Master's thesis

NTNU
Norwegian University of Science and Technology
Faculty of Economics and Management
Dept. of Industrial Economics and Technology Management

Eivind Andreas Falk
Frederik Løkka Hansen

Stochastic Short-Term Optimization of Energy Systems with Offshore Hydrogen Production

Green Hydrogen Production in the North Sea

Master's thesis in Industrial Economics and Technology Management
Supervisor: Asgeir Tomasgard
Co-supervisor: Paolo Pisciella, Hongyu Zhang
June 2023

NTNU
Norwegian University of Science and Technology

Eivind Andreas Falk
Frederik Løkka Hansen

Stochastic Short-Term Optimization of Energy Systems with Offshore Hydrogen Production

Green Hydrogen Production in the North Sea

Master's thesis in Industrial Economics and Technology Management
Supervisor: Asgeir Tomasgard
Co-supervisor: Paolo Pisciella, Hongyu Zhang
June 2023

Norwegian University of Science and Technology
Faculty of Economics and Management
Dept. of Industrial Economics and Technology Management

NTNU
Norwegian University of
Science and Technology

PREFACE

This master thesis is the culmination of a five year Master's Degree Programme in Industrial Economics and Technology Management offered by the Department of Industrial Economics and Technology Management at the Norwegian University of Science and Technology.

First and foremost, we express our appreciation to our main supervisor Asgeir Tomasgard for guiding academic insight. We have had the privilege of connecting with various esteemed industrial partners who have generously shared their expertise and insights, and we would like to express our sincere appreciation to all those who have contributed to the development of this work. Stefan Feltenmark, representing Volue, for sharing his knowledge on optimization models. We extend our gratitude to Hydepoint, through Martin Kjäll-Ohlsson, for key contributions in providing a comprehensive system design for offshore hydrogen production. We would also like to acknowledge the contributions of Elin Steinsland, Asbjørn Mortensen, and Erlend Røstbø from Moreld, whose insights have contributed in the development of a cohesive energy system. We extend our gratitude to Magnus Johansen from Arendal Fossekompani for his prompt assistance, and Leon Gosh from Cellect Energy S.L for sharing his expert knowledge on battery solutions. Sjur Westgaard, your expertise was very much appreciated and left a significant impact. We thank Nord Pool for providing us with data on power market transactions.

We deeply appreciate the swift responsiveness and willingness of all our partners to arrange meetings and assistance throughout the semester, enriching the quality and depth of this work. Finally, to our co-supervisors, Paolo Pisciella and Hongyu Zhang, we are profoundly privileged to have you as our co-supervisiors and very grateful for your genuine passion in sharing knowledge, and consistently providing invaluable and supportive feedback.

Eivind Andreas Falk
Frederik Løkka Hansen

Trondheim, June 2023

SUMMARY

In the next decades, the European energy supply will drastically increase its share of renewable power generation, as the future energy system will comprise renewable energy sources at its core. Hydrogen supply chains will play a vital role in integrating renewable technologies, but will also provide as a feedstock, fuel and energy carrier across a wide range of sectors. Meanwhile, the European Commission is planning to upscale the wind power capacity in the North Sea and provide the European continent with 40 GW renewables-linked electrolysis in 2030. Academia and industry have directed research efforts and investments to realize the ambitions of creating hydrogen corridors from the North Sea. Several companies have announced their investments in offshore systems, accelerating the race towards the production of hydrogen offshore. In that context, an offshore energy system consisting of an offshore wind farm and hydrogen platform in the North Sea has been studied. The so-called *hybrid* system is connected to the European mainland through a transmission cable to the power grid and a hydrogen pipeline. Energy from the wind farm can be utilized in hydrogen production or injected directly in to the mainland power grid. The objective of this thesis has been to implement the operational behavior of this system into an optimization framework that maximizes the revenue potential by participating in hydrogen and power markets. The optimization model provides decision-support by accurately estimating the expected revenues for a given system configuration of preference for a prospecting investor. A stochastic mixed integer planning model is formulated to account for uncertainty in wind power generation 36 hours ahead, by combining quantile regression with spline basis functions and a scenario generation method proposed by Pinson et al. (2009). Autoregressive structures are applied to forecast electricity prices in the day-ahead and intraday markets, and non-reversible commitments made in bidding auctions to capture risk. A compromise between computational tractability and modeling precision is made when modeling electrolyzer characteristics, that includes ramping constraints between operational states. A rolling horizon framework is implemented to solve the stochastic program.

The performance of the model is significantly influenced by the uncertainty associated with exogenous factors, as revealed by the results. In such scenarios, the role played by fuel cell batteries and the intraday market is crucial in effectively mitigating any potential violations of power purchase agreements. It is expected that a higher number of scenarios would result in more robust solutions. However, it is important to carefully assess the penalty costs and the number of scenarios to prevent the objective function from deteriorating and to avoid long solution times. This consideration is especially important due to the random processes involved in the scenario generation process. These aspects make it difficult to interpret the value of the stochastic solution, although the expected value problem by definition achieves a 6.8 % better solution. Furthermore, the perfect information case achieves an 8% better solution. Although higher transmission capacities yield greater revenues, they often require substantial grid reinforcements that may not be practically feasible. By modeling a 1000 MW electrolyzer capacity, which corresponds to an island mode configuration, the hydrogen break-even point is estimated to be approximately 5 EUR/kg when considering power sales. Selling hydrogen carries lower financial risks compared to power purchase agreements. The model proposed in this thesis could be iteratively employed with profitability tools for the project lifetime in the optimization of energy system designs. Future estimations of electricity and hydrogen prices, combined with equipment costs, will play a decisive role in determining the profitability and viability of projects involving offshore hydrogen production.

SAMMENDRAG

Fornybare energikilder utgjør kjernen av fremtidens energisystem. Verdikjeder av hydrogen vil spille en avgjørende rolle i integreringen av fornybar kraft, men vil også ha nytte som råstoff, drivstoff og energibærer på tvers av ulike sektorer. Samtidig planlegger den Europeiske kommisjon å øke vindkraftkapasiteten i Nordsjøen og forsyne det europeiske kontinentet med 40 GW grønn hydrogen innen 2030. Akademia og industrisektoren har rettet stort forskningsinnsats og allerede gjort store investeringer for å realisere ambisjonene om å skape forsyningskjeder av hydrogen i Nordsjøen. Med dette som bakgrunn er et offshore energisystem bestående av en offshore vindfarm og en hydrogenplattform i Nordsjøen blitt studert. Det såkalte hybridsystemet er koblet til det europeiske fastlandet via en overføringskabel til kraftnettet og en undervanns hydrogenrørledning. Energi fra vindparken kan brukes i hydrogenproduksjon eller sendes direkte inn på kraftnettet. Målet til denne oppgaven har vært å implementere systemets oppførsel inn i en optimaliseringmodell som maksimerer inntekt fra hydrogen- og kraftmarkeder. Optimeringsmodellen tilbyr beslutningsstøtte ved å nøyaktig estimere forventet inngående kontantstrømmer, også for ulike systemkonfigurasjoner dersom kapasiteter endres. Optimeringsmodellen er definert som et lineært stokastisk blandet heltallsproblem, som tar hensyn til usikkerhet i vindkraftproduksjon 36 timer frem i tid ved å kombinere kvantilregresjon og spline basisfunksjoner, og en scenariogenereringsmetode inspirert av Pinson et al. (2009). Regresjonsmodeller er benyttet til å prognostisere kraftpriser i day-ahead og intraday markedet, og straffekostnader ved underleveranser er modellert for å fange opp risiko ved budgivning til disse markedene. Nøyaktigheten i modelleringsbeskrivelsen av elektrolysørenes oppførsel er vektet mot problemstørrelse og løsningstid, og modellen håndterer også begrensninger som følger av overgang mellom ulike driftstilstander. En rullende horisont tilnærming er benyttet for å løse det stokastiske optimeringsproblemet over en bestemt tidshorisont.

Resultatene viser at modellen påvirkes betydelig av graden av usikkerhet knyttet til de eksogene faktorene. Selv om scenariobeskrivelsen fører til relativt robuste løsninger er brenselceller, batteripakker og intraday markedet viktige komponenter for å håndtere situasjoner med underproduksjon, selv om det er forventet at et høyere antall scenarioer fører til mer robuste løsninger. Det er viktig å vurdere straffekostnaden for brudd på avtaler av kraftsalg i sammenheng med antallet scenarioer som modelleres. Dette hensynet er av stor betydning ettersom tilfeldige prosesser er involvert i scenariogenereringsmetoden. Disse aspektene gjør det utfordrende å tolke den nøyaktige verdien av den stokastiske løsningen, selv om det deterministiske problemet oppnår en objektsfunksjonsverdi som er 6.8 % bedre. Videre vil modellen med perfekt informasjon om vind gi en 8.0 % bedre løsning. Høyere overføringskapasitet til kraftnettet kan gi betydelig inntektsøkning, men det vil kreve store investeringer i kraftnettet, som overgår det som er virker fornuftig. Ved å modellere en elektrolysørkapasitet på 1 000 MW, tilsvarende et energisystem dedikert til kun hydrogenproduksjon, anslås denne systemkonfigurasjonen å være konkurransedyktig med det opprinnelig studerte systemet dersom hydrogenprisen anslagsvis overstiger 5 EUR/kg. Salg av hydrogen innebærer lavere finansiell risiko enn avtaler av kraftsalg. Modellen som er foreslått i denne masteroppgaven finner nytte som et lønnsomhetsverktøy for å optimalisere energisystemets design over prosjektets levetid. Fremtidige estimater for kraft og hydrogenpriser spiller en avgjørende rolle for å estimere om investeringsbeslutninger i slike prosjekter kan være lønnsomme.

CONTENTS

LIST OF FIGURES

LIST OF TABLES

ACRONYMS

AFC Alkaline Fuel Cells.

AR Autoregressive.

BESS Battery Energy Storage System.

CET Central European Time.

DPP Discounted Payback Period.

EEV Expectation of the Expected Value Problem.

EU European Union.

EVPI Expected Value of Perfect Information.

HHV Higher Heating Value.

HPA Hydrogen Purchase Agreements.

HVAC High Voltage Alternating Current.

HVDC High Voltage Direct Current.

LCOH Levelized Cost of Hydrogen.

MED Multi Effect Distillation.

MET Norway The Norwegian Meteorological Institute.

MET-F MET Norway Forecasts.

MILP Mixed Integer Linear Programming.

MPC Model Predictive Control.

MSF Multi-Stage Flash Distillation.

NPV Net Present Value.

NWP Numerical Weather Prediction.

PEM Proton Exchange Membrane.

PEMEL Proton Exchange Membrane Electrolyzers.

PEMFC Proton Exchange Membrane Fuel Cells.

PI Perfect Information.

RO Reverse Osmosis.

SEC Specific Energy Consumption.

SOEC Solid Oxide Electrolysis Cells.

SOFC Solid Oxide Fuel Cells.

SS Stochastic Solution.

VSS Value of Stochastic Solution.

CHAPTER

ONE

INTRODUCTION

Over the next two decades, there is a pressing need for a profound transformation of Europe's energy system and its structure. The renewable share in the energy mix on the European continent is projected to reach 55-60% in 2030, and as high as 84% in 2050 (European Commission, 2020c). The energy supply will rely on an increasing share of geographically distributed renewable technologies. However, additional variable power grid injections from scheduled development compromise power system stability and demand substantial reinforcement investments, which in most cases are not considered techno-economic feasible. Energy storage inevitably co-exists with variable power generation. While direct electrification is often the most energy-efficient option for decarbonizing, a number of end-appliances benefit from renewable or low-carbon fuels such as sustainable gas, biofuels, methane, synthetic fuels, and low-carbon and renewable hydrogen.

To achieve emission reductions of 50 % by 2030 and net-zero by 2050, in accordance with the Paris Agreement and the European Green Deal, the European Commission has developed a hydrogen strategy on how hydrogen is implemented in industries by policy makers to become climate neutral economies. The European Union (EU) prioritizes renewable electricity and renewable hydrogen as the most sustainable solution and the future climate-neutral energy system has these two components as its core (European Commission, 2020a). Hydrogen is a feedstock, fuel and energy carrier applicable to a wide range of sectors. It is also a vector for storage as it offloads the grid in cases of energy abundance, providing a buffering function and enhancing the security of supply with daily to long-term seasonal storage. Hydrogen is currently representing only a modest proportion of the energy mix and the hydrogen supply chains are underdeveloped and still at the infancy level. The hydrogen ecosystem and its structure will depend on production and demand patterns, transportation costs and grid development. Nevertheless, hydrogen remains the most compatible and coherent option with EU climate neutrality and integrated energy system agenda. Trajectories suggest that hydrogen becomes intrinsic to the energy system in 2025-2030 and will play a nodal role in integrating renewable power generation. Demand-side policies will help to accelerate the progress on hydrogen networks, and at the same time, ensure national and regional interoperability by common quality standards and cross-border operational rules. The European Commission also proposes a certification scheme for domestic producers of renewable hydrogen. Eventually, hydrogen can be traded in a single market.

Although the European Commission prioritizes renewable hydrogen in the long term, the majority of hydrogen produced today cannot be classified as renewable. Approximately 96 % of the total production comes from steam reforming of hydrocarbons emitting 70 – 100 million tons of CO_2 annually. Carbonized hydrogen is still the most cost-competitive solution, but economies of scale for decarbonized hydrogen could be achieved with sufficient investments and public-private collaborations (European Commission, 2020a). One of many investment prospects emerges from the convergence between wind power generation and hydrogen energy.

Offshore wind energy, among other offshore technologies, has the greatest scale-up potential of approximately 300 GW capacity in 2050 from today's 12 GW (European Commission, 2020b). The short-term goal is to install 60 GW offshore wind capacity by 2030, which is considered both achievable and realistic. Approximately 77 % of total installed wind capacity in Europe is located in the North Sea region (McKenna et al., 2021), and experts predict future wind farms averaging 800 MW and 1100 MW for floating and fixed-bottom wind power, respectively (Beiter et al., 2022). The North Sea region is deemed to be the cornerstone of initiating the energy transition, and the EU has subsidized the development of hydrogen corridors from the North Sea to continental Europe (European Commission, 2020a). The EU Hydrogen Strategy targets 40 GW of renewables linked electrolysis by 2030. Offshore hydrogen storage systems are, at least in theory, deployable at any offshore location without relying on grid connection infrastructure (Dinh et al., 2021). Given these parameters, Norway has an opportune position to produce large-scale low-carbon and renewable hydrogen due to its geography and high wind speeds (Espegren et al., 2021). The concept of producing large-scale offshore hydrogen offshore has already sparked a large interest in the industry. Offshore hydrogen supply chains are unquestionably emerging in the near future.

The cost competitiveness of offshore hydrogen production has been a hot topic in academic research. The cost of fossil-based hydrogen is currently estimated at around 2 EUR/kg, while renewable hydrogen achieves 2.5 – 5.5 EUR/kg. However, technology for renewable hydrogen production is rapidly maturing and will soon reach economies of scale as renewable hydrogen is predicted to outperform fossil-based hydrogen in 2030. Preliminary academic studies on offshore hydrogen production have been concentrated on feasibility studies of investment cycles. A particular interest has been expressed in different offshore system layouts to compare and find the optimal configuration (Dinh et al., 2021; Lucas et al., 2022). The main alternatives being evaluated in research are if electrolyzers should be on-shore, on energy hubs/islands or tower integrated, and energy flows in electrical networks under these circumstances. As these studies are primarily economic assessments, system behavior tends to be aggregated and simplified in order to address system performance over long time horizons. Despite uncertainty in future technology and market prices, centralized production in floating structures or turbine tower integrated solutions is found to be unmatched compared to others in economic terms (Jang et al., 2022).

In terms of operational planning, many authors have already developed optimization models for hydrogen production with a focus on electrolyzer operation management. However, these models are based on onshore hydrogen production of typically a single electrolyzer, without consideration for the unmatched offshore project scale and offshore operating conditions. Different studies also estimate performance over longer time horizons, compared to our work, with grid-integrated systems that, in principle, cannot guarantee that the produced hydrogen is emission-free. A coherent model for operational planning of offshore hydrogen production systems is, to the extent of the authors' knowledge, not found in the literature, signifying this work as one of the first operational planning models for a large-scale offshore hydrogen production system in the North Sea. To our knowledge, few, if any, real world projects have been put into operation. There is no existing blueprint of the actual system design and dimensions easily available besides undisclosed corporate information. Therefore, a thorough review has been done of the core technological components comprising the conceptualized system. With the help of technology experts and research literature, system integrity is preserved.

Falk and Hansen (2022) studied a deterministic short-term optimization problem involving a hybrid offshore energy system with hydrogen production connected to an offshore wind farm, as well as hydrogen and the day-ahead market. However, the North Sea's challenging and volatile marine environment gives rise to abrupt and intensified atmospheric phenomena, leading to highly volatile wind power generation. This volatility poses significant risks when modeling realistic power purchasing agreements in both the day-ahead and intraday markets. This thesis stands apart from previous research on offshore energy systems with hydrogen production, and extends the work by Falk and Hansen (2022) by specifically investigating the short-term operational performance under the influence of uncertain power generation and power market prices. The primary objective of this thesis is to analyze the behavior and performance of the system by incorporating stochastic wind power generation in a scenario description, all while considering the fulfillment of power purchasing agreements. This approach enables a more precise estimation of how exogenous factors,

which guide power system behavior and performance, influence the economic viability of the system and investment decisions. To achieve this objective, a stochastic Mixed Integer Linear Programming (MILP) problem is proposed. The optimization model includes scenarios estimated using quantile regression and b-spline basis functions in order to represent wind power generation scenarios, and auto-regressive structures to forecast uncertain power market prices. The optimization model is implemented in a rolling horizon framework, allowing for quarter-hourly decision-making while forecasting wind data for the upcoming 36 hours. Notably, the practical applicability of the optimization model has been a key consideration, with execution time playing a central role.

The remainder of this thesis is structured as follows. Chapter 2 provides the reader with introductory insights on stochastic programming, the rolling horizon framework and the other mathematical modelling techniques that have been used in this thesis. Chapter 3 presents the problem description. The literature review is given in Chapter 4. Chapter 5 presents the modelling assumptions and strategies. The mathematical model for the stochastic short-term optimization problem is formulated in Chapter 6. Model implementation and instance generation are described in Chapter 7. Chapter 8 presents the results from the computational study in addition to managerial insights and discussion of the results. Concluding remarks are provided in Chapter 9. Finally, Chapter 10 gives a discussion of future research.

CHAPTER

TWO

BACKGROUND

This chapter aims to introduce the reader to certain topics that could ease the understanding of several later chapters in the thesis. Section 2.1 gives an introduction of stochastic model formulation and methods for assessing the performance of stochastic problems. Section 2.2 presents theory on the rolling horizon framework and how it can be used in optimization models. Section 2.3 introduces several mathematical modelling techniques that have been used in thesis.

2.1 Stochastic Programming

The theory presented in this section is based on Kall and Wallace (2003) and Pisciella (2012). A stochastic model aims at formulating and dealing with problem structures that involve uncertainty about parameter data. Stochastic models capture the future consequences of the decisions we make now, the *first-stage* variables. Recourse decisions, or second-*stage* variables are made as uncertainty is revealed. Because the first-stage decisions are non-reversible, they should be made with careful consideration of the uncertain future.

2.1.1 Formulation of Stochastic Problems

Stochastic models are typically defined in stages depending on how information is revealed. Many stochastic problems are formulated as two-stage problems which involve some irreversible decisions, some update on information about uncertain data, and recourse decisions made in response to this new information. We are solving problems that can be very generally described as

$$\begin{aligned} \text{“min”} \quad & g_0(x, \tilde{\xi}) \\ \text{s.t.} \quad & g_i(x, \tilde{\xi}) \leq 0, \quad i = 1, \ldots, m \\ & x \in \mathcal{X} \subset \mathcal{R}^n \end{aligned} \tag{2.1}$$

where $\tilde{\xi}$ is a random vector varying over a set $\Xi \subset \mathcal{R}^k$. More precisely, it is assumed that a collection $\mathcal{F}$ of subsets, or events, of Ξ, exists such that the probability distribution $\mathcal{P}$ on $\mathcal{F}$ is given. For every *subset* $\mathcal{A} \in \mathcal{F}$, which can be denoted an event, the probability $\mathcal{P}(\mathcal{A})$ is a known value. In this format, the meaning of “min” and the constraint is not precisely communicated.

So-called *deterministic equivalents* can be reformulated from (2.1).

$$g_i^+(x,\xi) = \begin{cases} 0 & \text{if } g_i(x,\xi) \leq 0 \\ g_i(x,\xi) & \text{otherwise} \end{cases} \tag{2.2}$$

is the i'th constraint in (2.1) and violated conditional that $g_i^+(x,\xi) > 0$ for a first-stage decision x and unveiling of the uncertain parameter ξ of $\tilde{\xi}$. After observing $\tilde{\xi}$, a recourse activity can be defined as $y_i(\xi)$ that can offset any observed violation of the constraints, given that

$$g_i(x,\xi) - y_i(\xi) \leq 0. \tag{2.3}$$

the recourse activity is assumed to incur an additional cost term, or penalty, $q_i y_i(\xi)$ per unit activity. Then the additional cost is represented by a *recourse function*, which can be defined as,

$$Q(x,\xi) = \min_y \left\{ \sum_{i=1}^{m} q_i y_i(\xi) \big| y_i(\xi) \geq g_i^+(x,\xi), i = 1, ..., m \right\} \tag{2.4}$$

The total cost comprises the sum of the first-stage costs and the recourse costs, modeled in (2.4). The decision-maker now aims to minimize

$$f_0(x,\xi) = g_0(x,\xi) + Q(x,\xi). \tag{2.5}$$

If modeling the expected value of the total costs, i.e. first- and second-stage costs, is acceptable to the decision-maker, the problem defined in (2.1) can be reformulated to a *deterministic equivalent*, commonly known as (two-stage) *stochastic program with recourse*,

$$\min_{x \in X} E_{\tilde{\xi}} f_0(x,\tilde{\xi}) = \min_{x \in X} E_{\tilde{\xi}} \{ g_0(x,\tilde{\xi}), Q(x,\tilde{\xi}) \} \tag{2.6}$$

where x is the first-stage decision.

In this thesis, one particular deterministic equivalent is modeled for stochastic problems given by (2.1) on the form,

$$\begin{aligned} \text{"min"} \quad & c^T x \\ \text{s.t.} \quad & Ax = b \\ & T(\tilde{\xi})x = h(\tilde{\xi}) \\ & x \geq 0 \end{aligned} \tag{2.7}$$

The recourse variables y are in this case specifically introduced as,

$$Wy = h(\xi) - T(\xi)x \tag{2.8}$$

where W is the known *recourse matrix*. The additional cost from the recourse problem is then,

$$Q(x,\xi) = \min_y \left\{ q^T y | Wy = h(\xi) - T(\xi)x, i = 1, \ldots, m, y \geq 0 \right\} \tag{2.9}$$

One deterministic equivalent of the particular stochastic instance in (2.7) is called a two-stage stochastic problem with recourse, and can be defined in a compact form,

$$\begin{aligned} \min \quad & c^T x + E_{\tilde{\xi}} Q(x,\tilde{\xi}) \\ \text{s.t.} \quad & Ax = b \\ & x \geq 0, \end{aligned} \tag{2.10}$$

or where the second-stage problem is casted from the recourse function

$$\begin{aligned} \min \quad & c^T x + E_{\tilde{\xi}}\left[q^T y(\tilde{\xi})\right] \\ s.t. \quad & Ax = b \\ & Wy(\tilde{\xi}) = h(\tilde{\xi}) - T(\tilde{\xi})x \\ & x \geq 0, y(\tilde{\xi}) \geq 0. \end{aligned} \tag{2.11}$$

If ξ is a finite and discrete stochastic variable, both stages can formulated in a single optimization problem. We start by defining the probabilities p_k, recourse variables y_k, quantities q_k, h_k, T_k for each realization of the uncertain parameter ξ_k, where $k = 1, \ldots, N$ is the discrete set of scenarios. The final discretized version of (2.11) is then reformulated as

$$\begin{aligned} \min_{x, y_1, \ldots, y_N} \quad & c^T x + \sum_{k=1}^{N} p_k q_k^T y_k \\ \text{s.t.} \quad & Ax = b \\ & T_k x + W_k y_k = h_k, \quad k = 1, \ldots, N \\ & x \geq 0, y_k \geq 0, \qquad k = 1, \ldots, N \end{aligned} \tag{2.12}$$

Although this discretized structure of the linear prrogramming problem is convenient for developing solution algorithms, it have the potential to grow very large in size depending on the number of scenarios that are modeled (Pisciella, 2012).

2.1.2 Evaluating the Performance of the Stochastic Problem

When modeling stochastic programs, it is important to evaluate if the impact of modeling uncertainty is significant (Leo & Engell, 2018). The value of a stochastic model generally increases in proportion to the significance of the uncertainty. In order to quantify the benefit of integrating wind speed variability in our model and estimate the value of obtaining more information on uncertain parameters, we determine recognized metrics such as the Value of Stochastic Solution (VSS) and the Expected Value of Perfect Information (EVPI).

Value of the Stochastic Solution

The value of the stochastic solution is reflected in the VSS parameter. In general, when there is significant uncertainty, the VSS can be quite significant. A high VSS value reflects a considerable benefit of considering uncertainty in the model. In academia, it is common to report on VSS when using a stochastic model. To determine VSS, we must also find the value of the Expectation of the Expected Value Problem (EEV). We find EEV by fixing the first-stage variables to the solutions found when solving the stochastic program with the expected value of the uncertain parameters and inserting them into the recourse problems.

VSS is described by Equation (2.13),

$$VSS = SS - EEV, \tag{2.13}$$

where Stochastic Solution (SS) denotes the objective function value of the the stochastic solution.

Value of Perfect Information

EVPI estimates the value of information and quantifies in simple terms how much one would be willing to invest in more information about uncertain parameters. Although the "P" stands for perfect, we can interpret EVPI as having more information and the cost to eliminate uncertainty

in the model (Wallace et al., n.d.). If we denote the solution with perfect foresight as Perfect Information (PI), the EVPI is mathematically defined as

$$EVPI = PI - SS \tag{2.14}$$

PI is determined by the expected value of the objective functions when solving each scenario as a deterministic problem.

2.2 Rolling Horizon Theory

Uncertain power generation makes it appropriate to incorporate the most recent information available to the decision-maker before any decisions on hydrogen production are taken in the next time period. This implies that the optimization problem is solved in a perpetual manner that requires continuous updates on information, emphasizing the need for a well-suited solution framework. When dealing with optimization problems that involve a temporal dimension, such as those encountered in energy systems with wind power modeling, a rolling horizon approach is commonly found in literature. Rolling horizon compromise between solution times and accuracy for comprehensive problem structures that otherwise would be hard to solve in a single iteration. The motivation for using a rolling horizon approach is that it is adaptive and flexible to the problem it is modeling and is appropriate for energy planning problems with indefinite time horizons and low interdependencies between early and later decisions (Andersson & Grönkvist, 2019). A rolling horizon framework generally solves shorter overlapping *subproblems* in an iterative process until decisions are made for the entire planning horizon. The rolling horizon approach will output the optimal policy for the planning horizon determined by the subproblems' solutions. Figure 2.1 illustrates the structure of the rolling horizon framework, which consists of fixed, current, forecasted and future decisions. The fixed decisions are implemented actions by the decision-maker, the current decision represents the optimal policies taken in the current time period, while forecasted decisions are decisions part of the subproblem but that are not implemented, but used for incorporation relevant information about the future for the current decisions. Future decisions are outside of the planning horizon of the subproblems, however scheduling will be done in the corresponding time periods when the rolling horizon approach progresses iteratively.

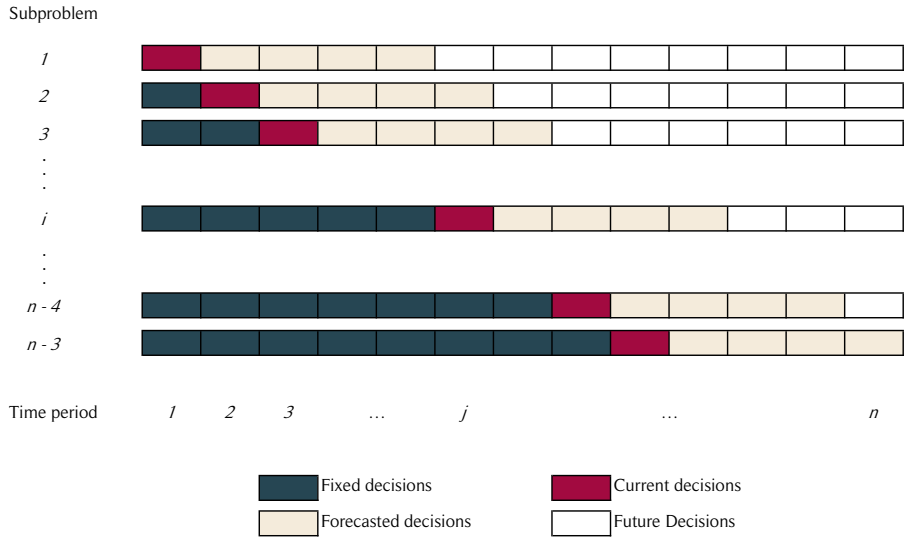

Figure 2.1: Information flow in the rolling horizon approach.

The size of the set of forecasted decisions, referred to as the forecasting section, directly impacts the amount of information available for determining the optimal scheduling policy in the current

time period. By fine-tuning the length of the forecasting period, we can incorporate future-relevant information for current decisions, while also adjusting the size of the set of current decisions to accommodate the frequency of changes in forecasted data. Considering the perpetual nature of solving interrelated subproblems, boundary conditions must be specified at the commencement and endings of subproblems. Because of the perpetual nature of finding optimal decisions, boundary conditions are specified at the beginning and the end of the subproblems. A mathematical description of the rolling horizon algorithm is presented next.

The rolling horizon methodology comprises a sequence of interconnected optimization problems, previously introduced as subproblems. Each subproblem, $\mathscr{P}_t$, corresponds to a specific time period $t \in \mathcal{T}$. Here, $\mathcal{T}$ represents the complete set of time periods within the global planning horizon. The global horizon is different from the subproblems' planning horizon, and depends on how many time periods we want to analyze, although in reality, only one subproblem is solved every 15 minutes. As these optimization problems are interlinked, each subproblem $\mathscr{P}_t$ is associated with a set of initial state-variables, denoted as $\mathcal{K}_t$, defined over $\mathscr{D}_t^{\mathcal{K}}$, a collection of interior state decision variables, denoted as $\mathcal{X}_t$, defined over $\mathscr{D}_t^{\mathcal{X}}$, and a set of end-state variables, denoted as $\mathcal{G}_t$, defined over $\mathscr{D}_t^{\mathcal{G}}$ (Falk and Løkka, 2022).

To establish the coupling between subproblem $\mathscr{P}_t$ and problem $\mathscr{P}_{t+1}$, where $t \in 1, \ldots, |\mathcal{T}| - 1$, it is assumed that $\mathscr{D}_t^{\mathcal{G}} \in \mathscr{D}_{t+1}^{\mathcal{K}}$. The objective function of subproblem $\mathscr{P}_t$, denoted as $f_t(\mathcal{X}_t)$, is defined such that the objective function value, $f_t : \mathcal{X}_t \to \mathbb{R}$, solely depends on the interior state variables. The feasible region of a given subproblem is defined by $g_t(\mathcal{K}_t, \mathcal{X}_t, \mathcal{G}_t) \leq 0$. As a result, the model formulation of the subproblem is given in (2.15).

$$
\begin{aligned}
\text{maximize} \quad & f_t(\mathcal{X}) \\
\text{subject to} \quad & g_t(\mathcal{K}_t\mathcal{X}_t, \mathcal{G}_t) \leq 0, \\
& \mathcal{K}_t \in \mathscr{D}_t^{\mathcal{K}}, \\
& \mathcal{X}_t \in \mathscr{D}_t^{\mathcal{X}}, \\
& \mathcal{G}_t \in \mathscr{D}_t^{\mathcal{G}},
\end{aligned} \tag{2.15}
$$

The rolling horizon approach can then be defined with the help of a constant r indicating the global planning horizon length that we want to solve for,

$$
\begin{aligned}
\text{maximize} \quad & \sum_{i=t}^{t+r} f_i(\mathcal{X}_i) \\
\text{subject to} \quad & g_t(\mathcal{K}_t\mathcal{X}_t, \mathcal{G}_t) \leq 0, \\
& \mathcal{K}_i = \mathcal{G}_{i-1}, && i \in \{t+1, \ldots, t+r\} \\
& \mathcal{K}_i \in \mathscr{D}_i^{\mathcal{K}}, && i \in \{t, \ldots, t+r\} \\
& \mathcal{X}_i \in \mathscr{D}_i^{\mathcal{X}}, && i \in \{t, \ldots, t+r\} \\
& \mathcal{G}_i \in \mathscr{D}_i^{\mathcal{G}}, && i \in \{t, \ldots, t+r\}
\end{aligned} \tag{2.16}
$$

2.3 Mathematical Modelling Techniques

Various mathematical techniques have been applied in this thesis. Some of the these are used to produce forecasts directly, while others are a small part of a larger framework. The techniques used in this thesis are introduced and briefly described in this section.

2.3.1 Autoregressive Models

There are many tools and models that can be used to analyse data that evolves over time. Autoregressive (AR) models can be used to perform time series analysis and are used in several fields to study time-evolving data sets. The model uses linear combinations of the p, usually referred to as the number of lags, most recently recorded values (Cryer & Kellet, 1991). An AR(p) is given by Equation (2.17) where X_t is the current value of the series ϕ_1,ϕ_2 and ϕ_p are the regression parameters and e_t is white noise.

$$X_t = \sum_{i=1}^{p} \phi_i X_{t-i} + e_t = \phi_1 X_{t-1} + \phi_2 X_{t-2} + ... + \phi_p X_{t-p} + e_t \tag{2.17}$$

AR models are relatively easy to implement and are often not computationally demanding. This has made the method a popular tool to assess time series, but also to forecast future behaviour. A way to simulate future behaviour is to randomly draw e_t from the standard normal distribution and to create future values. Bootstrapping is a similar procedure where e_t is drawn from empirical residuals instead.

2.3.2 Quantile Regression

Quantile regression is regression analysis method that is used to estimate conditional quantiles. Regression analysis is used to establish a relationship between an outcome y and a variable x. The study of a dataset with different quantiles, also called percentiles, allows a more complete assessment of the entire distribution of the data (Koenker & Hallock, 2001). This can be particularly useful in situations where decision-makers must consider the entire probability distribution of events, which is often the case for stochastic and chance constrained optimization problems. Furthermore, quantile regression makes no assumption on the probability distribution of the data, as it only uses empirical data to estimate quantiles. Quantile regression models can be formulated as a minimization problem of residuals. Koenker and Hallock (2001) formulated the minimization problem of residuals in a dataset of length n as shown in Equation (2.18), where ρ_θ is the loss function for a given quantile θ and $\xi(x_i, \beta)$ is a parametric function dependent on x and estimator β.

$$\underset{\beta \in \mathbb{R}}{\text{minimize}} \quad \sum_{t=1}^{n} \rho_\theta \left(y_t - \xi \left(x_t, \beta \right) \right) \tag{2.18}$$

The inclined absolute value function shown in Figure 2.2 is the loss function ρ_θ. The chosen quantile θ acts as a weighting mechanism for the loss function. For instance, a high θ will penalize the objective function in Equation (2.18) significantly when the residual $y_t - \xi(x_t, \beta)$ is positive. The quantile regression model will therefore adjust β to reduce the collective impact of positive residuals on the objective function. Conversely, negative residual are highly penalized for low values of θ. Finally, the optimization returns the regression estimator β for the θ-quantile. Quantile regression and its role in this thesis is further described in Section 4.2.2.

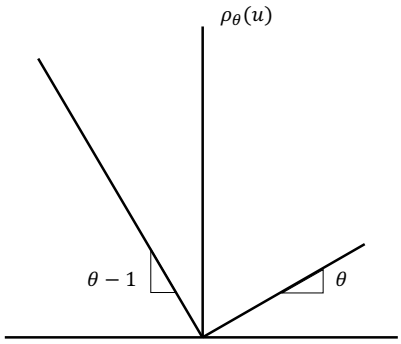

Figure 2.2: Loss function in quantile regression models. Adapted from Koenker and Hallock (2001).

2.3.3 Spline Basis Functions

Spline functions, or commonly referred to as splines, is an advanced mathematical tool used for interpolation. (Lyche & Morken, 2008) describe splines as a set of polynomial curves used to interpolate over a set of points. This can be useful is it is possible to a create smooth curves from data points, in other words create continuous functions from data points. The polynomial curves jointed to each other by knots, and both the number and position of knots can be determined by the user. There is a variety of different types of spline functions, such as cubic splines and natural cubic splines. Spline curves can be represented as a linear combination of basis splines, also called B-splines (Lyche & Morken, 2008). Basis spline functions can be used in combination with quantile regression as a way increase the accuracy of the quantile regression model. While implementation of spline basis functions can be a complex and extensive procedure, packages with spline tools are provided in several programming languages. Such packages have been used in this thesis to generate the necessary spline basis functions.

CHAPTER

THREE

PROBLEM DESCRIPTION

Large investments in offshore wind for the North Sea region are expected over the next decades. However, Europe's current power transmission grid is not dimensioned for the projected increase in wind capacity. It is ambitious to believe that the future power electrical grid will be able to withstand peak power production from the available variable renewable energy sources. Offshore hydrogen production presents itself as both an option and potentially a prerequisite to offload the power grid and limit curtailment. It could replace the need for a one-to-one ratio between installed power generation capacity and transmission capacity from offshore wind farms to onshore facilities. The designed energy system in this work is located at approximately 57°00'00.0"N 4°00'00.0"E, which places it centrally in the North Sea.

This thesis continues the work presented by Falk and Hansen (2022) with a study of a stochastic short-term optimization model of an offshore energy system with offshore hydrogen production. Deterministic formulation and perfect foresight of wind and power prices limits the practical use of the optimization problem presented by Falk and Hansen (2022). The energy system is inherently stochastic due to uncertain power production and power prices, and the study of the energy system under uncertainty can provide valuable insights in system behaviour. While stochastic short-term optimization could provide short-term production plans and potentially increase operational profitability, it could also increase the total value of similar renewable energy projects and assist in the decision-making process of investments in the energy sector. The next two sections explain more in detail about the objective of the optimization procedure and the technical description of the energy system. The stochastic short-term optimization problem optimization model is described in Section 3.1. The main components of the energy system are presented in Section 3.2.

3.1 Optimization Model Objective and Decision-making

The objective of the proposed optimization model is to maximize revenues from operating the energy system. By engaging in power markets and selling hydrogen, the objective of maximizing overall revenue per unit of available energy is achieved throughout the planning horizon while fulfilling power purchasing agreements. Revenues from power sales are generated by participating in the day-ahead and intraday market. The day-ahead market is the central scheduling mechanism for power exchanges and the intraday market provides balancing of the market participant's net position up until the delivery hour. The assumed income generation from hydrogen sales is derived from long-term Hydrogen Purchase Agreements (HPA), wherein the market participant has secured a fixed market price per kilogram of hydrogen.

The production plan for the upcoming time periods is optimized with respect to future power and hydrogen prices, along with the forecasted availability of wind energy. In order to optimize

decisions-making and avoid myopic decisions it is imperative to have information about future wind conditions. The unpredictable nature of future wind speed forecasts introduces uncertainty to the expected electrical power generation from the wind farm, making the future realized production exhibit a stochastic behavior. Uncertainty is therefore modelled up until the time instant of delivery. The stochasticity of wind power production is accounted for by a scenario generation approach. Information from the previous optimization problem is transferred to the subsequent optimization problem to determine future optimal production decisions. The information transfer includes pipeline storage level, operating states of the electrolyzers and battery energy storage in the current time period, which serve as initial conditions for the next optimization problem. Figure 3.1 provides a general description of the decision process in the optimization model.

The market clearing process, which occurs several hours before delivery, combined with the uncertainty of future power generation, can create situations where there is either a net energy surplus or a net energy deficit in future time periods with power market obligations, also referred to as power purchasing agreements. The day-ahead and intraday markets are cleared at different times, which implies that some time periods relies on forecasted market prices. As a price taker in the day ahead market, all offers on production are accepted to the day-ahead market at a forecasted price through self-bidding. The day-ahead market auction results are announced to the stakeholders at 13:00 Central European Time, for which all day ahead commitments for the next day's hours are decided. When day ahead commitments are decided, the market participant is obliged by contract to deliver the production volumes. If the market participant cannot meet its obligation in the day ahead market, a penalty fee per unit of energy is incurred. Given the length of the look-ahead horizon, certain optimization problems may involve forecasted day-ahead commitments, whereas there are always existing day-ahead commitments for the remainder of the current day.

System response to energy surplus and deficit is affected by market regulations. Intraday commitments are contracted at the time instant right before the delivery hour. Thus, the model cannot make additional intraday market commitments in the time periods that are within the current delivery hour, which implies that the commitments are uncertain. This implies that intraday market participation must be decided at a time that precedes the time period in the delivery hour. For surplus energy cases, where more energy is available than what is committed and contracted in the day-ahead market, it is possible to dedicate the excess electrical energy to increase hydrogen production and charge batteries if the capacities allow it. Conversely, in cases of energy deficit the model can reduce hydrogen production, discharge batteries, active fuel cells and curtail the surplus power. For time periods not within the current delivery hour, the model has the opportunity to make commitments in the intraday market for time periods in the upcoming delivery hour, and plan intraday operations in time periods with day-ahead obligations. In cases with energy surplus, the model can enrich the decision-making process with intraday day sale commitments in addition to the aforementioned mechanisms to avoid energy curtailment. Likewise, power purchase agreements can be made in the intraday market in cases of energy deficit in order to avoid a breach of contract for day-ahead obligations. Similar to day-ahead commitments, the intraday commitments are non-reversible and deviations from intraday purchasing agreements are penalized. In order to control the potential cost of unmet production levels, the model can adjust hydrogen production and activate system components in the manner described above to account for deviations in both day-ahead and intraday obligations.

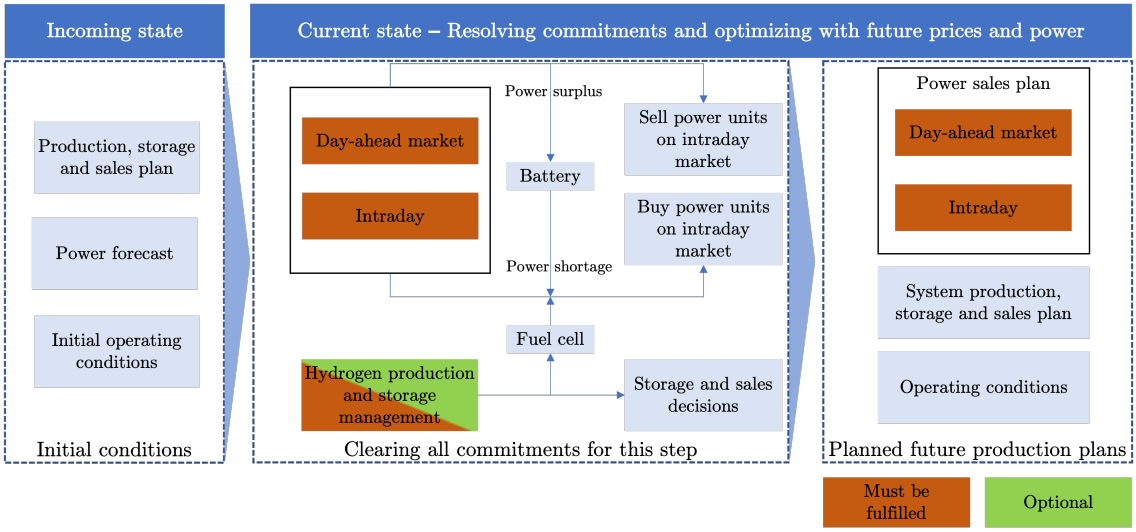

Figure 3.1: General description of optimization procedure

3.2 Energy System Components

The energy system disposes power from an offshore wind farm, and optimal usage of the energy resources is decided through the balancing of power market participation and hydrogen production. The energy system is described in Figure 3.2. The allocation of energy dedicated to power and hydrogen sales is determined in an electricity control center, which distributes electrical energy to either the transmission cable or an offshore platform with the necessary components to produce renewable hydrogen. Power grid connection via a unidirectional transmission cable between the offshore wind farm couples the energy system to the power markets. Green hydrogen can only be produced from renewable energy sources, thus the hydrogen can only be produced with electricity from the offshore wind farm and not from electricity from the grid. The key processes for power-to-hydrogen conversion in the energy system are sea water desalination, electrolysis, compression and storage, while fuel cell allows hydrogen-to-power conversion. Hydrogen is transported to the mainland hydrogen markets through a subsea pipeline.

Electrolysis converts water molecules into hydrogen gas, and electrolyzers are the most power consuming components in hydrogen production. Energy consumption per kg of hydrogen is described by a non-constant Specific Energy Consumption (SEC). A detailed modelling of of electrolyzer SEC can provide a more accurate description of overall system behaviour of real-time operations. Electrolyzers can transition from an idle (no production) to a producing state, vice versa. A transition from idle to producing halves production capacity for the time period of the transition. When in the producing state, electrolyzers can operate between a lower and upper capacity bound. Electrolyzers are aggregated into larger sets instead of individual description, and this set reduces in size for a given planning length to decrease the size of the problem.

The chosen state-of-the-art electrolyzer technology can only operate on high quality water, and not saline water in order to perform electrolysis. Desalination is the process of removing mineral solvents from sea water, and energy is required to pretreat sea water for electrolysis in the desalination process. Furthermore, compression of the outgoing hydrogen from the electrolyzers is required for storage. Compression, similarly to desalination, can be a complex process to model. However, compression and desalination SEC is marginal compared to electrolysis. Therefore, compression and desalination SEC is aggregated into a single constant parameter representing these auxiliary processes, as highly accurate behaviour modelling would have minimal impact on the accuracy on overall system behaviour. Furthermore, compression and desalination do not affect the bounds of hydrogen production capacity as these two processes are expected to have capacity limits well

above those of electrolysis in a real-life application. Compressed hydrogen is stored and transported via a pipeline. Compression at the production site and the inlet of the pipeline is needed to create a directional flow and overcome friction losses in the pipeline. A pipeline is considered the most viable option as it serves both as a storage and transportation device. Pipeline leakage is described by a loss coefficient. The pipeline also has a discharge capacity and storage capacity, in addition to a predefined terminal value for the last time period in the planning horizon.

Batteries and fuel cells are added to the energy system to provide flexibility and higher responsiveness when faced with fluctuations in wind power production. Battery charge and discharge are bounded by the installed capacity. A battery can either charge, discharge or remain unused in a given time period. The net change in the state of charge is contributed to the overall energy balance of the energy system. There is a loss associated with charging the batteries. Fuel cells converts hydrogen to electricity, which means that produced hydrogen can be reconverted to electricity to fulfill power market contracts. The energy output from hydrogen combustion is given by a constant SEC. There is an upper capacity limit on mass input to the fuel cells.

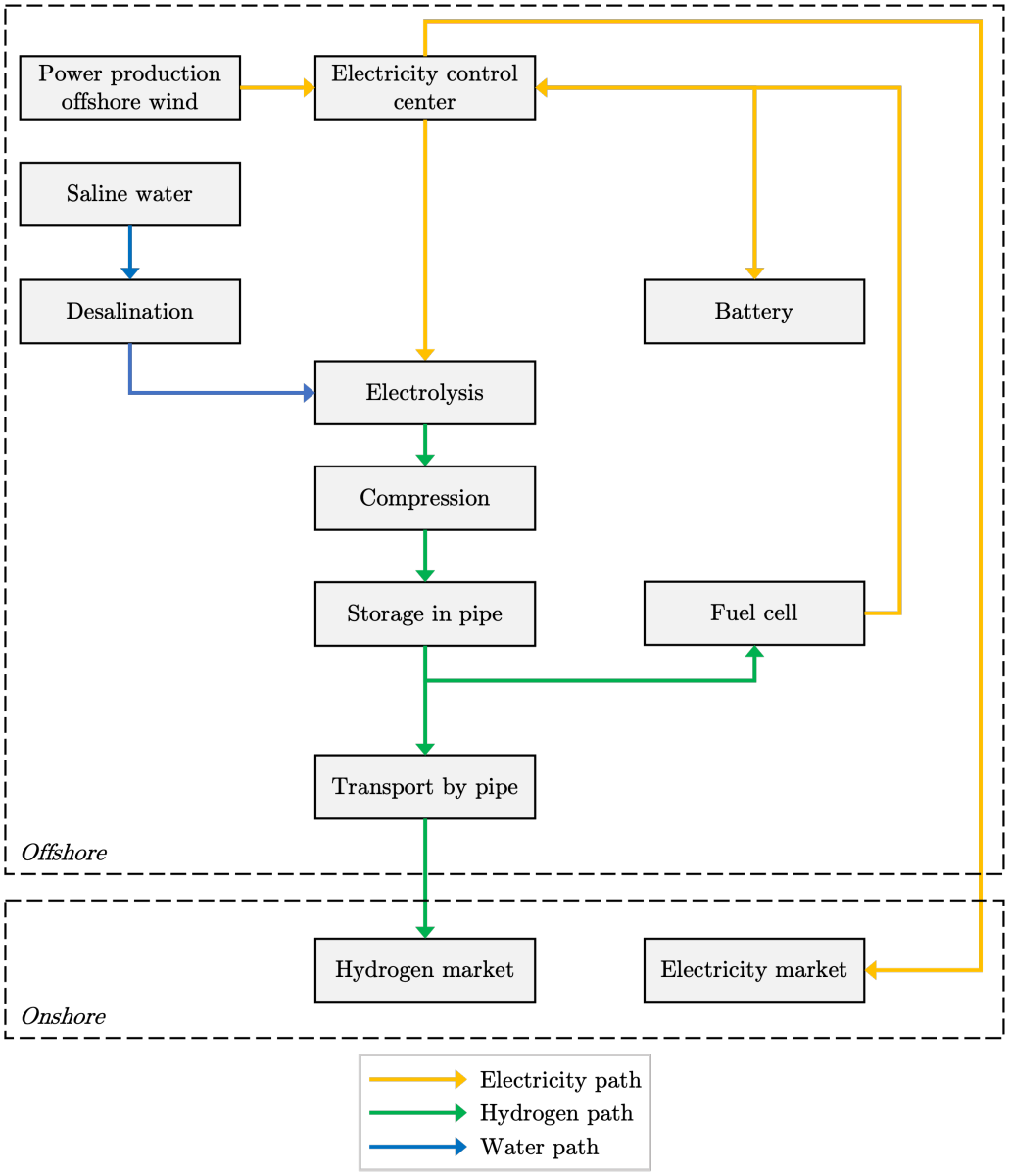

Figure 3.2: Schematic of the proposed energy system.

CHAPTER

FOUR

LITERATURE REVIEW

This chapters presents literature on offshore wind power generation and stochastic short-term optimization of energy systems with offshore hydrogen production. Substantial parts of the literature review stem from the research efforts in Falk and Hansen (2022) and have been synthesized in this thesis. Falk and Hansen (2022) used digital libraries and search engines such as Scopus, Google Scholar, Research Gate and Science Direct in combination with strategic strategic keywords and search filters to ascertain relevant literature. Rapid development in both research and commercialization of hydrogen technology led to the prioritization of more recent literature. The literature review also consists of consultations with industry experts, especially during the fall of 2022, and academic researchers. This has been an essential part of the literature review process in order to arrive at a sensible design for the offshore energy system studied in this thesis. The consultations has given the authors access to experience and knowledge that can be arduous to attain through publicly accessible channels. Research literature may promote an optimistic perspective on the availability and readiness of newer technology, contrary to companies whom seek reliable and proven solutions. In cases of contradictions, expert opinions have been given greater emphasis than research literature. The dynamic process of matching research literature and expert opinions made the literature review an iterative process in order to attain a more holistic and realistic system design.

The work related to short-term optimization in energy systems with hydrogen production presented in Falk and Hansen (2022), demonstrated that the studied problem spanned over several different fields of research. Offshore hydrogen production is mainly studied from a techno-economic view to evaluate profitability and investment decisions as well as technical feasibility. The operational aspect of short-term optimization is affiliated with operations research. Section 4.1 covers general literature related to short-term optimization of energy systems with offshore hydrogen production. Section 4.2 presents literature on the stochasticity of wind speed and power generation. This section aims to further investigate how wind power stochasticity can be integrated to the optimization problem presented in Falk and Hansen (2022). The main components of the energy system presented in Chapter 3 by Falk and Hansen (2022) are reviewed Section 4.3. Literature on power markets and electricity markets and electricity price forecasting is presented in Section 4.4. The literature review is presented as a synthesis in Section 4.5, followed by an overview on the research contribution of this thesis in Section 4.6.

4.1 Short-term Optimization of Offshore Hydrogen Production with Stochastic Power Generation Literature

This section provides a study of relevant literature related to short-term optimization of offshore hydrogen production with stochastic power generation. The search procedure is described in Section 4.1.1. In Section 4.1.2, offshore and onshore hydrogen production is studied, and the reviewed articles covers both both short-term optimization and techno-economic assessments of energy systems with hydrogen production. Section 4.1.3 presents a summary of relevant literature for short-term optimization of hydrogen production. The previous research in this field is highlighted and the thesis is positioned in the existing literature. Section 4.1.4 gives a further description of hydrogen production and stochastic power production.

4.1.1 Search Procedure

The strategy employed to gather and identify relevant literature on offshore energy systems with hydrogen production was a combination of approaches. It involved conducting a structured search in Scopus, along with a targeted keyword search in ScienceDirect and ResearchGate. The initial search in Scopus using the keywords "offshore," "energy," "system," "hydrogen," and "production" yielded a total of 179 papers. To refine the search, filters were applied, including limiting the Subject Area to "Energy" (resulting in 113 papers), Document Type to "Articles" (66 papers), and Language to "English." This filtering process yielded 64 articles that met the search criteria. Considering the importance of recent works, the search was further narrowed down to articles published in 2021 and 2022, resulting in 35 articles. A preliminary evaluation of titles and abstracts led to the selection of the papers presented in the next section for further investigation. Additionally, another search in Scopus using the keywords "offshore" and "electrolysis" generated 245 papers. Applying filters for Subject Area ("Energy"), Document Type ("Articles"), and Language ("English") narrowed down the results to 133, 75, and 68 papers, respectively. Finally, focusing on articles published between 2021 and 2022, a total of 31 papers were identified. After a brief review of titles and abstracts, 6 articles were selected for further investigation. Furthermore, our review was supplemented by consulting papers from key institutions and other relevant libraries.

4.1.2 Review of Offshore Energy Systems with Hydrogen Production Literature

The cost competitiveness of hydrogen production has recently drawn attention in academic research. The cost of fossil-based hydrogen is currently estimated around 2 EUR/kg and renewable hydrogen is reported to achieve 2.5 - 5.5 EUR/kg, although this finding is not consistent for all system design configurations. However, technology for renewable hydrogen production is rapidly maturing and will soon reach economies of scale as renewable hydrogen is predicted to outperform fossil-based hydrogen in 2030. Several authors have made economic-assessments of investment cycles in renewable hydrogen production systems, although not necessarily in an offshore setting. One of the studied articles (Lucas et al., 2022) addresses the profitability of hydrogen with power market participation for two different wind farm capacities, namely 25.2 and 150 MW. The electrolyzers up-time is restricted to either daily or nightly operation, or both. When not profiting from electricity sales, hydrogen production becomes competitive to power sale at electricity prices below 31 EUR/MWh for the 150 MW farm under the second scenario. The authors found that high electricity prices and low wind power capacities turns out as infeasible in most cases, and that income from commercial sales of oxygen turns out significant.

Dinh et al. (2021) developed an analytical model for assessing the economic viability of hydrogen production from offshore wind farms using Net Present Value (NPV) and Discounted Payback Period (DPP). A case study of a 101.3 MW wind farm in the East Coast of Ireland is conducted, considering Proton Exchange Membrane (PEM) electrolysers and underground hydrogen storage. The model incorporates hourly calculations for wind power output, electrolysis plant size, and hydrogen production based on varying wind speeds, and is integrated with potential future hy-

drogen supply chains, in order to take advantage of economies of scale during the construction, maintenance, and operation phases. Their findings suggest that offshore hydrogen production is financially viable only if hydrogen prices exceed 5 EUR/kg. Moreover, the authors identified the optimal investment level in underground storage capacity to be between 2 and 7 days.

There is a growing interest in determining the most profitable offshore hydrogen production layouts, leading to research exploring the economic feasibility of different design proposals for power-to-hydrogen configurations. This includes analyzing the placement of electrolyzers on-shore, on energy hubs/islands, or integrated into towers, as well as studying energy flows in electrical networks in these scenarios. Jang et al. (2022) evaluate the NPV and conducts sensitivity and probabilistic analyses to evaluate the economic feasibility of three distinct arrangements for hydrogen production; distributed production with stand-alone electrolyzers positioned next to turbine towers with pipeline network transportation, centralized production on offshore platforms in vicinity of the turbines, and onshore production supplied from an offshore wind farm. Based on a 12-hour daily uptime on production, the net present value analysis demonstrates that at the lowest hydrogen price of 13 EUR/kg none of the arrangements are profitable. It is only at a hydrogen price of 14 EUR/kg that the distributed and centralized cases begin to generate profits, whereas the onshore case requires a higher hydrogen price than 16 EUR/kg to turn profitable. When there is no access to power markets, the distributed, centralized, and onshore arrangements have probabilities of 80.3%, 71.5%, and 34.35%, respectively, of generating a positive net present value when selling hydrogen at 14 EUR/kg.

In the same direction, Luo et al. (2022) conducted a techno-economic analysis of hydrogen production with slight modifications, but still similar to that of Jang et al. (2022). In the study, the distributed configuration involves sourcing incoming feed water from a pipeline connected to the mainland, and the centralized design transports liquid hydrogen in vessels instead of gas in a pipeline. In their research, the performance of alkaline electrolyzers, Proton Exchange Membrane Electrolyzers (PEMEL), and Solid Oxide Electrolysis Cells (SOEC) was compared, and the results highlighted the promising potential of PEMEL in offshore hydrogen production, given the recent technological improvement in electrolyzer components. The paper further explores transportation methods and proposes the use of submarine pipelines and vessels for liquid hydrogen transport. Taking into consideration the commercial sale of oxygen, the economic potential increases, aligning with the findings of Lucas et al. (2022). Their preliminary estimation does not however consider transportation and storage costs. Moreover, the authors propose that selling hydrogen can be a competitive choice compared to selling electricity without subsidies.

Despite the fact that the cost of transportation assets greatly affects the Levelized Cost of Hydrogen (LCOH) (IEA, 2019), previous studies, including those reviewed in this paper, did not explore the costs of storage and transportation. However, Franco et al. (2021) addressed this issue in a comprehensive techno-economic evaluation for hydrogen offloading pathways in offshore hydrogen production platforms. Investigated offloading paths included hydrogen gas, liquid hydrogen, ammonia, and liquid organic hydrogen carriers, for either ship or pipeline transportation, along with a baseline case of onshore hydrogen production. To assess the LCOH, the authors outlined two scenarios. The first scenario considered a modest reduction in investment costs and no major breakthroughs in technology. In contrast, the second scenario adopted an optimistic outlook on technology progression with implemented support schemes expected from European hydrogen strategies. Out of all the explored pathways the transportation of hydrogen through pipelines emerges as the most favorable choice. In the baseline scenario, it yields a levelized cost of hydrogen amounting to 5.35 EUR/kg, but with the effective implementation of EU support and the achievement of set targets, this cost has the potential to decrease significantly to 2.17 EUR/kg. Unless the distances exceed 150-250 km, the transportation of hydrogen carriers by vessels does not surpass the use of pipelines in terms of competitiveness. Among the studied vessel transportation pathways, the process of liquefying hydrogen proves to be the most cost-effective with a cost of 2.94 EUR/kgH2 in the best-case scenario. One of the notable conclusions drawn from this study similar to Lucas et al. (2022), is that the commercialization of oxygen can substantially enhance the economic viability of hydrogen production, even within the lowest price range.

Bonacina et al. (2022) explored offshore liquid hydrogen production for ship refueling as a case study on refueling stations in the Mediterranean Sea. The pre-feasibility study aims to identify the

optimal electrolysis capacity that achieves minimum payback times, excluding transportation costs and power market interactions. The study utilized hourly deterministic wind profiles with cut-in and cut-off wind speeds, obtained from a meteorological database and transformed them using a wind turbine power curve. On the platform, a PEM electrolyzer, a water demineralization unit, and a liquefaction plant for compression and storage are incorporated. The analysis investigates the dependencies of wind farm and hydrogen production plant capacities on the payback time and levelized cost of hydrogen, revealing key insights into their relationships. The research findings demonstrate a clear inverse relationship between wind capacities and the LCOH. By analyzing various simulations across a wide range of wind capacities, the authors consistently observed that the minimum LCOH occurred when electrolyzer capacities were set between 80-90 % of the total installed wind capacity.

Jiang et al. (2021) conducted a study to determine the optimal PEM electrolyzer capacity for an offshore energy system with hydrogen production. The authors considered several factors, including expected costs from electrolyzer replacements with an advanced electrolyzer model that considers ageing, probabilistic hydrogen prices, and wind forecasts. Notably, to avoid distortions in their NPV-assessments and overly optimistic results, the authors accounted for electrolyzer degradation from operations. Investment costs of submarine cables, electrolyzers, storage and transport vessels have been accounted for, including operational and maintenance costs. Information gap decision theory is adopted together with a chance-constraint formulation to account for irregular hydrogen prices, and solved using particle swarm optimization. When applied to a case study of a 405 MW wind farm, the optimal electrolyzer capacity was found to be 336 MW, which aligns with the conclusions of Bonacina et al. (2022). The authors also observed that the NPV of offshore projects with hydrogen production are very sensitive to fluctuations in hydrogen prices. A minor deviation in the price could result in changes in the NPV by 10 – 40 %.

A comparison between SOEC and PEM electrolyzers is also conducted by Meier (2014), although under different circumstances. As the North Sea is widely regarded as the focal point of offshore hydrogen production in Europe, Meier (2014) evaluated Norway's role to capitalize on the country's offshore wind resource potentials, and leverage its emission reduction targets by producing hydrogen for the transportation sector. The case study indicates that the current costs of large-scale production and the comparison of hydrogen with prevailing fuel prices render offshore hydrogen production unprofitable. Neglecting transportation costs it is still not economically feasible for the system. The production costs of hydrogen using SOEC and PEM technologies coupled to a 100 mW wind farm were investigated under two different scenarios depicting a worst and best case scenario for wind power availability. In the conservative estimate, the annual wind power production is 258 GWh/year. The optimistic scenario assumes 404 GWh of production annually. This corresponds to hydrogen production amounts of 1530 and 8020 tons/year, respectively. Profitability is strongly influenced by several factors and design parameters should be carefully evaluated for large-scale production. Proves as concept development assistance and further research on this topic. When evaluating its cost-competitiveness, this study demonstrated that the current technology and market fuel prices on hydrogen substitutes do not achieve profitability, yet. The prices of hydrogen varied between 5.20 EUR/kg and 106.10 EUR/kg.

4.1.3 Review of Short-term Optimization of Hydrogen Production Literature

While the initial articles have extensively investigated system design parameters, which has been critical in order to develop an integrated system and provide a comprehensive understanding of system behavior, existing literature have primarily focused on economic assessments. Some of the reviewed articles so far have employed simplified representations of system components and wind power generation over the assessment period, which allows for aggregating system behavior over long horizons, usually spanning several years and without consideration for power market commitments in cases where power markets are modeled. Consequently, they do not propose specific solutions for short-term planning. In the following paragraphs, we will explore another segment of the literature comprising articles that have developed optimization models and commitment problems, and later developed suitable energy system planning algorithms to solve them. To provide

an overview of this section of the literature, the subsequent paragraphs delve into studies that specifically focus on relatively short-term models of energy systems with hydrogen production.

A Model Predictive Control (MPC) scheme was developed by Abdelghany et al. (2021) to optimize the switching operations of electrolyzers and fuel cells in grid-connected wind farms for non-renewable hydrogen production. Their model minimizes switching and cyclic degradation while meeting hydrogen demand and maximizing revenues from hydrogen and power sales. To accurately capture the system dynamics, a mixed-logic dynamic framework was employed to model electrolyzers and fuel cells, enabling different operational modes such as on, off, and standby. The focus was on minimizing unnecessary commutation cycles and preserving the electrolyzers' integrity with a higher level of accuracy compared to alternative methods. This study was conducted as part of the Haeolus project (Andrenacci et al., n.d.). By adopting a receding horizon strategy to update the wind forecast, an optimal control sequence for the electrolyzers was determined. The optimization problem was effectively solved within a 40-second time frame for each time step. However, the model is solved deterministic with wind power production forecasts updated for every time step, and without electricity market obligations, and a single 3 MW unit electrolyzer. Shortly after, the authors expanded their model (Abdelghany et al., 2022) by incorporating both low-level and high-level predictive control, utilizing shorter and longer timescales, respectively, while maintaining the same underlying logic. This enhancement resulted in a notable reduction in operational costs by 5%. The authors assert that their model can be applied to any hydrogen storage facility, provided that meeting the hydrogen demand remains the utmost priority.

Carr et al. (2016) conducted an optimization study on hydrogen refueling stations for vehicles in the UK, employing a rolling horizon approach. The switching policies of an electrolyzer with a capacity rating of 270 kW introduced a non-linear mixed integer programming model. The authors assumed perfect predictions for wind power generation, electricity prices, and hydrogen demand every half hour for the next 24 hours, which constituted the look-ahead period for each optimization routine. The overall planning horizon spanned 30 days, resulting in the solution of 1440 optimization problems using nonlinear solvers such as BONMIN and SCIP. To achieve their objectives, a multi-criteria objective function was developed to simultaneously maximize income, minimize costs from electricity sales and purchases, and minimize unmet hydrogen demand.

Grüger et al. (2019) developed an intelligent operating strategy of electrolyzers to optimize production costs and wind power utilization. Non-linear formulations of electrolyzer operation, compression and storage are modeled with piece-wise linear functions. Their model includes imperfect wind forecasts and intraday market access, where energy can be traded at an average price. However, contract fulfillment is not considered. A myopic optimization-simulation model is proposed that does not account for flexibility in hydrogen storage. Instead, their model investigates operational decisions in the current time step using heuristics. The implemented decisions are then simulated for 24 hours with a quarterly-hour resolution. The authors report that production costs are reduced by 9 percent with their approach and that wind energy utilization is increased by 19 percent. However, the study concluded that production was not profitable, as indicated by a LCOH of 16.125 EUR/kg.

Flamm et al. (2021) solved a deterministic receding horizon planning problem, with a focus on operational decisions made on a 1-minute time scale and a 4-hour look-ahead horizon. Their approach involved a two-stage strategy for modeling the operation of a single 100 kW unit PEM electrolyzer. In the first stage, an exact nonlinear representation was used to accurately model the electrolyzer's behavior, while a piece-wise linear approximation was employed for the subsequent stages. The electrolyzer model incorporated a detailed low-level control mechanism, enabling precise modeling of individual components. The study took into account various factors, including energy conversion efficiencies, thermal dynamics, and overload dynamics within the electrolyzer system. Through a high-level control formulation, the optimal power supply to the electrolyzer was computed. Hydrogen produced by the electrolyzer was stored in tanks, and power was sourced from both photovoltaic sources and the power grid. The problem was solved using a nonlinear solver, with a solution time of less than 1 second. However, it is important to note that the study did not consider the dynamics associated with startup and shutdown processes.

High wind power potentials are often located far from load centers. However, investments in grid

infrastructure are necessary in areas with limited remaining available capacity to accommodate additional power injections. Bødal and Korpås (2018) investigated the utilization of hydrogen production from stochastic wind power generation and hydro power in constrained power grids. They explore the role of hydrogen storage in supporting economically infeasible wind power projects that require significant power grid investments. The study employs a MILP model to optimize hydrogen dispatch using wind and hydro power within a defined geographical region in the north of Norway. A rolling horizon approach is adopted, evaluating operational decisions across 120 scenarios. The model penalizes power imports required to meet hydrogen demand and assesses the impact of uncertain wind power forecasts by comparing stochastic and deterministic solutions. The results demonstrate a 5.6% difference between the SS and the EEV, as well as a 37.6% difference between the PI solution and SS. The authors also investigate the effect of varying the number of scenarios and conclude the computational complexity increases without significant benefits with more than 27 scenarios.

The optimal control strategies for energy systems incorporating hydrogen storage and wind power generation were investigated by Schrotenboer et al. (2022). The researchers examined different power purchase agreement obligations in various scenarios, including unrestricted hydrogen gas sales and fixed demand policies with contractual obligations. Using backward dynamic programming, they solved a stochastic Markov decision process to determine an optimal conversion policy that maximizes profits from electricity and hydrogen operations. Their model includes operational decisions every day for the course of an entire year. A 4.5 MW wind turbine and 5 MW electrolyzer is modeled in their base case and the results demonstrated potential operational revenue gains of up to 51% through the incorporation of hydrogen storage units in renewable energy systems.

Author	Energy Source	Water Purification	Electrolyzis	Compression and Storage	Battery Energy Storage	Fuel Cell	Hydrogen Transportation
Lucas et al. (2021)	Offshore Wind Farm	Electrolyser Integrated	PEM	Compressed Gas			Pipeline
Dinh et al.(2020)	Offshore Wind Farm	Unspecified	PEM	Compressed Gas			Vessel
Jang et al. (2022)	Offshore Wind Farm		PEM	Compressed Gas			Pipeline
Luo et al. (2022)	Offshore Wind Farm		Alkaline, PEM, SOEC				
Franco et al. (2021)	Offshore Wind Farm	Unspecified	PEM	Multiple Technologies			Multiple Technologies
Bonacina et al. (2021)	Offshore Wind Farm	RO	PEM	Liquid Hydrogen			Vessel
Jiang et al. (2021)	Offshore Wind Farm		PEM	Compressed Gas			Vessel
Meier (2014)	Offshore Wind Farm	MSF	PEM, SOEC	Compressed Gas			Pipeline
Abdelghany et al. (2021)	Onshore Wind Farm		Unspecified	Compressed Gas		Yes	
Carr et al. (2016)	Onshore Wind Farm		PEM	Compressed Gas			
Gruger et al. (2018	Onshore Wind Farm		Alkaline	Compressed Gas			
Flamm et al. (2020)	Photovoltaic		PEM	Compressed Gas			
Bødal & Korpås (2018)	Offshore Wind Farm, Hydro		Unspecified	Compressed Gas			
Schrotenboer et al. (2022)	Offshore Wind Farm		Unspecified	Compressed Gas		Yes	
This work	Offshore Wind Farm	MSF	PEM	Compressed Gas	Lithium-ion	Yes	Pipeline

Figure 4.1: Comparison of energy system design to other research articles

Author	Hydrogen Demand	Electricity Markets	Power Purchase Agreements	Deterministic vs. Stochastic	Linear vs. Non-Linear Modeling	Planning Horizon	Time Granularity	Planning Model	Model Type	Solution Approach
Lucas et al. (2021)		Unspecified, Certain Prices		Deterministic		Years	Daily	Techno-economic Assessment	Economic Model	
Dinh et al.(2020)						Years		Techno-economic Assessment	Economic Model	
Jang et al. (2022)						Years	Yearly	Techno-economic Assessment	Economic Model	
Luo et al. (2022)						Unspecified		Techno-economic Assessment	Economic Model	
Franco et al. (2021)						Years	Yearly	Techno-economic Assessment	Economic Model	
Bonacina et al. (2021)	Yes			Deterministic	Non-linear	Yearly	Hourly	Techno-economic Assessment	Economic Model	
Jiang et al. (2021)				Stochastic	Non-linear	Years	1 Hour	Techno-economic Assessment	Chance Constrained Programming, Information Gap Theory	Particle Swarm Optimization With Stochastic Simulation
Meier (2014)				Deterministic		Years		Techno-economic Assessment	Economic Model	
Abdelghany et al. (2021)	Yes	Unspecified, Certain Prices		Determinstc	Linear	1 Day	Hourly	Operational Planning	Multi-level model predictive control	Receding Horizon, Simulation
Carr et al. (2016)	Yes	Unspecified Certain Prices			Non-linear	24 Hour Forecast, 30 Days Planning	30 Min	Operational Planning	Multi-Criteria Optimization	Rolling Horizon
Gruger et al. (2018	Yes	Intraday, Uncertain Prices		Stochastic	Linear	24 Hour Forecast, 1 Year Simulation	15 Min	Operational Planning	MILP	Heuristics, Simulation
Flamm et al. (2020)	Yes	Intraday, Certain Prices		Deterministic	Linear	4 Hour Forecast	1 Min	Operational Planning	MILP	Receeding Horizon
Bødal & Korpås (2018)	Yes	Unspecified, Certain Prices		Stochastic	Linear	1 Day	Hourly	Operational Planning	MILP	Rolling Horizion, Simulation
Schrotenboer et al. (2022)	Yes	Intraday Uncertain Prices	Yes	Stochastic	Non-linear	Monthly, Yearly	Hourly, Daily	Tactical Planning	Markov Decision Process	Backwards Dynamic Programming
This work		Day-ahead, Intraday, Uncertain Prices	Yes	Stochastic	Linear	36h Forecast, 36 Hours Planning	15 Min	Operational Planning	MILP	Rolling Horizon

Figure 4.2: Comparison of modeling aspects and solution techniques to other research articles

4.1.4 Hydrogen Production and Stochastic Power Generation Literature

From the 15 articles that were thoroughly studied in the master's project only a few included stochastic modelling. Jiang et al. (2021) used the Weibull distribution to account for probabilistic wind power production. However, it appears that scenarios have not been used to account for stochastic wind power production, but that the Weibull distribution has been used to generate data instead of creating possible future scenarios. Schrotenboer et al. (2022) also used the Weibull distribution, but similarly to the previous article did not use the distribution to generate forecasts or future scenarios but rather to generate data for the optimization problem's current periods. Thus, their model does not take into account future development of wind speeds. Also, the time step in the article was an entire day, not a quarter of an hour. Grüger et al. (2019) used historical data as well as imperfect forecasts from a real wind farm for their simulation model, but have not given a description as to how the inherent stochasticity of wind power has been accounted for in the imperfect forecasts.

Zhang et al. (2019) studied power-to-hydrogen-to-power versus lithium batteries for reduction in imbalance costs for grid-connected wind farms. The authors quantified wind power stochasticity with probability density functions of wind forecasting error. The statistical power-generation distribution is coupled together with installed capacities as to maximize NPV for a range of uncertain parameters described through a scenario sampling method and for statistical distributions of electricity.

Bødal and Korpås (2018) generated wind scenarios with the use of meteorological weather forecasts and historic wind power production. Future scenarios were sampled from a quantile forecast according to the method presented by Pinson et al. (2009). The quantile forecast was found through a local quantile regression algorithm, a method presented by Bremnes (2006). The two last-mentioned works were closely related to optimize operations of wind power farms for profit maximization of intermittent power production and power markets. Thus, it is natural to study how this research field has dealt with wind power forecasting and how this can be adopted into the model of this thesis.

4.2 Wind Power Stochasticity Literature

Stochastic wind power production is arguably the single most important contributor for the stochasticity of the optimization problem. The path from historical wind data and wind scenarios often consists of several steps. This section highlights the key steps made in this thesis in order to generate wind scenarios for the studied optimization problem. The search procedure to find literature on wind forecasting and scenario generation is described in Section 4.2.1. Forecasting methods for wind power production are reviewed in Section 4.2.2.

4.2.1 Search Procedure

There are mainly two types of research articles that have been reviewed. The first type is articles that focus on stochastic short-term optimization of hydrogen production, where the stochasticity related to variable wind power has been dealt with. Such articles are relatively close to the core of this thesis and have been studied in Section 4.1.3. The second type of articles are those where the main focus is on forecasting and/or scenario generation, both for wind power specifically and in more general terms. These articles are often related to optimization of power systems with wind power production. The search procedure has consisted of several steps. As a first step, articles on short-term optimization of hydrogen production were reviewed in order to study the method chosen by other authors within the field of operation research. The second step consisted of a strategic search on Google Scholar on forecasting methods for wind.

4.2.2 Review of Wind Power Forecasting and Stochasticity Literature

The path from historical wind data, as previously mentioned, to wind scenarios can be a process that consists of several steps. This process naturally depends on several factors. One important factor is to what extent the user has available data. The very least the user must have is historical data but sometimes the user has forecasts, as seen in Section 4.1.4. A user that does not have forecasts must either acquire it from a third-party or generate it themselves. Another important factor is if it suffices with a single forecast, often referred to as a point forecast, or if several forecasts depicting multiple possible values is needed for the optimization problem. For instance, for more robust optimization problems it could be necessary with a 90 % percentile forecast in order to get the desired robustness in the solution. The next important factor is if the user wants to generate scenarios instead of having forecasts in order to simulate more realistic power production outcomes. This section reviews various literature on these steps.

Deterministic Forecasting

There exists numerous methods to create deterministic forecasts, often referred to as point forecasts. Point forecasts only provide the user with one value for each time period and does not necessarily provide the user with information about the associated error. Hanifi et al. (2020) performed a detailed review of the state-of-the-art forecasting methods of wind power. There are three main categories of wind forecasting methods: physical, statistical and hybrid methods. Physical methods such as meteorological forecasts have been mostly used in the past, but in recent years the use of time-series and nonlinear machine learning models has increased. Hanifi et al. (2020) report that physical methods require more computational resources compared statistical methods. Physical methods are most suitable for medium (6 to 24 hours) to long-term (24 hours to a month) forecasting. Statistical methods such as time-series and artificial intelligence models have a better performance on short (0.5 to 6 hours) and medium-term forecasts. Furthermore, hybrid models are encouraged as to capitalize on the different strengths of the methods in order to achieve the best possible forecasts.

This thesis considers a 36-hour time horizon, and Hanifi et al. (2020) recommends the use of hybrid methods for this forecasting length. However, more complex forecasting method could cause an increase in computational time and decrease the time budget to find optimal solutions for optimization problems. Thus, the choice of forecasting methods could incur an overall loss to the optimization problem as optimal solutions are potentially not found. Hanifi et al. (2020) also emphasize the need to develop forecasting methods specifically for offshore wind prediction. This is due to different weather and operating conditions for onshore and offshore wind farms. Moreover, the main goal of the thesis is to short-term optimize production and not produce the best possible wind forecasts. Time series models are generally easier to implement compared to nonlinear machine learning models and have a lower computational burden, and can be used in the short-term forecasting to bridge the informational voids despite ignoring nonlinear trends in wind speed series (Yang et al., 2021).

Uncertainty Forecasting

Yang et al. (2021) studied uncertainty forecasting in their review of wind forecasting technologies. The authors divided uncertainty forecasting into risk index forecasting, probabilistic forecasting and scenario forecasting. Probabilistic forecasting consists of parametric and non-parametric methods. The former assumes a probability distribution for the studied variable, while the latter makes no assumptions on distributions and therefore based on empirical observations in its entirety. Scenario forecasting can convey information about forecasting uncertainty through the description of an ensemble of possible multi-period wind power realizations. The optimization problem in this thesis is formulated as a MILP accompanied by a scenario optimization approach in order to capture stochasticity. Scenario forecasting presents itself as the most viable option to keep the optimization problem linearly formulated. Yang et al. (2021) provide several examples of scenario-generation techniques, and this thesis adopts the method developed by Pinson et al. (2009). Pinson et al.

(2009) developed a method to produce wind power scenarios from quantile forecasts and historical values. Historical wind power data and historical forecasts are used as in a quantile regression model in order to arrive at an empirical distribution of prediction error related to forecasted wind power. The prediction errors are used to create a multivariate Gaussian random variable that is described by a covariance matrix. The covariance matrix is recursively updated with historical realizations of wind power and is in combination with quantile forecasts used to generate scenarios.

The scenario generation method chosen in this thesis requires quantile forecasts, perhaps more commonly known as quantile regression forecasts. Quantile regression is a nonparametric method to study the relationship between a response variable y and one or several predictor variables x. The relationship between response and predictor variables is described by regression parameters, originally referred to as estimators. These parameters are determined by minimization of empirical errors (Koenker & Bassett, 1978). Furthermore, quantile regression can be used to study forecast error. Prediction intervals can be created by fitting empirical forecast errors to realized values (Taylor & Bunn, 1999). Thus, historically registered data and historically forecasted values are required in order to determine the regression parameters to be used in future quantile forecasts. Koenker and Bassett (1978) formulated the quantile regression method as a minimization problem of the residuals in a dataset, demonstrated by Equation (4.1) where β is the estimator and θ is the quantile.

$$\underset{\beta \in \mathbb{R}}{\text{minimize}} \quad \left[\sum_{t \in \{t: y_t \geq x_t \beta\}} \theta \left| y_t - x_t \beta \right| + \sum_{t \in \{t: y_t < x_t \beta\}} (1 - \theta) \left| y_t - x_t \beta \right| \right] \tag{4.1}$$

Quantile regression is often modelled with a linear relation between response and predictor variables. This could be problematic as there might be a higher order polynomial relationship between input and output in a quantile regression model. Bremnes (2004) implemented a local quantile regression method to create probabilistic wind power forecasts for a wind farm based on Numerical Weather Prediction (NWP) point forecasts. The author argues that a simple polynomial could not necessarily describe the relation between response and predictor variables. Local quantile regression is a variant of quantile regression that uses weights to increase the mutual impact of data points with similar values on each other. Bremnes (2006) followed up this work with a comparison of the local quantile regression method to two other statistical methods, the Nadaraya-Watson estimator and a local Gaussian model, to estimate quantiles. None of the statistical methods in the study had a stand-out performance. He and Li (2018) constructed prediction intervals of wind power using a quantile regression neural network model combined with Epanechnikov kernel function and Unbiased cross-validation. Furthermore, the experiments conducted in the study revealed that the method was could construct prediction intervals and probability density curves with high accuracy.

Nielsen et al. (2006) also used quantile forecasts to account for the uncertainty of wind power forecasts. The forecasting horizon extended from 18 to 36 hours and meteorological forecasts from a prediction tool called WPPT were used as data. Thus, this article does not estimate quantile forecasts on period from 0 to 18 hours. The authors used basis spline functions instead of a local quantile regression in order to account for nonlinearities in the quantile regression model. Zarnani et al. (2019) found that quantile regression models outperformed clustering-based models in the estimation of prediction intervals for NWP models. More specifically, the spline-based quantile regression model had the highest performance compared to clustering-based models and other quantile regression models such as local quantile regression, kernel quantile regression and nonlinear quantile regression. The method presented by Nielsen et al. (2006) was also used by Møller et al. (2008) and Pinson et al. (2009). Furthermore, Møller et al. (2008) developed a time-adaptive quantile regression method based on the simplex method.

4.3 Technologies for Offshore Hydrogen Production Literature

In order to produce hydrogen offshore, several technical components are required. Due to technological advancements in recent years, a literature review of the core components facilitating renewable hydrogen production and their state-of-the-art technologies has been conducted. The selection and integration of system components is based on academic articles and meetings with industry experts conducted in the fall of 2022. The search procedure is briefly explained in Section 4.3.1, and reviews of the system components are presented in Section 4.3.2.

4.3.1 Search Procedure

The evaluation of state-of-the-art technologies integrated into a system necessitates an assessment of their feasibility for real-world application. Prioritizing high performance and reliability is imperative in this regard. Several reviewed research articles investigate the performance of pertinent component technologies in their feasibility studies. Additionally, Fragiacomo and Genovese (2020) provided a valuable foundation for scrutinizing the efficacy and characteristics of the fundamental components. Seeking guidance from industry experts also proved useful in identifying suitable technologies for the system. For each component outlined in Section 3.2, a targeted search was conducted on Google Scholar using unique keywords for the component and the process, such as "name of the component" AND "hydrogen" AND "efficiency" OR "performance" OR "energy consumption". Given the swift advancements in the state-of-the-art technologies, attention has been given to latest research. Furthermore, an essential avenue for relevant literature involved studying the sources cited in the articles examined in Section 4.1.2 and 4.1.3.

4.3.2 Review of Technologies for Offshore Hydrogen Production Literature

Desalination

The objective of this section is to determine the candidate solution that can provide the required feed water quality for PEMEL-electrolyzers. Desalination is the process of removing mineral solvents from saline water through a chemical process. This is accomplished by splitting the incoming streamflow into two streams: a stream of high-quality water, known as the permeate, and a stream of highly saline water, known as the concentrate, which should be properly disposed of to avoid harm to marine environments. The dominant technologies for commercialized desalination of large-scale sea water are Reverse Osmosis (RO) and Multi-Stage Flash Distillation (MSF), (Mehrjerdi, 2020; Wittholz et al., 2008), with Multi Effect Distillation (MED) included by some (Ghaffour et al., 2013; Raluy et al., 2006). RO, as the name suggests, is the reversed process of osmosis where two fluids of different salinities would mix due to equilibrium forces. Applying sufficient mechanical pressure, a semi-permable membrane can reversely separate the fluids of different salinities (Stoughton, 2018). 80 % of the global desalination capacity is based on RO and todays commercialized RO systems achieves total dissolved solids up to 99,8% (Stoughton, 2018), lower energy consumptions and higher efficiencies than the thermal based MSF and MED processes (Aladwani et al., 2021; Ghaffour et al., 2013). The thermal based systems MSF and MED instead use forced circulation to evaporate saline water in a process comprising several stages at different temperature and pressure levels, using the energy from an electric boiler. Condensate is then collected in every stage. According to Ghaffour et al. (2013), the advanced technology has the potential to not only surpass MSF and RO in terms of cost but also deliver significantly higher quality permeate.

All state-of-the-art technologies have undergone extensive research and development in efforts to reduce costs. Only the most reliable state-of-the-art technology that produces the acceptable quality levels will suffice, as the PEMEL operates on dionized water with total dissolved solvent ratings

below 0,5 parts per million parts of water (Ghaffour et al., 2013; NEL ASA, 2022). Commercialized RO systems cannot in reality achieve the acceptable quality levels due to physical properties of membranes independent on how much pressure that is applied, in addition to issues with membrane degradation and refueling of chemicals (Al-Mutaz & Ghunaimi, 2001). Although MSF and MED are more expensive in terms of capital investments and operational expenses, the thermal processes perform significantly better with respect to water quality and is the preferred technology for large-scale sea water desalination (Europe, 2022).

Electrolysis

The fundamental process of hydrogen production resides in electrolysis. Several production techniques exist, however stringent regulations would classify any technique involving fossil-fuels as non-renewable and thus non-applicable to the system. Electrolysis, thermolysis and photolysis, are renewable production methods, but as neither heat nor photons but electricity is the input energy to the process, electrolysis is the only viable option (Nikolaidis & Poullikkas, 2017). Electrolysis is incomparably energy-intensive to the other processes on the platform and utilize electric potentials to split a water molecule into hydrogen and oxygen, producing heat in the process. When the electricity is produced by renewable energies, the hydrogen is the cleanest energy carrier available since hydrogen-fueled combustion processes only have water vapor as exhaust (Felseghi et al., 2019). Various electrolyzers exist, differing in size, power ratings, and thermodynamic properties, and it is important to select the appropriate technology for the energy system. Not all electrolyzers are designed to operate on saline water; they have specific water requirements. When evaluating water quality, the standard parameter is particles per million, and since sea water has an average salinity of around 35,000 particles per million parts of water, desalination becomes an indispensable step for offshore hydrogen production.

Among the state-of-the-art electrolyzer technologies available today, two noteworthy ones are alkaline electrolyzers and the more recent PEMEL (Chi & Yu, 2018). Alkaline electrolysis paved the way as the first widely implemented large-scale method, while PEMEL has gained traction in the commercial market in recent years. SOEC, a high-temperature water electrolysis technique, presents a promising and relatively new method for hydrogen production that is still in the process of being fully commercialized. Unfortunately, the operational temperature range of SOEC, which typically ranges from 500 to 1000 °C, poses challenges for its suitability in offshore applications. In an offshore setting, limited resources to manage unforeseen events that could cause production interruptions imposes a stringent tolerance for operational risks as maintenance could require longer lead times. In numerous research papers focusing on energy systems with variable power input, PEMEL has been utilized to provide the necessary flexibility (Abdelghany et al., 2021; Durakovic et al., 2023; Jiang et al., 2021). Additionally, Schiebahn et al. (2015) emphasizes the importance of highly dynamic electrolyzers in power-to-gas applications with variable power. A highly dynamic behavior can be identified by excellent performance in terms of start-up time and ramping times. Furthermore, maintaining low energy consumption in stand-by mode requires is also of importance. In terms of coupling with variable renewable energy sources, PEMEL demonstrates a significant advantage over other electrolysis technologies (Andrenacci et al., n.d.). Cockerill (2020) highlights the valuable benefits of PEMEL, including a broad dynamic operating range and rapid response times for ramp-up and ramp-down capabilities. Apart from its operational benefits, PEMEL is also characterized by its compact size, which makes it the preferred choice in situations where space is limited, as is the case in the proposed system. In recent years, there has been a gradual commercialization of PEMEL, with several electrolyzer suppliers now offering this technology. This indicates that there is an expectation for additional commercialization in the foreseeable future. (Andrenacci et al., n.d.) have identified a decrease in capital expenditures and improved efficiency by 2030, surpassing the present-day standards.

Most of the research papers on hydrogen production adopt the assumption of a constant efficiency for the electrolyzer. This assumption involves calculating the energy requirement for 1 kg of hydrogen by dividing the higher heating value of hydrogen by the specific energy consumption of the process. Jiang et al. (2021) have shown that the efficiency of PEMEL is influenced by both current density and operational time. This indicates that the efficiency of the electrolyzer is

dependent on the amount of energy supplied to it. The decline in membrane conductivity due to aging accounts for the latter aspect, indicating that the assumption of constant efficiency is not adequately precise for an operational model. In Figure A.1 in the Appendix, it can be observed that as the power input increases, the efficiency decreases. Furthermore, the efficiency curve exhibits non-linearity, and it also declines with the lifetime of the electrolyzer, as indicated by Figure A.2, which illustrates the impact of decreasing electrolyzer efficiency on hydrogen output.

Storage, Compression and Transportation

Hydrogen gas produced by electrolyzers at low pressures needs to be compressed to achieve higher volumetric density. One key disadvantage of hydrogen is its low energy density per unit volume. Therefore, it is important to assess storage options, particularly high pressure, or liquid storage, as these methods can increase the volumetric energy density. However, it is important to consider that achieving such density may require a significant amount of energy. Thus, it is required to evaluate compression, storage, and transport as interrelated. The compressor technology must align with the maximum pressure ratings of the fluid state. Although several compressor technologies are available, each designed for different requirements, research highlights stationary storage methods or gas pipelines for offloading hydrogen (Dinh et al., 2021; Lucas et al., 2022; Meier, 2014). Compared to above-ground storage methods, Dinh et al. (2021) advocates gaseous underground storage for large-scale capacities and lower operational risks. Meier (2014) adopted a hydrogen pipeline as the preferred method over 100 MW. Other solutions include storing hydrogen in a liquid state or energy dense molecules, like ammonia, methylcyclohexane and organic hydrogen carriers. According to (Wijayanta et al., 2019), liquefied hydrogen can become a competitive and effective long-term solution given a strong market demand for hydrogen. However, this represents a more expensive solution as the supply cost can increase by 50 – 150 % when transportation method and distance are included. Concerns about the safety risks associated with offshore liquefaction of hydrogen were also raised by industry (Moreld, personal communication, October 19, 2022). Brändle et al. (2021) argue that pipeline transportation offers superior economic benefits and serves as a foundation for the development of a large-scale hydrogen market. Franco et al. (2021) studied various offloading solutions for hydrogen and their findings promote pipeline as the economic viable option. However, other storage and transportation methods than pipelines become relevant where pipelines are infeasible (Elberry et al., 2021). Nevertheless, the North Sea already has an extensive natural gas pipeline network. In cases where existing pipelines can be retrofitted costs can be significantly reduced.

According to Sheffield et al. (2014), pipelines generally operate within the range of 10-12 bar, with the potential to reach pressures as high as 100 bar. Representatives from Moreld (personal communication, October 19, 2022) stated that offshore transport pipelines could be designed to operate within the pressure range of 40 to 60 bar. As a result, it is not essential for compressors to achieve exceptionally high pressures; instead, their main role is to compress large quantities of hydrogen at lower pressure levels. The compressor's SEC is outlined by Fragiacomo and Genovese (2020) in Equation (4.2), while Martín and Luceño (2022) establish Equation (4.3) to calculate the SEC based on the cumulative work required for multi-stage compression.

$$e = \frac{E}{m} = \frac{RT}{\eta^C}\left[\left(\frac{p_{out}}{p_{in}}\right)^{\frac{n-1}{n}} - 1\right], \tag{4.2}$$

$$e_{total} = \frac{E_{total}}{m} = N\frac{RT}{(n-1)\eta^C}\left[\left(\frac{p_{out}}{p_{in}}\right)^{\frac{n-1}{n}\frac{1}{N}} - 1\right]. \tag{4.3}$$

where m is the mass flow, R is the gas constant of hydrogen, C is the compressor efficiency, p_{out} is the compressor output pressure, p_{in} is the compressor input pressure, n is the polytropic coefficient, N is the number of stages and T is the compressor temperature. The SEC of compression is evidently characterized by nonlinearity.

An analysis conducted by Witkowski et al. (2017) recommended the integration of multi-stage centrifugal and two-stage reciprocating compressors with large mass flow to accommodate high mass flows for effective transportation in pipelines. One type of compressors that can achieve the technical requirements is large-scale centrifugal compressors (Tsiklios et al., 2022). Tsiklios et al. (2022) also discuss the relationship between pressure losses and transmission distance, which can require re-compression at intervals of 100 to 600 km. In a study conducted by Kaiser et al. (2022), a pipeline spanning 2800 km was modeled to facilitate the transfer of 77 TWh of energy per year. The pipeline was designed to operate at a nominal pressure of 100 bar, with pressure losses of 0.1 bar per km and leakage losses of 0.5%. To compensate for these losses, recompression stations were strategically placed at intervals of 500 km. In a separate case study, Khan et al. (2021) considered a 1500 km long pipeline with an inlet pressure of 70 bar, outlet pressure of 28 bar, and recompression stations positioned every 500 km. As centrifugal compressors are currently under development (Khan et al., 2021), their study modeled instead 7 reciprocating compressors, each of 16 MW capacity which is able to compress 4311 tons per day, or 50 kg/s.

Battery

Intermittent power generation is a challenge for renewable hydrogen, as it can lead to a discontinuation in the production. To address this issue, a Battery Energy Storage System (BESS) is a promising technology for storing large amounts of electrical energy (Lebedeva, 2018). Recent research by Woznicki et al. (2020) also found that linking a non-grid-connected offshore wind farm to a BESS results in the most cost-effective production of renewable hydrogen. More specifically, lithium-ion batteries are regarded as the most promising technology for supporting offshore hydrogen production (Arendals Fossekompani, personal communication, 25.10.2022). Lithium-ion batteries are widely adopted in energy-intensive industries that take advantage of BESS, as they offer higher energy densities and lower weights, making them suitable for responsive applications with high cyclability. A BESS can provide power to prevent sudden interruptions in hydrogen production during periods with significant wind power variability. In addition, at least in theory, a BESS system would be able to support power market deliveries to avoid contract breaches. It is worth noting that a BESS cannot replace wind as an energy source over extended time periods, which would be techno-economical infeasible. In this thesis, lithium-ion batteries can provide delivery support to power market commitments, if necessary, and provide energy to avoid electrolyzer shutdowns. A BESS comprises various components, such as battery units, control and power conditioning systems, safety mechanisms, and interfaces.

When selecting the most appropriate BESS, key properties of interest are energy capacity, charge- and discharge capacities, state of charge, C-rating, number of charge-discharge cycles, and depth of discharge. The state of charge of a battery is considered 100% when it is fully charged, while a 0% state of charge indicates complete discharge. The battery's C-rating indicates how much of the energy's capacity that can be discharged during a specific time duration (POWER SONIC, n.d.). A C rating of 1 means that the battery can be charged and discharged in 1 hour, while a C rating of 4 would imply that the battery can fully charge and discharge in 15 minutes. Maintaining the battery's state of charge within the range of 20% to 80% is critical to prevent battery degradation over time (Arendal Fossekompani, personal communication, October 10, 2022). The number of charge-discharge cycles also strongly affects a battery's state of health, with its depth of discharge playing a crucial role in battery performance degradation over time (Bordin et al., 2017).

Fuel Cells

The integration of fuel cells within the hydrogen energy systems enables power-to-gas and gas-to-power conversions, providing operational flexibility. This flexibility within hydrogen energy systems proves advantageous when there is a requirement to convert the produced hydrogen back into electricity. This need arises when the wind power producer's power market commitments exceed the available output from the wind farm. When power production is low, it may also be necessary to shut down some or all of the electrolyzers, resulting in additional costs for shutdown and startup. However, the incorporation of fuel cells can, in theory, prevent the necessity of shutting

down production if the drop in production is only for a momentary timeframe. Multiple fuel cell technologies have been developed, showcasing different degrees of technological advancements and commercialization. Proton Exchange Membrane Fuel Cells (PEMFC) and Alkaline Fuel Cells (AFC) have several similar characteristics. Unlike other fuel cell technologies, AFC and PEMFC offer rapid start-up and ramping times. This dynamic behavior makes them particularly suitable for energy systems that depend on variable energy availability. On the other hand, the other fuel cell technologies have slower response times and operate at higher temperatures. Given the safety considerations associated with offshore energy systems, it is unlikely that components with high operating temperatures would be integrated. As a result, PEMFC and AFC are the most suitable options in terms of dynamic behavior and operating temperature.

Just as with electrolyzers, different fuel cell technologies come with their own set of requirements and operating conditions. Practical implementations involve the use of auxiliary systems like pumps, ventilation, and instrumentation. It is crucial to assess the compatibility of these auxiliary systems within the offshore production context. The efficiency of hydrogen fuel cells is calculated by dividing the electric output energy by the energy content of the consumed hydrogen. The efficiency of PEMFC is non-linear and varies based on the operating conditions. Figure A.3 illustrates the relationship between the desired output current and the efficiency. Achieving high efficiency and high power output in hydrogen fuel cells involves a trade-off. According to sources such as PowerCellution (n.d.) and Ballard (n.d.), hydrogen fuel cells can reach a peak efficiency of 50% - 60%. Furthermore, the electrical output of fuel cells can be sustained indefinitely by continuously supplying fuel. The available research literature on hydrogen fuel cells does not provide a definitive verdict on whether PEMFC outperforms AFC. Nevertheless, industry experts and fuel cell manufacturers consistently advocate for PEMFC as the more favorable option. Notably, industry experts from Moreld (personal communication, October 19, 2022) express a distinct preference for PEMFC over AFC. Nel ASA advises the integration of PEMFC and PEMEL due to the observed synergies between the two technologies, as noted by Cockerill (2020). According to Ferchau (2019), PEMFC and Solid Oxide Fuel Cells (SOFC) are the two primary fuel cell technologies available today.

Power Transmission

There are power losses associated with the transmission of electricity from offshore to onshore, which depend on the chosen transmission mode. The available options are High Voltage Alternating Current (HVAC) and High Voltage Direct Current (HVDC). The total energy losses comprise constant losses caused by elements such as transformers and collection cables (Kucuksari et al., 2019), as well as variable losses primarily driven by line capacity and length. Research by May et al. (2016) demonstrated significantly lower power losses with HVDC configurations compared to HVAC over long distances. HVDC is considered the most suitable transmission mode for large-scale offshore power transmission (Rahman et al., 2021).

4.4 Power Markets and Electricity Price Forecasting Literature

Rapid deployment of wind power is essential for energy transition progression. However, the inherent volatility and unpredictable nature of high wind speeds not only introduce stability concerns within the power system but also present challenges for power producers in fulfilling their commitments within power markets (Karanfil & Li, 2017). Academic studies often adopt a simplified approach, restricting the analysis of models to a single market as observed by Heredia et al. (2018) and Finnah et al. (2022). While the inclusion of balancing and reserve markets is tempting, our analysis focuses specifically on the day ahead and intraday markets in order reduce modeling complexities. A wind power producer can find great benefit in the interplay between operations in both (Kraft et al., 2023) because wind is subject to forecasting errors (Narajewski & Ziel, 2020b). Typically, the optimization process begins with day-ahead scheduling to determine market commitments. Subsequently, intraday scheduling is utilized to enhance daily operational efficiency

and address any inaccuracies in the forecasts (Kraft et al., 2023) The markets are introduced in Subsection 4.4.1 and 4.4.2, and forecasting techniques are presented in Subsection 4.4.3.

4.4.1 The Day Ahead Market

The central scheduling mechanism for physical trade of electric energy in Europe is organized in day ahead auctions. As the name suggests, this process is conducted a day ahead of operation. Each market participant submits a set of price-volume bids to a power exchange for each load hour of the following day, typically at noon (Engmark et al., 2018). From the submitted demand and supply bids, an equilibrium is found by the marginal bid that determines a unique price-vector for each hour. The market clearing price, usually referred to as the system price, is announced to all market participants and their respective dispatch volumes after the matching algorithm is performed (Engmark et al., 2018). This market design analogies to day ahead markets across Europe and is common for deregulated electricity markets and not exclusive to the Nordic region.

4.4.2 The Intraday Market

Unexpected circumstances such as imperfect supply or demand predictions, outages, poor forecasts, or intentional non-compliance with market commitments for strategic purposes, can cause a discrepancy between anticipated and actual levels of production and consumption. In the intraday market participants are able to adjust their net position after day ahead market closure. The purpose of the intraday market is usually to improve financial performance and account for forecast errors (Kraft et al., 2023). The intraday market offers a valuable tool for generators and consumers to modify their pre-agreed quantities based on updated information. These markets are recognized as valuable for wind power generators, as the intermittent and unpredictability of wind power makes bidding challenging (Karanfil & Li, 2017) The process of intraday scheduling pertains to the immediate hours ahead aiming to arrange for the current or imminently commencing hour (Weitzel & Glock, 2018). Usually the scope of the control horizon open for trading can span from the next hour to several hours ahead. However, Narajewski and Ziel (2020a) describe that most trades in the German intraday market are arranged a few hours before delivery, which is significant for the scheduling problem. Thus, the intraday market becomes highly relevant for close-to-realtime decisions.

4.4.3 Electricity Price Forecasting

Electricity prices are highly influenced by daily, weekly, and seasonal trends, which is why multivariate modeling frameworks are frequently found on this topic in the literature (Marcjasz, 2020). Not only is electricity price forecasting very complex, but modeling performance is also dependent on the origin of data. This field of literature distinguishes between so called first-class models, which constructs 24 separate models for each individual hour, and second-class models that produce a single model for 24 hours ahead prediction as one time series (Ziel, 2016). The motivation of the former technique is that when prices are announced simultaneously, this approach becomes intuitive at a first glance. The more advanced methods belonging to the second-class are enriched with regressors such as long-term trends, public holidays, non-linear effects (price spikes), fundamental regressors, time-varying time of the week effects, but more importantly, time-varying cross hour-dependencies (Ziel, 2016) For instance, as the renewable share increases in the energy mix, the electricity prices tend to decrease. Another example is the strong hourly correlation between electricity prices in the late evening (22:00 – 00:00) on day *D-1* and early morning (00:00-03:00) on day *D+1*. This dependency is much stronger than the correlation between prices on the same hour for consecutive days (Ziel, 2016). The forecasting techniques in the second-class includes various types of time-series, but the majority of machine-learning models are found in this category. Both approaches are relevant in the forecasting literature and the application depends on the model design. However, as the number of regressors increases the potential of capturing dependencies, at least in theory, it also increases the risk of overfitting the model. In those cases, the least shrinkage

and selection operator can be used to automatically extract significant explanatory variables (Marcjasz, 2020). On the contrary, models based on empirical testing and expert knowledge, usually referred to as expert models, provides simple autoregressive structures with a fixed set of parameters. The obvious advantage of these models lies in their simple interpretation and implementation, with negligible overfitting complications. Even though this approach might involve less accuracy, this type of pricing behavior has been extensively studied and is widely acknowledged in the field of price prediction literature (Finnah et al., 2022).

4.5 Synthesis of the Literature Review

The existing literature on offshore energy systems with hydrogen production reveals a predominant focus on economic assessments and life cycle cost evaluations in terms of net present value and discounted payback time. As these studies are primarily economic assessments, system behavior tends to be aggregated and simplified in order to address system performance over long time horizons. Nonetheless, the literature favors centralized production in floating structures or turbine tower integrated solutions with pipeline storage, despite uncertainties in future technology and market prices. Shifting our attention to articles dedicated to operational planning programs, it becomes apparent that a number of authors opt for a rolling horizon framework when solving their scheduling problems, despite differences in look-ahead times and time resolutions. Highly sophisticated models of onshore systems have been developed that capture the complex interplay of switching between operational states and thermodynamic effects. The authors also estimate performance over longer time horizons, compared to our work, with grid-integrated systems that in principle cannot guarantee that the produced hydrogen is emission-free. Furthermore, simplifications are made on modeling exogenous factors such as power market interactions and wind power forecasting, neglecting power market auctions and the uncertain characteristics of the wind speed. Additionally, the developed operational models typically model a single electrolyzer unit, without considerations for the unmatched offshore scale and meteorological conditions unique to the marine environment. In an offshore setting, wind power prediction is more difficult compared to onshore wind forecasting due to sudden atmospheric phenomena that are felt more acutely and amplified in the vast and flat offshore environment (Foley et al., 2012). This makes offshore wind forecasting more challenging, and uncertain wind power generation gains relevance. A coherent model for operational planning of offshore hydrogen production systems is, to the extent of the authors' knowledge, not found in the literature, signifying this work as one of the first operational planning models for an isolated large-scale offshore hydrogen production system in the North Sea.

4.6 Our Contribution

The main contribution of this thesis is a short-term operational model for a large-scale offshore energy system with hydrogen production. By simultaneously considering price differences and the financial implications of not meeting power purchasing agreements, the model seeks to maximize net income. The model achieves this objective by scheduling the optimal split between hydrogen and electricity sales for every quarterly hour, considering the uncertainties associated with wind power generation and power market prices. A key novelty of this work lies in the integration of an advanced wind power scenario generation algorithm, complemented by real-time updates on power purchasing agreements. The system incorporates state-of-the-art technologies and accurate capacities, tailored to the specific offshore context. In order to account for the changing offshore conditions, a stochastic framework is employed to schedule hydrogen production and power market commitments, emphasizing the acknowledgement that the committed power one day ahead may differ from the available power generation at the delivery hour. Furthermore, the system design developed in this work serves as an accurate representation of the offshore system, and the model can be theoretically applied to any offshore system with hydrogen production and onshore power grid connection. This work can be helpful as assistance in the development phase of offshore energy system alike the one presented in this thesis.

CHAPTER

FIVE

MODELLING ASSUMPTIONS AND STRATEGIES

In this chapter the modeling assumptions for the optimization model is presented. Section 5.1 describes the modeling assumptions related to each of the system components. Further on, hydrogen and power markets are treated in Sections 5.2 and 5.3. The chapter wraps ups with the presentation of modeling assumptions for wind power scenarios in Section 5.4.

5.1 Technical Components of the Energy System

5.1.1 Desalination

MSF and MED are more expensive, but thermal distillate designs perform better with respect to quality measures for large-scale sea water desalination. MSF has been selected as the most appropriate system due to its superior reliability, which is given a high priority. It is widely acknowledged that water desalination processes are typically characterized by their high energy intensity and significant SEC. However, it is important to note that in comparison to the energy consumption of electrolysis, the energy consumption of desalination can be relatively minor. Consequently, the extent to which desalination processes are incorporated into the investigation of energy systems with hydrogen production can vary considerably. Dinh et al. (2021) specifically modeled desalination as a distinct process, Lucas et al. (2022) integrated the energy consumption of desalination with the SEC of electrolysis. In contrast, Carr et al. (2016) and Jiang et al. (2021) did not consider water purification in their respective studies. This aspect should be considered when desalination is modeled. Rather than treating desalination as an individual process, it is assumed that the desalination process operates continuously, without any interruptions or ramping constraints that may hinder hydrogen production. The detailed dynamics, such as maximum up-times, startup and shutdown constraints, ramp-up and ramp-down limitations, concentrate disposal, and thermodynamic effects related to water temperature, salinity, and operating pressures on performance, are not explicitly modeled but incorporated into the SEC parameter. All energy requirements for pump operations, heat exchangers, and irreversibilities in the thermal process are consolidated into the SEC constant.

5.1.2 Electrolyzer

Considering that the modeled energy system relies on wind energy, PEMEL electrolyzers are a suitable choice. This observation also aligns with expert opinions, which identify PEMEL as the optimal choice for offshore hydrogen production in the context of an offshore wind park. The modeling of the electrolyzers is inspired by the work of Varela et al. (2021) and results from the

project work (Falk & Hansen, 2022). At any given time period, the electrolyzers will either be in an idle or producing state. When an electrolyzer is idle, it does not consume energy or produce any hydrogen. When producing, the electrolyzer will consume energy $e^{E}_{s\varepsilon t}$ to produce hydrogen $m^{E_{H2}}_{st}$. Transitioning from an idle to producing state between consecutive time periods prepares the electrolyzer for full production in the next time period, and can only operate at half capacity in the current. Switching between operating states is indicated by the binary variables $z^{Up}_{s\varepsilon t}$ and $z^{Down}_{s\varepsilon t}$, which reflect the required energy consumption during transitions as these processes are subject to ramping, which is assumed to be linear. This is a less advanced approach compared to the original formulation in the project work, where each electrolyzer is associated with three operating states as shown by Figure 5.1: idle, producing, and standby, involving a total of six possible state transitions. Electrolysis is a highly energy-intensive process, and precise modeling of its properties is desirable, especially when studying decisions with short-term resolution (Andrenacci et al., n.d.). However, approximating real-world properties should be weighed against the computational budget. Results from the project work demonstrated some reasonable tradeoffs and have been considered when developing an efficient, yet descriptive, formulation of electrolyzer behavior. Our preliminary findings in the project work did not suggest that the standby state provided any significant benefit, as it was rarely utilized. Matute et al. (2021) also did not consider it to be profitable for electrolysis facilities to switch between standby and idle states in practice. Incorporating the standby state makes the problem computationally intractable for the given planning horizon and time-granularity. Removing the standby state reduces the number of binary variables controlling operating states from three to one per platform will operate more than 400 electrolyzer modules. The former formulation also produced a cumbersome non-linear model, making it much harder to solve. Issues with problem size and wind speed uncertainty allows for a more detailed description in the near future that of compared to uncertain decisions relatively far ahead in time. The set $\mathcal{E}$ represents a clustering of electrolyzers on the platform approximating the true number of electrolyzer units, while $\mathcal{E}^{Agg}$ is a further clustering of the electrolyzers and even more simplified representation of the true set size. Each subproblem is partitioned into a set of time periods for each of the generated set.

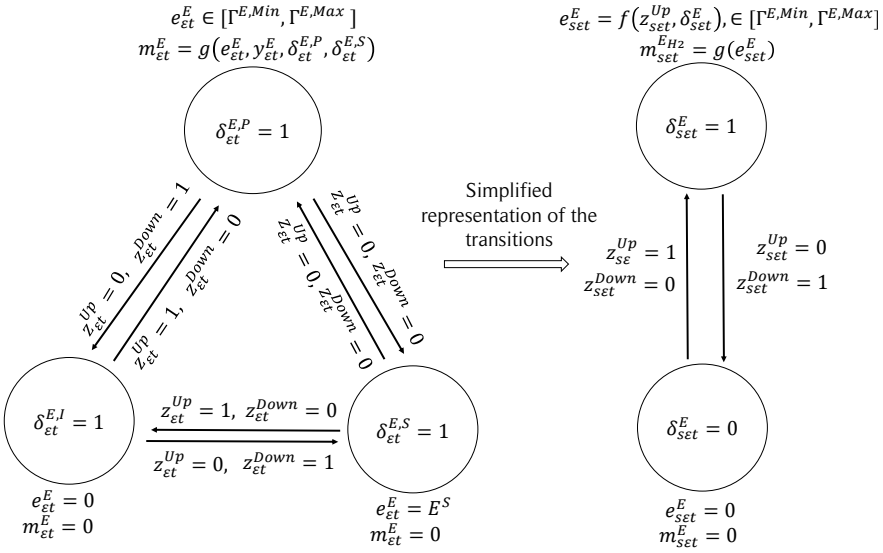

Figure 5.1: Comparison of the more advanced state transitions modeling in project work (left) by Falk and Hansen, 2022 and the less advanced approach adopted in this thesis (right). In the left approach, the binary variables indicating the idle, standby and producing states are indicated by the superscripts (I),(S) and (P). Although some notation differ, the figure illustrates the modeling complexity of implementing three operating states and corresponding state transitions, as opposed to modeling only two operating states.

5.1.3 Compression, Storage and Transportation

Pipelines are considered the most cost-effective by academia and industry. The most viable option for storage and transport is therefore to assume a pipeline, either from retrofitting existing pipeline

network or developed specifically for the hydrogen project. The pipeline stores and transport the produced hydrogen from the North Sea to the European mainland. Compression of hydrogen gas is a complex process, and fluid mechanic modelling within the pipeline extends way beyond the scope of this work. Accurately modeling the compression of hydrogen gas, as shown in Equation (4.2), involves a complex process that requires considering multiple design parameters. Figure 5.2 showcases the adiabatic compression curve represented by Equation (4.2). The rise in SEC is evident at lower pressures, with adiabatic compression demonstrating higher SEC compared to isothermal compression, which better reflects actual compressor operations. According to the findings of Bossel and Eliasson (2003), multi-stage compression with cooling outperforms adiabatic compression in terms of efficiency. As a result, the corresponding SEC curve for this process would be positioned between the curves for adiabatic and isothermal compression. This specific approach is intentionally designed to minimize compressor work and has gained widespread adoption, as supported by insights from industry experts (Moreld, personal communication, October 19, 2022).

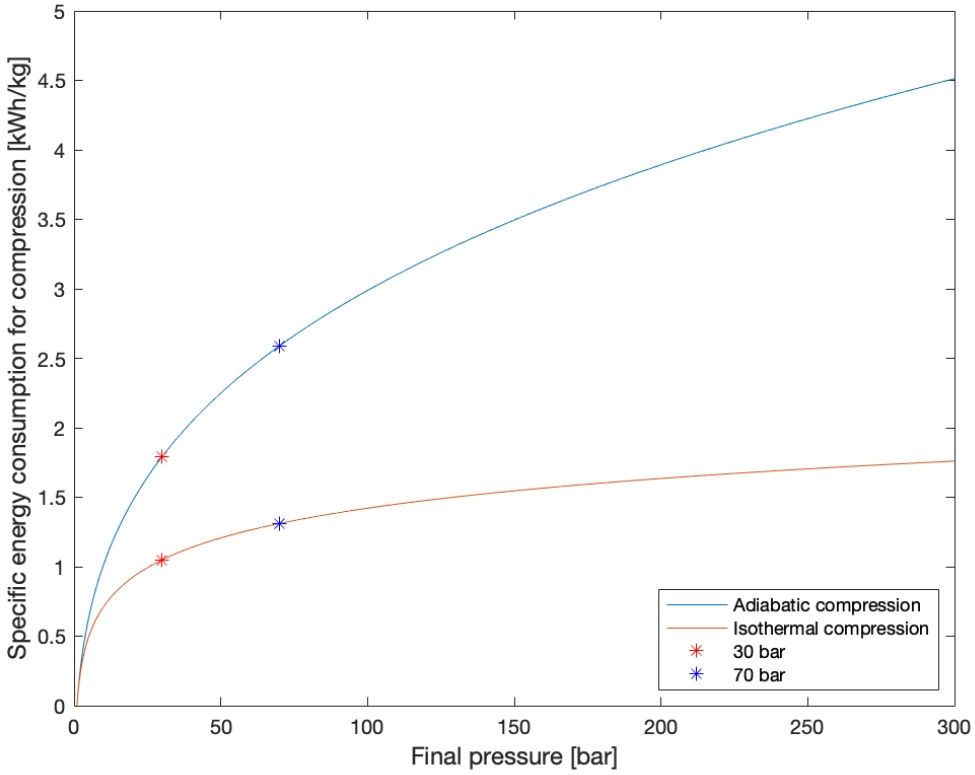

Figure 5.2: SEC for adiabatic and isothermal compression processes. Figure adapted from Bossel and Eliasson (2003).

For this task, we model a single compression unit and the compression process described by Equation (4.2). A constant SEC. The project work demonstrated that the energy consumption of compression is negligible compared to electrolysis. It is assumed that all hydrogen from electrolysis can be compressed. A storage balance equation governs the quantity of hydrogen in the pipeline during each time period. The incoming flow represents the hydrogen produced from electrolysis, while the outgoing flows include the hydrogen sold at a fixed price through contracts, and hydrogen consumed by the fuel cells. Friction losses in the pipeline contribute to minor energy loss. A maximum discharge rate is given. To preserve operability of our model, we include a terminal value for pipeline storage amount.

5.1.4 Fuel Cell

Based on the findings of the literature review, PEMFC stands out as the most suitable fuel cell technology. Throughout the planning horizon, the extraction of hydrogen from the pipeline for electricity generation is possible, accounting for irreversible losses during the process. To simplify the model, individual fuel cells are treated as a single entity operating symmetrically. While the potential for heat recovery exists, it is assumed that heat dissipates into the surroundings without additional utilization. A capacity limit on hydrogen consumption is imposed, and the relationship between electricity generation and fuel consumption as determined by the SEC constant.

5.1.5 Battery

As lithium-ion battery systems are commonly used in energy systems with renewable energy, and the preferred BESS technology suggested after consulting with Arendal Fossekompani a number of lithium-ion battery packs with 4C-ratings is assumed to be installed on the offshore hub (M. Johansen, personal communication, October 25, 2022). Cyclic degradation and ageing of batteries cause capacity degradation over time. However, with respect to the short planning horizon of the model, degradation effects are assumed negligible. Therefore, the round-trip efficiency of the lithium-ion batteries is assumed to be constant. The state of charge is determined by monitoring various parameters, including voltage level, temperature, and electron flow during charging and discharging processes. Typically, a battery management system handles these functions, but they are not addressed in this project. Aspects in regard to optimal and safe operation to prevent thermal events, release of gases and toxicity due to battery failure, have not been considered. Although, to prevent exorbitant activation of the batteries, charging and discharging cause a small penalty in the objective function. The battery charge and discharge rates must respect the C-rating, and energy storage balance equation is provided.

5.1.6 Power Transmission

Based on the studies of Rahman et al. (2021), an estimated value for total energy losses in offshore HVDC configurations is 5%. The transmission cable capacity must not be violated. When modeling the transfer capacity, resistive loss is included.

5.2 Hydrogen Market

The energy system in this work is likely to operate in a hydrogen market dominated by long-term HPAs (M. Kjäll-Ohlsson, personal communication, January 13, 2023). This implies that the energy system in a real-life application would need to deliver a required amount of hydrogen. The production requirement is not necessarily easy to formulate in a short-term optimization. The HPA could have hourly, daily and weekly demands. This planning horizon is larger than the horizon considered in this thesis, as the model focuses on short-term optimization. A tactical planning problem may be need in order to decompose the HPA. The model would also need to account for the possibility to produce more than what is required by the HPA obligations. Stochasticity of wind power generation may also make it unreasonable to have hourly, or even daily, hydrogen demand constraints as the problem may turn infeasible. Due to the complexity of formulating HPA as demand requirements, it has been assumed that the model can sell hydrogen at a fixed price and is not subjected to demand constraints on hydrogen production.

5.3 Power Markets

The wind power producer engages in trading activities on the Nord Pool power exchange, specifically in the "NO2" (Kristiansand) bidding zone in Norway. The wind power producer exclusively

participates in the day-ahead and intraday markets. It is assumed that the predicted market prices in both markets are solely influenced by historical electricity prices. Notably, the wind power producer is strictly prohibited from both overproducing and underproducing. In the event of a default, Nord Pool possesses the authority to suspend the member from further trading and/or clearing (Nord Pool AS, 2020). An event of default is determined by Nord Pool as a breach of one or more obligations, among various other criteria. The consequences of such a default must be highly financially unattractive. This suspension risk is incorporated into our model through a substantial penalty, acknowledging its significant impact for power markets integrity. The modeling approach employed encompasses the pertinent quantity and price risks from day-ahead clearing to intraday gate closure. The analysis primarily focuses on day-ahead commitments, which enable optimal pre-positioning in terms of risk, both in quantity and price, for recourse actions when wind power generation and intraday information are realized. It should be noted that quarterly products have not yet been implemented in the Nordic region. Currently, the availability of quarterly and half hourly products is restricted to the German market. However, given the increasing prominence of variable production in the energy mix, it is reasonable to anticipate the introduction of similar products in the near future, and have been adopted in this thesis.

5.3.1 Day-ahead Market

The wind power producer submits price-accepting bids to Nord Pool based on forecasted day-ahead prices. This process, also called self-schedule bidding, assumes the participant to be a price-taker. Bids from single market actors are, in reality, not necessarily accepted. However, wind power generation plants have a low marginal cost in the market supply curve, and the volume offered on the day-ahead market is incomparably small to the total traded volume. This assumption reduces the complexity of bidding modeling. Bids are submitted to the market operator at 12:00 CET, and corresponding prices for day *D+1* become known at 13:00 CET. day-ahead commitments made at 12:00 CET are first-stage variables determined in a day-ahead clearing subproblem. The promised commitments in $\mathcal{T}^{D+1}$ are scenario-independent. In the next subproblems, recourse actions are taken in each wind power generation scenario. The recourse actions, in time periods with delivery commitments, depends on the uncertain wind power generation through the energy balance constraint. Wind power generation is realized in the current time period. To manage expected deficits from scheduled day-ahead obligations, energy can be redirected from hydrogen production, in addition to coverage by fuel cells, batteries and intraday purchase, as a last resort. It is assumed that payment is linked to actual delivery, including resistive losses in the transmission cable.

Day-ahead Price Forecast

Because the day-ahead market is cleared once per day, there will be time periods in the subproblem's planning horizon that do not contain any information about the market price. Before 12:00 CET on a given day *D*, bids have not yet been submitted for day *D+1*; only day-ahead commitments for the remainder of day *D* exist. Nevertheless, the model should be able to estimate the possible revenue generation from day-ahead sales for the remaining time periods of the planning horizon. A simple auto-regressive structure based on a first-class expert model classification mentioned in Ziel (2016), is developed to predict future spotprices. The simple, yet effective forecast makes the algorithm fast, which is relevant for the model. While some authors (Finnah et al., 2022; Maciejowska et al., 2016; Narajewski & Ziel, 2020b) incorporate a weekday dummy variable in their auto-regressive models, preliminary studies did not find weekday correlation to be statistically significant in predicting future day-ahead prices.

The expert regression model for hour h on day d is formulated as

$$P_{d,h}^{Dah} = \beta_{h,0} + \beta_{h,1} P_{d-1,h}^{Dah} + \beta_{h,2} P_{d-2,h}^{Dah} + \beta_{d-7,h} P_{d-7,h}^{Dah} + \epsilon_{d,h}, \tag{5.1}$$

assuming that the error term $ln(\epsilon) \sim N(0, \sigma_h^2)$.

5.3.2 Intraday Market

The purpose of the ideal intraday market is to provide balancing mechanism and not targeting a high volume per se (Karanfil & Li, 2017). It also not the intention to propose an arbitrage strategy in our model, but to make optimal day-ahead commitments with the higher priority and then balance if necessary. It is desirable to have optimal bids in both markets, however, the focus has been to model the intraday market as an opportunity rather than purely speculative by representing price processes and sales and purchase demands patterns. Also, production uncertainty would require advanced forecasting models to make any justified forecasted decisions on the intraday market. When bidding into the day-ahead market or forecasting day-ahead decisions, intraday decisions are not modeled. It also makes sense to impose volume constraints in the intraday market for two main reasons. Firstly, the volume traded on the intraday market is incomparably small to the day-ahead market. Supplying bulk volumes and large shares of the total volume on the intraday as a single market participant is not necessarily incorrect, but the modeled energy system capacity is disproportionate and not in harmony with the current state of the intraday market. Second, selling surplus of energy always requires a counterparty on the intraday market. This means that the producer might not manage to find a counter-party to allocate the entire production surplus. Negative prices are disregarded as it reduces the complexity of the problem, although the majority of trades on Nord Pool's intraday exchange have positive prices. With access to Nord Pool's database, it is possible to separate the intraday transactions into selling and purchasing volumes and prices. To control the traded volume on a given day D, an intraday to day-ahead volume ratio is defined and multiplied by the day-ahead commitment per time period to give an upper bound for intraday trades. Furthermore, to prevent competing bids that negate each other and artificially inflate bidding volumes, we can only submit either a sell or an ask bid on a given price level for each time period in the horizon. The intraday price forecast is also updated at the time of the day-ahead clearing process for model implementation purposes. There are various approaches to manage the intraday scheduling problem. One way is to consider the whole intraday horizon as one market clearing process with a one-time commitment. Other authors have chosen more intricate models with intraday auctions occurring every hour before each gate-closure, starting from the time of market opening. A hybrid variant of the latter has been implemented that combines hourly auctions with deterministic prices and volumes in the form of forecasts. We acknowledge the missed opportunity for revenue-increasing re-positioning in reaction to the volatility of the true continuous price process with continuously updated bids and dynamic prices and volumes, however, a multistage framework with multiple active contracts is not in the scope of this work. Non-reversible commitments apply at gate-closure, which imposes non-anticipativity constraints over the time periods in the upcoming delivery hour. The commitments are then modeled under a separate set of time periods, and penalized in the event of under-delivery. Intraday decisions are allowed in time periods associated with day-ahead commitments, but are not penalized as they are planned events, and not bound by obligations. The interrelationship between day-ahead and intraday commitments and auctions at particular moments makes model formulation complicated.

Intraday Price Forecast

Intraday prices are dynamic and determined by bilateral transactions, unlike the day-ahead auction where the last accepted bid determines the price for all transactions. In theory, the final average price of the load hour is unknown up until gate-closure indicating that all intraday prices are essentially uncertain. A simple auto-regressive model is developed to forecast intraday prices. The model incorporates an integrated term, looking at the difference between the previous day intraday price for the corresponding hour. It also incorporates the day-ahead price, as auto-regressive structures that estimates intraday prices usually do. It follows a first-class expert model approach. Intraday prices are forecasted for all time periods where there exist day-ahead commitments. Namely, before the day-ahead clearing process we can only use intraday data up until day *D-1* to predict prices for day D and *D+1*, and day-ahead market data up until day *D-1*. After day-ahead clearing, information on day-ahead prices for day *D+1* becomes available which is accounted for in the regression. Finnah et al. (2022) assume that the intraday prices can be explained by cross hour dependencies of previous intraday prices, time-varying day of the week variables and the spotprices

up until day d.

The expert model or hour h on day d is formulated as,

$$P_{d,h}^{Int} = \alpha_{h,0} + \alpha_{h,1}(P_{d-1,h}^{Int} - P_{d-2,h}^{Int}) + \alpha_{h,2}P_{d-1,h}^{Dah} + \epsilon_{d,h}, \tag{5.2}$$

After the day-ahead bid submission, the regression data set is updated, and intraday prices for the next day is estimated with new information on day-ahead prices,

$$P_{d,h}^{Int} = \alpha_{h,0} + \alpha_{h,1}(P_{d-1,h}^{Int} - P_{d-2,h}^{Int}) + \alpha_{h,2}P_{d,h}^{Dah} + \epsilon_{d,h}, \tag{5.3}$$

5.4 Wind Power Scenarios

The optimization problem is continuously updated with the most recent wind speed data at the beginning of each time period. Updated scenarios take into account the new information, which could result in more accurate results as modeling uncertainty is reduced up until the delivery hour. Forecasting error usually increases with forecasting horizon and time since the last forecast, and updated forecast information at every time instant could provide more proficient results closer to delivery times. As information is continually updated at each time instant, a perpetual stochastic optimization problem is practically being solved. However, the newly registered wind data must undergo a procedure in combination with the available forecasts to produce scenarios. This process can be time-consuming and complex. It is however not affected by the decisions of the energy system and can therefore be treated separately. The procedure to generate wind power scenarios from historical observations and forecast is described with more details in Section 7.5.2. The optimization problem is assumed to have scenarios accessible as initial values at the beginning of each time period, and the time spent to generate new scenarios is not included in the solution time of the optimization problem.

CHAPTER

SIX

MATHEMATICAL MODEL AND FORMULATION

In this chapter, we present the mathematical formulation of a stochastic mixed integer linear program used to analyze the short-term operational planning problem associated with offshore production of hydrogen and electricity. A sequence of subproblems is solved using a rolling horizon approach. The submission of non-reversible power market bids at certain time points impacts the mathematical structure of subproblems. Slight modifications must be made in subproblems that involve first-stage day-ahead and intraday decisions, those which involve only first-stage intraday decisions, and subproblems without first-stage decisions but recourse actions. For practical purposes, we will refer to the subproblem with both day-ahead and intraday first-stage decisions as the day-ahead clearing subproblem.

The nomenclature for the model is outlined in Section 6.1. Then, a visual representation of a small section of the global planning horizon is presented to the reader in Figure 6.1. The figure depicts the partitioning of the subproblems and provides a visual guide of the diverse modeling sets and their respective domains, and how they relate. Readers are encouraged to refer to this figure when reading the mathematical formulations, aiding in better understanding of this section. We then adopt a structured approach in which each system component is treated sequentially. The remainder of the chapter is structured as follows. Section 6.2 presents the formulation of all the technical components in the system. Section 6.3 connects the energy production and energy requirements within the system through energy balances. Following up, the day-ahead market, intraday and objective functions formulations are presented in Sections 6.4, 6.5 and 6.6. Required non-anticipativity constraints are presented in Section 6.7. Modeling constraints found in all of the subproblems are represented by simplified notation introduced in Section 6.8. At the end of this chapter, the three types of subproblems solved in the rolling horizon are finally represented in Sections 6.9 - 6.11.

6.1 List of Symbols

Superscripts

Agg	Aggregated
Aux	Auxiliary
B	Battery
D	Day
Dah	day-ahead
Dis	Discharge
$Down$	Shutdown
E	Electrolyzer
El	Electric power
F	Fuel cell
H	Hour
$H2$	Hydrogen
HHV	Higher Heating Value
Int	Intraday
Max	Maximum
Min	Minimum
P	Pipeline
Sys	System
T	Transition
Up	Startup

Sets

$\bar{\mathcal{T}}^{Dah}$	Set of time periods with day-ahead commitments, $\bar{\mathcal{T}}^{Dah} \subset \mathcal{T}$
$\bar{\mathcal{T}}^{Int}$	Set of time periods with intraday commitments, $\bar{\mathcal{T}}^{Int} \subset \mathcal{T}$
$\hat{\mathcal{T}}^{Dah}$	Set of time periods with forecasted day-ahead decisions, $\hat{\mathcal{T}}^{Dah} \subset \mathcal{T}$
$\mathcal{B}$	Set of batteries
$\mathcal{E}$	Clustered set approximating the true number of electrolyzers
$\mathcal{E}^{Agg}$	Aggregated set of electrolyzers
$\mathcal{S}$	Set of wind power scenarios
$\mathcal{T}$	Set of time periods in planning horizon, $\mathcal{T} \subset \mathcal{T}_0$
$\mathcal{T}^{\mathcal{E}^{Agg}}$	Set of time periods for aggregated set of electrolyzers $\mathcal{T}^{\mathcal{E},Agg} \subset \mathcal{T}$
$\mathcal{T}^{\mathcal{E}}$	Set of time periods for true set of electrolyzers $\mathcal{T}^{\mathcal{E}} \subset \mathcal{T}$
$\mathcal{T}^{D+1}$	Set of time periods in the next day $\mathcal{T}^{D+1} \subset \mathcal{T}$

$\mathcal{T}^{H+1}$	Set of time periods in the next hour $\mathcal{T}^{H+1} \subset \mathcal{T}$
$\mathcal{T}_0$	Set of time periods in the planning horizon including the initial-state period

Indices

ε	Electrolyzer
s	Scenario
t	Time period

Parameters

$\bar{r}_t^{Dah}$	day-ahead commitment	[MWh]
$\bar{r}_t^{Int+}$	Intraday sale commitment	[MWh]
$\bar{r}_t^{Int-}$	Intraday purchase commitment	[MWh]
$\delta_{s\varepsilon 0}^{E}$	Initial state of electrolyzer	[–]
η^{B}	Round-trip efficiency of batteries	[–]
η^{El}	Efficiency of electrical power transmission cable	[–]
η^{H2}	Efficiency of hydrogen transmission pipeline	[–]
γ^{E}	Specific energy consumption of electrolyzers	[MWh/kg]
γ^{F}	Specific energy consumption of fuel cells	[MWh/kg]
γ^{Aux}	Specific energy consumption of auxiliary systems	[MWh/kg]
$\Gamma^{B,Max}$	Charge and discharge capacity of batteries	[MWh]
$\Gamma^{E,Max}$	Maximum energy input to electrolyzer	[MWh]
$\Gamma^{E,Min}$	Minimum energy input to electrolyzer	[MWh]
$\Gamma^{F,Max}$	Maximum hydrogen input to fuel cells	[kg]
$\Gamma^{P_{H2},Dis}$	Discharge capacity of hydrogen pipeline	[kg]
$\hat{E}_{st}^{Wind}$	Wind power generation forecast	[MWh]
$\hat{p}_t^{Int+}$	Intraday selling price forecast	[EUR/MWh]
$\hat{p}_t^{Int-}$	Intraday buying price forecast	[EUR/MWh]
$\hat{p}_t^{Dah}$	day-ahead price forecast	[EUR/MWh]
λ^{B}	Penalty from activating batteries	[EUR/MWh]
λ^{Dah}	Default cost from day-ahead contract breach	[EUR/MWh]
λ^{Int+}	Default cost from intraday contract breach	[EUR/MWh]
λ^{Shed}	Cost of load shed	[EUR/MWh]
$\overline{DC}_s$	Total default cost from day-ahead and intraday contract breach	[EUR]
$\Phi^{B,Max}$	Storage capacity of batteries	[MWh]
$\Phi^{P_{H2},Max}$	Storage capacity of hydrogen pipeline	[kg]
a	Linearization constant	[–]

b	Linearization constant	[−]
C_s^B	Total cost of battery activation	[EUR]
C_s^{Shed}	Total cost of energy shed	[EUR]
D_t^{Int+}	Maximum intraday selling volume	[MWh/kg]
D_t^{Int-}	Maximum intraday buying volume	[MWh/kg]
DC_s^{Dah}	Total default cost from expected day-ahead contract breach	[EUR]
DC_s^{Int+}	Total default cost from expected intraday contract breach	[EUR]
e_{sb0}^B	Initial state of batteries	[MWh]
$ET^{\mathcal{E},Agg}$	Energy consumption in electrolyzer during state transition fopr aggregated set	[MWh]
$ET^{\mathcal{E}}$	Energy consumption in electrolyzer during state transition for true set	[MWh]
HHV^{H2}	Higher Heating Value of Hydrogen	[MWh/kg]
I_s^{Dah}	Total income from day-ahead operations	[EUR]
I_s^{H2}	Total income from hydrogen sales	[EUR]
L^P	Terminal value of hydrogen storage level	[kg]
$m_{s0}^{P_{H2}}$	Initial state of hydrogen storage	[kg]
NI_s^{Int}	Net income from intraday operations	[EUR]
P^{Max}	Capacity of power transmission cable	[MWh]
p_s	Probability of scenario s	[−]
p_t^{Dah}	day-ahead price	[EUR/MWh]
p_t^{H2}	Hydrogen price	[EUR/kg]

Variables

$\delta_{s\varepsilon t}^E$	Binary variable associated with electrolyzer operating state	[−]
Δ_{st}^{Dah}	Deviation from day-ahead commitment under scenario s	[MWh]
Δ_{st}^{Int+}	Deviation from intraday commitment under scenario s	[MWh]
δ_{st}^{Int+}	Binary variable associated with intraday sale	[−]
δ_{st}^{Int-}	Binary variable associated with intraday purchase	[−]
μ_{st}^{Dah}	Underdelivery associated with day-ahead commitment	[MWh]
μ_{st}^{Int+}	Undelivery associated with intraday commitment	[MWh]
θ_{st}^{Int+}	Energy surplus in system	[MWh]
$e_{s\varepsilon t}^E$	Energy input to electrolyzer	[MWh]
$e_{sbt}^{B,Cha}$	Electrical charging of battery	[MWh]
$e_{sbt}^{B,Dis}$	Electrical discharging of battery	[MWh]
e_{sbt}^B	Energy storage in battery	[MWh]
e_{st}^{Shed}	Curtailed energy within the energy system	[MWh]
$m_{s\varepsilon t}^{E_{H2}}$	Hydrogen production from electrolysis	[kg]

$m_{st}^{F_{H2}}$	Hydrogen consumption in fuel cells	[kg]
$m_{st}^{P_{H2}}$	Hydrogen storage level in pipeline	[kg]
r_{st}^{Dah}	Electricity sold to the day-ahead market	[MWh]
r_{st}^{H2}	Hydrogen sold	[kg]
$r_{st}^{Int_+}$	Electricity sold on the intraday market	[MWh]
$r_{st}^{Int_-}$	Electricity purchased on the intraday market	[MWh]
r_t^{Dah}	First-stage day-ahead decision	[MWh]
$z_{s\epsilon t}^{Down}$	Binary variable associated with shutdown of electrolyzer	[−]
$z_{s\epsilon t}^{Up}$	Binary variable associated with startup of electrolyzer	[−]

Figure 6.1: An overview of some of the different modeling sets and their associated domains in each subproblem.

6.2 Technical Components Formulation

6.2.1 Electrolyzer

When in an operating state, an electrolyzer consume energy $e^{E}_{s\varepsilon t}$ between the minimum and maximum capacity ratings. A transition from an idle to producing state in consecutive time periods reduce the production capacity for that time period, as indicated by the binary variable $z^{Up}_{s\varepsilon t}$,

$$e^{E}_{s\varepsilon t} \leq \Gamma^{E,Max}\delta^{E}_{s\varepsilon t}(1-\frac{1}{2}z^{Up}_{s\varepsilon t}), \qquad s\in\mathcal{S}, \varepsilon\in\mathcal{E}, t\in\mathcal{T}^{\mathcal{E}}, \quad (6.1)$$

$$e^{E}_{s\varepsilon t} \geq \Gamma^{E,Min}\delta^{E}_{s\varepsilon t}, \qquad s\in\mathcal{S}, \varepsilon\in\mathcal{E}, t\in\mathcal{T}^{\mathcal{E}}. \quad (6.2)$$

Since the planning horizon is modeled with the help of two separate electrolyzer modeling sets, $\mathcal{E}$ and $\mathcal{E}^{Agg}$, upper and lower capacity limits must also be specified for the set of electrolyzers in $\mathcal{E}^{Agg}$ over $\mathcal{T}^{\mathcal{E},Agg}$ in Equation (6.3) and Equation (6.4), similar to the above constraints,

$$e^{E}_{s\varepsilon t} \leq \Gamma^{E,Max}\delta^{E}_{s\varepsilon t}(1-\frac{1}{2}z^{Up}_{s\varepsilon t}), \qquad s\in\mathcal{S}, \varepsilon\in\mathcal{E}^{Agg}, t\in\mathcal{T}^{\mathcal{E}^{Agg}}, \quad (6.3)$$

$$e^{E}_{s\varepsilon t} \geq \Gamma^{E,Min}\delta^{E}_{s\varepsilon t}, \qquad s\in\mathcal{S}, \varepsilon\in\mathcal{E}^{Agg}, t\in\mathcal{T}^{\mathcal{E}^{Agg}}. \quad (6.4)$$

We must establish the link between energy consumption and hydrogen output. This is accomplished in Equation (6.5) through the SEC. However, the SEC is derived from electrolyzer's efficiency $\eta_{\varepsilon t}$, which is a nonlinear function in terms of energy ratios,

$$e^{E} = \gamma^{E} m^{E_{H2}}, \quad (6.5)$$

where

$$\gamma^{E} = \frac{HHV^{H2}}{\eta^{E}_{\varepsilon t}}. \quad (6.6)$$

Figure A.2 in the Appendix shows that the relationship between energy input and hydrogen output is close to linear. We develop a set of equations to approximate this relationship with the help of energy ratios R^{E} and R^{H2}. The energy ratios are normalized expressions for energy input and output with respect to the electrolyzer's maximum rating.

$$R^{H2} = a\cdot R^{E} + b, \quad (6.7)$$

$$R^{H2} = \frac{e^{H2}}{\Gamma^{Max}}, \quad (6.8)$$

$$R^{E} = \frac{e^{E}}{\Gamma^{Max}}, \quad (6.9)$$

$$e^{H2} = m^{H2} HHV^{H2}. \quad (6.10)$$

By combining Equations (6.7) - (6.10), an expression that couples the electrolyzer energy input and hydrogen output is formulated,

$$e^{E} = \left(\frac{HHV^{H2}}{\Gamma^{Max}} m^{H2} - b\right)\frac{\Gamma^{Max}}{a}. \quad (6.11)$$

The appropriate expression that provides the hydrogen production rate as a function of the energy input for corresponding sets $\mathcal{E}$ and $\mathcal{E}^{Agg}$, are given by Equation (6.12) and (6.13),

$$e^{E}_{s\varepsilon t} = \left(\frac{HHV^{H2}}{\Gamma^{E,Max}} m^{E_{H2}}_{s\varepsilon t} - b\right)\frac{\Gamma^{E,Max}}{a}, \qquad s\in\mathcal{S}, \varepsilon\in\mathcal{E}, t\in\mathcal{T}^{\mathcal{E}}, \quad (6.12)$$

$$e^{E}_{s\varepsilon t} = \left(\frac{HHV^{H2}}{\Gamma^{E,Max}} m^{E_{H2}}_{s\varepsilon t} - b\right)\frac{\Gamma^{E,Max}}{a}, \qquad s\in\mathcal{S}, \varepsilon\in\mathcal{E}^{Agg}, t\in\mathcal{T}^{\mathcal{E}^{Agg}}. \quad (6.13)$$

An electrolyzer startup is indicated by Equations (6.14) - (6.16) for $\mathcal{E}$, and Equations (6.17) - (6.19) for $\mathcal{E}^{Agg}$,

$$z^{Up}_{s\varepsilon t} \leq 1 - \delta^{E}_{s\varepsilon,t-1}, \qquad s \in \mathcal{S}, \varepsilon \in \mathcal{E}, t \in \mathcal{T}^{\mathcal{E}}, \quad (6.14)$$

$$z^{Up}_{s\varepsilon t} \leq \delta^{E}_{s\varepsilon t}, \qquad s \in \mathcal{S}, \varepsilon \in \mathcal{E}, t \in \mathcal{T}^{\mathcal{E}}, \quad (6.15)$$

$$z^{Up}_{s\varepsilon t} \geq \delta^{E}_{s\varepsilon t} - \delta^{E}_{s\varepsilon,t-1}, \qquad s \in \mathcal{S}, \varepsilon \in \mathcal{E}, t \in \mathcal{T}^{\mathcal{E}}, \quad (6.16)$$

$$z^{Up}_{s\varepsilon t} \leq 1 - \delta^{E}_{s\varepsilon,t-1}, \qquad s \in \mathcal{S}, \varepsilon \in \mathcal{E}^{Agg}, t \in \mathcal{T}^{\mathcal{E}^{Agg}}, \quad (6.17)$$

$$z^{Up}_{s\varepsilon t} \leq \delta^{E}_{s\varepsilon t}, \qquad s \in \mathcal{S}, \varepsilon \in \mathcal{E}^{Agg}, t \in \mathcal{T}^{\mathcal{E}^{Agg}}, \quad (6.18)$$

$$z^{Up}_{s\varepsilon t} \geq \delta^{E}_{s\varepsilon t} - \delta^{E}_{s\varepsilon,t-1}, \qquad s \in \mathcal{S}, \varepsilon \in \mathcal{E}^{Agg}, t \in \mathcal{T}^{\mathcal{E}^{Agg}}, \quad (6.19)$$

Similarly, a shutdown process is modeled by Equations (6.20) - (6.22) for $\mathcal{E}$, and Equations (6.23) - (6.25) for $\mathcal{E}^{Agg}$,

$$z^{Down}_{s\varepsilon t} \leq \delta^{E}_{s\varepsilon,t-1}, \qquad s \in \mathcal{S}, \varepsilon \in \mathcal{E}, t \in \mathcal{T}^{\mathcal{E}}, \quad (6.20)$$

$$z^{Down}_{s\varepsilon t} \leq 1 - \delta^{E}_{s\varepsilon t}, \qquad s \in \mathcal{S}, \varepsilon \in \mathcal{E}, t \in \mathcal{T}^{\mathcal{E}}, \quad (6.21)$$

$$z^{Down}_{s\varepsilon t} \geq \delta^{E}_{s\varepsilon,t-1} - \delta^{E}_{s\varepsilon t}, \qquad s \in \mathcal{S}, \varepsilon \in \mathcal{E}, t \in \mathcal{T}^{\mathcal{E}}. \quad (6.22)$$

$$z^{Down}_{s\varepsilon t} \leq \delta^{E}_{s\varepsilon,t-1}, \qquad s \in \mathcal{S}, \varepsilon \in \mathcal{E}^{Agg}, t \in \mathcal{T}^{\mathcal{E}^{Agg}}, \quad (6.23)$$

$$z^{Down}_{s\varepsilon t} \leq 1 - \delta^{E}_{s\varepsilon t}, \qquad s \in \mathcal{S}, \varepsilon \in \mathcal{E}^{Agg}, t \in \mathcal{T}^{\mathcal{E}^{Agg}}, \quad (6.24)$$

$$z^{Down}_{s\varepsilon t} \geq \delta^{E}_{s\varepsilon,t-1} - \delta^{E}_{s\varepsilon t}, \qquad s \in \mathcal{S}, \varepsilon \in \mathcal{E}^{Agg}, t \in \mathcal{T}^{\mathcal{E}^{Agg}}. \quad (6.25)$$

Non-negative and binary constraints on the variables must be defined,

$$e^{E}_{s\varepsilon t} \geq 0, \qquad s \in \mathcal{S}, \varepsilon \in \mathcal{E}, t \in \mathcal{T}^{\mathcal{E}}, \quad (6.26)$$

$$m^{E_{H2}}_{s\varepsilon t} \geq 0, \qquad s \in \mathcal{S}, \varepsilon \in \mathcal{E}, t \in \mathcal{T}^{\mathcal{E}} \cap \mathcal{T}_0, \quad (6.27)$$

$$e^{E}_{s\varepsilon t}, m^{E_{H2}}_{s\varepsilon t} \geq 0, \qquad s \in \mathcal{S}, \varepsilon \in \mathcal{E}^{Agg}, t \in \mathcal{T}^{\mathcal{E}^{Agg}}, \quad (6.28)$$

$$z^{Up}_{s\varepsilon t}, z^{Down}_{s\varepsilon t} \in \{0,1\}, \qquad s \in \mathcal{S}, \varepsilon \in \mathcal{E}, t \in \mathcal{T}^{\mathcal{E}}, \quad (6.29)$$

$$\delta^{E}_{s\varepsilon t} \in \{0,1\}, \qquad s \in \mathcal{S}, \varepsilon \in \mathcal{E}, t \in \mathcal{T}^{\mathcal{E}} \cap \mathcal{T}_0, \quad (6.30)$$

$$\delta^{E}_{s\varepsilon t}, z^{Up}_{s\varepsilon t}, z^{Down}_{s\varepsilon t} \in \{0,1\}, \qquad s \in \mathcal{S}, \varepsilon \in \mathcal{E}^{Agg}, t \in \mathcal{T}^{\mathcal{E}^{Agg}}. \quad (6.31)$$

We denote the set of Equations (6.1) - (6.4), (6.14) - (6.28) as $\mathbf{\Omega^E_1}(\mathbf{x}) \leq \mathbf{0}$, Equations (6.12) - (6.13) as $\mathbf{\Omega^E_2}(\mathbf{x}) = \mathbf{0}$, and Equations (6.29) - (6.31) as $\mathbf{\Upsilon^E}(\mathbf{x}) \in \{\mathbf{0}, \mathbf{1}\}$, as the set of electrolyzer constraints found in the three different types of subproblems.

6.2.2 Compression, Storage and Transportation

Equations (6.32) and (6.33) are the corresponding pipeline storage balance equations modeled ovcr $\mathcal{E}$ and $\mathcal{E}^{Agg}$. The amount of hydrogen stored in the pipeline is determined by the hydrogen amount from the previous time period, the hydrogen produced by all electrolyzers, less the hydrogen sold and hydrogen combusted in the fuel cells.

$$m^{P_{H2}}_{st} = m^{P_{H2}}_{s,t-1} + \sum_{\varepsilon \in \mathcal{E}} m^{E_{H2}}_{s\varepsilon t} - r^{H2}_{st} - m^{F_{H2}}_{st}, \qquad s \in \mathcal{S}, t \in \mathcal{T}^{\mathcal{E}} \cap \mathcal{T}_0. \quad (6.32)$$

$$m^{P_{H2}}_{st} = m^{P_{H2}}_{s,t-1} + \sum_{\varepsilon \in \mathcal{E}^{Agg}} m^{E_{H2}}_{s\varepsilon t} - r^{H2}_{st} - m^{F_{H2}}_{st}, \qquad s \in \mathcal{S}, t \in \mathcal{T} \backslash \mathcal{T}^{\mathcal{E}}. \quad (6.33)$$

The amount of hydrogen stored in the pipeline cannot exceed the maximum pipeline storage capacity,

$$m^{P_{H2}}_{st} \leq \Phi^{P_{H2},Max}, \qquad s \in \mathcal{S}, t \in \mathcal{T}. \quad (6.34)$$

Equation (6.35) restricts the hydrogen discharge rate of the pipeline for hydrogen sales,

$$r_{st}^{H2} \leq \Gamma^{P_{H2},Dis}, \qquad s \in \mathcal{S}, t \in \mathcal{T}. \quad (6.35)$$

The amount of hydrogen stored in the pipeline in the last time period in the planning horizon must at least be equal to a predefined terminal value,

$$m_{st}^{P_{H2}} \geq L^{P}, \qquad s \in \mathcal{S}, t := |\mathcal{T}|. \quad (6.36)$$

Non-negative constraints are defined for pipeline storage amount and hydrogen sale variables,

$$m_{st}^{P_{H2}} \geq 0, \qquad s \in \mathcal{S}, t \in \mathcal{T}_0, \quad (6.37)$$

$$r_{st}^{H2} \geq 0, \qquad s \in \mathcal{S}, t \in \mathcal{T}. \quad (6.38)$$

We denote the set of Equations (6.34) - (6.38) as $\mathbf{\Omega_1^P}(\mathbf{x}) \leq \mathbf{0}$, and Equations (6.32) - (6.33) as $\boldsymbol{\Omega_2^P(x) = 0}$, as the set of pipeline constraints found in all subproblems.

6.2.3 Fuel Cell

Equation (6.39) relates the electricity production in fuel cells and hydrogen consumption from storage through fuel cell operating efficiency and SEC,

$$e_{st}^{F} = m_{st}^{F_{H2}} \gamma^{F}, \qquad s \in \mathcal{S}, t \in \mathcal{T}. \quad (6.39)$$

For convenience, the maximum electricity production capacity of the fuel cells is implicitly given by the above equation and the maximum inlet flow of hydrogen represented by Equation (6.40),

$$m_{st}^{F_{H2}} \leq \Gamma^{F,Max}, \qquad s \in \mathcal{S}, t \in \mathcal{T}. \quad (6.40)$$

Non-negativity constraints are imposed on the fuel cell variables,

$$m_{st}^{F_{H2}}, e_{st}^{F} \geq 0 \qquad s \in \mathcal{S}, t \in \mathcal{T}. \quad (6.41)$$

We denote Equations (6.40) - (6.41) as $\boldsymbol{\Omega_1^F(x) \leq 0}$ and Equation (6.39) as $\boldsymbol{\Omega_2^F(x) = 0}$, when referring to fuel cell constraints found in all subproblems.

6.2.4 Battery

Battery capacities in terms of charge and discharge rates must not violate the maximum charge and discharge capacities,

$$e_{sbt}^{B,Cha} \eta^{B} \leq \Gamma^{B,Max}, \qquad s \in \mathcal{S}, b \in \mathcal{B}, t \in \mathcal{T}, \quad (6.42)$$

$$e_{sbt}^{B,Dis} \leq \Gamma^{B,Max}, \qquad s \in \mathcal{S}, b \in \mathcal{B}, t \in \mathcal{T}. \quad (6.43)$$

The energy stored in the batteries cannot exceed the storage capacity of the batteries,

$$e_{sbt}^{B} \leq \Phi^{B,Max}, \qquad s \in \mathcal{S}, b \in \mathcal{B}, t \in \mathcal{T}. \quad (6.44)$$

Energy conservation in the battery system is expressed in Equation (6.45),

$$e_{sb,t-1}^{B} + e_{sbt}^{B,Cha} \eta^{B} - e_{sbt}^{B,Dis} = e_{sbt}^{B}, \qquad s \in \mathcal{S}, b \in \mathcal{B}, t \in \mathcal{T}_0. \quad (6.45)$$

At last, we include the non-negativity constraints on the variables related to the batteries,

$$e_{sbt}^{B,Cha}, e_{sbt}^{B,Dis} \geq 0, \qquad s \in \mathcal{S}, b \in \mathcal{B}, t \in \mathcal{T}, \quad (6.46)$$

$$e_{sbt}^{B} \geq 0, \qquad s \in \mathcal{S}, b \in \mathcal{B}, t \in \mathcal{T}_0. \quad (6.47)$$

We denote the set of Equations (6.42) - (6.44), and (6.46)-(6.47) as $\boldsymbol{\Omega_1^B(x) \leq 0}$, and Equation (6.45) as $\boldsymbol{\Omega_2^B(x) = 0}$ when referring to battery constraints found in all subproblems.

6.2.5 Power Transmission

Power delivery day-ahead r_{st}^{Dah}, and intraday r_{st}^{Int+} cannot not violate the transmission capacity between the offshore hub and the mainland power grid. In time periods with promised day-ahead deliveries $\bar{\mathcal{T}}^{Dah}$, the sum of day-ahead and intraday power transfers cannot exceed the cable capacity. A separate constraint holds for time periods without day-ahead commitments, but forecasted day-ahead decisions $\hat{\mathcal{T}}^{Dah}$. The intraday market is not modeled over $\hat{\mathcal{T}}^{Dah}$, thus intraday market operations are not included.

$$r_{st}^{Dah} + r_{st}^{Int+} \leq P^{Max}, \qquad s \in \mathcal{S}, t \in \bar{\mathcal{T}}^{Dah}, \tag{6.48}$$

$$r_{st}^{Dah} \leq P^{Max}, \qquad s \in \mathcal{S}, t \in \mathcal{T} \backslash \bar{\mathcal{T}}^{Dah}. \tag{6.49}$$

Power markets decisions are defined as non-negative variables,

$$r_{st}^{Dah}, r_{st}^{Int+} \geq 0, \qquad s \in \mathcal{S}, t \in \bar{\mathcal{T}}^{Dah}, \tag{6.50}$$

$$r_{st}^{Dah} \geq 0, \qquad s \in \mathcal{S}, t \in \mathcal{T} \backslash \bar{\mathcal{T}}^{Dah}. \tag{6.51}$$

We denote the set of Equations (6.48) - (6.51) as $\boldsymbol{\Omega_1^T(x) \leq 0}$ when referring to power transmission formulations found in all subproblems.

6.3 Energy Flows

As multiple sets are incorporated throughout the planning horizon, slight modifications are made to the energy balance equation at various time intervals. In the case where both $\mathcal{T}^{\mathcal{E}}$ and $\bar{\mathcal{T}}^{Dah}$ apply, the energy balance equation for the system model the true electrolyzer set and intraday sales. Equation (6.52) is a general formulation modeled in all subproblems. However, when solving a subproblem with first-stage intraday decisions, $\mathcal{T}^{\mathcal{E}}$ and $\mathcal{T}^{H+1}$ overlap, as illustrated in Figure 6.1. Equation (6.52) is therefore not valid over $\mathcal{T}^{H+1}$, and must be omitted. On the left side of the equation, the wind energy availability, battery discharge to the system, and fuel cell electricity production must be accounted for by all energy-consuming processes listed on the right side, including total batteries charging, energy shedding, day-ahead delivery, intraday sales delivery, and total consumption by transitions, production and auxiliary processes associated with operating the electrolyzers.

$$\begin{aligned} \hat{E}_{st}^{Wind} + \sum_{b \in \mathcal{B}} e_{sbt}^{B,Dis} + e_{st}^{F} = \sum_{b \in \mathcal{B}} e_{sbt}^{B,Cha} + e_{st}^{Shed} + r_{st}^{Dah} + r_{st}^{Int+} + \\ \sum_{\varepsilon \in \mathcal{E}} \left[ET^{\mathcal{E}}(z_{s\varepsilon t}^{Up} + z_{s\varepsilon t}^{Down}) + e_{s\varepsilon t}^{E} + m_{s\varepsilon t}^{E_{H2}} \gamma^{Aux} \right], \qquad s \in \mathcal{S}, t \in \mathcal{T}^{\mathcal{E}} \backslash \mathcal{T}^{H+1}. \end{aligned} \tag{6.52}$$

For the remaining time periods that involves day-ahead commitments, the only difference is that the set $\mathcal{E}$ is replaced by $\mathcal{E}^{Agg}$,

$$\begin{aligned} \hat{E}_{st}^{Wind} + \sum_{b \in \mathcal{B}} e_{sbt}^{B,Dis} + e_{st}^{F} = \sum_{b \in \mathcal{B}} e_{sbt}^{B,Cha} + e_{st}^{Shed} + r_{st}^{Dah} + r_{st}^{Int+} + \\ \sum_{\varepsilon \in \mathcal{E}, \mathcal{A}gg} \left[ET^{\mathcal{E},Agg}(z_{s\varepsilon t}^{Up} + z_{s\varepsilon t}^{Down}) + e_{s\varepsilon t}^{E} + m_{s\varepsilon t}^{E_{H2}} \gamma^{Aux} \right], \qquad s \in \mathcal{S}, t \in \bar{\mathcal{T}}^{Dah} \backslash \mathcal{T}^{\mathcal{E}}. \end{aligned} \tag{6.53}$$

In the remaining time periods of the planning horizon, there are no day-ahead commitments and thus no intraday decisions to be made. Equation (6.54) is the energy balance equation over $\hat{\mathcal{T}}^{Dah}$. The constraint is identical to the one above, except that the term related to intraday sale is left

out.

$$\hat{E}_{st}^{Wind} + \sum_{b\in\mathcal{B}} e_{sbt}^{B,Dis} + e_{st}^{F} = \sum_{b\in\mathcal{B}} e_{sbt}^{B,Cha} + e_{st}^{Shed} + r_{st}^{Dah} + \sum_{\varepsilon\in\mathcal{E},Agg} \left[ET^{\mathcal{E},Agg}(z_{s\varepsilon t}^{Up} + z_{s\varepsilon t}^{Down}) + e_{s\varepsilon t}^{E} + m_{s\varepsilon t}^{E_{H2}}\gamma^{Aux} \right], \qquad s \in \mathcal{S}, t \in \hat{\mathcal{T}}^{Dah}. \quad (6.54)$$

We denote the set of Equations (6.52) - (6.53) as $\boldsymbol{\Omega_2^{Sys}(x) = 0}$ when referring to energy flow formulations found in all subproblems.

6.4 Day-ahead Market

The expected future day-ahead deviation Δ_{st}^{Dah} depends upon the realization of wind power generation in $\mathcal{D}+1$ in constraint (6.55). Given the first-stage day-ahead variables, r_t^{Dah}. This constraint is unique for the day-ahead clearing subproblem and replaces the general energy balance constraint (6.54).

$$\Delta_{st}^{Dah} = \sum_{b\in\mathcal{B}} e_{sbt}^{B,Cha} + e_{st}^{Shed} + r_t^{Dah} + \sum_{\varepsilon\in\mathcal{T}^{\mathcal{E},\mathcal{A}gg}} \big[ET^{\mathcal{E},Agg}(z_{s\varepsilon t}^{Up} + z_{s\varepsilon t}^{Down}) + e_{st}^{E} + m_{s\varepsilon t}^{E_{H2}}\gamma^{Aux} \big] - \hat{E}_{st}^{Wind} - \sum_{b\in\mathcal{B}} e_{sbt}^{B,Dis} - e_{st}^{F}, \qquad s \in \mathcal{S}, t \in \mathcal{T}^{D+1}. \quad (6.55)$$

The first-stage day-ahead decisions cannot exceed the transmission cable capacity,

$$r_t^{Dah} \leq P^{Max}, \qquad s \in \mathcal{S}, t \in \mathcal{T}^{D+1}. \quad (6.56)$$

In subsequent subproblems, the first-stage decisions $r_t^{Dah}, t \in \mathcal{T}^{D+1}$ are input as parameters, $\bar{r}_t^{Dah}$. Recourse actions for the day-ahead market is modeled in Equation (6.57). Equation (6.57) includes the actual day-ahead delivery, any intraday purchases made and the slack variable representing any underproduction,

$$r_{st}^{Dah} + r_{st}^{Int-} + \mu_{st}^{Dah} = \bar{r}_{st}^{Dah}, \qquad s \in \mathcal{S}, t \in \bar{\mathcal{T}}^{Dah}. \quad (6.57)$$

Non-negative constraints are imposed in constraint (6.58) on the day-ahead-related variables,

$$r_t^{Dah}, \Delta_{st}^{Dah} \geq 0, \qquad s \in \mathcal{S}, t \in \mathcal{T}^{D+1}. \quad (6.58)$$

$$\mu_{st}^{Dah} \geq 0, \qquad s \in \mathcal{S}, t \in \bar{\mathcal{T}}^{Dah}. \quad (6.59)$$

We denote Equation (6.57) and (6.59) $\boldsymbol{\Omega_2^{Dah}(x) = 0}$ when referring to the day-ahead constraint that is found in all subproblems.

6.5 Intraday Market

Solving a subproblem at any time period *hh:45 - h(h+1):00* involves determining the first-stage intraday decisions for the next delivery hour $t \in \mathcal{T}^{H+1}$. Notice that the day-ahead clearing subproblem at *11:45-12:00* contains both intraday *and* day-ahead first-stage variables. In $\mathcal{T}^{H+1}$, the energy balance equation is modeled with an extra slack variable θ_{st}^{+} indicating an excess energy production in the system, which is not penalized as opposed to the energy shed variable, when day-ahead commitments are accounted for.

$$\hat{E}_{st}^{Wind} + \sum_{b\in\mathcal{B}} e_{sbt}^{B,Dis} + e_{st}^{F} = \sum_{b\in\mathcal{B}} e_{sbt}^{B,cha} + e_{st}^{Shed} + r_{st}^{Dah} + \theta_{st}^{+} + \sum_{\varepsilon\in\mathcal{T}^{\mathcal{E}}} \left[ET^{\mathcal{E}}(z_{s\varepsilon t}^{Up} + z_{s\varepsilon t}^{Down}) + e_{st}^{E} + m_{s\varepsilon t}^{E_{H2}} \gamma^{Aux} \right], \qquad s \in \mathcal{S}, t \in \mathcal{T}^{H+1}. \quad (6.60)$$

Depending on the amount of surplus energy available for intraday commitments, the over-commitment Δ_{st}^{Int+}, which is penalized in the objective function, under scenario s when submitting intraday sale bids is expressed as

$$\Delta_{st}^{Int+} = r_{st}^{Int+} - \theta_{st}^{+}, \qquad s \in \mathcal{S}, t \in \mathcal{T}^{H+1}. \quad (6.61)$$

Since we adopt a rolling horizon approach the first-stage intraday variables, r_{st}^{Int+} for sales and r_{st}^{Int-} for purchases, are input as parameters $\bar{r}_{st}^{Int+}$ and $\bar{r}_{st}^{Int+}$ in subsequent subproblems.

Constraint (6.62) accounts for the deviation between the actual intraday sales delivery and the committed quantity, where μ_{st}^{Int+} denotes any underproduction.

$$r_{st}^{Int+} + \mu_{st}^{Int+} = \bar{r}_{t}^{Int+} \qquad s \in \mathcal{S}, t \in \bar{\mathcal{T}}^{Int}. \quad (6.62)$$

Constraint (6.63) ensures that we can either trade sales or purchases in the intraday market, not both,

$$\delta_{st}^{Int+} + \delta_{st}^{Int-} \leq 1, \qquad s \in \mathcal{S}, t \in \bar{\mathcal{T}}^{Dah}. \quad (6.63)$$

The intraday sale and purchase decisions are upper bounded by the parameters D_t^{Int+} and D_t^{Int-}, which are volume restrictions on intraday trading reflecting that the intraday market is trading smaller volumes than the day-ahead.

$$r_{st}^{Int+} \leq D_t^{Int+} \delta_{st}^{Int+}, \qquad s \in \mathcal{S}, t \in \bar{\mathcal{T}}^{Dah}. \quad (6.64)$$
$$r_{st}^{Int-} \leq D_t^{Int-} \delta_{st}^{Int-}, \qquad s \in \mathcal{S}, t \in \bar{\mathcal{T}}^{Dah}. \quad (6.65)$$

Intraday purchases are financial costs and contractual obligations to trading counterparties. On the other hand, the wind power producer has an active role in delivering intraday sales. Therefore, non-anticipativity constraints in $\bar{\mathcal{T}}^{Int}$ for all subproblems are formulated for the intraday purchases, but not for the actual intraday delivery, which is subject to wind power uncertainty.

$$r_{st}^{Int-} = \bar{r}_{t}^{Int-}, \qquad s \in \mathcal{S}, t \in \bar{\mathcal{T}}^{Int} \quad (6.66)$$

Non-negative and binary restrictions are imposed on the intraday variables,

$$r_{st}^{Int+}, r_{st}^{Int-} \geq 0, \qquad s \in \mathcal{S}, t \in \bar{\mathcal{T}}^{Dah}. \quad (6.67)$$
$$\delta_{st}^{Int+}, \delta_{st}^{Int-} \in \{0,1\}, \qquad s \in \mathcal{S}, t \in \bar{\mathcal{T}}^{Dah}. \quad (6.68)$$
$$\mu_{st}^{Int+} \geq 0, \qquad s \in \mathcal{S}, t \in \bar{\mathcal{T}}^{Int}. \quad (6.69)$$
$$\theta_{st}^{+}, \Delta_{st}^{Int+} \geq 0, \qquad s \in \mathcal{S}, t \in \mathcal{T}^{H+1}. \quad (6.70)$$

We denote the set of Equations (6.63) - (6.65), (6.67) and (6.69) as $\boldsymbol{\Omega_1^{Int}(x) \leq 0}$, Equation (6.62) as $\boldsymbol{\Omega_2^{Int}(x) = 0}$, and Equation (6.68) as $\boldsymbol{\Upsilon^{Int}(x) \in \{0,1\}}$, for later convenience.

6.6 Objective Function Terms

The term I_s^{Dah} summarizes the income generated from day-ahead market contracts and non-contractual day-ahead decisions under scenario s,.

$$I_s^{Dah} = \sum_{t\in\bar{\mathcal{T}}^{Dah}} p_t^{Dah} \bar{r}_t^{Dah} + \sum_{t\in\hat{\mathcal{T}}^{Dah}} \hat{p}_t^{Dah} r_{st}^{Dah}. \quad (6.71)$$

The net income from intraday market operations under scenario s is the sum all contractual arrangements in $\bar{\mathcal{T}}^{Int}$, and non-contractual operations in time periods with day-ahead obligations, $\bar{\mathcal{T}}^{Dah}$.

$$NI_s^{Int} = \sum_{t \in \bar{\mathcal{T}}^{Int}} \hat{p}_{st}^{Int+} \bar{r}_t^{Int+} - \hat{p}_{st}^{Int-} \bar{r}_t^{Int-} + \sum_{t \in \bar{\mathcal{T}}^{Dah} \setminus \bar{\mathcal{T}}^{Int}} \hat{p}_{st}^{Int+} r_{st}^{Int+} - \hat{p}_{st}^{Int-} r_{st}^{Int-}. \tag{6.72}$$

The term $\overline{DC}_s$ represents the total default cost from under-delivery in scenario s of power market commitments in $\bar{\mathcal{T}}^{Dah}$ and $\bar{\mathcal{T}}^{Int}$, respectively.

$$\overline{DC}_s = \sum_{t \in \bar{\mathcal{T}}^{Dah}} -\lambda^{Dah} \mu_{st}^{Dah} \sum_{t \in \bar{\mathcal{T}}^{Int}} -\lambda^{Int+} \mu_{st}^{Int+}, \tag{6.73}$$

Separate expressions for the expected future default cost for the day-ahead and intraday market are defined. Any over-commitment, in $\mathcal{T}^{D+1}$ or $\mathcal{T}^{H+1}$, is penalized by a default cost rate of λ^{Dah} and λ^{Int} per unit MWh accordingly,

$$DC_s^{Dah} = \sum_{t \in \mathcal{T}^{D+1}} -\lambda^{Dah} \Delta_{st}^{Dah}, \tag{6.74}$$

$$DC_s^{Int+} = \sum_{t \in \mathcal{T}^{H+1}} -\lambda^{Int+} \Delta_{st}^{Int+}. \tag{6.75}$$

The total cost of energy shedding in the planning horizon under a given scenario is captured by C_s^{Shed},

$$C_s^{Shed} = \sum_{t \in \mathcal{T}} -\lambda^{Shed} e_{st}^{Shed}. \tag{6.76}$$

Batteries cannot charge and discharge at the same time. Instead of introducing more binary variables a small penalty is imposed for charging and discharging in the objective function to make sure it will never be profitable to discharge and charge in the same time period,

$$C_s^B = \sum_{b \in \mathcal{B}} \lambda^B \left[\sum_{t \in \mathcal{T}} e_{sbt}^{B,Cha} + e_{sbt}^{B,Dis} \right]. \tag{6.77}$$

Finally, we include hydrogen sales in scenario s over the entire planning horizon of the subprpoblem,

$$I_s^{H2} = \sum_{t \in \mathcal{T}} \eta^{H2} p_t^{H2} r_{st}^{H2}. \tag{6.78}$$

6.7 Non-anticipativity Constraints

Decisions in the current time period are implemented by the wind power producer. Non-anticipativity constraints are required for several variables, but not all, because variables are interlinked. One way of defining non-anticipativity constraints in order to reduce the number of additional constraints, is to make the variable take the average value across all scenarios. For simplicity, a vector $\mathcal{X}$ defines the variables, represented as $\mathcal{X}_i$, that requires non-anticipativity constraints in the current time period,

$$\mathcal{X} = \left[e_{s\epsilon t}^{E}, e_{sbt}^{B,Cha}, e_{sbt}^{B,Dis}, e_{st}^{F}, r_{st}^{Dah}, r_{st}^{Int+}, r_{st}^{Int-}, r_{st}^{H2}, \hat{E}_{st}^{Wind} \right].$$

For $i = \{1\}$, the non-anticipaitivity constraints are

$$\mathcal{X}_i\big|_{s=s^*} = \frac{1}{|\mathcal{S}|} \sum_{k \in \mathcal{S}} \mathcal{X}_i\big|_{s=k}, \qquad s^* \in \mathcal{S}, \varepsilon \in \mathcal{E}, t := 1. \tag{6.79}$$

For $i = \{2,3\}$, the non-anticipaitivty constraints are

$$\mathcal{X}_i\big|_{s=s^*} = \frac{1}{|\mathcal{S}|}\sum_{k\in\mathcal{S}} \mathcal{X}_i\big|_{s=k}, \qquad s^* \in \mathcal{S}, b \in \mathcal{B}, t := 1. \tag{6.80}$$

For $i = \{4,5,\ldots,9\}$, the non-anticipaitivty constraints are

$$\mathcal{X}_i\big|_{s=s^*} = \frac{1}{|\mathcal{S}|}\sum_{k\in\mathcal{S}} \mathcal{X}_i\big|_{s=k}, \qquad s^* \in \mathcal{S}, t := 1. \tag{6.81}$$

For convenience, Equations (6.66), and (6.79) - (6.81) are label as $\boldsymbol{\Omega^{\mathcal{X}}(x) = 0}$, to represent non-anticipativity constraints found in all the subproblems.

When solving a subproblem with first-stage intraday decisions, non-anticipativity constraints are formulated for intraday sales and purchasing over $\mathcal{T}^{H+1}$, respectively, as

$$r_{st}^{Int+} = \frac{1}{|\mathcal{S}|}\sum_{k\in\mathcal{S}} r_{kt}^{Int+}, \qquad s \in \mathcal{S}, t \in \mathcal{T}^{H+1}, \tag{6.82}$$

$$r_{st}^{Int-} = \frac{1}{|\mathcal{S}|}\sum_{k\in\mathcal{S}} r_{kt}^{Int-}, \qquad s \in \mathcal{S}, t \in \mathcal{T}^{H+1}. \tag{6.83}$$

The observant reader noticed that the first-stage day-ahead variables in $\mathcal{T}^{D+1}$ defined in Equation (6.58) are scenario-independent in its formulation, and thus require none non-anticipativity constraints.

6.8 Simplified Notation

For easier reading, we define the vectors $\boldsymbol{\Omega_1(x)}$, $\boldsymbol{\Omega_2(x)}$ such that

$$\boldsymbol{\Omega_1(x)} = \left[\boldsymbol{\Omega_1^E(x), \Omega_1^P(x), \Omega_1^F(x), \Omega_1^B(x), \Omega_1^T(x), \Omega_1^{Int}(x)}\right] \tag{6.84}$$

$$\boldsymbol{\Omega_2(x)} = \left[\boldsymbol{\Omega_2^E(x), \Omega_2^P(x), \Omega_2^F(x), \Omega_2^B(x), \Omega_2^{Sys}(x), \Omega_2^{Dah}(x), \Omega_2^{Int}(x),}\right] \tag{6.85}$$

A final formulation of the mathematical constraints that apply to all subproblems defined in the rolling horizon algorithm, becomes

$$\left[\boldsymbol{\Omega_1(x)}\right]^T \leq \left[\mathbf{0}\right]^T, \tag{6.86}$$

$$\left[\boldsymbol{\Omega_2(x)}\right]^T = \left[\mathbf{0}\right]^T, \tag{6.87}$$

$$\left[\boldsymbol{\Omega^{\mathcal{X}}(x)}\right]^T = \left[\mathbf{0}\right]^T, \tag{6.88}$$

$$\boldsymbol{\Upsilon^E(x)}^T \in \{0,1\}, \tag{6.89}$$

$$\boldsymbol{\Upsilon^{Int}(x)}^T \in \{0,1\}. \tag{6.90}$$

where T is the transposition operator.

6.9 Subproblems with First-Stage Day-ahead and Intraday Decisions

The day-ahead subproblem is solved in time period *11:45 - 12:00*, and finds the first-stage day-ahead and intraday decisions in $\bar{\mathcal{T}}^{D+1}$ and $\bar{\mathcal{T}}^{H+1}$ simultaneously. The complete mathematical description of this subproblem is given below.

$$\max \sum_{s\in\mathcal{S}} p_s \Big[I_s^{H2} + I_s^{Dah} + NI_s^{Int} + \overline{DC}_s + DC_s^{Dah} + DC_s^{Int+} + C_s^{Shed} + C_s^{B} \Big],$$

$$\Delta_{st}^{Dah} = \sum_{b\in\mathcal{B}} e_{sbt}^{B,Cha} + e_{st}^{Shed} + r_t^{Dah} +$$
$$\sum_{\varepsilon\in\mathcal{T}^{\mathcal{E},\mathcal{A}gg}} \Big[ET^{\mathcal{E},Agg}(z_{s\varepsilon t}^{Up} + z_{s\varepsilon t}^{Down}) + e_{st}^{E} + m_{s\varepsilon t}^{E_{H2}}\gamma^{Aux} \Big] - \hat{E}_{st}^{Wind} - \sum_{b\in\mathcal{B}} e_{sbt}^{B,Dis} - e_{st}^{F}, \quad s\in\mathcal{S}, t\in\mathcal{T}^{D+1},$$

$$\hat{E}_{st}^{Wind} + \sum_{b\in\mathcal{B}} e_{sbt}^{B,Dis} + e_{st}^{F} = r_{st}^{Dah} + e_{st}^{Shed} + \theta_{st}^{+} + \sum_{b\in\mathcal{B}} e_{sbt}^{B,Cha} +$$
$$\sum_{\varepsilon\in\mathcal{T}^{\mathcal{E}}} \Big[ET^{\mathcal{E}}(z_{s\varepsilon t}^{Up} + z_{s\varepsilon t}^{Down}) + e_{st}^{E} + m_{s\varepsilon t}^{E_{H2}}\gamma^{Aux} \Big], \qquad s\in\mathcal{S}, t\in\mathcal{T}^{H+1},$$

$$\Delta_{st}^{Int+} = r_{st}^{Int+} - \theta_{st}^{+}, \qquad s\in\mathcal{S}, t\in\mathcal{T}^{H+1},$$

$$r_{st}^{Int+} = \frac{1}{|\mathcal{S}|}\sum_{k\in\mathcal{S}} r_{kt}^{Int+}, \qquad s\in\mathcal{S}, t\in\mathcal{T}^{H+1},$$

$$r_{st}^{Int-} = \frac{1}{|\mathcal{S}|}\sum_{k\in\mathcal{S}} r_{kt}^{Int-}, \qquad s\in\mathcal{S}, t\in\mathcal{T}^{H+1},$$

$$\big[\boldsymbol{\Omega_1(x)}\big]^T \le \big[\mathbf{0}\big]^T,$$
$$\big[\boldsymbol{\Omega_2(x)}\big]^T = \big[\mathbf{0}\big]^T,$$
$$\big[\boldsymbol{\Omega^{\mathcal{X}}(x)}\big]^T = \big[\mathbf{0}\big]^T,$$
$$\boldsymbol{\Upsilon^{E}(x)} \in \{0,1\},$$
$$\boldsymbol{\Upsilon^{Int}(x)} \in \{0,1\},$$
$$\Delta_{st}^{Dah} \ge 0, \qquad s\in\mathcal{S}, t\in\mathcal{T}^{D+1},$$
$$\Delta_{st}^{Int+}, \theta_{st}^{+} \ge 0, \qquad s\in\mathcal{S}, t\in\mathcal{T}^{H+1}.$$

6.10 Subproblems with First-Stage Intraday Decisions

Subproblems starting in time period *hh:45 - h[h+1]:00*, finds the first-stage intraday decisions over $\mathcal{T}^{H+1}$.

$$\max \sum_{s\in\mathcal{S}} p_s \left[I_s^{H2} + I_s^{Dah} + NI_s^{Int} + \overline{DC}_s + DC_s^{Int+} + C_s^{Shed} + C_s^{B} \right],$$

$$\hat{E}_{st}^{Wind} + \sum_{b\in\mathcal{B}} e_{sbt}^{B,Dis} + e_{st}^{F} = r_{st}^{Dah} + e_{st}^{Shed} + \theta_{st}^{+} + \sum_{b\in\mathcal{B}} e_{sbt}^{B,Cha} + \sum_{\varepsilon\in\mathcal{T}^{\mathcal{E}}} \left[ET^{\mathcal{E}}(z_{s\varepsilon t}^{Up} + z_{s\varepsilon t}^{Down}) + e_{st}^{E} + m_{s\varepsilon t}^{E_{H2}} \gamma^{Aux} \right], \qquad s\in\mathcal{S}, t\in\mathcal{T}^{H+1},$$

$$\Delta_{st}^{Int+} = r_{st}^{Int+} - \theta_{st}^{+}, \qquad s\in\mathcal{S}, t\in\mathcal{T}^{H+1},$$

$$r_{st}^{Int+} = \frac{1}{|\mathcal{S}|} \sum_{k\in\mathcal{S}} r_{kt}^{Int+}, \qquad s\in\mathcal{S}, t\in\mathcal{T}^{H+1},$$

$$r_{st}^{Int-} = \frac{1}{|\mathcal{S}|} \sum_{k\in\mathcal{S}} r_{kt}^{Int-}, \qquad s\in\mathcal{S}, t\in\mathcal{T}^{H+1},$$

$$\left[\boldsymbol{\Omega_1}(\boldsymbol{x})\right]^T \leq \left[\mathbf{0}\right]^T,$$

$$\left[\boldsymbol{\Omega_2}(\boldsymbol{x})\right]^T = \left[\mathbf{0}\right]^T,$$

$$\left[\boldsymbol{\Omega}^{\mathcal{X}}(\boldsymbol{x})\right]^T = \left[\mathbf{0}\right]^T,$$

$$\boldsymbol{\Upsilon}^{\boldsymbol{E}}(\boldsymbol{x}) \in \{0,1\},$$

$$\boldsymbol{\Upsilon}^{\boldsymbol{Int}}(\boldsymbol{x}) \in \{0,1\},$$

$$\Delta_{st}^{Int+}, \theta_{st}^{+} \geq 0, \qquad s\in\mathcal{S}, t\in\mathcal{T}^{H+1}.$$

6.11 Subproblems without First-Stage Decisions

Subproblems that are purely modeling recourse decisions is reprsented by the complete formulation

$$\max \sum_{s\in\mathcal{S}} p_s \left[I_s^{H2} + I^{Dah} + NI_s^{Int} + \overline{DC}_s + C_s^{Shed} + C_s^{B} \right],$$

$$\left[\boldsymbol{\Omega_1}(\boldsymbol{x})\right]^T \leq \left[\mathbf{0}\right]^T,$$

$$\left[\boldsymbol{\Omega_2}(\boldsymbol{x})\right]^T = \left[\mathbf{0}\right]^T,$$

$$\left[\boldsymbol{\Omega}^{\mathcal{X}}(\boldsymbol{x})\right]^T = \left[\mathbf{0}\right]^T,$$

$$\boldsymbol{\Upsilon}^{\boldsymbol{E}}(\boldsymbol{x}) \in \{0,1\},$$

$$\boldsymbol{\Upsilon}^{\boldsymbol{Int}}(\boldsymbol{x}) \in \{0,1\}.$$

CHAPTER

SEVEN

IMPLEMENTATION AND INSTANCE GENERATION

The implementation phase encompasses various aspects, which are explored in this chapter. The technical parameter values of the components in the energy system are highlighted in Section 7.1. Section 7.2 gives an overview of the technical parameter model data and its implementation in the rolling horizon framework. Hydrogen prices are described briefly in Section 7.3. Subsequently, an overview of the data sets used for electricity prices is provided in Section 7.4. To generate forecasts for electricity market prices, we demonstrate the forecast procedure along with relevant model statistics. Section 7.5 presents the implementation process for wind power data, including the generation of wind power forecasts and the creation of wind power generation scenarios. In Section 7.6, we delve into the computational study, discussing all the test instances that were conducted. In Section 7.7, we provide details about the hardware and software utilized for the test instances, and also discuss solver attributes.

7.1 Technical Data on System Components

7.1.1 Electrolyzer Data

The energy system needs to accommodate the maximum power generation by the wind farm, necessitating a combined capacity of 1 000 MW for the electrolyzers and the transmission cable. As a default configuration, both the electrolyzers and transmission cables have individual ratings of 500 MW each. 500 MW is used as a base value for electrolysis to determine the minimum and maximum capacity ratings, and the energy cost from startup and shutdown processes per electrolyzer unit. In addition, the modeling sets $\mathcal{E}$ and $\mathcal{E}^{Agg}$ requires adjustments in the capacities. When in a producing state there is a minimum energy requirement to operate the electrolyzers (Andrenacci et al., n.d.). This lower limit is approximated by setting the minimum energy consumption to 10 % of the rated capacity, which translates to 0.625 MWh as a lower limit, and 6.25 MWh as an upper limit for $\mathcal{E}$. For the set $\mathcal{E}^{Agg}$, the minimum and maximum bounds are 1.25 MWh and 12.5 MWh. The energy consumption during transitions is taken to be the average of the energy consumption between being idle and when operating at the minimum capacity, under the condition that these processes are linear. This implies that startup and shutdown require 5% of the rated capacity, which implies that electrolyzers in $\mathcal{E}$ require 0.03125 MWh and electrolyzers in $\mathcal{E}^{Agg}$ require 0.625 MWh when starting up or shutting down. The determine the conversion rate between electrolyzer power supply and hydrogen output, the nonlinear relationship in Figure A.2 has been approximated as a linear curve $y = ax + b$ and then determining a and b. The Higher Heating Value (HHV) for hydrogen is assumed to be 0.039772 MWh/kg, according to Jiang et al. (2021).

Reading of the chart of Figure A.2, $b \approx 0$ and $a \approx 0.64$. Equation (6.12) and (6.13) become,

$$e^E_{s\varepsilon t} = \frac{HHV^{H2}}{0.64} m^{E_{H2}}_{s\varepsilon t}, \qquad s \in \mathcal{S}, \varepsilon \in \mathcal{E}, t \in \mathcal{T}^{\mathcal{E}}. \quad (7.1)$$

$$e^E_{s\varepsilon t} = \frac{HHV^{H2}}{0.64} m^{E_{H2}}_{s\varepsilon t}, \qquad s \in \mathcal{S}, \varepsilon \in \mathcal{E}^{Agg}, t \in \mathcal{T}^{\mathcal{E}^{Agg}}. \quad (7.2)$$

Reformulation of Nonlinear Constraints

The current electrolyzer formulation is nonlinear because of the startup penalty in Equations (6.1) and (6.3). Both constraints are reformulated in order to keep the model linear. A product of two binary variables σ_1, σ_2 is reformulated into a linear equivalent by introducing a third binary variable x, demonstrated in Equations (7.3) - (7.5).

$$\sigma_1 \cdot \sigma_2 = x, \quad (7.3)$$

$$\sigma_1 + \sigma_2 \geq 2x, \quad (7.4)$$

$$\sigma_1 + \sigma_2 \leq 1 + x. \quad (7.5)$$

Equations (6.1) and (6.3) in linear form becomes,

$$e^E_{s\varepsilon t} \leq \Gamma^{E,Max}(\delta^E_{s\varepsilon t} - \frac{1}{2} x^E_{s\varepsilon t}), \qquad s \in \mathcal{S}, e \in \mathcal{E}, t \in \mathcal{T}^E. \quad (7.6)$$

$$e^E_{s\varepsilon t} \leq \Gamma^{E,Max}(\delta^E_{s\varepsilon t} - \frac{1}{2} x^E_{s\varepsilon t}), \qquad s \in \mathcal{S}, e \in \mathcal{E}^{Agg}, t \in \mathcal{T}^{E,Agg}. \quad (7.7)$$

7.1.2 Pipeline Storage and Transportation Data

Equation (7.1) has been used to determine the maximum hydrogen production given 1 000 MW electrolyzer capacity. It seems reasonable to assume that the pipeline would be dimensioned for the highest possible power generation of the energy system, which is the installed capacity of 1 000 MW. This could be the outcome if the energy system was not integrated with the power markets. Furthermore, it has been considered reasonable to assume that the maximum rate of charge/discharge can be scaled simply as a function of time. Maximum hydrogen production in terms of mass per time unit is thereby calculated as 4022.931 kg/quarter, 16 091.723 kg/h, 386 201.348 kg/day and 140.963 kton/year. This is according to Wind and Gas (2020) equivalent to a pipe size of approximately 12 inches (30.48 cm) in diameter, which is also in accordance with the work of Khan et al. (2021). Andersson and Grönkvist (2019) state that a pipeline with diameter $D_2 = 1.4$ m could store 12 tons of hydrogen per km of pipeline. The storage capacity of a 12 inch pipeline is found by comparing the cross sections of pipelines with diameters 12 inch and 1.4 m, and their respective cross sections are given by Equation (7.8) and (7.9).

$$\frac{\pi \cdot D_1^2}{4} = 0.0730 m^2, \quad (7.8)$$

$$\frac{\pi \cdot D_2^2}{4} = 1.539 m^2. \quad (7.9)$$

Since the pipeline of 1.4 m diameter could store 12 tonnes of hydrogen per 1000 m, the pipeline storage capacity for this project can be calculated as shown in Equation (7.10)

$$\frac{0.0730}{1.539} \cdot 12 t/km = 0.569 t/km. \quad (7.10)$$

The location of the exiting end of the pipe is uncertain, but a pipeline length of approximately 217.5 km could allow for several possible locations along the coast of Southern Norway. This is

valid under the assumption that the pipeline is roughly the same length as the distance measured on a map, although it would be somewhat longer in real life. With a pipeline of length 217.5 km, the capacity of the pipeline can be estimated to approximately 123.8 tonnes. There are many factors that affect the true storage capacity such as distance, pressure, temperature etc. The approximation made here does however provide a sufficiently good estimate of the dimension of the storage capacity. With 500 MW electrolyzers capacity at full production (2011.465 kg/quarter), the energy system can produce at full capacity for 14.1 hours without discharging until the pipeline is full. According to Khan et al. (2021), the energy system in our case study exhibits an outlet pressure of approximately 18 bar. Reducing the outlet pressure below this threshold would result in an increased mass flow rate. Although theoretically, the output pressure could be reduced to 0 bar, it is more practical to consider atmospheric pressure (1 bar) as the minimum viable pressure. Consequently, the discharge rate may exceed 4022.931 kg per time step Khan et al. (2021). Furthermore, Khan et al. (2021) elucidates that the gas flow rate is proportional to the square root of the difference between the squares of the input and output pressures. Specifically, when the output pressure is set at 1 bar, the gas flow rate experiences a marginal increase of less than 4% compared to an output pressure of 18 bar. Therefore, it is reasonable to assume a charge/discharge rate of 4022.931 kg per time step, given the specified dimensions. Additionally, based on the findings in Section 4.3.2, leakage losses are assumed to be 0.5%, implying a hydrogen transfer efficiency of 99.5%.

7.1.3 Fuel Cells Data

Ballard (n.d.) is among many companies that provide fuel cell modules specifically certified for marine applications, including vessel transportation. These modules exhibit a fuel peak efficiency of 56 % and possess the flexibility to be scaled from a modest 0.2 kW system to several MWs. PowerCellution (n.d.) also offers systems that have been meticulously designed and developed in compliance with maritime regulations. Their fuel cells demonstrate a net energy output of 200 kW, with reported fuel efficiency reaching 54 %. The peak efficiency is not reported for maximum operating capacity. It is expected that the fuel cells will most likely be in full operation when activated, a lower efficiency is deemed more appropriate. Reading from the graph in Figure A.3 in the Appendix, which reports the efficiency and specific fuel consumption of their offered fuel cells. The specific fuel consumption is taken to be 65 g/kWh, which translates to 0.01548 kg/MWh. Considering the requirement for backup energy, the clustered fuel cell capacity is rated 40 MW, as the fuel cell system will function in parallel with the batteries. The fuel cell modules are interconnected in parallel and collectively treated as a single container unit, capable of delivering 10 MWh per specified time period.

7.1.4 Battery Data

Based on consultations conducted with battery experts regarding battery characteristics, the system incorporates five battery packages with a total capacity of 40 MW. The BESS consists of containerized lithium-ion batteries arranged in a 40 ft. rack configuration (ECO Power, n.d.). These units can be connected in parallel to achieve the desired overall capacity. Considering the variable nature of wind power, a capacity of 40 MW is considered a reasonable smoothing capacity for the batteries (personal communication with Hydepoint in the fall, 2022). To meet the requirement of complete charging or discharging within a specific time period, the batteries have a C-rating of 4. This corresponds to an aggregate maximum charge and discharge rate of 10 MWh per time period, and 2 MWh for each battery. According to Schimpe et al. (2018), stationary lithium-ion battery containers exhibit a round-trip efficiency of 70-80 %. Although the batteries themselves exhibit high energy conversion efficiencies, auxiliary equipment significantly contributes to energy losses at lower utilization rates. Considering the harsh marine environment in which the batteries are situated, extensive auxiliary systems are expected to ensure safe operation. It is, however, worth noting that batteries have been and continue to be extensively researched, with lithium-ion battery efficiencies anticipated to improve in the future. An appropriate value of round-trip efficiency is taken to be 0.85. The value of λ^B is determined to be 100 EUR/kg based on pretesting of the

model and observing the charge and discharge patterns.

7.1.5 Auxiliary Systems Data: Desalination and Compression

Cummins (2021) reports that electrolyzers require 9 litres of water per kg of hydrogen. This corresponds to an 11.11 % hydrogen recovery per kilogram of water. Ghaffour et al. (2013) reports that the total energy required to desalinate 1 m^3 of water is 10-16 kWh. Assuming an optimistic value of 10 kWh, this results in a SEC per kg hydrogen produced in the desalination system as 0.0009 MWh/kg. Considering the available technology and the possibility of further advancements of MSF, particularly in reheating, the achieved SEC reported in the next decade is probably even lower. It makes, therefore, sense to assume that the more efficient systems today will soon be average performing in the end of the decade. Khan et al. (2021) found that the input pressure in the pipeline was set to 70 bar in the analysis of optimal pipeline design. By fixing the pipe inlet pressure to 70 bar the SEC of the compressor will be constant as the pressure ratio between the compressor inlet and outlet pressure is constant. PEMEL have an output pressure, which is the inlet pressure to the compressor, of 30 bar (Cummins, 2021; Nel Hydrogen, 2021). With the assumptions of adiabatic compression and pipeline inlet pressure fixed at 70 bar, which is the compressor output pressure, compressor SEC of 0.7972 kWh/kg can be read from Figure 5.2. In practice, mass flow is adjusted by changing the pressure difference between input and output pressure in a pipeline. Thus, both pipe inlet and outlet pressure could be adjusted to find optimal SEC for a given state, but this is out of the scope of this project.

7.1.6 Power Transmission Data

The examined energy system is interconnected with the onshore power grid via a transmission line that has a capacity of 500 MW. This capacity corresponds to a power transfer capability of 125 MWh during each time step. Based on the studied articles in Section 4.3.2, the total energy losses associated with the power transfer process are set at 5%, resulting in a transfer efficiency of 95%.

7.2 Model Data

This section describes the process and result of model data generation and its implementation in the rolling horizon framework. System parameter estimation relies on guidance provided by industry experts and information from literature studies. Hydepoint, the industrial partner providing technical support in this work, encouraged a 50 % split between transmission and electrolyzer capacity for the system configuration. Key design parameters are given in Table 7.1.

Table 7.1: Key technical parameters of the system design.

System parameter	Value	Unit
Electrolyzer installed capacity	500	[MW]
Power transmission installed capacity	500	[MW]
Fuel cell installed capacity	40	[MW]
Battery installed capacity	40	[MW]
Pipeline installed capacity	123 800	[kg]

To accommodate the 15-minute time granularity, the design parameters of various components need to be adjusted. This involves properly distributing the capacity among the units in the

electrolyzer and battery sets. These additional design parameter values can be found in Table A.1 in the Appendix.

7.2.1 Boundary Conditions

Boundary conditions must be specified for the first problem instances that provide day ahead commitments to the first subproblem in the rolling horizon. Also, the mathematical models in the algorithm require input boundary conditions, at $t = 0$. The initial values are related to the operational status of electrolyzers, hydrogen storage amount in the pipeline and battery state of charge. The initial values are shown in Table A.7, also found in the Appendix.

7.3 Hydrogen Price

Prices in the current hydrogen market can range from 10 EUR/kg to 60 EUR/kg (Jovan & Dolanc, 2020). These prices are however not necessarily reflective of future market prices as a hydrogen economy is not yet established and still relatively high production costs. The optimization model presented in this thesis assumes a fixed unit price for hydrogen. This is, as described in 5.2 due to long-term HPAs that are expected. Several authors have studied the production costs of hydrogen. Long-term productions costs could according to economic theory provide a basis for long-term prices. Maggio et al. (2019) report that production costs ranging from 2 to 20 EUR/kg have been used in research literature. Dinh et al. (2021) found that for their configuration of an offshore energy system was only financially viable for hydrogen prices above 5 EUR/kg. There are however several costs that the work in this thesis does not consider, as opposed to other literature that considers overall profitability and investment decisions. Initial testing and observation of preliminary results during the development of the model suggested that a hydrogen price of 4 EUR/kg could be reasonable starting point. Thus, the hydrogen price is set at 4 EUR/kg the base case.

7.4 Electricity Prices

The data regarding electricity prices for bidding zone NO2 in the calendar year 2022 has been gathered from both Nord Pool's public website and through private access to Nord Pool's database. Prices are reported on an hourly basis for this particular bidding zone. In order to align with the time granularity of 15 minutes, prices are duplicated across all time periods within each hour. The implementation of electricity markets is discussed in the subsequent sections, starting with the day-ahead market followed by the intraday market. Regression models for day-ahead and intraday prices are constructed using the Julia software and leveraging the "GL.jl" library.

7.4.1 Day Ahead Market Data and Price Forecast

We examine the average value, variance, and standard deviation of the day-ahead prices per hour. The day-ahead price for the third hour on 28.03.2022 is missing, and it has been replaced with the average value of the prices for the corresponding hour of the previous and next day. Upon initial investigation of the data set, clear seasonal patterns are evident, as depicted in Figure 7.1.

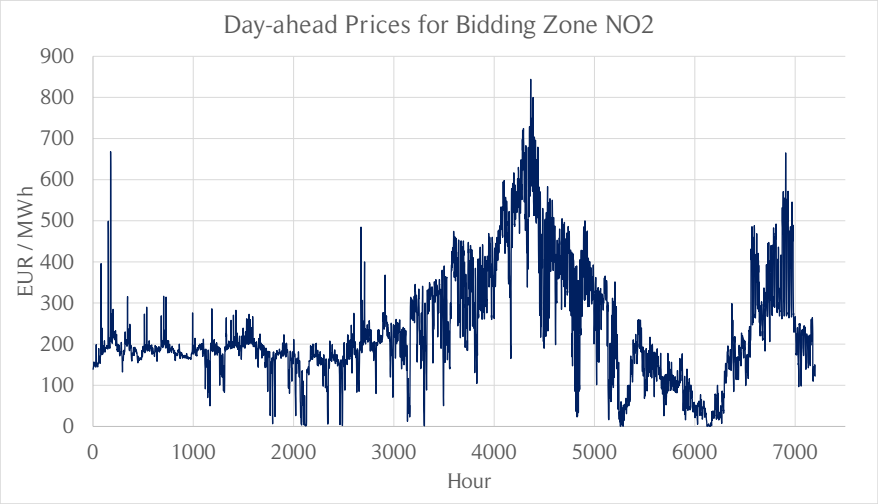

Figure 7.1: Reported Day-ahead prices for the calendar year of 2022 by Nord Pool.

A comparison of the average day-ahead prices are found in Figure A.4 in the Appendix. It is apparent that the price variation does not follow a typical pattern associated with the seasons. The prices exhibit abnormally high prices during the summer, which can be attributed to the energy crisis resulting from the energy deficit in Europe following the invasion of Ukraine. It is worth noting that from the seasons' definition and the provided data set, there is a smaller amount of data available for the winter months compared to the other seasons, as data from January and February 2023 is not included in the winter month's data set. However, even with this limitation, the highest prices are still observed in December although prices during the summer months are exceptionally high. Since we are studying a relatively short time frame in the optimization model, these effects are assumed to have an negligible impact. Additionally, a weekday effect is observed in the data set, illustrated by Figure A.5 in the Appendix, as weekdays generally exhibit higher prices compared to weekends.

The implementation of the expert-class auto-regressive model described in Equation (5.1) is carried out and tested using the complete data set. A summary of model performance is provided in Table 7.2, while Table 7.3 presents the statistical properties of the explanatory parameters. The auto-regressive model developed for this data set explains 81.3 % of the variance in day-ahead prices in the first hour, which is sufficient precision for modeling. As observed in Figure 7.2 the auto-regressive structure predicts the spot prices relatively well. The prices are continuously updated for each subproblem, considering both the time periods with certain prices, denoted as $\bar{\mathcal{T}}^{Dah}$, and the time periods with uncertain prices, denoted as $\hat{\mathcal{T}}^{Dah}$, as illustrated in Figure 6.1. For every subproblem, the price vector is updated, and after the market clearing at 13:00 CET, actual prices for day *D+1* are included in $\bar{\mathcal{T}}^{Dah}$. This approach allows the wind power producer to submit bids based on a forecast of the day-ahead prices, which adds an element of realism to the modeling process. When the respective time periods are solved, the wind power producer receives payment based on the actual price, not the forecasted price used in the self-bidding process.

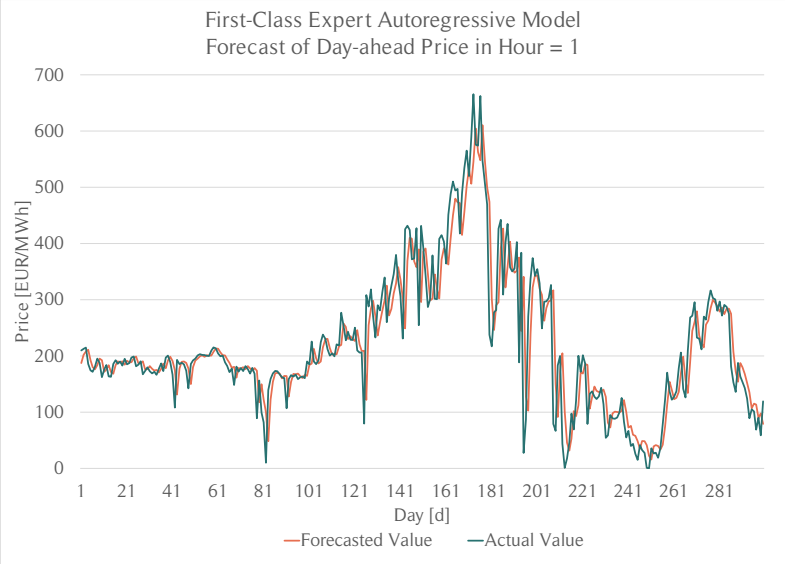

Figure 7.2: Results from autoregressive structure with lags *D-1*,*D-2* and *D-7* trained on the complete data set. Similar models are developed for each hour of the day.

Table 7.2: Regression statistics of the developed auto-regressive model developed to predict day-ahead prices for hour 1.

Multiple R	R squared	Adjusted R square	Standard error	Observations
0.902 %	0.813	0.811	53.937	300

Table 7.3: Statistical properties of the regression parameters in the model used to predict day-ahead prices for hour 1.

	Coefficients	Standard Error	t Stat	P-value	Lower 95%	Upper 95%
$\beta_{1,0}$	13.692	6.783	2.019	0.0444	0.343	27.042
$\beta_{1,1}$	0.682	0.057	11.890	0.000	0.569	0.795
$\beta_{1,2}$	0.182	0.060	3.018	0.003	0.063	0.300
$\beta_{1,3}$	0.072	0.039	1.830	0.068	-0.005	0.150

7.4.2 Intraday Market Data and Price Forecast

The data set used for intraday prices does not include day-ahead data for the 25th of February 2022. To ensure the integrity of the data set, only data from the 26th of February 2022 onwards has been utilized. The data set is then divided into separate files for selling and purchasing transactions between bidding zone NO2 and other bidding zones. In each data set, the average price and traded volume are calculated. Some hours in the calendar year have negative prices, which are replaced with zeros. The calendar year contains several hours where no price information is available. This leads to discontinuities in the data set, as depicted in Figures A.6 and A.8 found in the Appendix. It is important to note that this does not indicate a price of zero if trades were to occur, but rather reflects the reporting format. In order to maintain consistency within the data set, the open source library *Impute.jl* in Julia software is utilized to interpolate and generate intraday prices for all the missing hours. The modified data set, highlighting the interpolated data, is illustrated in Figures 7.3 and 7.4 below. Due to tail-effects resulting from the interpolation, the data set is restricted to include data from the 1st of March 2022 until the 23rd of December 2022. To ensure consistency between the day-ahead and intraday markets, only spot prices for the corresponding time periods are included.

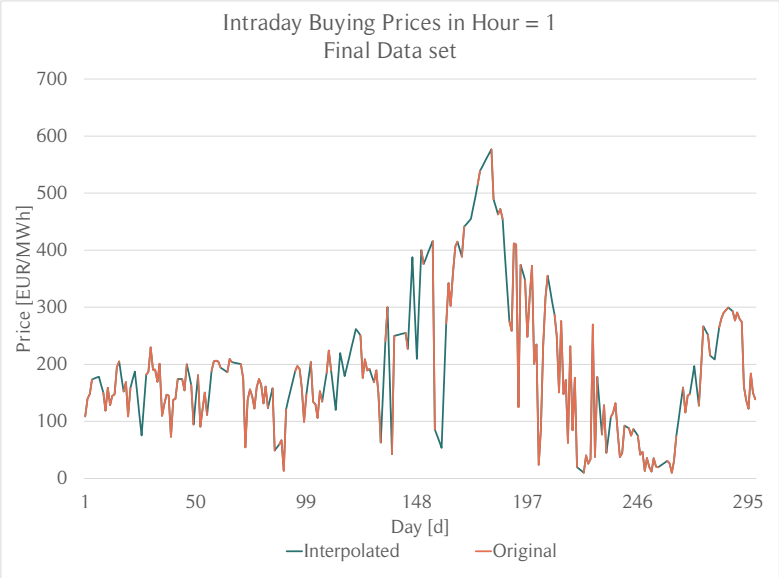

Figure 7.3: Final time-series after recombining the original intraday buying prices time-series and the interpolated time-series for 01.03.22 - 23.12.22

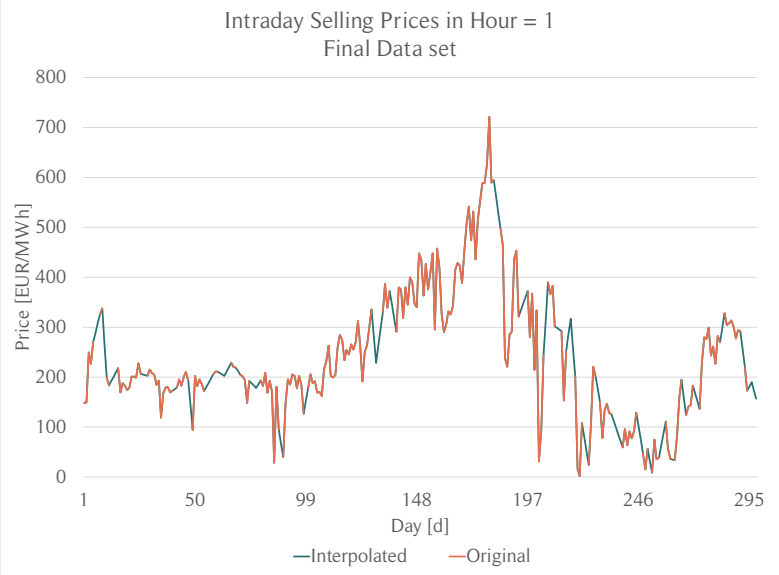

Figure 7.4: Final time-series after recombining the original intraday selling prices time-series and the interpolated time-series for 01.03.22 - 23.12.22

The intraday prices data set reveals interesting observations. Figure A.10, found in the Appendix, illustrates the difference between day-ahead and intraday selling prices. In the earlier months of 2022, intraday selling prices tend to be lower than day-ahead prices. However, during the autumn months, intraday selling prices surpass day-ahead prices. Conversely, the buying prices exhibit a similar pattern, with higher values compared to day-ahead prices in the autumn months, and lower values in the earlier months.

Comparing the total traded volumes between intraday and day-ahead markets reveals a significant difference. The total volume traded intraday (selling) represents only 1.3% of the day-ahead market volume. The largest disparity occurs on the 15^{th} of March 2022, with intraday trading volume at 551.1 MWh compared to the day-ahead volume of 201,402.30 MWh. Similarly, the total purchased volume on the intraday market for the calendar year only accounts for 1.54% of the day-ahead market volume. The most substantial difference occurs on the 7^{th} of December 2022, with an intraday volume of 1842.6 MWh compared to the day-ahead volume of 116,093.8 MWh. To visualize the day-to-day variations between the markets, the reader is referred to Figures A.12

for sales and A.13 for purchases, both found in the Appendix.

The auto-regressive model, as described in Equation (5.2), is utilized to forecast intraday prices. Table 7.4 reports the regression statistics, showcasing its ability to explain 90.4% of the variation in intraday selling prices for the first hour of the day. Both explanatory variables demonstrate statistical significance, highlighting the strong correlation between the intraday price and the corresponding day-ahead price for the corresponding hour. To visualize the model's performance, Figure 7.5 plots the predicted intraday selling prices against the actual observed prices for the first hour of the day throughout the year.

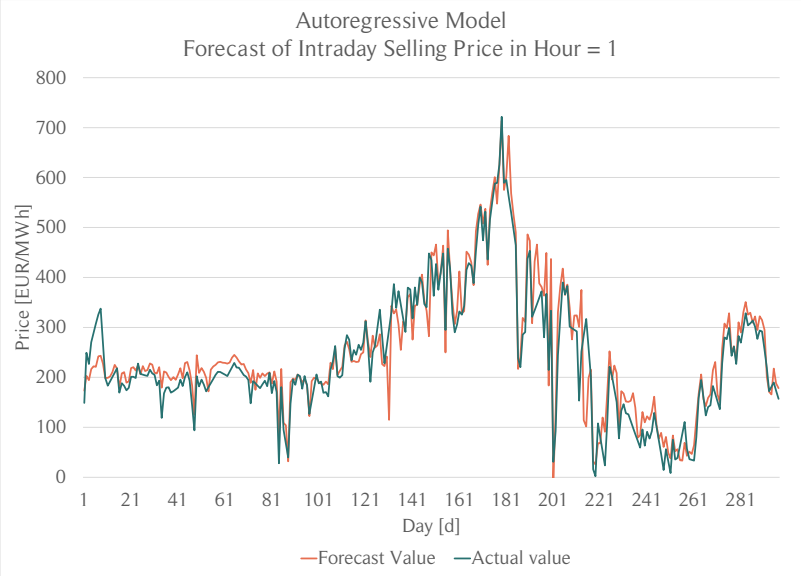

Figure 7.5: Results from auto-regressive structure developed for predicting intraday sales prices and trained on the complete data set. The graph illustrates the prediction of prices in the first hour of the day. Similar models are developed for each hour of the day.

Table 7.4: Regression statistics on the auto-regressive model developed to predict intraday selling prices for hour 1.

Multiple R	R squared	Adjusted R square	Standard Error	Observations
0.951	0.904	0.903	38.832	297

Table 7.5: Statistical properties of the regression parameters in the auto-regressive model used to predict intraday selling prices for hour 1.

	Coefficients	Standard Error	t Stat	P-value	Lower 95%	Upper 95%
$\alpha_{1,0}$	28.040	4.682	5.988	0.000	18.825	37.256
$\alpha_{1,1}$	0.215	0.043	5.031	0.000	0.131	0.299
$\alpha_{1,2}$	0.949	0.019	51.262	0.000	0.912	0.985

7.5 Wind Forecasting and Scenario Generation

The model presented in this work uses wind power scenarios to model stochasticity. Scenarios of future wind power production must therefore be generated. The central steps to generate wind power scenarios are described here. Firstly, the wind data used in this thesis is presented. Subsequently, a description of the wind forecasting and quantile forecasting techniques are given. Finally, the wind power scenario generation method is presented.

7.5.1 Wind Data

The data used in this thesis is acquired from The Norwegian Meteorological Institute (MET Norway). MET Norway provides NWP forecast products for large parts of Northern Europe, especially in Scandinavia. The particular product used in this thesis is the MET Nordic dataset. More specifically, the historical forecasts derive from the *MET Nordic operational archive* and the historical weather data derives from the *MET Nordic rerun archive version 3*. The dataset contains a large variety of information on historical forecasts and post-processed data on historic weather with one hour resolution (MET Norway, 2023). Forecasts are available every 6^{th} hour with forecast horizons longer than 36 hours. Analyses of weather parameters are available every hour. Ideally, power production data from an actual offshore wind would be used as historical data. This is however not easily accessible due to the low amount of wind farms far offshore. The estimated and analyzed data from MET Norway is a substitute for this data.

The dataset has a grid resolution of 1 km and data was extracted for the closest grid point to 57°00'00.0"N 4°00'00.0"E. The extracted parameters are historical wind speeds and historical forecasts of wind speeds between for 2021 and 2022. These parameters are however given for a height of 10 meters, and offshore wind turbines are over 100 meters tall. Thus, all the extracted data has been scaled up from 10 to 100 meters with a method used by Solbrekke and Sorteberg (2022). The method is given by Equation (7.11), where $\alpha(t)$ is the hourly varying exponential power law coefficient, and where $v_{h_2}(t)$ and $v_{h_1}(t)$ are recorded wind speeds at heights h_2 and h_1 for a given time t, respectively.

$$v_{h_2}(t) = v_{h_1}(t) \left(\frac{h_2}{h_1} \right)^{\alpha(t)}, \tag{7.11}$$

The dataset made available in their work contains monthly values of the alpha exponent in the period of 1996 to 2019 (288 values). This study period is however not the same as the data set from MET Norway, and the exponential alpha cannot therefore not be applied directly to the MET Nordic dataset. The exponential alpha values for 1996 to 2019 were averaged in order to create 12 exponential alpha values, one for each month. Thus, historical data and historical forecasts made in month n were scaled with the corresponding exponential alpha value shown in Table A.5 found in the Appendix. A turbine curve converts wind speed to wind power for a given turbine. The turbine curve was empirically fitted with data from the dataset used by Kächele et al. (2022).

7.5.2 Wind Forecasting

Several methods have been used in this thesis in order to produce wind power scenarios. Pinson et al. (2009) provided a comprehensive methodology to produce scenarios from historical data, and the scenario generation process in this thesis is based on this work. The process from historical data to scenarios can be divided into three major steps. The first step is the point forecasts, the second step is the quantile forecasts, and the third step is the scenario generation procedure.

Point forecast describes a single prediction of a future outcome. This forecast does not convey information about the distribution of the prediction error, which in many cases can be large. As stated in Section 4.2.2, Hanifi et al. (2020) recommend hybrid methods for the 36-hour time horizon this thesis considers. The forecasts in the database are updated every 6^{th} hour and are deterministic. The MET Norway Forecasts (MET-F) are in fact point forecasts of MET Norway best prediction of future weather. The historic MET-F used in this work are updated every 6^{th} hour. The value of real-time observations of realized wind speeds in this 6 hour period is not necessarily capitalized on as sudden unforeseen changes in wind speeds are not accounted for in the forecasting model. Prediction errors, especially in the short term, could thus be substantial as forecasts are not updated frequently.

Several authors have studied the performance of time series models for wind speed and wind power forecasting. Grigonytė and Butkevičiūtė (2016) developed an ARIMA(3,1,1) model to forecast wind power production with a time step of 1 hour and a forecasting horizon of 24 hours. Wang et

al. (2018) developed an ARMA(4,1) model with a time step of 15 minutes and a forecasting horizon of 24 hours. Based on relevant literature, an autoregressive model has been developed to provide point forecasts over the 36-hour time period. While the long-term forecast error is relatively large for AR models, these models have reportedly good performance in the short-term. AR models are also relatively easy to implement and has low computational complexity. The AR model was modelled with four lag terms. Bootstrapping has been applied to produce point forecasts after a study of the residuals.

For real-time applications, MET Norway provides through *MET Nordic operational real-time* hourly updated forecasts for the last three days. Furthermore, other third parties may potentially also be used to receive forecasts on an on-demand basis. This implies that the AR model used in this thesis would likely not be used in a real-life application. The AR was calibrated for a dataset with 15000 data points and the description of the AR(4) model is presented in Table 7.6. The AR model is used to forecast wind speed, and wind power values have been found with the empirically fitted turbine curve available from Kächele et al. (2022). The two forecasting methods are combined in a manner that is described in the next section.

Table 7.6: Statistical properties of the developed AR(4) forecasting model

	Coef.	**Std. Error**	**t**	**Pr(>|t|)**	**Lower 95%**	**Upper 95%**
Intercept	0.339	0.022	15.68	<1e-54	0.296	0.381
X1	1.039	0.008	127.26	<1e-99	1.023	1.055
X2	0.000	0.012	0.000	0.0283	-0.049	-0.003
X3	0.000	0.012	0.000	0.3377	-0.034	0.012
X4	0.000	0.008	0.000	<1e-05	-0.052	-0.020

7.5.3 Quantile Forecasting

Quantile forecasting is based on quantile regression models and have been used to quantify the prediction error of the point forecasts. Spline basis functions have been implemented in order to model the unknown non-linear relation between quantiles and forecasted power. In order to account for a growing prediction error, which naturally occurs for both AR forecasts and NWP forecasts, quantile parameters are computed for each individual horizon length. This approach might lead to a problem called quantile-crossing. Quantile-crossing is a phenomenon that can occur when quantiles are calculated individually, such as in this case. Constraints are added to prevent quantile-crossing in the training set. $\mathcal{Q}$ is the set of quantiles, $\mathcal{F}$ is the set of all forecasting length, and $\mathcal{S}$ is the set that contains all basis spline knots. Quantile estimators α and β are calibrated for a given quantile $\theta \in \mathcal{Q}$ and a given forecasting length $f \in \mathcal{F}$. y is the realized power value, x is the forecasted power value for the given forecasting horizon whilst $b(x)$ is the natural B-spline basis of x. The model is calculated over the training set $\mathcal{T}$. u and v are dummy variables used to linearize the minimization problem. q^- denotes the value of the previously calculated quantile and is activated after the first quantile for a given forecasting length has been calculated. The quantile model in this thesis can be formulated as the following linear minimization problem:

$$\text{minimize} \quad \sum_{t\in\mathcal{T}} \theta u_t + (1-\theta)v_t \tag{7.12}$$

$$\text{subject to} \quad y_t - [\alpha^p - \alpha^n] - \sum_{s\in\mathcal{S}} b_s(x_t)\,[\beta_s^p - \beta_s^n] = u_t - v_t, \qquad t \in \mathcal{T}, \tag{7.13}$$

$$\alpha^p - \alpha^n + \sum_{s\in\mathcal{S}} b_s(x_t)\,[\beta_s^p - \beta_s^n] \geq q^-, \qquad t \in \mathcal{T}, \tag{7.14}$$

$$\alpha^p, \alpha^n, \beta_s^p, \beta_s^n, u_t, v_t \geq 0, \qquad t \in \mathcal{T}, s \in \mathcal{S}. \tag{7.15}$$

α is defined as the difference between α^p and α^n, and β_s is found in the same manner. The optimization problem is solved for every quantile at every forecasting length, thus for every combination

of θ and f. Thus, the output from this procedure is estimators α for every $\theta \in \mathcal{Q}, f \in \mathcal{F}$ and β_s for every $\theta \in \mathcal{Q}, f \in \mathcal{F}, s \in \mathcal{S}$. The estimators are used to estimate the quantile forecast $q(\theta, f)$ given in Equation (7.16), where $b(x)$ is the natural B-spline basis of forecasted power values x using the same knots as in the parametrization of estimators.

$$q(\theta, f) = \alpha(\theta, f) + \sum_{s \in \mathcal{S}} b_s(x)\beta_s(\theta, f) \tag{7.16}$$

Estimation of regression estimators with the current formulation of the quantile regression model has a relatively high computational burden. Recalibration of $\alpha(\theta; f)$ and $\beta_s(\theta; f)$ at the beginning of every subproblem in the rolling horizon model would reduce the time budget of 15 minutes drastically. In order to reduce this computational burden, the quantile regression model has been made static. This implies that the parametrization of the regression estimators is conducted before the rolling horizon model is initiated. This could to some extent result in outdated regression estimators, particularly in cases of extensive rolling horizon iterations and large seasonal variations.

Quantile regression estimators were parameterized for AR forecasts and MET-F individually. The same dataset of 15000 data points used in the calibration of the AR(4) model was used for the parametrization of the quantile regression estimators. The basis spline knots ranged from 0 to 1 with 0.1 increments. The quantile forecasts generated from the two forecasting methods indicated that the MET Norway forecasts outperformed the AR-forecast in most cases. MET-F had superior medium and long-term performance as well as a better ability to predict large future shocks in power generation. However, while the MET-F predicted shocks to a greater extent, the AR model demonstrated a substantial ability to respond to shocks. The ability to react to unexpected large short-term variations in wind power production without large computational burdens could become particularly useful as the MET-F is updated every 6^{th} hour. Empirical observations of the resulting quantile curves for both models suggested that switching from the AR(4)-model to MET-F at a forecasting horizon of 4 hours could be sensible. A linear weighting scheme was implemented in order to avoid "unnatural shocks" in the merging of the two quantile forecasting models. The quantile forecasts of AR(4) and MET-F were weighted with a factor of 1-to-0 up until a forecasting horizon of 2 hours, 0.5-to-0.5 at 4 hours, and 0-to-1 at 6 hours and beyond. As previously mentioned, the main focus of this work is not to create the most accurate forecasting methods, but to have a reasonable set of scenarios to test the behaviour of the hydrogen production and trade system. The proposed hybrid forecasting method should be subject to in-depth statistical analysis, but this is not in the scope of this work. Figure 7.6 demonstrates quantile forecasts from 0 to 1 with 0.05 steps between quantiles.

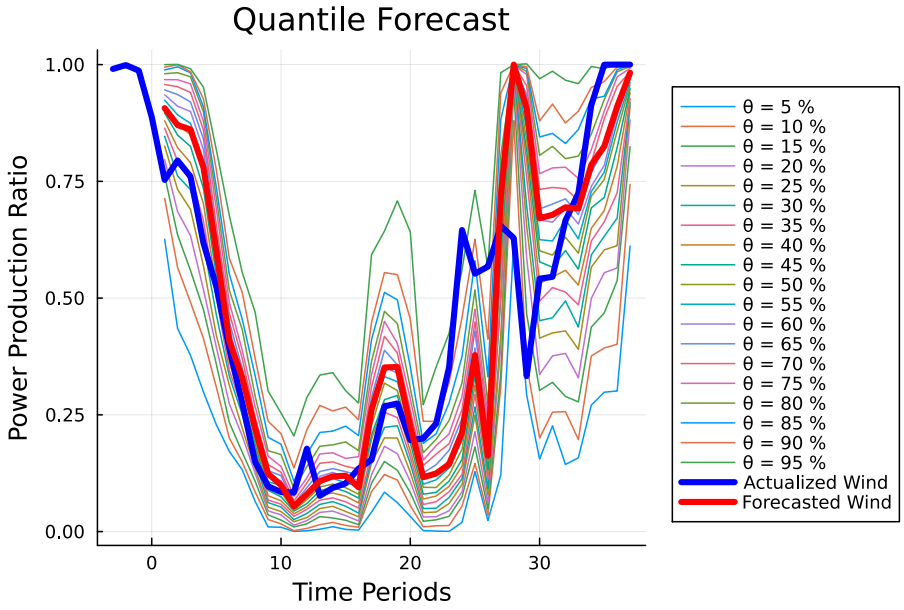

Figure 7.6: Quantile forecast for a 36-hour forecasting horizon

7.5.4 Wind and Power Scenario Generation

This section describes how historical observations and quantile forecasts are used to generate scenarios for the optimization model. Pinson et al. (2009) provides a method to generate scenarios from probabilistic forecasts of wind power generation. The method factors in the structural interdependence of forecasting error by introducing a multivariate Gaussian random variable. This variable is defined by zero mean and a continuously updated empirical covariance matrix. Furthermore, the method integrates the probabilistic distribution of forecasted power production to generate scenarios.

The probabilistic forecasts required in the method by Pinson et al. (2009) are in this case quantile forecasts. Quantile forecasts provide a nonparametric estimation of prediction intervals for future realizations of wind power. A collection of quantile forecasts be seen as a discrete probability distribution of possible outcomes. A curve can be fitted between each quantile and its corresponding estimated power value to create a cumulative distribution function F. This operation is done for every forecasting length. The cumulative distribution function denotes the probability of having a power level p or lower at a given time. The uniformly distributed random variable Y describes the possible return values of F, that are between 0 and 1. When Y is transformed into a normally distributed variable for an entire forecasting length, a multivariate Gaussian variable denoted as X is created. The multivariate Gaussian variable describes the interdependence between wind power values in a time-series. X is a vector of normally distributed variables and is defined by a vector of mean values μ and a covariance matrix Σ. The covariance matrix is recursively updated when new observations of power production are registered, and an exponential memory loss scheme has been applied in order to adjust for long-term variations. The recursive updating procedure proposed by Pinson et al. (2009) is shown in Equation (7.17), where X_t is the observation of the random variable X at time t which is used to update covariance matrix Σ_t with λ as the memory loss factor.

$$\Sigma_t = \lambda \left(\frac{t-2}{t-1} \right) \Sigma_{t-1} + \left(1 + \lambda \left(\frac{1}{t-1} - 1 \right) \right) X_t X_t^\top \tag{7.17}$$

An element-wise division of Σ by $\sigma\sigma^\top$, where the vector σ contains the square root of the elements in the main diagonal of Σ, is conducted to recalibrate the matrix. Scenarios are generated by using a multivariate Gaussian random number generator with μ and matrix Σ to obtain X. The steps described above are backtracked and the scenario generation method is summarized and contextualized in Figure 7.7. The accompanied code provides a more detailed description of how each step has been implemented as well as assumptions and adjustments that have been made.

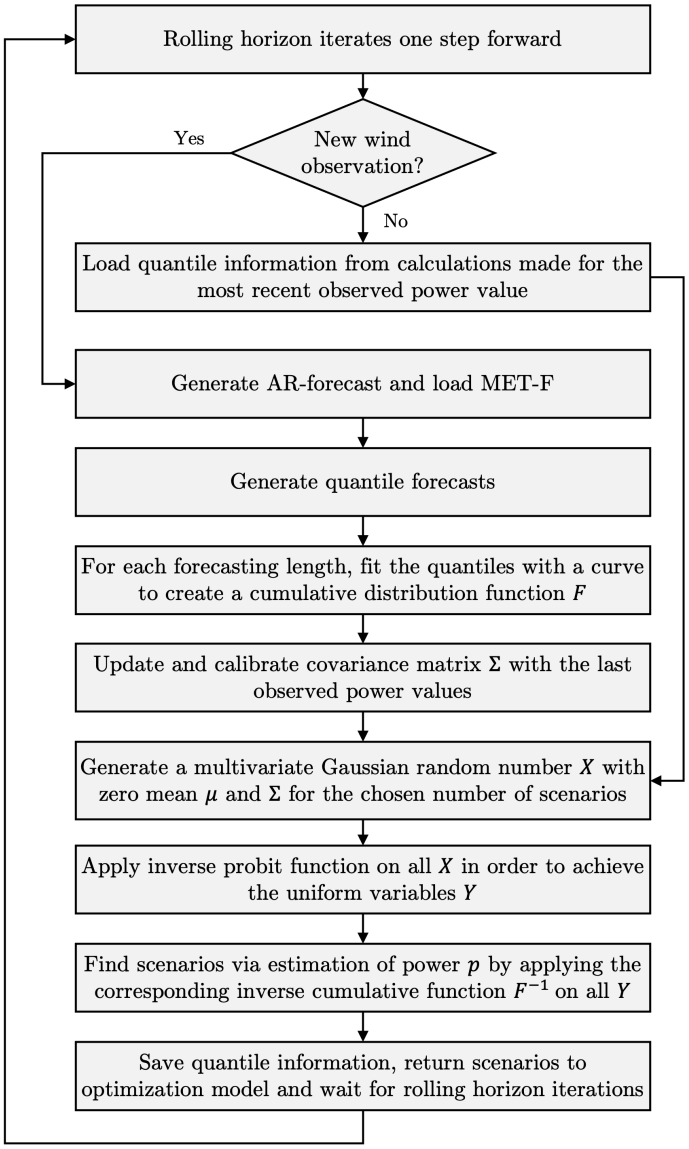

Figure 7.7: Map of the process flow of the scenario generation procedure

New scenarios are generated every quarter hour. As stated in Section 7.5.1, the dataset is of hourly resolution. This thesis considers an optimization problem with a time resolution of 15 minutes. The hourly data has been converted to quarter hour values after the completion of all forecast and scenario generation processes. The conversion was performed via the use of linear interpolation. The conversion could have been done before the forecasting and scenario generation processes, but this would create linear trends in the data that not necessarily exist. These trends would have been captured by the autoregressive model as well as in the parametrization of quantile estimators. Conversion after these processes was therefore considered to cause the least inaccuracy. The covariance matrix is therefore only updated once an hour due to the hourly resolution of the original dataset. Figure 7.8 shows the results of the scenario generation for 20 scenarios.

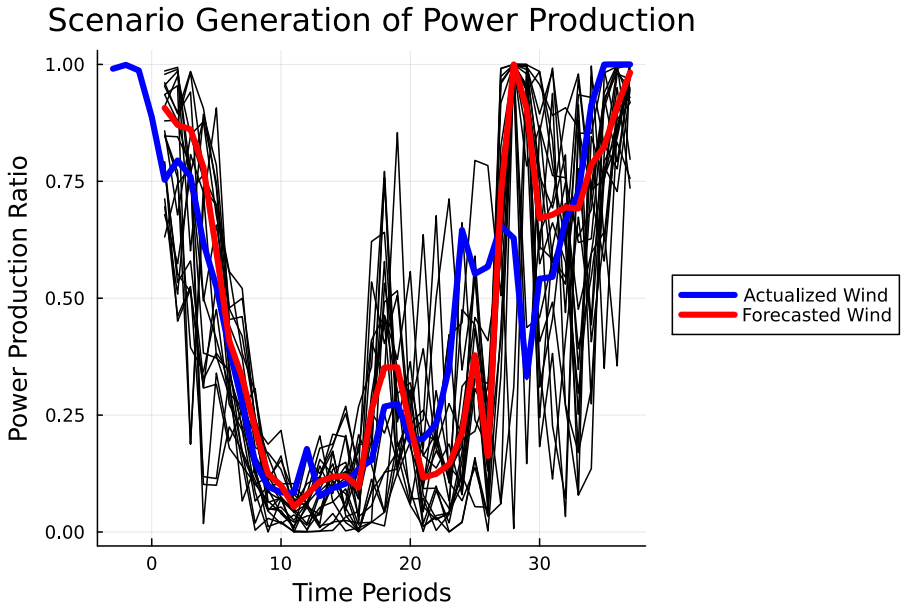

Figure 7.8: Scenario generation of 20 scenarios

7.6 Test Instance Generation

The key objectives of the computational study is to assess the value of using a stochastic formulation in regard to power market commitments and to study the behavior of the energy system. The modeling of the stochastic nature of wind power generation is complex and results in a substantial increase in problem size. In order to test the functionality and performance of the implemented model, several test instances are created to illuminate the optimal model design parameters given the available computational resources. Both model specific parameters and energy system parameters have been altered in the test instances in order to assess overall performance. Motivation and description of the test instances are accounted for in this section. Modeling parameters for the base case are described in Table A.6 in the Appendix. Technical parameters value of the base case model are given in Table A.1 in the Appendix. Initial values for all test instances are stated in Table A.7 in the Appendix. If not otherwise indicated, test instance parameters are the same as for the base case.

7.6.1 Seven Days Operation

The base case is studied over a seven day period. An extended global planning horizon reveals information on how the model performs over a longer time periods. Furthermore, this could also disclose characteristics on energy system behaviour that is can not be captured over shorter planning horizons. Furthermore, one week of operations allows us to study how the model deal with hydrogen storage over a longer period of time. As shown by Falk and Hansen (2022), the issue related to subproblem-endings in a rolling horizon framework could affect the behaviour of the pipeline. This test, as opposed to a smaller testing period, can also to a greater extent capture how variations of exogenous factors affect system behaviour over time. Such combinations can for instance be large or small variability in both high wind power generation and power prices. Operations over one week correspond to 672 iterations in the rolling-horizon framework. The starting point of the seven day period is set at 08.10.2022:10:30.

7.6.2 Number of Wind Power Scenarios

In stochastic programming it is important to determine a set of scenarios and corresponding probabilities in such a way that the first-stage decisions have the *hedging property*. This is the ability to hedge very well against outcomes not included in the scenario set (Narum, 2020). Such decisions can also be thought of as robust solutions. The number of scenarios must be selected based on a compromise between computational tractability and risk management. In general, the number of scenarios increases the computational cost exponentially and thus impacts model performance. As stated, varying the number of scenarios is a way to manage risk (Eyvindson & Kangas, 2016). Effective risk management plays a crucial role when choosing between stochastic programming and deterministic approaches. If operational risk is given a high priority, the need for several scenarios is elevated. Consistent non-delivery of the agreed transferred amount of power can be interpreted as an event of default by Nord Pool, which can lead to severe financial consequences. It is important to acknowledge this risk element when participating in power markets. The size of the scenario set could influence how risks are taken into consideration by the model. The model has been tested for 10, 20, 30, 40 and 50 number of wind power scenarios.

7.6.3 The Role of the Intraday Market

Renewable power producers are generally exposed to uncertain weather and variable production, a risk that can be mitigated with accurate forecasts. The intraday market plays a significant role in balancing the power system, as discussed earlier. Due to its importance, it can be interesting to study how the system behaves when it has unlimited trading opportunities intraday, and also how the system performs without access to the intraday market. The current intraday volumes may not adequately represent the volumes anticipated in 2030, where renewable and variable energy sources such as wind and solar are expected to constitute a significantly larger share of the energy mix. The market is highly dynamic, and larger amounts of variable energy sources could further increase volatility in market prices. The intraday market is an important mechanism to manage under and overproduction. Other mechanisms such as energy storage systems can also contribute to balancing the net energy position of the energy system. Fuel cells and battery both possess risk-hedging properties, but only to a certain extent due to capacity limitations. Exclusion of intraday operations could illustrate how the system responds to under- and overproduction, and might indicate appropriate investment levels in fuel cells and batteries. Investigation the impact of excluding intraday market operations can how reliant the energy system is on the intraday market to fulfill its power purchasing agreements.

Hydrogen production is part of the European strategy, and sales are expected to be actualized through HPAs. While this thesis has assumed constant hydrogen price and no delivery requirements, there will in real-life applications be a demand requirement for hydrogen production in order to fulfill the HPAs. Although the contracts are assumed to be of long-term character, there may be hourly, daily or even weekly demand that must be satisfied. The energy system may have an excess of energy if the wind farm generates more power than can be used for hydrogen production and day-ahead commitments. Energy shedding and curtailment will occur if the batteries cannot absorb the excess energy and the energy system is without access to the intraday market. Conversely, the energy system may need to reallocate energy to power market deliveries in cases of low power production. Furthermore, under-delivery on day-ahead commitments may occur if the generated power by the wind farm is less than the day-ahead obligations, the activation of fuel cells cannot offset the deviation, and there is no access to the intraday market. Access to intraday market may alleviate the consequences of energy surplus and deficit in cases where an energy system with intraday trading opportunities cannot regulate itself. The role of the intraay market is therefore tested in this instance. The model is solved for the base case with three different cases of intraday trading. The first case consist of no access to intraday market, while the second case is identical to intraday assumptions made for the base case. The model has in the third case unlimited access to the intraday market.

7.6.4 What-If Analysis of Capacity Limits

Capacity limits have an impact on the utilization of resources in the energy system. A what-if analysis is performed to study the sensitivity of the proposed model to changes in capacities. This test aims to provide insight as to how the system could have performed with different investment decisions on capacity limits. It could be useful for decision-makers to understand the potentially added value of upgrades in capacity limits and how the energy system and profitability would benefit from early-stage capacity investments decisions.

Electrolyzer Capacity

In cases of wind power generation that exceeds day-ahead commitments, the excess wind power production can be utilized in hydrogen production, intraday sales or battery charging. The energy that cannot be absorbed by the system must be curtailed. If commitments to the day-ahead market are robust in the sense that the first-stage decisions are very conservative, the system can benefit from a higher electrolyzer capacity. Increasing the electrolyzer capacity could be one way of dealing with overproduction and at the same time generate revenues from hydrogen sales. The system performance has in this test been studied with electrolyzer capacities of 500, 600, 700, 800 and 1 000 MW.

Fuel Cell Capacity

Fuel cells provides the energy system the opportunity to convert hydrogen to electricity. This option can be useful in cases of low power production where the model wants to increase in power in the system to fulfill power market obligations or support hydrogen production processes. The fuel cell capacity determines the maximum amount of hydrogen that can be converted to electricity in each time period. The impact of the capacity limit is studied in this test with fuel cell capacities of 40, 50, 60, 70 and 80 MW.

Power Transmission Capacity

The day-ahead market can generate large revenues for a wind farm owner. The power transmission capacity determines the upper bound on how much electricity that can be sold to the power market. M. Kjäll-Ohlsson (personal communication, October 28, 2022) expressed that a realistic transmission line capacity could be somewhere between 300 and 700 MW for an installed offshore wind power capacity of 1 000 MW. Thus, system behaviour has been tested for a power transmission capacity of 300, 400, 500, 600 and 700 MW.

7.6.5 Electrolyzer Modeling - Number of Electrolyzers in $\mathscr{E}$ and Time Periods in $\mathscr{T}^{\mathscr{E}}$

The number of electrolyzers in $\mathscr{E}$ serves as a primary determinant of problem size. In order to depict operational states and requisite ramping processes, multiple binary variables are associated with each electrolyzer. Despite efforts to minimize this count while preserving realistic behavior, employing the entire set of variables throughout the planning horizon may render the problem computationally demanding within a given time limit. The proposed formulation introduces symmetry, which can be problematic as the solver may spend significant resources exploring isomorph solutions; mathematically distinct yet practically identical solutions, due to the components being identical. Consequently, an extensive enumeration tree may arise. To mitigate symmetry and enforce an electrolyzer ordering to reduce solution times, lexicographic ordering constraints can be implemented. However, predicting their performance proves difficult. Preliminary tests did not demonstrate success in incorporating these additional constraints. Subproblems may prove challenging to solve optimally within the given time limit of 15 minutes or yield suboptimal bounds. To

address the problem's magnitude, the planning horizon has been divided into two parts: one set of time periods representing the actual number of electrolyzers in the system and another set representing an approximation thereof based on available computational power. Rather than striving for optimality in solving the "exact problem," which is typically unattainable, an alternative strategy involves solving a slightly modified problem and exploring all solutions to identify an improved solution. The complexity of the problem is also dependent on the number of time periods the clustered set $\mathcal{E}$ is modeled, denoted as $\mathcal{T}^{\mathcal{E}}$. This test instance aims to study the trade-offs between accurate electrolyzer modeling and computational complexity. The model has been tested where $\mathcal{E}$ takes represents 20, 50, 100, 150, 200 and 400 electrolyzers in addition to evaluating the model with $\mathcal{T}^{\mathcal{E}}$ being 5, 10, 15, 20 and 25 time periods.

7.6.6 Hydrogen Price

Hydrogen has been assumed to be sold via HPAs. This is reflected by constant hydrogen prices. Hydrogen prices are in combination with power prices central for decision-making by the model as revenues between the sale of hydrogen and electricity are considered simultaneously. Changes in hydrogen prices should alter the profitability of hydrogen production, and this test instances aims to examine how the energy system is affected by changes in hydrogen prices. System behaviour is evaluated with hydrogen prices of 2, 3, 4, 6, 8, 10, 15 and 20 EUR/kg.

7.6.7 Model Performance - Value of Perfect Information and Value of the Stochastic Solution

Test instances that estimate PI and SS are generated. The stochastic framework introduces modeling complexity and more importantly problem size, which makes the optimization models much harder to solve. We estimate the value of perfect information to evaluate how much information about future wind power generation the model is able to control. Then we estimate the SS in order to determine how well the stochastic model performs in comparison to the deterministic problem. The perfect information case is implemented by running the model using the realized wind power generation over the global planning horizon. The EEV is calculated by modeling the wind power generation point-forecast in the day-ahead clearing subproblem and the subproblems with first-stage intraday decisions. The recourse subproblems are then solved using the scenario description combined with the first-stage decisions found in previous time periods. Because the pipeline storage can be quite different in the last time period for the different cases, we have to account for the unsold hydrogen in the pipeline as well. EVPI and VSS is also separately estimated when default costs are included.

7.7 Hardware and Software

All test instances have been conducted on the shared supercomputer cluster Solstorm, offered by the Norwegian University of Science and Technology. Technical specifications of the hardware and software is given in Table 7.7.

Table 7.7: Technical specifications of modeling software and solver hardware.

Description	Technical Specification
Type	HP BL686 G7
Processor	4xAMD OPTERON 6274
GHz	2.2
Cores	64
Threads	64
Memory	128 GB
Disk	300 GB SAS 15'rpm
Compiler	Julia
Compiler version	Julia 1.8.2
Solver	Gurobi
Solver version	Gurobi 10.0

7.7.1 Solver Attributes

The proposed model is implemented with the Gurobi solver. It is fundamental that a solution can be provided in less than 15 minutes – the wind power producer needs the production plan before the next time period starts. Gurobi offers the opportunity to define model attributes such as a time limit, which has been adopted for the computational study. It is by no means said that all subproblems will use all of the 15 minutes, and could find significant sufficient solutions in shorter times depending on the design parameters. A MIPGap can be defined in the solver. However, setting a suitable gap MIPGap is hardly general to define as the computational study involves different system design parameters, modeling formulations and thus different problem sizes. Initial testing has indicated that good solutions are typically found fast.

CHAPTER

EIGHT

COMPUTATIONAL STUDY

The test instances described in Section 7.6 have been implemented, test and analyzed. This chapter presents and provides a discussion of the computational results. The aim is to study both how the model presented in this thesis performs as well as assess the behaviour of an offshore energy system with hydrogen production under uncertainty. Section 8.1 presents the computational results. Section 8.2 discusses the computational results and provides managerial insights.

8.1 Results

In order to better communicate the value of stored hydrogen in the pipeline, hydrogen sales [EUR], and net income are denoted with "*" to highlight that we value the unsold hydrogen in the pipeline. Accordingly, if net income is presented with "*", the unsold hydrogen is included. The same logic is applied when evaluating the value of perfect information and the value of the stochastic solution, where "objective function value*" indicates that the unsold hydrogen in the pipeline is included, and "objective function value**" is an extension of the former by also including penalties on under-delivery in the day-ahead and intraday market, as well as cost of energy shed. Percentages of revenues generated from hydrogen and electricity are based on net income. In this part, the key observations are presented in the text. To view more details related to the tables in each subsection, the reader is referred to the Appendix. To avoid confusion, curtailment is often used interchangeably with energy shed. The same is true for under-delivery which is sometimes used instead of actual deviation, which must not be mixed up with the expected deviation when submitting bids. When referring to electrolyzer energy consumption, that includes the total energy requirement, not just for a single electrolyzer.

8.1.1 Seven Days Operation

This test instance serves to provide insight in the behaviour of the energy system over a longer time period. Table 8.1 summarizes the most central results for the base case tested over a week. For the parameters in the base case, the model tends to favor participation in the power market over hydrogen market participation. The model diverts almost one half more power to the day-ahead market compared to electrolysis and hydrogen production. Furthermore, the revenues from electricity sales are more than three times as large as the revenues from hydrogen production. This suggests that access to power markets increases overall project profitability for the given configuration. However, the costs from day-ahead deviation are not included in the net income. The penalty for not delivering is set to a very high number in order to avoid contract breach, but the real penalty that would incur is prone to uncertainty. Thus, the real net income for electricity

sales would in practice be somewhat lower. In reality, the day-ahead deviation could be further reduced by placing purchase orders in the intraday market with a high unit price. Furthermore, participation in other power markets, such as various balancing and reserve markets, could be activated in order to clear a power deficit that occurs after the closing of the intraday market. The price achieved in these markets is uncertain, which makes the actual penalty for not delivering ambiguous.

Table 8.1: Main results from applying the rolling horizon approach to one week of operation.

Description	**Unit**	**Value**
Day-ahead Commitment	[MWh]	45 580.8
Actual Day-ahead Deviation	[MWh]	2 167.0
Day-ahead Delivery Success	[%]	95.2
Electrolysis	[MWh]	31 306.1
Energy Shed	[MWh]	6 447.1
Hydrogen Production	[kg]	503 725.8
Hydrogen Sales*	[EUR]	1 730 248.5
Day-Ahead Sales	[EUR]	6 113 813.2
Net Income*	[EUR]	7 755 543.9
Hydrogen Sales	[%]	22.3
Electricity Sales	[%]	77.7

The model is severely penalized for deviation in power sale commitments. This implies that it would be beneficial for the model to avoid or reduce day-ahead deviation as much as possible. System behaviour is therefore heavily influenced by day-ahead deviations, and it is natural to commence the analysis of system behaviour by observing the day-ahead deviations. It is observed in Figure 8.1 that a day-ahead deviation occurs in cases where the wind power is lower than the day-ahead commitments. Moreover, it can be observed that day-ahead deviations do not occur frequently over the one week period. However, when deviations first occur they are often of a high value. The design of the energy system and the optimization model handle small deviations well, but struggle to plan for and respond to large deviations.

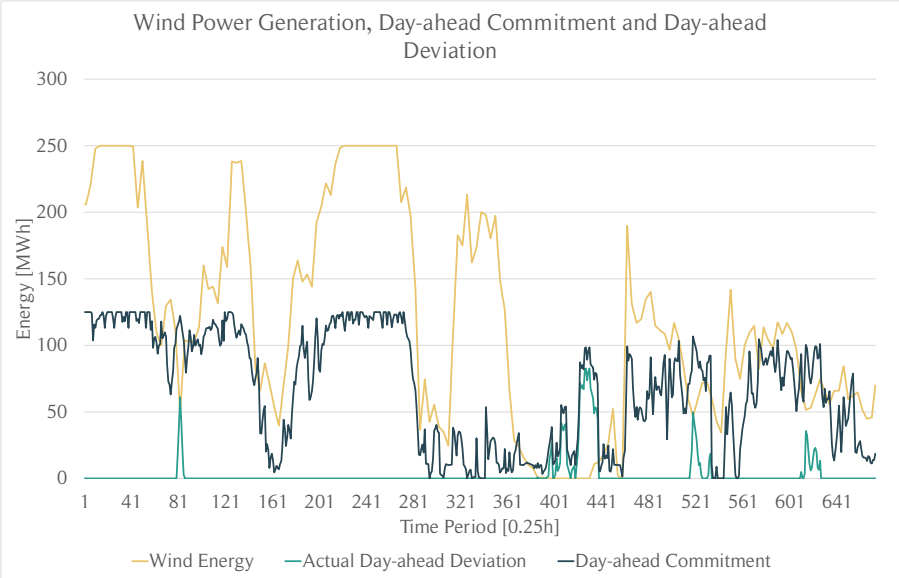

Figure 8.1: Illustration of the interplay between available energy resource, promised day-ahead deliveries and incurred deviations.

Day-ahead deviations and behaviour of components in the energy system are inspected closer in Figure 8.2. The activation of batteries, an intraday market and fuel cells demonstrate how various components in the energy system could be used in order to reduce the day-ahead deviation. Fuel cells are observed to be activated to either reduce or eliminate this deviation. From time period

300 the model starts to drastically increase hydrogen storage levels, as can be seen in Figure 8.3. The figure also suggests that there is always enough hydrogen stored in the pipeline for the fuel cells to be activated and even operate at full capacity. Furthermore, it can observed in Figure 8.1 that a prolonged duration of low power generation initiates approximately at time period 400, which explains the energy deficit Figure 8.2 for the same period. These observations could suggest that the model is "stockpiling" hydrogen for future activation of fuel cells. The model is observed to have fuel cells in continuous use for over 57 time periods in the period of lower power generation. Over this period, the fuel cells consume approximately 34 tons of hydrogen that is converted to power. One can observe that the fuel cells operate at maximum capacity whenever there is a day-ahead deviation. They are operate when day-ahead deviation is zero. This implies that fuel cells can be an important tool to minimize the penalties for unmet delivery.

The model considers the activation of fuel cells, batteries and intraday purchases simultaneously. The main application area of the fuel cells is expected to be for deviation reductions. However, the fuel cells could also be activated to support hydrogen production processes. Fuel cells operate at almost maximum capacity at period 372 despite there being no energy deficit, meaning that the wind power generation is high enough to deliver on the day-ahead contract. It appears that the fuel cells have been activated in this period in order to prevent shutoff for some electrolyzers and also activate several other electrolyzer units. Also, the fuel cells are activated in time period 66 to charge up batteries. This could be done in an attempt to hedge against future low power production that one of the scenarios could describe.

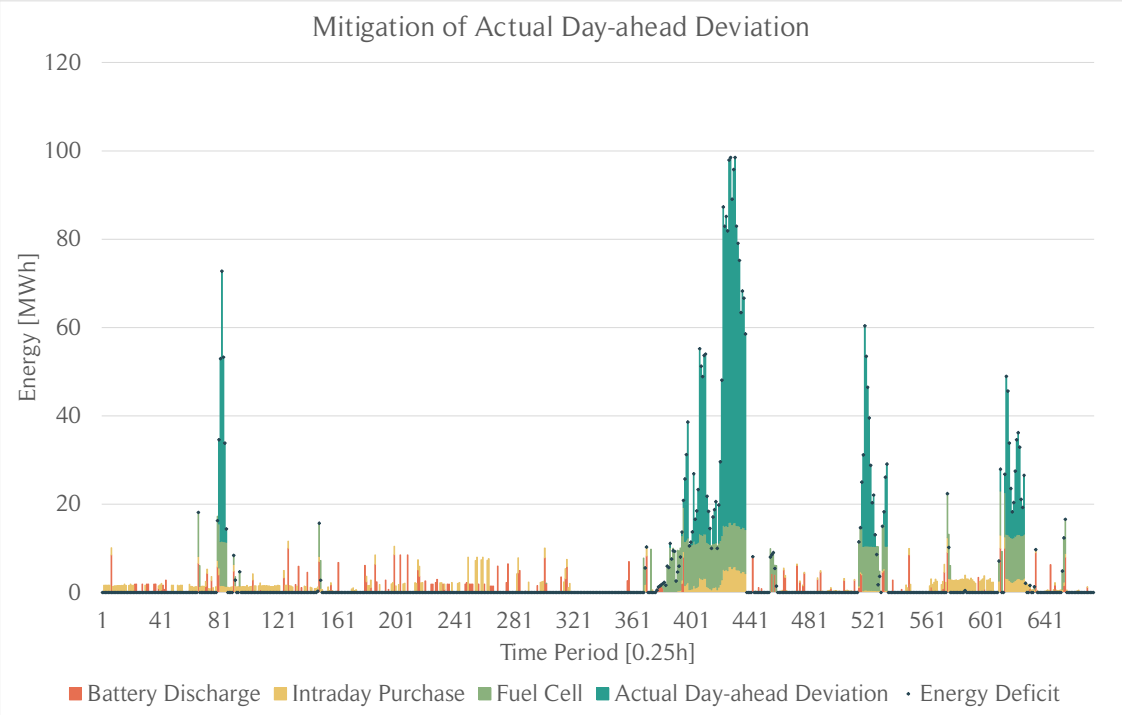

Figure 8.2: The figure illustrates how the model minimizes the penalty cost from under-delivery by activating the fuel cells, batteries and purchasing power intraday.

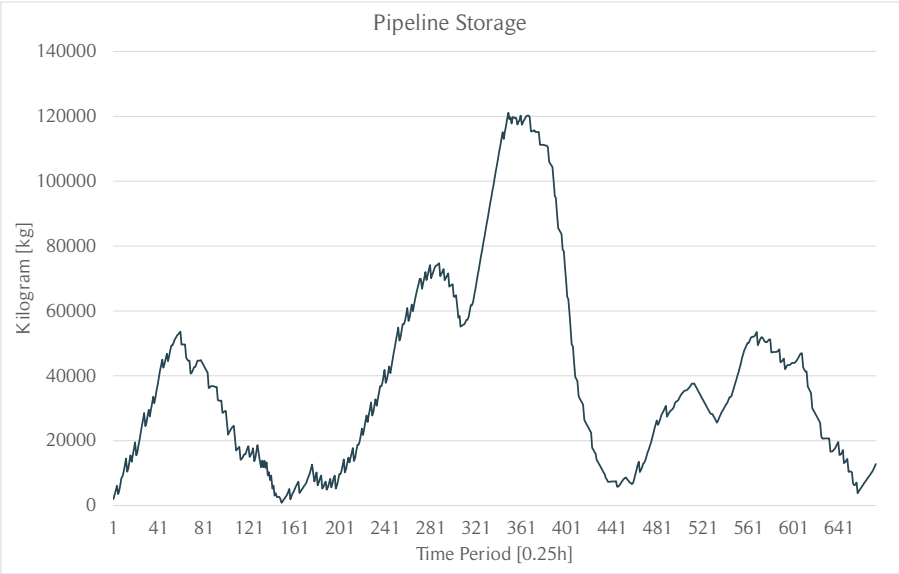

Figure 8.3: Hydrogen storage level in the pipeline during the 7 days operation of the energy system

The model generally decides to alternate between battery discharge, fuel cells and intraday purchases during the studied time period. Practically, the model has the opportunity to use fuel cells to generate more power in every time period, which is not the case for intraday purchases. Intraday purchases in periods where fuel cell could be activated then indicate that the model often prefers to buy power from the intraday markets instead of converting hydrogen to power. This could be explained with relative price differences between intraday and hydrogen. As there is a high conversion loss for hydrogen-to-power, the intraday price needs to be relatively large in order to offset this loss. It is therefore often more profitable for the model to sell hydrogen compared to activating fuel cells when intraday access is available. Batteries and intraday purchases allows the energy system to increase the available energy, and when energy from these sources can be used to fulfill the day-ahead contract, then the power from the wind farm can be used to produce hydrogen.

Energy shed also conveys key information on overall system performance. Several large spikes in energy shed can be observed in Figure 8.4. These spikes are due to electrolyzers being shutoff instead of producing. This could seem counter-intuitive as it would more profitable for the system to continue the production of hydrogen in this period, or that it might turn on electrolyzer and produce at half the installed capacity. However, it could happen that the model in the current time period has one scenario value with zero wind power generation in the subsequent period. There is an energy cost associated with the shutdown of electrolyzers. This means that the model avoids having this shutoff cost being potentially added as penalty in the subsequent period, as one of the scenarios could indicate the possibility of zero power production the next period. This shows that the model is highly sensitive to extreme fluctuations, especially cases of extremely low power generation. This sensitivity is rooted in the high penalty for under-delivery.

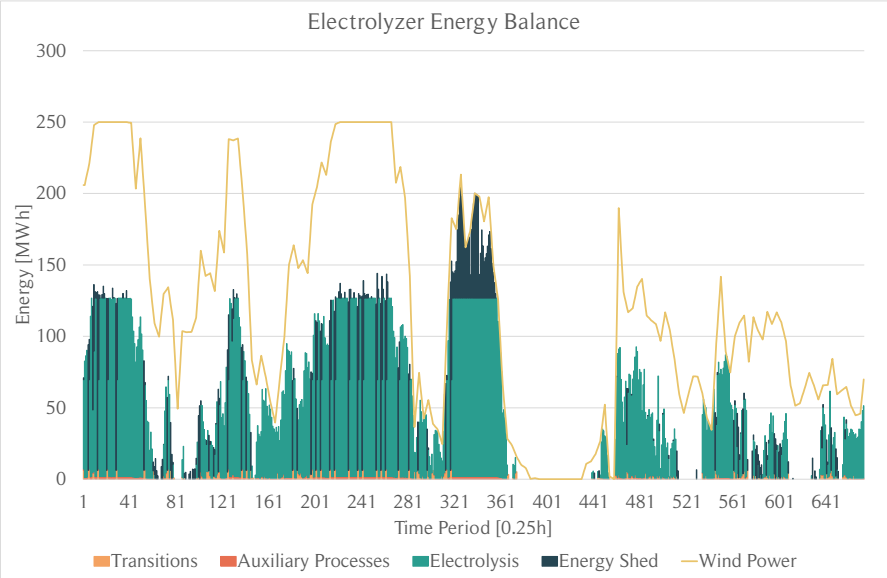

Figure 8.4: Electrolysis energy balance. The figure illustrates the electrolyzers operation during the studied time period.

8.1.2 Changing the Number of Wind Power Generation Scenarios

The impact of the number of wind power scenarios is presented in Table 8.2. A general observation is that an increase in the number of scenarios do not necessarily incur systematic variations in energy system performance, while the solution time expectedly increases. This could suggest that the underlying scenario generation process may create ambiguous results in the different model runs. The number of scenarios has several implications for the output of the scenario generation procedure. Scenarios are drawn randomly based on a covariance matrix and quantile distributions. A larger number of scenarios provides a more representative view on possible future realizations of wind power as more values from the entire quantile distributions are drawn. Thus, the probability of having extreme values in one of the scenarios increases in proportion to the number of scenarios. The presence of more extreme scenario values could be an explaining factor for what may be considered inconsistent system behaviour. However, the behaviour tends to become more prudential as more scenarios are added.

Table 8.2: Main results from running the optimization model with different number of wind power generation scenarios.

	Unit	$\mathcal{S}$ **= 10**	$\mathcal{S}$ **= 20**	$\mathcal{S}$ **= 30**	$\mathcal{S}$ **= 40**	$\mathcal{S}$ **= 50**
Day-ahead Commitment	[MWh]	16 110.5	16 428.8	16 322.7	16 369.4	16 644.9
Intraday Purchase	[MWh]	184.2	231.7	256.7	276.0	303.4
Actual Day-ahead Deviation	[MWh]	231.5	178.1	172.8	190.9	191.2
Actual Day-ahead Deviation	[%]	1.4	1.1	1.1	1.2	1.1
Intraday Sale Commitment	[MWh]	45.7	35.8	31.2	13.7	14.7
Battery Discharge	[MWh]	111.0	82.7	98.2	93.1	100.3
Fuel Cell	[MWh]	85.7	95.7	123.9	139.5	188.8
Energy Shed	[MWh]	1 753.7	1 663.9	2 452.0	2 320.1	1 980.6
Energy Shed	[%]	6.7	6.4	9.4	8.9	7.6
Hydrogen Production	[kg]	134 857.1	131 513.9	120 794.8	123 688.6	126 165.3
Hydrogen Sales*	[%]	25.7	24.7	23.0	23.3	22.8
Net Electricity Sales*	[%]	74.3	75.3	77.0	76.7	77.2
Average Runtime	[s]	21.5	55.1	87.7	118.9	171.2

As discussed in Section 8.1.1, the model is severely penalized for not delivering the agreed quantity of power and this could interfere with the "true" value of having more scenarios. Since the penalty of not delivering is relatively large, it could mean that it suffices with one scenario with very

low power production in order to adjust itself against over-commitments. Again, as the number of scenarios increases, it is more likely that the number of extreme scenarios could occur. The high penalization could cause the model to hedge against the associated tail-distribution of over-committing, especially in the day-ahead market. If the number of scenarios were to increase infinitely there could theoretically be one scenario that projects zero power generation in every future time period. The high penalty could then lead the model to choose the lowest possible level of power market participation as it wants to avoid this penalty. The solution could in this case become practically robust as it never risks over-commitments. It has been observed that participation in the intraday market, more specifically intraday purchases, acts as a mechanism to reduce day-ahead deviation. An increase in intraday purchases can be observed in Table 8.2 when the number of scenarios increases. Larger numbers of scenarios may capture more of the wind power stochasticity as a wider span of future realization is represented through the various scenarios. Variation in scenario values, and in this case short-term variation, could lead the model to purchase more power from the intraday market. This would allow the model to hedge against the lowest scenario power value for the upcoming time periods that will be locked for further intraday trading. Fuel cell activity can also be observed to increase when more scenarios are included in the model. A similar reasoning can be projected to the fuel cell behaviour.

There is an increasing trend in curtailment and it occurs periodically across different scenarios, which raises concerns. The abrupt shutdown of electrolyzers is particularly puzzling, given the availability of sufficient wind power for their operation. One possible explanation for this behavior is that the current subproblem has least one wind power scenario which contains a sudden drop in wind power generation for the subsequent time period. This becomes more likely with a larger number of scenarios. To prevent potential delivery issues in the subsequent time period, the model chooses to shut down all electrolyzers instead of running them at minimum capacity, ensuring optimal performance for fulfilling day-ahead commitments. However, as the wind power rebounds in the following time period, the model becomes fully capable of meeting the power demand. Regrettably, the electrolyzers start up during this time and can therefore only produce for half of the installed capacity, leading to significant curtailment as illustrated in Figure 8.5.

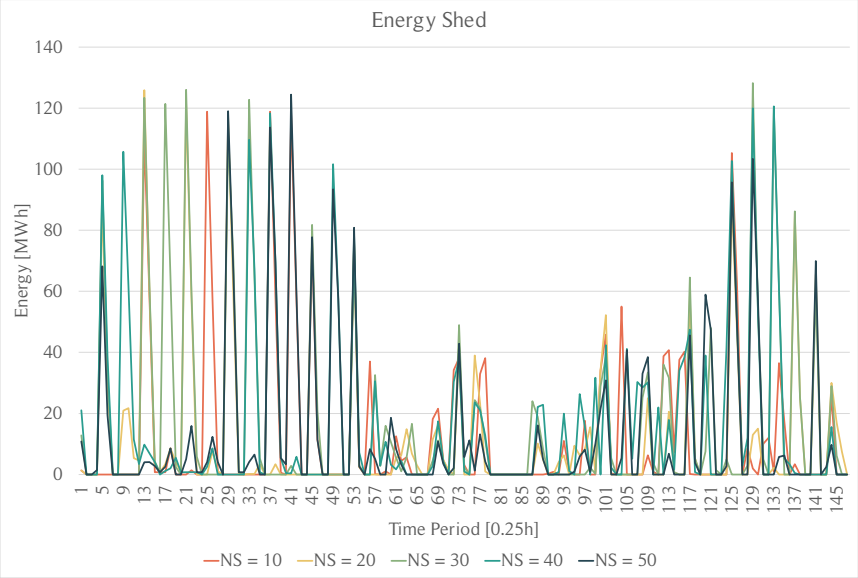

Figure 8.5: Energy shed with different number of scenarios.

The fact that an increase in a number of scenarios increases the absolute number of low-power scenarios could explain the increase intraday purchases and fuel cell activity. As the penalty is substantial, low-power scenarios are heavily penalized and the model would want to avoid these by intraday-purchases. It is therefore plausible that the model buys more from the intraday than it needs to, meaning that it needs to shed the surplus energy. This could also explain the decrease in intraday delivery. The model wants to avoid further penalties on unmet intraday deliveries and therefore reduces these commitments. However, this is not necessarily consistent with the

increase in day-ahead commitments. The fluctuating outcomes of random processes in the model are therefore likely to have a large impact on model solutions.,

8.1.3 The Role of the Intraday Market

The role of the intraday market has been studied in order to assess the impact of intraday purchases and sales on the model and energy system behaviour. Test results from three different degrees of market access are presented in Table 8.3. It is observed when that relaxing the volume constraints results in a substantial decrease in day-ahead deviations. Furthermore, energy shed is reduced considerably which could be attributed to the increase in hydrogen production. Net income does not increase with intraday trading due to costs associated with intraday purchases despite the increase in hydrogen production. Fuel cell activity is significantly reduced when the model has higher access to the intraday market. Higher intraday access also leads to higher average runtimes for the model.

Table 8.3: Key model results for different intraday market policies.

	Unit	No Intraday Access	Limited Intraday Trading	Unlimited Intraday Trading
Day-ahead Commitment	[MWh]	16 423.4	16 428.8	16 426.9
Intraday Purchase	[MWh]	0.0	231.7	4 250.0
Actual Day-ahead Deviation	[MWh]	193.9	178.1	0.0
Actual Day-ahead Deviation	[%]	1.2	1.1	0.0
Intraday Sale Commitment	[MWh]	0.0	35.8	271.5
Intraday Sale Delivery Success	[%]	0.0	100.0	100.0
Auxiliary Processes	[MWh]	119.2	124.6	189.0
Electrolyzer Transitions	[MWh]	203.7	195.0	50.6
Battery Discharge	[MWh]	102.1	82.7	36.6
Fuel Cell	[MWh]	109.5	95.7	1.5
Energy Shed	[MWh]	1 852.5	1 663.9	1 019.5
Energy Shed	[%]	7.1	6.4	3.9
Hydrogen Production	[kg]	125 822.3	131 513.9	199 547.8
Hydrogen Sales*	[EUR]	476 537.3	502 635.8	797 914.5
Net Income*	[EUR]	2 032 794.6	2 037 856.0	1 892 034.4
Hydrogen Sales*	[%]	23.4	24.7	42.2
Electricity Sales*	[%]	76.6	75.3	57.8
Average Runtime	[s]	53.8	55.1	453.2

It could appear counter-intuitive that the day-ahead commitments do not increase when the model has larger access to the intraday market. This is predominantly due to the fact that the model does not include decisions in the intraday market when day-ahead decision are made, as there is a large uncertainty associated with forecasting intraday market prices for time periods relatively far in the future. Under the condition that the day-ahead prices are always higher than intraday prices, the model could in theory commit as much power as possible as it would always be able to buy cheaper power from the intraday market and sell to the day-ahead market. However, arbitrage situations could arise with unlimited intraday market access as there is no upper bound on day-ahead commitments in the model formulation. This could theoretically lead to the trading of infinitely high volumes. For the more general case, some probability distribution of intraday-prices would be weighted against the known day-ahead prices in order to determine the optimal sale quantity.

Energy shedding is influenced by a combination of factors such as price evaluations, the non-reversible nature of intraday decisions, and the model's objective to avoid under-delivery penalties. One could expect that full access to intraday markets would eliminate the occurrence of energy shedding. It would also be expected that the model could sell excess energy instead of curtailing it. One possible explanation is that the model adjusts its energy allocation based on price evaluation. It seems plausible that the model tends to purchase power in the intraday market if the intraday buying price is lower, replacing the need to inject power into the grid. The energy system is however not able to eliminate curtailment as shown in Table 8.3, which is can be surprising considering the penalty associated with shedding. It is observed in Figure 8.6 that the model occasionally has purchased power in a period where it experiences energy shedding. It is also observed that this occurs at times where the generated wind power is at its maximum possible value, which would be sufficient to cover both maximum day-ahead commitments and support maximum hydrogen

production. When intraday decisions are made, which occur once every hour, they are non-reversible and made prior to the realization of wind power production. Given that the day-ahead commitment is fixed, the model anticipates the worst-case scenario and seeks to avoid under-delivery of its market obligations when the wind power is anticipated to diminish. Unlimited intraday trading can therefore contribute to high levels of energy shedding as it simultaneously eliminates day-ahead deviations.

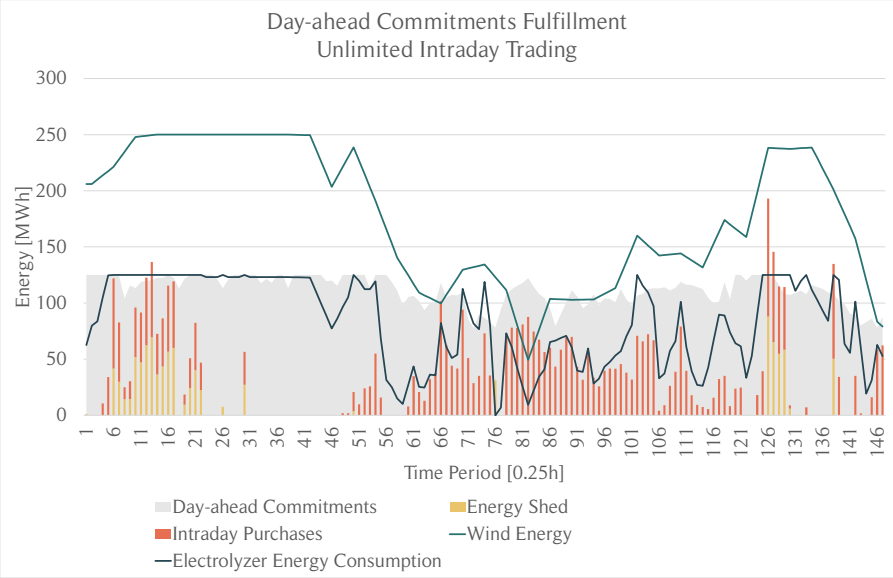

Figure 8.6: This figure primarily illustrates the relationship between the day-ahead delivery (not shown), energy curtailment, intraday purchases in regards to fulfilling day-ahead contracts.

Any extreme scenario with low wind power production would incentivize the model to purchase large intraday volumes. Then, if the wind power generation is abundant at the time of delivery, the power injection to the grid must decrease according to Equation (6.57) and as seen in Figure A.17, as a net surplus power injection to the grid is prohibited. This happens to minimize the risk of under-delivery, which, if realized, incurs a penalty of a factor of 1000 higher than from curtailment. In comparison, the consequences of energy curtailment are considered less dramatic compared against expected under-delivery. This could also explain why the model responds by maximizing hydrogen production with unlimited access to intraday trading, as deviating from market contracts is far more costly than curtailment. Moreover, intraday purchases are power injections into the power system by other parties, freeing more available energy for other purposes, such as hydrogen production. The model can balance risk mitigation and at the same time generate revenues from the "missing" energy that is supposed to be injected to the power grid. The model weights the unit cost in the intraday market against the foregone revenues from producing hydrogen when deciding on which power source to use for fulfilling the power market obligations. This artificial increase in hydrogen production is a result of the intraday bidding process.

Furthermore, an increase in the upper volume bound on intraday sale and purchase causes considerably higher activity in the intraday market than under a restricted trading scheme. This can be observed from Figure 8.7 as intraday sales increase significantly when the energy system has unlimited access to the intraday, and Figure 8.8 suggests the same for intraday purchases. The same hours in the two cases are being traded, which is reasonable considering similar wind power scenarios are modeled. The difference in intraday volumes signals that the ability to be able to trade higher intraday volumes is substantially valued by the model. One would expect the model to prioritize selling electricity in the intraday market rather than dedicating energy to hydrogen production, especially considering the lower selling price for hydrogen and the efficiency loss in the electrolyzer process. However, the increase in intraday purchases shows that the model is more concerned about fulfilling existing power market obligations than generating more income in the intraday market when access to the intraday market is granted. This concern also provides an explanation of the higher frequency of intraday purchases compared to intraday sales.

There are two concerns, however, regarding intraday sales. Firstly, when submitting intraday bids at gate-closure time, the model take into account already engaged contracts. Failure to fulfill the initial obligations incurs penalties, making it a first-priority to fulfill them. If the wind power producer expects that intraday purchases will be required to meet the initial commitments, it does not make sense to speculate in intraday sales, even at highly attractive prices. Secondly, it is not possible to both sell and buy power in the same time period, forcing the model to choose between the two. Additionally, selling power intraday would entail additional market obligations, possibly requiring support from the fuel cell and battery in the upcoming delivery hour. Based on the results, it is apparent that such behavior carries considerable risk. In summary, although larger trading volumes in the intraday market lead to increased activity, the model faces challenges and constraints when selling power intraday. Prioritizing intraday purchases to fulfill existing commitments, the inability to simultaneously sell and buy power, and the risks associated with additional market obligations all contribute to the model's cautious approach to intraday selling.

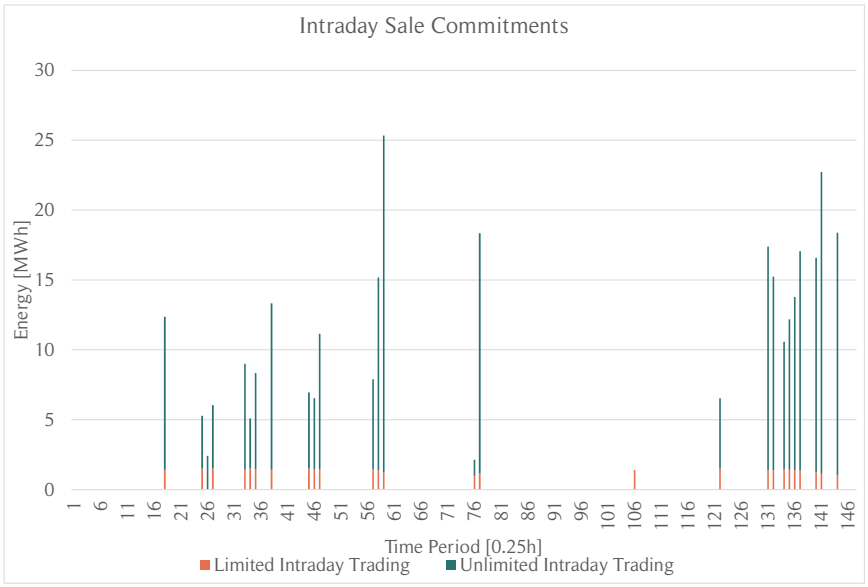

Figure 8.7: A comparison between the intraday sale commitments over the planning period for limited and unlimited intraday trading policies.

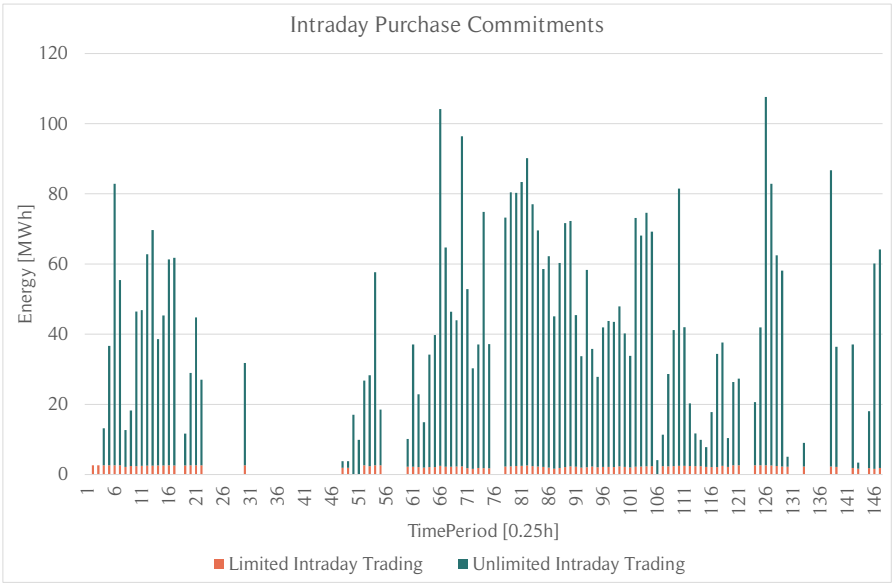

Figure 8.8: A comparison between the intraday purchase commitments over the planning period for limited and unlimited intraday trading policies.

The increase in intraday trading access has a notable impact on fuel cell activity. Considering the efficiency loss of over 50% in fuel cells, it becomes apparent that it in many cases would be more profitable to purchase from the intraday market to cover the day-ahead position rather than activating fuel cells and incurring high losses from selling energy as hydrogen instead of electrical power. As such, a sufficiently large intraday market could essentially render fuel cells obsolete, replacing their role with market transactions. Fuel cells offer flexibility to energy systems with limited market access, but their relevance diminishes when the market needs can be effectively met through the intraday market. However, it should be noted that fuel cells still play a significant role in reducing day-ahead deviations, particularly in scenarios with limited or no access to the intraday market, as clearly shown in Figure 8.9.

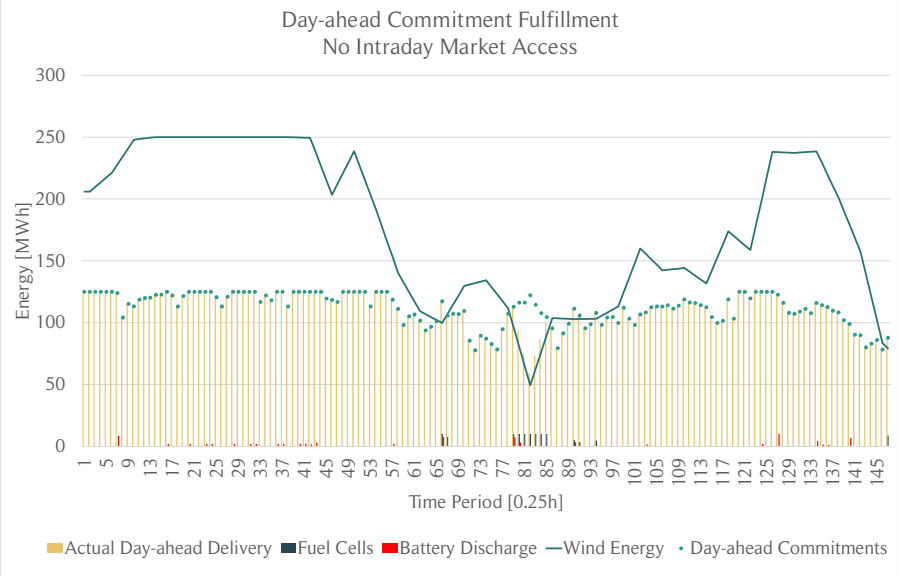

Figure 8.9: Plot highlighting the utility of fuel cells and batteries when the energy system is decoupled from intraday market trading.

The fuel cells help mitigate costs associated with fluctuations in power generation and day-ahead contracts. Given the substantial penalties involved, even minimal activation of fuel cells can result in significant cost savings, which underscores their importance in the overall energy system. Fuel cells contribute to the optimization of energy systems when they are included as decision variables in the bidding process. There is however a risk of over-commitment in relation to the purchases of power in the intraday market, causing the system to curtail and receive penalties similar to those of over-commitments in the day-ahead market. However, due to the absence of hedging options other than batteries and fuel cells, intraday sales are not as attractive. Consequently, the model avoids taking excessive risks in over-committing to intraday sales, as it would require significant fuel cell and battery capacity to secure both large day-ahead and intraday commitments, as mentioned earlier.

It can be seen in Table 8.3 that the net income is lower for unlimited intraday trading compared to no and limited intraday trading. This is due to the larger costs associated with intraday purchases. However, the net income for unlimite intraday trading has not been adjusted for the costs of under-delivery as opposed to no and limited intraday trading. A high penalty would reduce the net income substantially and leave unlimited intraday traing as the best performing case. The inclusion of intraday markets comes at the expense of higher computational complexity and longer solution times. The sale of hydrogen takes a larger part of net income when the access to intraday trading increases. This could be due to the model's ability to compare intraday prices to hydrogen prices, meaning that it directs wind farm power to hydrogen production and uses the intraday market to fulfill the day-ahead contract. Again, the model is not allowed to use power from the power markets to produce hydrogen, as this power cannot be guaranteed to be entirely renewable. Access to the intraday market provides the model with more room to identify situations with degrees of arbitrage.

8.1.4 What-If Analysis

Increased Electrolyzer Capacity

Electrolyzer capacity is a central part in planning of investments. An analysis of the implications of electrolyzer capacity could reveal impacts on operational revenues that are not captured in NPV-analyses. The results are presented in Table 8.4. It can be observed that commitments in the day-ahead market decrease with increasing electrolyzer capacity, in addition to decreases in day-ahead deviation. Hydrogen production is increased, and the decreasing revenues from power sale results in larger relative contribution to net income from the sale of hydrogen. The net income is increasing, for cases with same day-ahead deviation, as electrolyzer capacity increases. Energy shedding also tends to reduce with higher electrolyzer capacity.

Table 8.4: Key findings when studying the impact on system performance under different electrolyzer capacities.

	Unit	500 MW	600 MW	700 MW	800 MW	1 000 MW
Day-ahead Commitment	[MWh]	16 428.8	14 408.1	13 130.5	12 462.2	12 195.4
Actual Day-ahead Delivery	[MWh]	16 019.2	14 182.2	12 990.1	12 335.2	12 071.3
Intraday Purchase	[MWh]	231.7	173.5	133.5	120.1	117.2
Actual Day-ahead Deviation	[MWh]	178.1	53.1	7.5	7.5	7.5
Actual Day-ahead Deviation	[%]	1.1	0.4	0.1	0.1	0.1
Electrolyzer Transitions	[MWh]	195.0	213.0	243.3	231.0	227.5
Battery Discharge	[MWh]	82.7	112.7	83.0	46.7	22.0
Fuel Cell	[MWh]	95.7	51.5	33.7	26.6	26.6
Energy Shed	[MWh]	1 663.9	1 747.1	1 383.6	1 237.1	1 068.0
Energy Shed	[%]	6.4	6.7	5.3	4.7	4.1
Hydrogen Production	[kg]	131 513.9	158 025.4	182 022.9	194 857.3	201 970.4
Hydrogen Sales*	[EUR]	502 635.8	619 618.3	719 892.4	772 580.9	800 932.8
Total Net Income*	[EUR]	2 037 856.0	1 981 681.6	1 976 179.9	1 982 658.3	1 987 789.9
Hydrogen Sales*	[%]	24.7	31.3	36.4	39.0	40.3
Net Electricity Sales*	[%]	75.3	68.7	63.6	61.0	59.7
Average Runtime	[s]	57.2	66.2	61.0	72.6	95.0

Increasing the capacity of electrolyzers has a noticeable impact on day-ahead commitments and day-ahead deviation. As the electrolyzer capacity increases, there is a decrease in day-ahead commitments, shown in Figure 8.10, and subsequently a lower day-ahead deviation.

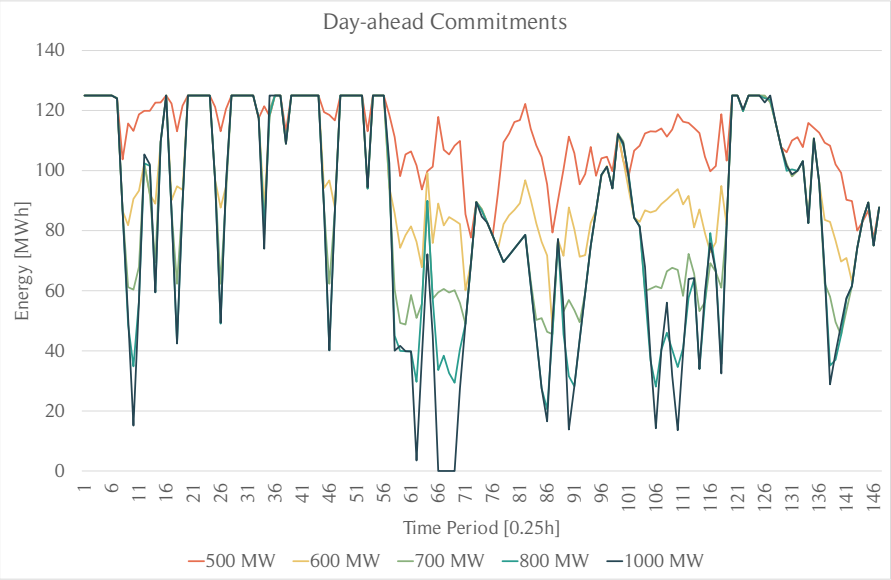

Figure 8.10: The change in day-ahead commitments as the total electrolyzer capacity changes. Higher electrolyzer capacities are associated with lower day-ahead commitments.

The reduction in day-ahead deviation is also accompanied by a decrease in fuel cell and battery

activity, likely due to the lower day-ahead commitments. When comparing the net incomes of the 500 MW capacity case to the net income generated with a capacity of 1 000 MW, a significant decrease in day-ahead deviation is observed. The distribution of income also varies considerably between the two cases, with hydrogen contributing 24.7% and 40.3% of the income in the base-case and 1 000 MW capacity case, respectively. Notably, the day-ahead deviation remains the same for cases with electrolyzer capacities of 700 MW, 800 MW, and 1 000 MW. This implies that the net incomes of these cases can be directly compared. With that in mind, it is observed from Table 8.4 that the net income increases as the electrolyzer capacity decreases, primarily due to the corresponding increase in hydrogen production, visualized in Figure 8.11. As with higher possibilities of obtaining income with hydrogen it is beneficial to have less exposure on the risks of operating in the power markets, given the high price of under-delivery. For an investor, it would be of interest to determine the cost of additional capacity and assess how much it would contribute to revenue growth. However, it remains uncertain how expensive it is to offset the day-ahead deviation in an ideal market scenario. The storage level develops quite differently in the analyses as seen in Figure 8.12, requiring to consider the unsold hydrogen in the pipeline when determining how total hydrogen revenues change between the cases which is captured in Figure A.19, as found in the Appendix.

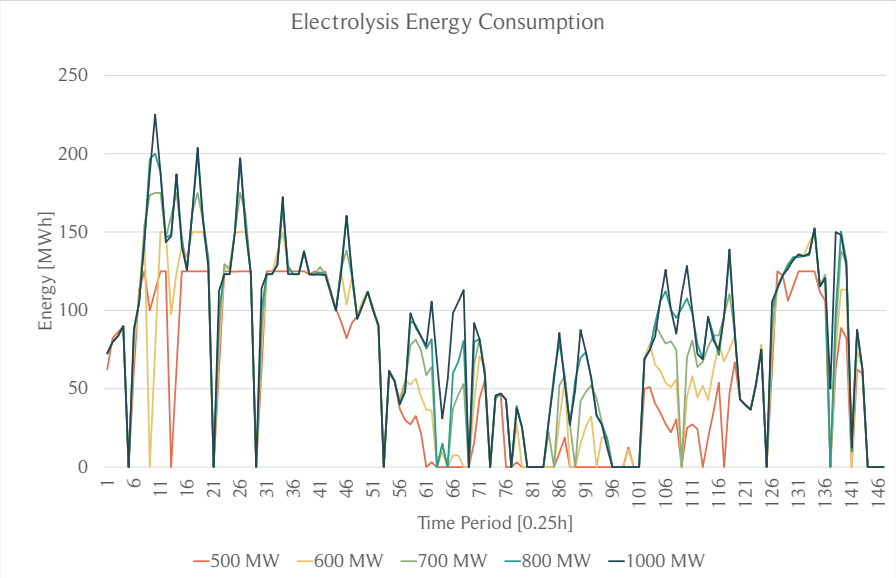

Figure 8.11: The energy requirement for electrolysis tends to increase with higher electrolyzer capacity on the platform.

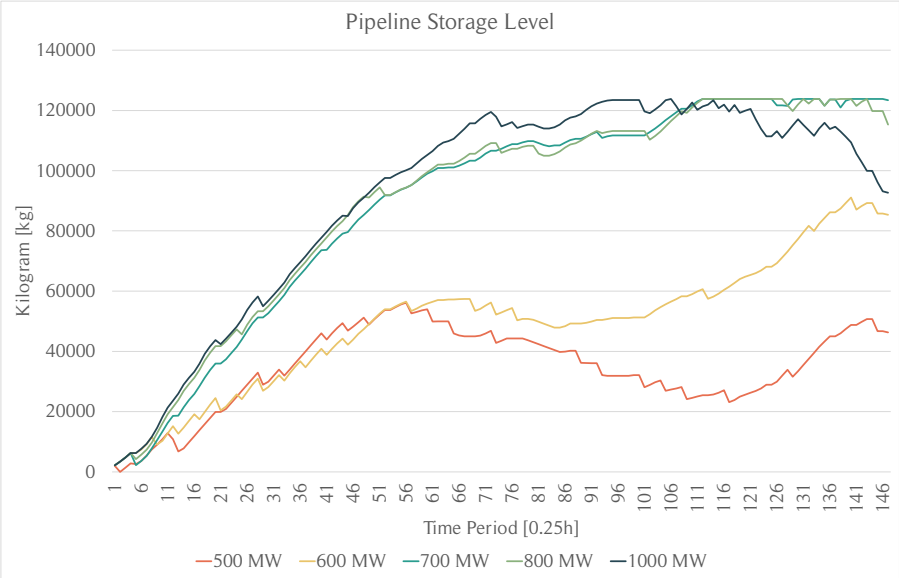

Figure 8.12: The graph illustrates how differently the storage amount in the pipeline is developing for the different electrolyzer capacities.

It is important to consider the financial consequences of under-delivery and energy-shedding in this particular test instance. A higher hydrogen production capacity does not necessarily mean that hydrogen is prioritized over day-ahead sales. Instead, it could indicate that when power market obligations are fulfilled, an opportunity to produce more hydrogen comes with higher capacities. Operational risk could also play a part in the explanation of this model behaviour. Day-ahead commitments carry more risk compared to hydrogen production, and an increase in hydrogen production capacity could entail lower risk compared to day-ahead commitments yielding approximately equivalent revenues from the same resources. Expansion of the production capacity could allow the achievement of comparable revenues to lower electrolyzer capacities, even with efficiency losses and price differences in consideration. It is important to note that although the base-case capacity generates higher net income, the day-ahead deviation and energy curtailment, as defined in the model, offsets these gains. This could potentially make the 1 000 MW capacity more profitable in terms of net income from operations. However, the difference in day-ahead deviation is not convincing enough to render any of the higher capacities as techno-economic viable configurations from the observed penalties. If there any real-world mechanism to compensate for this deficit, as there likely is through various power markets, the base-case capacity could potentially earn roughly the same as the 1 000 MW capacity when the deficit is compensated at competitive market prices, even though the other configuration requires a significant investment in additional 500 MW electrolysis.

The expectation that increased hydrogen production capacity would lead to reduced energy shedding seems reasonable in theory. However, in practice, this result is not consistently observed. Despite having the capability to produce more hydrogen when market commitments are fulfilled, it is still observed in Table 8.4 that curtailment remains significant. This discrepancy can be attributed to how the model reacts to wind power scenarios with low power generation, as discussed earlier. Similarly to the case in Section 8.1.2, the shutdown of electrolyzers could occur in order to reduce expected day-ahead deviation in upcoming time-periods where one of the scenarios involves low power generation. This model behavior is shown in Figure 8.13. If wind power generation increases again, the electrolyzers may not be able to consume all the energy, resulting in curtailment. For instance, in the case of a 1 000 MW hydrogen production capacity, during time period 52, the day-ahead commitment is 94.44 MWh, while the recorded power production is 203 MWh. Although the electrolyzers were operating at 90.75 MWh in the previous time period, they completely shut down. The subsequent time period shows a power production of 191.1 MWh and a day-ahead commitment of 125 MWh, indicating no specific reason to shut down the electrolyzers unless a significant decrease in wind power production was anticipated by the model. This behavior occurs inconsistently, but typically in time periods with high commitments as shown in

Figure 8.13. Namely, operating in the hydrogen market does not entail the need for instantaneous fulfillment of the obligations, and therefore requires less flexibility. On the other hand, operating in the electricity market requires quite some level of flexibility, and the cost of flexibility might be quite high. This justifies a higher involvement in the hydrogen market, when it is possible. One would also anticipate a higher energy requirement from electrolyzer transitions with an increase in capacity and the number of electrolyzers, as transitions make up a percentage of the capacity. Despite the presence of more electrolyzers operating at higher capacity, energy requirement seems only to slightly increase, but it is not a consistent observation.

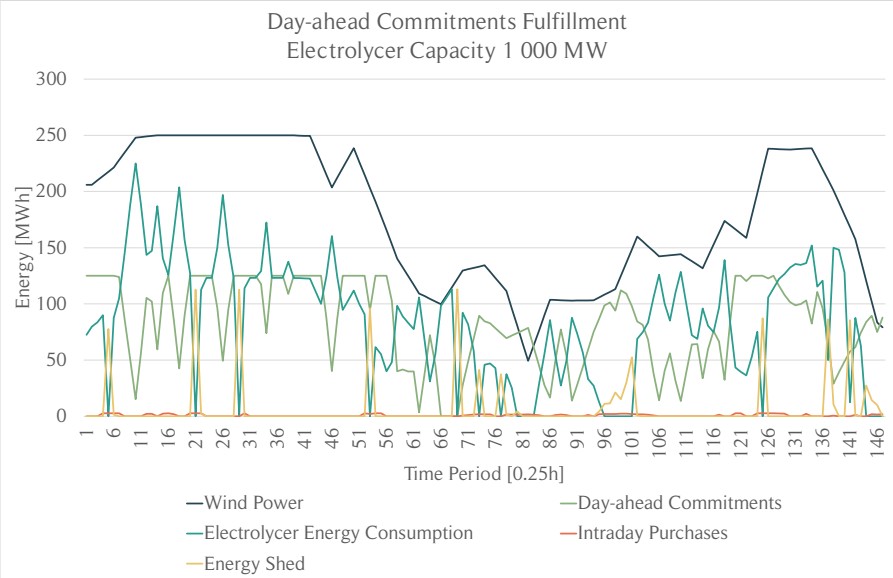

Figure 8.13: Illustration that most importantly highlights the sudden energy shedding in regards to fulfilling day-ahead contracts.

Fuel Cell Capacity

Fuel cells give the energy system the option to increase the energy availability in a given time period. Additional energy can be useful for hydrogen production and particularly to reduce under-deliveries. Results for different fuel cell capacities are shown in Table 8.5. Slight increase in day-ahead commitments and relatively large decreases in day-ahead deviation is observed for higher fuel cell capacities. Table 8.5 also also shows a reduction in hydrogen revenues despite a minor positive trend in hydrogen production. Furthermore, energy shedding decreases for larger fuel cell capacity, and so does the energy consumption by electrolyzer state transitions.

Table 8.5: Key findings from testing the model with different fuel cell capacities.

	Unit	40 MW	50 MW	60 MW	70 MW	80 MW
Day-ahead Commitment	[MWh]	16 428.8	16 458.0	16 489.0	16 531.8	16 578.3
Actual Day-ahead Delivery	[MWh]	16 019.2	16 063.0	16 117.4	16 170.5	16 230.9
Intraday Purchase	[MWh]	231.7	235.8	227.4	230.1	228.1
Actual Day-ahead Deviation	[MWh]	178.1	160.0	144.8	132.1	120.1
Actual Day-ahead Deviation	[%]	1.1	1.0	0.9	0.8	0.7
Electrolyzer Transitions	[MWh]	195.0	182.5	185.0	175.6	165.0
Fuel Cell	[MWh]	95.7	115.4	134.2	159.5	180.7
Energy Shed	[MWh]	1 663.9	1 590.4	1 535.0	1 469.6	1 441.6
Energy Shed	[%]	6.4	6.1	5.9	5.6	5.5
Hydrogen Production	[kg]	131 513.9	132 534.5	132 680.7	133 589.6	133 535.8
Hydrogen Sales*	[EUR]	502 635.8	501 609.0	497 305.0	494 395.6	488 688.7
Day-Ahead Sales	[EUR]	1 556 594.7	1 560 282.3	1 564 015.6	1 568 425.6	1 573 472.4
Total Net Income*	[EUR]	2 037 856.0	2 040 434.7	2 040 518.1	2 041 767.8	2 041 643.8
Hydrogen Sales*	[%]	24.7	24.6	24.4	24.2	23.9
Net Electricity Sales*	[%]	75.3	75.4	75.6	75.8	76.1
Average Runtime	[s]	56.3	53.9	53.0	67.5	64.1

A consistent marginal increase in day-ahead commitment volumes is observed in Table 8.5. Despite the increase in total commitments, the absolute day-ahead deviation decreases, which is opposite to the previously studied test instances. This observation is summarized by an increase in day-ahead delivery success for an increase in fuel cell capacity. Fuel cells can lead to a higher ability to deliver the committed amount of power in the day-ahead market. This again leads to reduced penalties from contrct violations. Intraday participation shows no particular response to a change in fuel cell capacity. There is however a noticeable decrease in energy shed when fuel cells have a larger capacity.

There is a slight positive trend in hydrogen production when the capacity is increased. There is however a decrease in the energy consumption for electrolyzer transitions with higher fuel cell power ratings. This could indicate that fuel cells can prevent electrolyzer from shutting off in cases of low realized power production. It could also be that fuel cells are considered when planning future periods, where some scenarios could take zero as power value, and that the model plans that fuel cells can be used to keep electrolyzers going if this scenario does in fact materialize. This allows the model to prevent shutting of electrolyzers as the energy system can generate enough power to keep them going. This situation also relies on how day-ahead commitments for such a situation have been done, so that there is in fact more than enough power to fulfill the contract so that power from fuel cells can be directed to the electrolyzers and not contribute to fulfilling the contract.

This situation could also explain why the energy shed is considerably lower for high capacities. The fuel cells can in fact prevent the electrolyzers from shutting down, meaning that there is no reduction in hydrogen production capacity in the subsequent period. This leads to higher utilization of the available energy and does in fact point towards fuel cells lowering energy curtailment and promoting higher efficiency of the overall energy system.

Hydrogen sales are lowered when fuel capacity is increased. This could seem to be in contrast with the increase in hydrogen production that is observed. However, the increase in fuel cell activity implies that hydrogen is combusted in the fuel cells to generate electricity. An increase in day-ahead revenues could point to this, as more electricity is delivered. The overall impact of fuel cell capacity is negligible on the total net income. However, the day-ahead deviation decreases meaning that the overall profits would increase for higher fuel cell capacities. This could explain the fact that the ratio between hydrogen revenues and power revenues shifts slightly towards a higher contribution from electricity sales.

Increased Power Transmission Capacity

Power transmission capacity is, like electrolyzer capacity, a fundamental decision in the investment phase of the offshore energy system. Due to both material and installation costs, it is paramount that the transmission capacity is dimensioned appropriately. The model performance when changing the power transmission capacity are seen in Table 8.6, and do have a large effect on the behaviour of the entire energy system. Higher power transmission capacity results in a substantial increase in day-ahead commitments, and thus electricity revenues, accompanied by higher activation of fuel cells, intraday purchases and partly battery discharges. The day-ahead deviation increases with transmission capacity nevertheless. While hydrogen production and hydrogen sales decrease, energy shedding experiences non-systematic changes when transmission capacity increases.

Table 8.6: Key findings from the sensitivity analysis on transmission cable capacity.

	Unit	300 MW	400 MW	500 MW	600 MW	700 MW
Day-ahead Commitment	[MWh]	10 163.7	13 257.0	16 428.8	19 846.0	23 501.8
Actual Day-ahead Delivery	[MWh]	10 078.0	13 051.9	16 019.2	18 983.3	21 566.3
Intraday Purchase	[MWh]	81.7	150.3	231.7	354.9	459.1
Actual Day-ahead Deviation	[MWh]	4.0	54.8	178.1	506.8	1 476.4
Actual Day-ahead Deviation	[%]	0.0	0.4	1.1	2.6	6.3
Δ Day-ahead commitment	[%]	-38.1	-19.3	0	20.8	43.1
Δ Actual day-ahead deviation	[%]	-97.8	-69.3	0	184.5	728.9
Auxiliary Processes	[MWh]	220.2	171.5	124.6	95.1	61.2
Electrolyzer Transitions	[MWh]	225.8	179.3	195.0	105.5	70.1
Battery Discharge	[MWh]	59.6	75.5	82.7	84.4	73.0
Fuel Cell	[MWh]	27.3	50.9	95.7	305.6	489.7
Energy Shed	[MWh]	1 155.5	1 487.7	1 663.9	982.8	892.8
Energy Shed	[%]	4.4	5.7	6.4	3.8	3.4
Hydrogen Production	[kg]	232 520.3	181 053.3	131 513.9	100 384.9	64 657.0
Hydrogen Sales*	[EUR]	922 358.9	711 285.7	502 635.8	324 455.9	134 634.6
Day-Ahead Sales	[EUR]	968 001.5	1 262 226.5	1 556 594.7	1 880 514.5	2 228 076.6
Cost Intraday Purchases	[EUR]	9 481.0	16 994.6	26 041.9	38 694.8	50 051.0
Net Income*	[EUR]	1 883 808.5	1 960 836.2	2 037 856.0	2 169 120.7	2 314 185.0
Hydrogen Sales*	[%]	49.0	36.3	24.7	15.0	5.8
Electricity Sales*	[%]	51.0	63.7	75.3	85.0	94.2
Average Runtime	[s]	76.3	58.4	55.1	102.4	112.4

Day-ahead commitments increase drastically as transmission capacity increases (Figure 8.14) and the system over-commits systematically, which is observed by the large increase in day-ahead deviation, referred to Figure A.20 in Appendix, and decrease in delivery success. The increase in intraday purchases, as shown in Figure 8.15, fuel cell activity and in most cases batteries are responds in order to reduce the deviations. As a result from steadily higher over-commitments, hydrogen production is reduced accordingly as power is being directed to the power markets to fulfill the commitments. As over-commitments increase with higher transmission capacity, an increasing amount of energy is diverted to avoid large penalties, sacrificing hydrogen production. Systematic over-commitment unfortunately leads to systematic low levels of power available to produce hydrogen, as seen in Figure A.21, also attached to the Appendix.

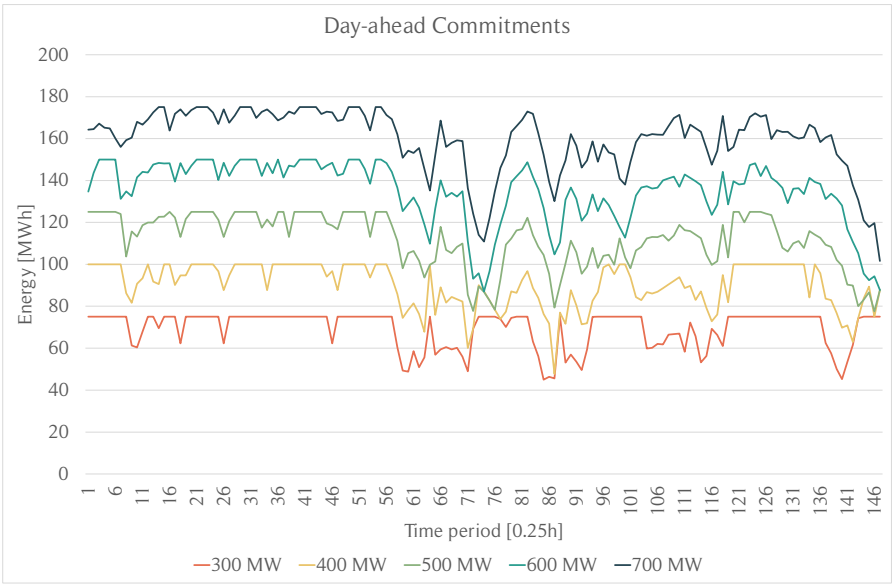

Figure 8.14: Comparison of the day-ahead commitments made with different transmission cable capacities. Changing the transmission cable capacity significantly increases the day-ahead commitments.

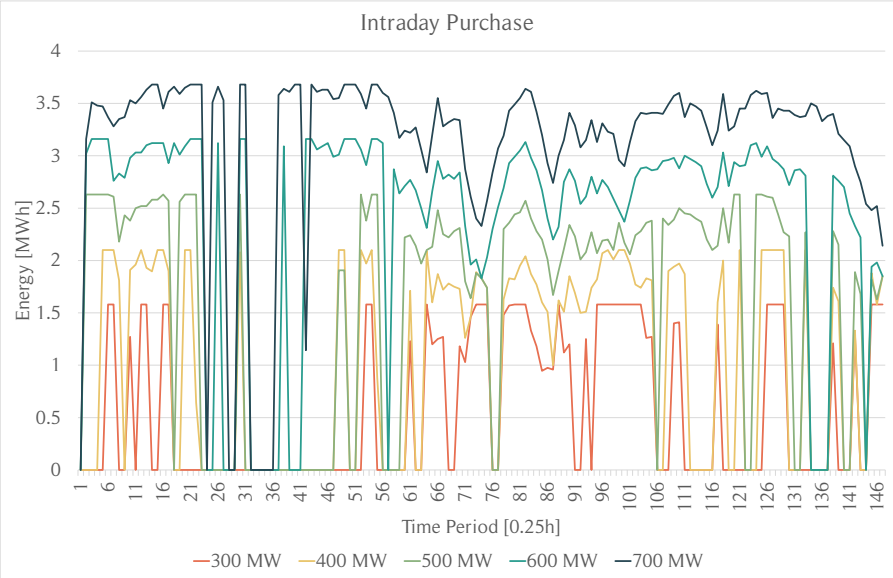

Figure 8.15: The total volume purchased intraday is compared under different transmission cable capacities.

It is observed in Table 8.6 that energy shedding both decreases and increases when the capacity moves in either direction from the base case. As stated in Section 7.6.3, the combined total installed capacity of power transmission and electrolyzer is 1 000 MW. The hydrogen production in the "300 MW"-case is more than three and a half time higher compared to the "700 MW"-case, despite the installed electrolyzer capacity only being less than two and a half between the two cases. Furthermore, it is observed that energy consumption from electrolyzers transitions increases for low transmission capacities. As energy shedding is heavily penalized, the electrolyzers become more susceptible to transitioning between operating states to avoid incurred costs of energy shedding. Another contributing factor is that the transition energy cost increases when electrolyzer capacity increases as per reported in the previous section. The high day-ahead commitments could lead to situations where all power needs to be directed to minimize day-ahead deviations, thus leaving little available power for the electrolyzers and necessitating a shutdown of the electrolyzers. When it is discovered that for instance, the power generation is above the day-ahead commitment, the model suffers from reduced capacity due to the electrolyzers being shut off in the previous period. As the energy system has more available energy for hydrogen production when the transmission cable has low capacity, this could lead to substantial energy shedding. Furthermore, over-commitments happen less frequently when the transmission capacity decreases. Lower capacity constraints would decrease the probability of cases where the power generation is lower than the first-stage day-ahead commitments. These factors, in combination with a higher electrolyzer capacity, lead to a higher hydrogen production when transmission capacity is reduced.

It becomes apparent that when the model has a low power transmission capacity, it has a stronger ability to effectively manage hydrogen production. According to this line of argument, the energy shed should increase when power transmission capacity increases. This is however not the case for transmission capacity above the base case. As stated above, the model systematically over-commits when the transmission capacity is high. The upper bound on power sale is to a great extent decided by first-stage day-ahead decisions as the intraday trading limit is a function of the day-ahead commitments. As the model consistently commits larger volumes of power to the day-ahead market, the upper bound on power sales increases as these are directly related to the committed power day-ahead in Constraints (6.64) and (6.65). This implies that the model in cases with higher power transmission capacity has a higher bound on power sales. The bound on power sale becomes low in cases with low transmission capacity as the bound is limited by the actual day-ahead commitment, despite potentially having a lot higher power generation than what was planned for. This, in combination with electrolyzer capacity and shutdown implications, causes higher energy shed in cases of lower transmission capacity and lower energy shed in cases with higher transmission capacity. It is also important to factor in that the model does not have the opportunity to participate in the intraday market at every time period, due to zero demand

and/or supply. This could naturally increase energy shed as day-ahead commitment is fulfilled and electrolyzers operate at maximum capacity.

The two effects described above impact the overall energy shed in opposite ways. For the studied cases it appears that the effect of higher bounds on power sales reduces energy shedding to a greater extent than stronger the effect of hydrogen production management, as the lowest energy shed is found for a transmission capacity of 700 MW. Furthermore, low transmission capacity increases the impact of hydrogen revenues on net income, and vice versa for electricity sales, as is to be expected. The net income increases with transmission capacity, as shown in Figure 8.16. This is likely due to the price differences between hydrogen and day-ahead power sale, as can be seen in Figure A.18, and that these effects are enforced when the upper bounds are adjusted for each market. However, the considerable day-ahead deviation found with higher transmission capacity could infer substantial consequences on profitability in the end.

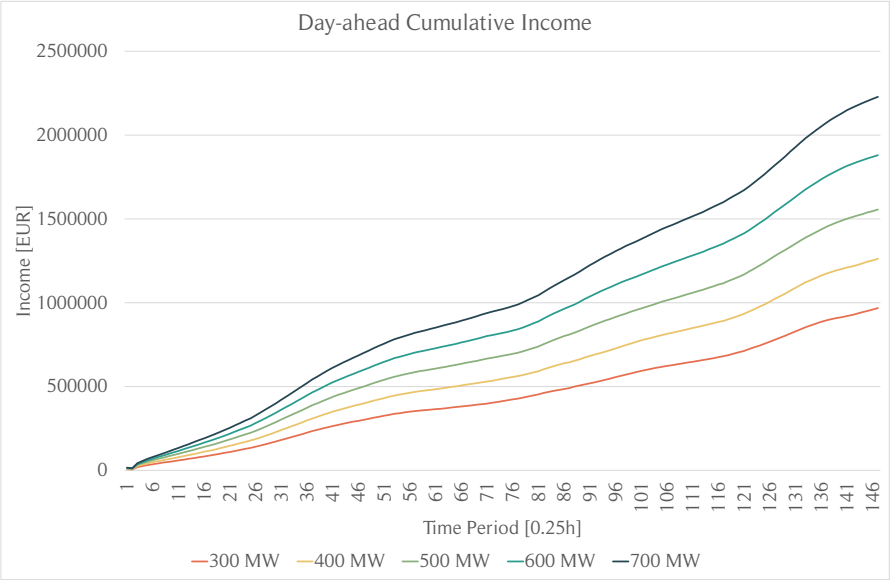

Figure 8.16: With time the income from day-ahead operations under higher transmission cable capacities increases at a high rate.

The model submits day-ahead bids 12-36 hours ahead of delivery and the wind power scenarios are identical across all configurations for this particular test instance. Independent of the transmission capacity, the cases face the same risk profile when submitting day-ahead bids, which is reflected in the lowest producing scenario. To understand the increased electricity revenues and the strong correlation with higher under-delivery, one must recognize the price difference between power and hydrogen. This price difference, in combination with higher upper bounds on transmission capacity, inevitably leads to higher bids inconsequentially on how the power generation actually develops 12-36 hours later.

8.1.5 Size of $\mathcal{E}$

The number of electrolyzers directly affects how accurate electrolyzer behaviour can be modelled. The larger size of $\mathcal{E}$ results in a higher granularity for the modelling of electrolyzers. The idea behind varying the number of electrolyzers allows to study the trade off between more accurate modelling and computational complexity. The results from increasing the number of electrolyzers are presented in Table 8.7. The most important variables, such as day-ahead commitments and deviation, hydrogen production and energy shed do not have a uniform behaviour in this test instance. However, the average solution time increases substantially as the number of electrolyzers increases.

Table 8.7: Key findings from the sensitivity analysis on number of electrolyzers.

	Unit	$\mathcal{E} = 20$	$\mathcal{E} = 50$	$\mathcal{E} = 100$	$\mathcal{E} = 150$	$\mathcal{E} = 200$	$\mathcal{E} = 400$
Day-ahead Commitment	[MWh]	16 428.8	16 429.9	16 427.5	16 428.3	16 427.7	16 428.6
Intraday Purchase	[MWh]	231.7	243.0	236.0	247.0	237.6	252.1
Actual Day-ahead Deviation	[MWh]	178.1	177.5	178.6	178.5	177.0	177.5
Actual Day-ahead Deviation	[%]	1.1	1.1	1.1	1.1	1.1	1.1
Intraday Sale Commitment	[MWh]	35.8	33.3	33.2	31.5	35.8	28.9
Auxiliary Processes	[MWh]	124.6	131.6	132.5	131.4	129.6	134.9
Electrolyzer Transitions	[MWh]	195.0	165.0	156.3	161.3	177.8	137.9
Battery Discharge	[MWh]	82.7	84.3	89.9	82.4	76.5	84.9
Fuel Cell	[MWh]	95.7	94.5	92.9	97.0	97.1	92.5
Energy Shed	[MWh]	1 663.9	1 242.5	1 181.7	1 260.9	1 355.3	1 058.7
Energy Shed	[%]	6.4	4.8	4.5	4.8	5.2	4.1
Hydrogen Production	[kg]	131 513.9	138 967.8	139 880.2	138 725.5	136 779.6	142 365.7
Hydrogen Sales*	[EUR]	502 635.8	532 665.3	536 719.7	531 047.0	523 245.8	546 699.6
Day-Ahead Sales	[EUR]	1 556 594.7	1 556 695.9	1 556 537.9	1 556 623.7	1 556 546.9	1 556 651.4
Net Income*	[EUR]	2 037 856.0	2 066 316.9	2 071 333.0	2 063 567.0	2 058 054.1	2 079 222.3
Hydrogen Sales*	[%]	24.7	25.8	25.9	25.7	25.4	26.3
Electricity Sales*	[%]	75.3	74.2	74.1	74.3	74.6	73.7
Average Runtime	[s]	54.3	71.1	90.4	119.3	145.8	300.8

The impact of increasing the number of electrolyzers leads to a higher allocation of activities in the hydrogen market. While there is a slight increase in net income for larger electrolyzer sets, there is no definitive trend; neither in intraday sales or purchases as the volume of intraday trades shows both increases and decreases. Similarly, the day-ahead deviation does not provide a justification for using larger sets. The behavior of the energy system appears to be consistent regardless of the size of the electrolyzer set, which may be attributed to the dynamic operating point of the electrolyzers. One would expect that a higher number of electrolyzers would offer more flexibility in regulating hydrogen production, particularly in terms of ramping processes and transitioning between states. A more detailed analysis of the electrolyzers' behavior would help identify the optimal number of electrolyzers needed to effectively switch states.

In cases where the system needs to shut down electrolyzers, the minimum energy requirement for operating an electrolyzer with 200 units is 0.0625 MWh, while for 20 units, it is 0.625 MWh. If there is only enough energy to operate an additional 0.50 MWh, the model cannot turn on an electrolyzer in the set of 20 units. However, with 200 electrolyzers, it would be possible to turn on 8 electrolyzers. In theory, a higher number of electrolyzers provides more operational flexibility, and although the overall results are inconsistent, there seems to be a decrease in energy shedding with a higher number of electrolyzers. Although the solutions do not demonstrate noteworthy differences overall, the amount of curtailment could be an indicator of the value of higher modeling accuracy. It is important to keep in mind that the number of electrolyzers does not impact the curtailment resulting from maximum electrolyzer production in situations with surplus energy in the system.

Increases in the size of the true electrolyzer set do not seem to have a significant impact on model solutions. The planning and consequences of day-ahead commitments appear to be the same across all test cases. However, the model tends to increase the amount of energy allotted to hydrogen production for larger electrolyzer sets, which leads to higher revenues from hydrogen sales. The slight differences in variable values could also be attributed to the optimality gap, which varies among the different cases. Additionally, it is worth noting that the solution time increases rapidly as the set size increases. It is important to remember that the electrolyzer sets are modeled for a total of five time periods. Preliminary testing did not give convincing results that increasing this number of time periods is of any considerable value, and the solution times are likely to increase exponentially if combined with a larger modeling set of the electrolyzers. It is uncertain that utilizing larger electrolyzer sets would offer practical value to the model. A larger set of electrolyzer could offer marginally better management of electrolyzer, but at the cost significantly longer solution times. A potential increase in the size of the electrolyzer set must be considered together with potential increases in other sets, such as number of scenario and number of time periods with true electrolyzer sets. Increases in numerous sets would cause an exponential increase in size, and there is a risk that solutions cannot be found within the real-life time limits. It can also be concluded that the base case with a set size of 20 is a sufficient formulation, as there are no significant differences in solutions compared to larger sets.

8.1.6 System Performance with Different Hydrogen Prices

Changes in hydrogen price can affect revenues from hydrogen in two ways. A price change causes a scaling of the revenue per unit hydrogen with all other things being equal. A change in hydrogen price can also affect system behaviour as the model could favor hydrogen production instead of power sale when relative price differences are taken into consideration. The results presented in Table 8.8 suggest however that changes in overall system behaviour are small when compared to the large relative changes in hydrogen price per kilogram.

Table 8.8: Key findings of system performance with different hydrogen prices per kilogram hydrogen.

	Unit	2 EUR	3 EUR	4 EUR	6 EUR	8 EUR	10 EUR	15 EUR	20 EUR
Day-ahead Commitments									
Day-ahead Commitment	[MWh]	16 441.7	16 441.7	16 428.8	16 292.9	16 129.6	16 117.6	16 075.7	16 069.1
Intraday Purchase	[MWh]	228.1	228.1	231.7	238.2	237.7	240.2	251.5	248.5
Actual Day-ahead Deviation	[MWh]	178.5	178.0	178.1	179.2	182.4	181.9	182.4	182.3
Actual Day-ahead Deviation	[%]	1.1	1.1	1.1	1.1	1.1	1.1	1.1	1.1
Auxiliary Processes	[MWh]	120.9	122.9	124.6	124.4	126.1	129.5	127.1	132.9
Electrolyzer Transitions	[MWh]	210.0	189.4	195.0	199.4	197.8	185.6	197.2	170.3
Battery Discharge	[MWh]	79.8	82.5	82.7	88.5	98.6	101.9	93.8	98.1
Fuel Cell	[MWh]	98.8	97.9	95.7	89.6	86.6	86.5	87.7	85.3
Energy Shed	[MWh]	1 888.9	1 765.5	1 663.9	1 810.6	1 859.5	1 670.1	1 861.1	1 509.4
Energy Shed	[%]	7.2	6.8	6.4	6.9	7.1	6.4	7.1	5.8
Hydrogen Production	[kg]	127 587.2	129 721.3	131 513.9	131 284.2	133 123.0	136 682.9	134 206.6	140 253.0
Hydrogen Sales*	[EUR]	243 102.8	371 205.6	502 635.8	754 989.5	1 022 885.5	1 314 003.0	1 932 930.8	2 700 710.6
Day-Ahead Sales	[EUR]	1 557 467.7	1 557 470.9	1 556 594.7	1 545 171.5	1 528 890.2	1 528 164.4	1 523 954.7	1 523 529.6
Intraday Sales	[EUR]	4 666.8	4 667.6	4 667.5	4 512.3	4 538.1	4 230.6	3 850.6	3 863.9
Net Income	[EUR]	1 700 664.9	1 855 266.2	1 853 701.4	2 163 668.1	2 282 317.6	2 594 205.3	2 278 395.8	4 150 239.7
Net Income*	[EUR]	1 779 429.1	1 907 533.6	2 037 856.0	2 278 292.1	2 529 873.6	2 819 771.8	3 432 844.6	4 200 387.7
Hydrogen Sales*	[%]	13.7	19.5	24.7	33.1	40.4	46.6	56.3	64.3
Electricity Sales*	[%]	86.3	80.5	75.3	66.9	59.6	53.4	43.7	35.7
Average Runtime	[s]	58.1	58.6	55.5	57.5	57.0	58.3	54.9	56.8

It can be seen that the revenue contributions from hydrogen sales increase when the hydrogen price increases. This is expected as the scaling of hydrogen unit price scales the revenues correspondingly with all others being equal. It can also be seen that total day-ahead commitments tend to decrease when hydrogen price increases, and logically, electrolyzer power consumption increases. The power consumption of electrolyzers increases when hydrogen prices increase. The increase in the amount of produced hydrogen is however relatively small. Thus, the monetary increase in hydrogen sales is driven by the scaling of revenues and not a large increase in hydrogen production. It appears that the direct sale of electricity remains more profitable for hydrogen prices up to 20 EUR/kg. This could seem counter-intuitive at first as the relative hydrogen price is considerably larger than the power prices. The decision between selling power and selling hydrogen is based on the relative price differences between the periods. The hydrogen price remains constant throughout the test period while power prices vary. A higher hydrogen price would increase the number of situations where hydrogen is relatively more profitable compared to power market sales. 20 EUR/kg is however relatively higher than every power price in the studied time period. This implies that it is not relative price differences that result in large commitments in the day-ahead market. It is however a possibility that the production of hydrogen does not increase significantly due to capacity limits on production. Thus, the true value and implications of higher hydrogen prices on system behaviour is not necessarily captured by only varying the hydrogen price without other changes in energy system design.

8.1.7 Value of Perfect Information

The results of the perfect information case is given in Table 8.9 together with the results of the stochastic solution.

Table 8.9: Comparing the objective function values of the perfect information solution and stochastic solution together with key system performance metrics.

	Unit	Perfect Information	Stochastic Solution
Objective Function Value	[EUR]	1 947 099.1	1 853 733.2
Objective Function Value*	[EUR]	2 208 027.9	2 037 887.8
Objective Function Value**	[EUR]	2 206 680.9	-177 737 990.8
Day-ahead Deviation	[MWh]	0.0	178.1
Intraday Sale Deviation	[MWh]	0.0	0.0
Energy Shed	[MWh]	1.3	1 663.9

Without consideration of the unsold hydrogen in the pipeline, the $EVPI$ is

$$EVPI = PI - SS = (1\ 947\ 099.1 - 1\ 853\ 733.2)\ \text{EUR} = 93\ 365.9\ \text{EUR}, \tag{8.1}$$

or 5.0 % better. If we include the value of the unsold hydrogen but no default cost, the $EVPI$ is

$$EVPI^* = PI^* - SS^* = (2\ 208\ 027.9 - 2\ 037\ 887.8)\ \text{EUR} = 170\ 140.1\ \text{EUR}. \tag{8.2}$$

In other words, the perfect information solution is 8.4% better than the stochastic solution. Conversely, when accounting for the default cost from under-deliveries, the $EVPI$ becomes

$$EVPI^{**} = PI^{**} - SS^{**} = (2\ 206\ 680.9 - (-177\ 737\ 990.8))\ \text{EUR} = 179\ 944\ 671.7\ \text{EUR} \tag{8.3}$$

It is obvious that the perfect information case is better than the stochastic solution when including penalties. Yet, the negative objective function value of the stochastic solution becomes dramatically worse when including penalties, which stems from a high penalty cost in the model. As mentioned earlier, that doesn't suggest that 179 944 671.7 is the true value. In order to obtain the true value one would need to investigate the real costs of eliminating the delivery deficit first, and then compare the the two objective function values.

8.1.8 Value of the Stochastic Solution

The results of solving the expectation of the expected value problem is compared to the stochastic problem is given in Table 8.9.

Table 8.10: Comparing the objective function values of the expected value solution and the stochastic solution, and key system performance metrics.

	Unit	Expected Value Solution	Stochastic Solution
Objective Function Value	[EUR]	1 910 153.2	1 853 733.2
Objective Function Value*	[EUR]	2 176 216.2	2 037 887.8
Objective Function Value**	[EUR]	-468 232 743.7	-177 737 990.8
Day-ahead Deviation	[MWh]	470.1	178.1
Intraday Sale Deviation	[MWh]	0.0	0.0
Energy Shed	[MWh]	314.0	1 663.9

The VSS is computed according to Equation (2.13). When comparing the objective function terms, as reported as net income without taking into account the cost of load shed or default cost from power market contracts, the VSS is reported as

$$VSS = SS - EV = (1\ 853\ 733.2 - 1\ 910153.3)\ \text{EUR} = -56\ 420.1\ \text{EUR} \tag{8.4}$$

When including the unsold hydrogen in the pipeline,

$$VSS^* = SS^* - EV^* = (2\ 037\ 887.8 - 2\ 176\ 216.3)\ \text{EUR} = -138\ 328.5\ \text{EUR} \tag{8.5}$$

However, it is necessary to include the penalties for both the stochastic and the expected value solution in order to make a fair comparison. The total shedding over the planning horizon is 1

663.9 MWh and 314.0 MWh, respectively for SS and EV. The total day-ahead deviation over the planning horizon is 178.1 MWh and 470.1 MWh, for SS and EV. Since the battery activation cost is only for modeling and not representing any financial cost, it is not included.

$$VSS^{**} = SS^{**} - EV^{**} = (-177\ 737\ 990.8 - (-468\ 232\ 743.7)) = 290\ 494\ 752.9 \text{ EUR} \quad (8.6)$$

The inclusion of penalties reveals that the stochastic solution outperforms the deterministic problem significantly. However, evaluating the value of the stochastic solution compared to the deterministic model is challenging due to the complexity of accurately estimating the true cost of market penalties in the model. The value of 290 494 752.9 EUR serves as compelling evidence that the stochastic solution is superior to the deterministic solution, by definition, and is a preferred modeling choice, because it explicitly considers the risk of not meeting demand.

8.2 Managerial Insights and Discussion

The model has been tested over shorter and longer time periods in order to reveal the modelled behaviour of the energy system. Both modelling parameters and energy system design parameters were manipulated to study the model under different operating conditions. The results presented in Section 8.1 provides a foundation for the further analysis of model behaviour and operational performance made here. Projects similar to the energy system described in this thesis are to the authors' knowledge still in the investment phase. This has also been reflected in the available literature on offshore hydrogen production, where a large part of the current research efforts studies profitability of such projects. Short-term optimization focuses on optimizing decisions in an operational planning horizon. Models such as the one presented in this thesis would typically be applied to a real-life case study to assess how the proposed solution would improve operations and profitability. This is evidently not possible for this thesis due to the non-existence of operational offshore energy systems with hydrogen production. The results of the work in this thesis can still provide valuable insights for decision-makers. A study of the operational performance of the energy system could give more accurate estimations of revenues and cash flows, which are often used in NPV analyses to assess profitability of investment decisions. Furthermore, decision-makers could receive valuable information on the operational implications for different installed capacities on certain components. This suggests that the model presented in this thesis could be used iteratively with project life-time profitability tools to optimize energy system designs.

This section intends to contextualize the results in order to provide value to decision-makers. Several aspects and implications of the results in Section 8.1 are analyzed further in this section. Additional test instances have been identified, generated and tested to provide more insight in model behaviour. The results have been placed in both an operational and strategic context to reveal the co-dependence of operational decisions and investment decisions in the investment phase of a planning process. The assumption of being a price-taker in the power markets is discussed in Section 8.2.1. The intraday bidding process is addressed in Section 8.2.2. The implications of non-delivery in the power market on risk management are discussed in Section 8.2.3. A small study of the energy system under no access to power markets has been conducted in Section 8.2.4. The impact of the scenario generation method is explored in Section 8.2.5. A discussion of model design and energy system design is undertaken in Section 8.2.6. Finally, the profitability of power market participation is examined in Section 8.2.7.

8.2.1 Price-Taker Assumption

There are several important implications to consider in regard to increased participation in intraday markets. The model formulation is based on the price-taker assumption, which is the premise that market prices are not impacted by the participation of the wind power producer. Although this is a reasonable assumption for day-ahead market, intraday power prices within the current market would be significantly affected by the substantial increase in supply and demand caused by an energy system with unlimited intraday trading opportunities. The intraday market could in some extreme cases become as large as the day-ahead market. However, the provided data set has established that it is not typical to trade large volumes in the intraday market. Unlimited trading volumes would have a profound impact on pricing and may even pose technical and physical challenges in the management of such a large intraday market. The available transmission and production capacity are also reflected by the observed prices in the data set.

It is however worth noting that power markets, including the day-ahead market, could experience substantial growth in the coming years as a result of electrification efforts in many parts of Europe. The German intraday market already offers quarterly products, which can reduce the potential risks associated with trading surplus energy from the anticipated wind farm power within the upcoming hour. As the proportion of variable energy sources in the energy mix rises, quarterly products will progressively gain relevance in the Nordic Market. In this context, the possibility of an "unlimited intraday trading" scenario becomes more plausible as the intraday market becomes more liquid. Whether or not this scenario becomes a reality, one clear advantage of having high access to intraday markets is the reduction in day-ahead deviations for the energy system. The

model would always have the opportunity to avoid penalties by adjusting day-ahead commitments based on intraday trading opportunities.

8.2.2 A Complicated Intraday Bidding Process

Upon further investigation, it can be argued that the optimization model under full intraday access resembles a trading algorithm for both the day-ahead and intraday markets. This can seem surprising as the model does not consider intraday prices when day-ahead commitments are made. However, the model can in this case maximize revenues by comparing prices between the hydrogen market and the intraday market. Briefly explained, the model performs intraday purchases to cover the day-ahead contract and instead diverts the power from the wind farm to hydrogen production. This highlights the potential benefits of high access to intraday markets and the importance of capturing price differentials to optimize the energy system's financial performance.

The dynamics of the bidding process make the intraday modeling challenging, which is arguably why some authors choose a simpler modeling approach. Such approaches can consist of not modeling sequential intraday auctions and commitments. There are several aspects that make the bidding process intricate. There are for instance numerous regulations and products related to intraday trading, and possibilities to withdraw orders or placing bids well ahead of delivery hours. It is generally also possible to place both sale and buy orders, which can lead to numerous intraday contracts being active simultaneously. The inclusion of such aspects could result in a model that to a large extent would speculate in arbitrage opportunities, which is not the focus of this work. Intraday bids are therefore not modeled together with day-ahead bids.

Intraday transactions are based on bilateral arrangements and finding an optimal bid can be difficult as the market brings together multiple parties. The parties can have different net positions, financial and data resources to make their own informed decisions that align with the decisions of the wind power producer. Furthermore, one could argue that the upper bounds on intraday trades are too restrictive. In a case of energy abundance, it is possible to lower the selling price, or even selling at negative prices, to make the offer more attractive to other parties. With the same logic, another party could accept a buy order if the offered price is high enough. The unpredictability of modeling the intraday bidding process can be reflected in the fact that the traded volume can be anywhere between 5 MWh to several hundred MWh per hour. As observed, the wind power producer is trading a considerable higher volume of purchase contracts compared to sale contracts. This could, with correlated production patterns between variable power producers of similar scale, cause technical concerns for the grid infrastructure. The current implementation is justified by the idea that trading constraints should reflect the demand and supply. It might be the case that the value of the intraday market to the wind power producer is not accurately represented with hard volume restrictions and could potentially benefit from other modeling strategies of the intraday market dynamics. In retrospect, a more appropriate approach could have been to estimate intraday prices as a function of the requested volume to be sold or purchased.

8.2.3 Risk Management: Non-delivery Penalties and Power Market Exclusion

The occurrence of under-delivery in certain test instances does not imply exclusion of wind power producers from the Nordic Power Exchange. However, it highlights the need for balancing mechanisms. Minimizing the under-delivery is desirable for a number of reasons, and insights can be gained by comparing the relative decrease (or increase) of under-deliveries as a percentage of the promised commitment. The base-case exhibits a relatively low deviation ($\sim$1%). In contrast, increasing the transmission capacity leads to relatively significant increases in day-ahead over-commitments. With a 700 MW transmission cable, the total under-delivery is 728.9 % higher than the base-case scenario. At first glance, a total deviation of 6.8 % from the promised delivery is substantial. It is therefore important to discuss the financial implications of this finding. It can be difficult to determine the tolerable level of under-delivery, but the true cost ultimately depends on the financial burdens from actions taken to correct this under-delivery. As emphasized earlier,

the intraday market is crucial in addressing imbalances in the net position which can serve as a cost-estimator for covering the production deficit. Repeated under-delivery must however be taken seriously as participation in power markets requires the ability to deliver promised commitments. The tolerance level for observed under-delivery should be evaluated against the quality of the power generation forecasts.

The penalty costs in the original formulation are extremely high. To investigate the impact of the penalty parameter value, the base case is tested with a substantial lower penalty. Penalties for under-delivery in all power markets are set to 1 000 EUR/MWh and the cost of energy shed is adjusted to 500 EUR/MWh. All other system characteristics remain unaffected. As seen in Table 8.11, it is evident that the penalty costs does have a profound impact. A lower penalty encourages higher commitments which is accompanied by larger amounts of under-delivery.

Table 8.11: Key findings from the impact of lower penalty costs.

	Unit	**1 000 000**	**1 000**
Day-ahead Commitment	[MWh]	29106.0	29616.9
Actual Day-ahead Deviation	[MWh]	188.8	203.3
Energy Shed	[MWh]	3919.2	15.4
Energy Shed	[%]	7.5	0.0
Hydrogen Production	[kg]	306086.2	363418.7
Day-Ahead Sales	[EUR]	2834662.4	2903469.5
Cost Intraday Purchases	[EUR]	40162.0	15488.5
Average Runtime	[s]	65.6	540.7

One of the main implications of lower penalty cost is the weighting of extreme scenarios, and low-power scenarios in particular. Low-power scenarios have been seen to determine model behaviour extensively as the expected deviation costs are significant. It can also be seen in Figure 7.8 that the number of extreme scenarios can be limited to only a few, and often just one scenario. This scenario could be a statistical outlier from stochastic processes in the scenario generation method. It could therefore be argued that the weight given to this scenario by a high penalty cost does not necessarily reflect the true expected cost. A lower penalty cost will reduce the impact of such extreme scenarios.

The penalty costs affect to a great extent how the model reacts sudden changes in wind power production within the generated scenarios. Large short-term variations in wind speed can cause deviations in commitments that the model needs to adjust for. It can be seen in Figure 8.17 that there are only minor differences in day-ahead commitment patterns for a low and high penalty cost. Most of the differences are observed for commitments that are close to the capacity limit of the transmission cable. This is likely due to lower impact of extreme scenarios, which in this case would be low-power scenarios. Reduced impact of extreme scenarios could be one of the explanatory factors behind the increase in day-ahead deviation with a lower penalty. When deviations are not as severely punished as before, the model evaluates candidate solutions that previously were suboptimal. An example of this behavior could be to prevent shutdown of electolyzers in cases where only a single scenario projects a low power value. Such cases can also explain why hydrogen production has increased significantly between the two cases and how energy shedding has been almost eliminated in its entirety. A simple numerical example could illustrate such situations.

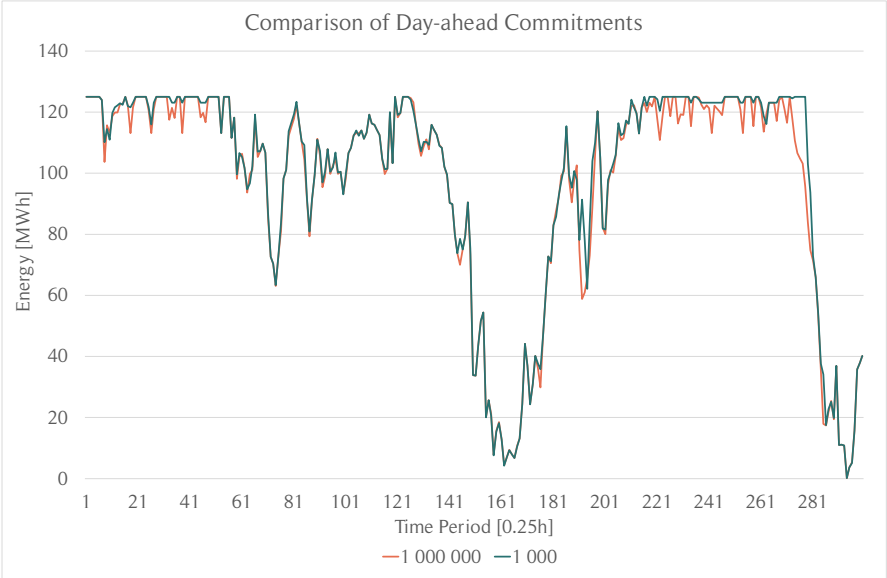

Figure 8.17: Comparison of day-ahead commitments for day-ahead penalties of 1 000 000 EUR/MWh and 1 000 EUR/MWh.

The costs of day-ahead deviation are evaluated against the costs of energy shedding and lost hydrogen revenues when electrolyzers are decided to be turned off. This has been observed in Figure 8.4 where the model responded to forecasted wind power variations in a more sensitive manner when a high penalty was in place. This lead to what in hindsight can be characterized as unnecessary shutdowns of the electrolyzers. However, the relative difference between these two aforementioned costs changes with a lower penalty cost. The day-ahead deviation in a single time period would in a worst case situation be 125 MWh, with a penalization of 1 000 EUR/MWh. For this simple example it is assumed that 20 scenarios are generated and that the true power value is given by one of them. If 19 out of 20 scenarios expect power generation at maximum capacity and the remaining scenario projects zero power generation, the expected deviation cost of not turning off electrolyzer before the subsequent time period would be 6 250 EUR. The expected shedding would in 19 out of 20 scenarios become half of the maximum hydrogen production capacity subtracted by start-up energy costs, due to the shutdown of electrolyzers. With an associated shedding cost of 500 EUR/MWh, this would correspond to a shedding cost of 26 718.75 EUR. Additionally, the revenues from lost hydrogen sales must be added to the calculations. Had the electrolyzer not been turned off, the energy system would have been able to produce approximately one additional ton of hydrogen, with a value of 4 000EUR. Battery discharges, fuel cell activation and intraday purchases would naturally have an impact on the final differences between the situation described here. However, the model would still prefer to keep electrolyzers in operation and instead risk having a higher day-ahead deviation in the subsequent period.

These types of situations could explain the difference in electrolyzer consumption in Figure 8.18 and the energy shedding in Figure 8.19, where the model produces hydrogen for a low penalty and sheds for high penalty for given periods. The dimensions of the number suggests that the line of argument in the numerical example could be valid for an even lower penalty for energy shedding. Furthermore, these types of situation could explain the increase in day-ahead deviation described by Table 8.11, while hydrogen production increases and energy shedding decreases. The same penalty for under-delivery during operation is imposed on the model when it makes bid submissions to the power exchange and accounts for the expected under-delivery. The increase in total day-ahead commitments could therefore also be explained by the reduced impact of low-power scenarios.

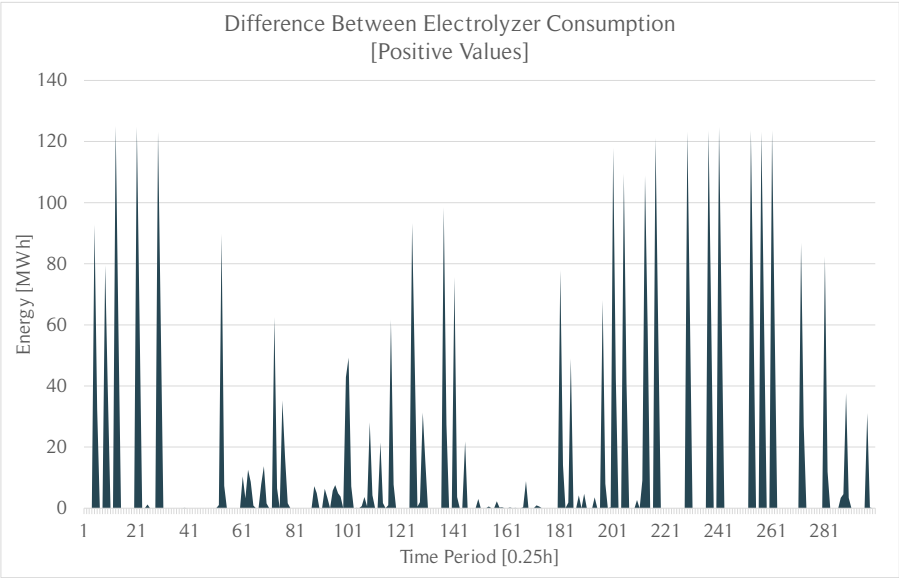

Figure 8.18: Difference between electrolyzer consumption for day-ahead penalties of 1 000 000 EUR/MWh and 1 000 EUR/MWh.

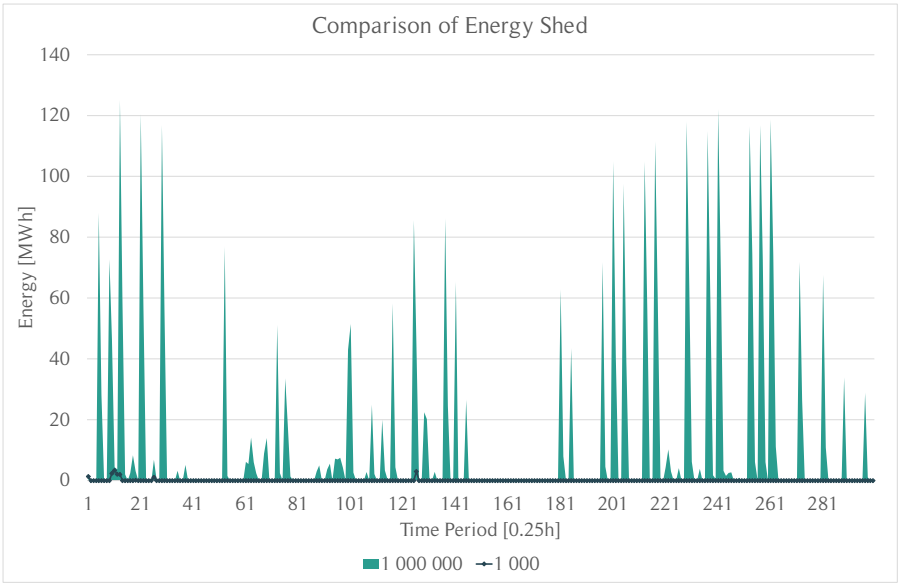

Figure 8.19: Comparison of energy shed for day-ahead penalties of 1 000 000 EUR/MWh and 1 000 EUR/MWh.

A central question in regard to modeling with difference penalty costs is raised by the revenue and cost distributions from operation imperfections in Table 8.11. How should decision-makers assign a cost estimate of the large energy shed and small day-ahead deviation under a high penalty cost, as compared to the much smaller energy shed and slightly higher day-ahead deviation with a smaller penalty? This dilemma encounters different perspectives on how to effectively model the costs of these imperfections. While there are many factors that influence the choice of penalty cost, such as the forecast quality and model formulation, the real-world financial implications should be the main contributor in the selection of appropriate penalty values. It was argued in Section 8.1.3 that with no volume restrictions on intraday trading, the net position can be adjusted as needed, which has also been confirmed when testing the model under these circumstances. In other words, the penalty cost should under optimal conditions reflect this cost. Choice of optimal penalty becomes even more complex when several balancing mechanisms are available. Such mechanisms are in this case fuel cells and batteries, which can be cheaper to utilize although with limited capacities. Real-life operations would also be influenced by other various balancing and reserve markets, which could complicate the matter even further. Despite all available balancing mechanisms, there would

always be a small possibility that the contract as a worst consequence is defaulted. Repeated cases of contract default could lead to exclusion from the power markets. Power producers with variable renewable energy sources are themselves victims of the stochastic nature of wind and weather. In other words, power producers could be penalized for exogenous factors that are beyond their control. Hard penalization of day-ahead deviation could disincentives new wind farm projects. However, too soft penalization could lead to systematic over-commitment from power producers. Thus, efforts from both power producers and policy makers must be made to ensure maximum economic efficiency and reduce curtailment.

8.2.4 Decoupling from Power Markets - *Island Mode*

Several of the authors that figure in the literature review have studied different offshore configurations. While the energy system in this thesis is interconnected to hydrogen and electricity markets, similar future offshore energy systems could be isolated from the power markets. A power grid decoupled energy system, or what is commonly referred to as "island mode", has been studied in order to assess the revenues of system that can only generate revenues with production and sale of hydrogen. More specifically, an examination of which hydrogen prices would yield comparable revenues between the island mode setting to the hybrid system has been conducted. This examination could provide value to decision-makers if it currently is uncertain if similar offshore energy systems will be connected to the power grid. The net income of the base-case is established as a benchmark for comparison, which amounted to 2 037 856.0 EUR. The results are presented in Table 8.12.

Table 8.12: Key findings of island mode assessment.

	Unit	2	4	5	6	8	10	15
Technical Performance								
Electrolysis	[MWh]	25 667.9	25 667.9	25 667.9	25 667.9	25 667.9	25 667.9	25 667.9
Auxiliary Processes	[MWh]	391.2	391.2	391.2	391.2	391.2	391.2	391.2
Electrolyzer Transitions	[MWh]	12.5	12.5	12.5	12.5	12.5	12.5	12.5
Battery Discharge	[MWh]	0.0	0.0	0.0	0.0	0.0	0.0	0.0
Fuel Cell	[MWh]	0.0	0.0	0.0	0.0	0.0	0.0	0.0
Energy Shed	[MWh]	56.6	56.6	56.6	56.6	56.6	56.6	56.6
Energy Shed	[%]	0.2	0.2	0.2	0.2	0.2	0.2	0.2
Hydrogen Production	[kg]	413 072.8	413 072.8	413 072.8	413 072.8	413 072.8	413 072.8	413 072.8
Financials								
Hydrogen Sales	[kg]	365 297.9	372 081.0	372 294.0	385 018.1	372 986.7	385 702.1	372 643.5
Hydrogen Sales	[EUR]	726 940.2	1 480 887.6	1 852 145.3	2 298 569.9	2 968 973.3	3 837 709.5	5 561 724.6
Hydrogen Sales*	[EUR]	823 992.5	1 648 007.8	2 060 000.8	2 471 938.7	3 295 970.1	4 119 991.0	6 180 067.3

The results indicate that the island mode generates 18.8 % less revenue compared to the hybrid mode in the base-case. This suggests a break-even price for hydrogen of approximately 4.9 EUR/kg, which shows a relatively modest increase from the initial price level. However, to achieve this, an additional 500 MW of electrolyzer capacity would be required, necessitating a comparison between the investment in transmission cable and the electrolyzers. It is important to note that the profitability of the hybrid configuration is influenced by both power market and hydrogen prices. Additionally, specific hydrogen demand contracts may undermine these results if they require a specific amount of hydrogen on a regular basis, potentially reducing the profitability of the hybrid mode.

A second observation is that the battery and fuel cells remain inactive over the planning period. Having an aggregated electrolyzer capacity of 1 000 MW requires a minimum energy consumption of 25 MWh to keep all of the electrolyzers operating. However, recorded wind energy production never reaches such low levels (49.42 MWh lowest, 250 MWh highest) and the model utilizes the dynamic operating range to maintain continuous operation without shutdowns. This suggests that fuel cells and batteries may potentially be omitted in the design of the energy system in an island mode configuration.

8.2.5 Scenario Generation and Wind Power Stochasticity

Scenarios have been seen to have a large effect on the value of stochastic solution. While scenarios can capture elements of the probability distribution of stochastic parameters, it has been observed that statistical outliers can have a large effect on model behaviour. The likelihood of statistical deviations increases when many scenarios are generated over a long period of time as the scenario generation method contains random processes. However, the value of including statistical outliers in decision-making tools can be essential for risk management, as rare events can incur large costs if not considered. The scenario generation method used in this thesis and the handling of wind power stochasticity is discussed in this section. The next three paragraphs looks at the impact of scenario diversity, the application of the utilized scenario generation method to offshore wind farms and, finally, a brief elaboration of wind data sources is given.

Scenario Diversity

An increase in the number of scenarios presents both advantages and disadvantages. Extremely low wind power scenarios raise the risk of over-commitment. Conversely, the inclusion of additional wind power scenarios with high energy availability serves to increase the likelihood of higher production which helps to mitigate this risk by bolstering the model's confidence in its bidding strategy. The model consistently seeks to achieve an optimal balance between risk and income generation, making decisions that maximize the expected income. It carefully evaluates the trade-off between over-committing and the corresponding penalties in each scenario, taking into account the value of committing additional energy units. Moreover, as the number of scenarios increases, it is reasonable to anticipate that the day-ahead commitment will align closely with the scenario featuring lower production, while the inclusion of additional scenarios helps to enhance bidding confidence. This could however be counterbalanced by a low value for the day-ahead deviation penalty. Thus, the choice of penalty would influence the effects and implications of scenario diversity. It is therefore crucial to assign an appropriate penalty value before making an assessment of potential changes that have to be made in terms of scenario diversity. Such changes could be various scenario reduction and bundling techniques, so that the impact of statistical outliers are reduced.

An increased number of scenario would not only give a larger set of potential outcomes. It would also increase the solution time of the problem substantially. The model has in this thesis been given a maximum of 15 minutes to solve each subproblem. This could give the decision-maker little time to implement the operational schedule proposed by the model. In practice, the model would likely have less than 15 minutes to find a solution. It could also happen that the model is not able to find any feasible solution for the given time limit, if the number of scenarios is excessive. It is therefore important not to increase the problem size without considering the impact of high computational complexity. This is especially important if the accuracy is only marginally improved by an increased number of scenarios.

Scenario Generation Method

While the scenario generation method appears to perform well when power values are not at a maximum over longer time periods, it does not always perform too well when power generation is at full capacity over a long time period. This could be due to the covariance matrix having problems when numerous quantiles take the value of 1, denoting 100 % power production. When historically realized values are 1, it is not clear which quantile should be considered in the recalibration process. Also, when numerous quantiles are 1, it is difficult to generate future scenarios from the quantile distribution when drawing random numbers from the distributions. It is for instance not clear which quantile $Y = 0.5$ belongs to if a total of 15 separate quantiles have the value 1. This directly affects the covariance matrix. Also, forecasted wind speeds instead of forecasted power production could perhaps be applied directly in the quantile regression models.

There is however one issue that could arise if the quantile regression model is applied to forecasted

wind values. The highest quantile will have the highest wind speed value compared to the other quantiles. An issue here is that there is no theoretical upper bound on the 100%-quantile. Some measures must then be used to model this quantile with a proper exponential tail. Furthermore, the upper quantile would be the first quantile to go over the upper wind speed for the turbine. The wind turbine is shut off if the wind speed exceeds this upper bound, which is equivalent to zero power generation. This would lead the upper quantile in terms of wind speed to become the lowest quantile when converted to power values. This could cause issues in the parametrization of estimators in the quantile model.

The covariance matrix is also slightly sensitive to starting conditions as the effect of exponential smoothing is large for small numbers of iterations. It could perhaps be useful to train and initialize the covariance matrix over a larger set. Furthermore, it could be that the method provided by Pinson et al. (2009) is not necessarily suitable for offshore winds. Offshore winds are stronger compared to onshore winds, and power generation could be at maximum for longer time periods for offshore wind farms compared to onshore wind farms.

Wind Data Sources

The model developed in this thesis has been provided data from MET Norway. The methods described in Section 7.5.1 were necessary to scale and convert wind speeds to appropriate values that could be used be the model, in addition to linear interpolation to create data with 15 minute resolution. These methods are however not ideal as actual production data should be used by the model. The historical data is a post-processed product from MET Norway, meaning that it is not actual measured data. There are to the authors' knowledge relatively few offshore wind farms in the North-Sea. Furthermore, there are no floating offshore wind farms situated far out in the North-Sea. This makes it challenging to access real observed data, which would be useful for the work in this thesis.

8.2.6 Model Design and Energy System Design

Operational decisions are heavily influenced by energy system design. The design of the energy system is particularly shaped by investment decisions made early in the lifetime of a project. This implies that the decision on installed capacity on system components may only be made once. It could also be possible to expand capacities in the operational stage of the project, however this would require certain early-stage decisions that would in practice create real options. It has for instance been observed in Section 8.1.4 that over-dimensioning of electrolyzer and fuel cells capacity can lead to significantly better solutions. This suggests that the decision-maker could invest in over-dimensioning of certain component capacities to increase operational profits. It could therefore be essential that the decision-maker considers the added value of flexibility from over-dimensioning as decisions on installed capacities in a worst case can only be made once. Modelling choices made to control problem size and computational complexity also influence the operational decisions as simplifications of real-life behaviour lead to theoretically suboptimal solutions. This section first expands on the design of the model in this thesis. This is followed by a discussion on energy system design starting with electrolyzer capacity and followed by fuel cells and batteries, pipeline and finally power transmission cable.

Model

The challenge of solving a model with a 36 hours look-ahead horizon is the problem size. This issue requires careful consideration of the mathematical formulation in the development of the stochastic optimization model. Small changes can lead to drastic results on solution performance and significantly longer solution times, as demonstrated when increasing the size of $\mathcal{E}$ or reducing the under-delivery penalty. In the first case, the number of binary variables increases exponentially given the scenario description, and the original formulation had over 4 million binaries in the preliminary testing phase. In the second case, a high penalty narrows the candidate solution space

dramatically, as many solutions are cut off from having negative objective function values. The opposite is true when decreasing the penalty. These examples demonstrate how model performance and problem complexity can be very sensitive to changes in parameters. The original formulation was downsized from 400 electrolyzers to 20 after the model made use of the computational resources and even crashed to due lack of random-access memory in the computer cluster.

A strength of the proposed model is that it can incorporate large amounts information simultaneously and that the acquisition of new information imitates the real-life process. This allows a more accurate information flow as the submission of market bids and revealing of market prices is approximated to real-life conditions. The model also incorporates risk-assessment by modeling the consequences of under-delivery on the submitted bids. Too optimistic bidding would be the consequence if these financial consequences were not modeled, and true income would be considerably less without this aspect taken into consideration. The strategy of sequential intraday auctions resembles real-life market behavior, although the possibility of arbitrage has not been considered. Sequential intraday auctions and arbitrage raises concerns of interference with hydrogen production, and literature suggests that a multi-stage model would be needed instead of two-stage model. This would require a different approach and formulation. Furthermore, the stochastic processes in the model formulation would most likely result in chaotic model behavior. Commitments to intraday purchasing contracts could be done as soon as any wind power scenario projects low power generation, which could to an irrational and excessive trading behavior. However, a different approach could have been taken to model supply-demand patterns of the intraday market in order to capture a dynamic range of intraday prices for different volumes. The hard constraint on intraday trading volume does not provide the needed flexibility to adjust the net position in the power markets.

Electrolyzer Capacity

Increase in electrolyzer capacity was seen in Section 8.1.4 to increase the overall performance of the energy system. The decrease in energy shedding could be a sign of less curtailment and thus larger efficiency. Moreover, the decrease in day-ahead deviation could potentially assign a high value of over-dimensioning electrolyzer capacity in the energy system. Over-dimensioning consists of having a larger combined electrolyzer and power transmission capacity that supersedes the installed capacity of the wind farm. The value of reduced day-ahead deviation is to a large extent given by the penalty cost and could be significant in cases of high penalty costs. The investment decision on electrolyzer capacity should therefore include an assessment of the added operational value of flexibility and over-dimensioning. As high electrolyzer capacity tends to decrease power market commitments and deviations, fuel cells and batteries could become less essential to the energy system. It could be argued that investment costs in these components would be lowered. Investments in high electrolyzer capacity could therefore reduce the investment costs in other components and potentially reduce the overall investment cost of the energy system. This should however be subjected to a comprehensive analysis of investment costs and operational benefits.

Decision-makers could find that it for a given economic environment would not be profitable to invest in a substantially over-dimensioned energy system. Electrolyzer costs are however expected to fall and efficiency is expected to increase as the technology matures. While the value of increased electrolyzer capacity is uncertain, it is certain that there is a positive value that could be exploited. The physical footprint of the energy system does however impose physical constraints as to the amount of equipment that can be fitted on the floating hydrogen production site. This is a key point of difference between onshore and offshore hydrogen production sites. Expansion of electrolyzer capacity at a later time could in offshore applications be technically infeasible due to lack of space. Decision-makers must therefore consider to over-dimension the physical footprint of the production site if capacity expansion at a later time would be feasible. Expanding electrolyzer capacity could therefore be considered a real option, and the value of the option should be included in the investment phase of the energy system. By extension, over-dimensioning of the physical footprint of the offshore production site could also be considered a real option.

Fuel Cells and Batteries

The overall value of fuel cells must be evaluated from both the operational value of flexibility and the investment costs. The operational value from fuel cells could be quantified by finding the true value of the deviation penalty. This value would then be aggregated over the lifetime of the fuel cells which would provide an estimation of the reduction in deviation costs that the fuel cells are able to provide. Batteries provide in many ways the same operational flexibility as fuel cells. The role of fuel cells and batteries is minimal when the energy system is not coupled to the power markets. Activation of fuel cells and batteries could be triggered in some particular cases, but are most of the time expected to remain inactive. Batteries and especially fuel cells take a pivotal role when the energy system has access to power markets, and they are frequently activated to find optimal solutions.

Activation of fuel cells is a mechanism that can reduce the deviation of day-ahead commitments. It is important in the evaluation of fuel cell capacity to conduct an economic assessment that considers the costs associated with the use of fuel cells to other alternative methods in the reduction of day-ahead deviation. Determining the value of fuel cells is complex as it involves an evaluation of price differences when mitigating day-ahead deviations. If the price of hydrogen is high, the use of fuel cells for electricity generation may lead to a higher cost level compared to power purchases on the intraday market, as high revenues from hydrogen sales are foregone. If the intraday buying prices are relatively high compared to the hydrogen price, it makes more sense to use fuel cells at a high capacity.

To assess the potential savings from using fuel cells instead of the intraday market, it could be interesting to evaluate price differences between hydrogen and intraday purchases over time. An appropriate fuel cell capacity can be estimated by incorporating investment costs. Furthermore, it is argued that fuel cells can be activate to avoid shutdowns of the electrolyzers by providing the minimum energy requirement. Cost are incurred in subsequent time periods due to reduced production capacity resulting from previous shutdowns along with the energy consumption during shutdowns. This must be compared to the cost of continuing operation. In that case, the fuel cell capacity could be optimally designed to keep the electrolyzers running at minimum capacity but avoid shutting them down.

The impact of transitions should be considered if it is costly to avoid electrolyzer shutdowns and transitions in general. Additionally, transitions accelerate the degradation of electrolyzers. Minimizing the number of commutation cycles is a topic explored in the reviewed papers. Maintenance and potential replacement costs are associated with electrolyzers, and it should be possible to estimate the cost of a single transition and compare it to the value of hydrogen. It is worth noting that fuel cells require maintenance, while intraday purchases do not. Any maintenance requirement would result in the shutdown of fuel cells, leaving the system without backup power. While fuel cells could power other critical system components, it is important to consider the low round-trip efficiency of hydrogen power-to-gas-to-power. In such cases, it may be more sensible to directly power these components with energy from the wind farm.

Similarly to investments in electrolyzer capacity, the investment decision of fuel cells can be seen as a real option. The line of argument in terms of electrolyzer capacity and physical footprint being real options applies to fuel cells as long as they are situated offshore. While it has been assumed in this thesis that fuel cells are installed at the offshore facility, it is not required that the fuel cells are situated offshore. They could be placed on an onshore facility, and it might also be more profitable do it so. An onshore location does however have some other practical implications. One implication could for instance be that hydrogen designated for sale and hydrogen designated for fuel cells "share" the same discharge rate. Another implications is that the power from fuel cells would need to be transferred to the offshore facility via the power transmission cable and not directly injected into the energy system when placed offshore. Thus, the practical application of onshore fuel cells could be different compared to offshore placement. While the equipment costs would remain the same for onshore and offshore placement, it would be reasonable to assume that installing costs are substantially lower for onshore installation. It is therefore important for decision-makers to consider the operational flexibility and practical application of fuel cells that have been described here to the investment costs associated with having fuel cells as a part of the

energy system.

The batteries are frequently and consistently utilized across the test instances, but it can only provide a burst of energy. During several time periods with low power production, the fuel cells need to assume the role of supplying energy instead of the batteries. While batteries are known for their higher efficiency compared to fuel cells, their ability to mitigate or cover under-deliveries day-ahead contracts is limited in terms of energy provision. This work provides an estimation of the utilization rate of batteries, offering a more precise understanding of their application. To assess the value of incorporating lithium-ion batteries in the energy system, one can evaluate the financial implications weighing the lost revenues resulting from allocating energy to the batteries charging against the cost of under-delivery, operational costs associated with their maintenance, degradation, and eventual replacement. This economic assessment helps determine the overall economic feasibility of installing and operating the batteries. Batteries are however prone to degradation. The inclusion of batteries when coupled to power markets could provoke behaviour that is consistent with that of a trading algorithm as it charges and discharges to profit on price differences in the power markets. This behaviour is observed in Figure 8.2 where the battery discharges in periods where day-ahead commitments are lower than the generated power in a given time period. The degradation of battery life is the cumulative degradation from battery cycles, where each independent cycle induces stress on the battery (Xu, 2016). As a result, frequent charge and discharge of batteries could make it necessary to replace them often, which would be costly for the overall profitability of the energy system. The main purpose of batteries is to provide operational security by peak-shaving and balancing ultra short-term variation in power. While batteries play a crucial role for safe operations in the energy system, it can be argued that batteries should not be included in the decision-making processes related participation and activity in the power market.

Pipeline

This study did not consider the constraints imposed by hydrogen demand, despite the fact that hydrogen sales are realized through HPAs It is important to account for purchasing agreements as they influence investment decisions in hydrogen production and help mitigate excessive risks for the investors (personal communication with Martin Kjäll Olsson in the fall, 2022). In the presence of HPAs, there is a requirement to determine the necessary quantity of hydrogen that must be produced in order to fulfill one or multiple contracts. It is also possible to have multiple active HPAs with different start and end dates simultaneously as the energy system is likely to serve multiple customers. HPAs are typically active over longer time periods, which means there could be hourly, daily, and potentially weekly hydrogen demands that need to be met. Demand constraints must then be implemented within the rolling horizon framework appropriately. From a risk perspective, it is reasonable to ensure that the contracts can be honored and not violated during periods of low production. Even from an economic standpoint, assuming risk neutrality, it makes sense to utilize storage as a form of hedging against periods with low power production. For instance, producing and storing hydrogen during periods of low electricity prices and high power production can be beneficial. In such cases, producing more hydrogen than the immediate demand should be rewarded in the objective function. The upper bound of pipeline capacity is thus relevant to the optimization model and could vary depending on the storage capacity required to fulfill the delivery of hydrogen through the contracts.

The pipeline capacity analyzed in this project is specifically designed to suit the requirements of the studied energy system. As mentioned in the introduction, the European Commission has set a target of achieving 60 GW of offshore wind capacity by the end of the decade. In practice, due to economies of scale, it is highly feasible to integrate the pipeline into a larger network that includes a main pipeline connecting multiple offshore hydrogen systems, as illustrated in Figure 8.20.

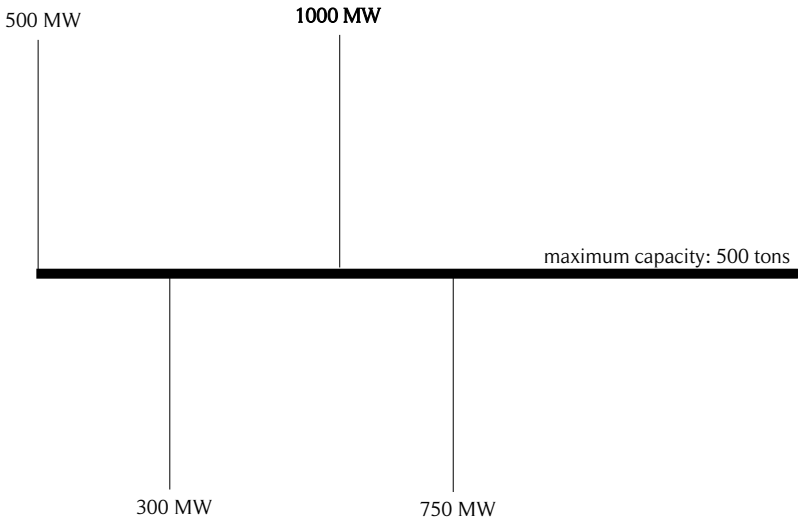

Figure 8.20: Example of potential hydrogen pipeline setup in the North-Sea.

However, while this integration may be advantageous from an investment standpoint, it would significantly increase the complexity and difficulty of the modeling process. The model would need to consider the available capacity not only within its own pipeline but also within the main pipeline, which relies on the production of other offshore energy systems. This integration would also introduce additional complexities when modeling hydrogen demands, posing further challenges to the modeling process.

Power Transmission Cable

It is not unlikely that energy systems similar to the one described in this thesis will be connected to the power markets, regardless if the energy system intends to sell electricity in the power markets or not. Electricity from power markets could be essential to ensure safe operations of hydrogen production as the power from the wind farm has ultra short-term fluctuations. Other solutions, such as a diesel aggregate unit, could also be used to ensure safe operations. This work assumes however that the power transmission cable is used for access to the intraday and day-ahead market, where power sales in the day-ahead market play a large role. Results have shown that larger transmission capacity increases the revenues from electricity sales. However, this is at the expense of a larger day-ahead deviation. The overall operational profitability of the power transmission cable is therefore difficult to assess as the costs and implications of day-ahead deviation are uncertain.

There is a clear trend that the income from electricity sales is higher than hydrogen sales. A transmission cable allows direct and instant transmission of renewable electricity. Compared to hydrogen production, which undergoes the process of production, transportation and distribution and combustion, the transfer of electrical energy is a much more efficient method to transport energy to onshore locations. It is important to recognize that subsea transmission cables are expensive. Transportation distance is an important cost driver, although the capacity rating would also impact the investment cost. The electrical infrastructure would require immense upgrades with higher capacity levels than 500 MW. Investigating the current available capacity in the power grid (DataArena, 2023), injecting anything above 500 MW seems, even in 2030, as a long shot. It would require a transformation of the entire electrical infrastructure to be able to handle this amount of power, which the wind power producer would be responsible of financing. Therefore, it is expected that the current transmission capacity of 500 MW would be sufficient. Although this is considered a stand-alone project, several initiatives to produce renewable power are required in the energy transitions. This would put enormous pressure on the need for reinforcement of the power grid.

It is difficult to decide the appropriate transmission capacity based solely on these results, as the

net income from electricity sales finances not only the cable, but also other parts of the project. Without considering the investment costs of other components, it is difficult to propose any definite answer on the reasonable transmission capacity.

8.2.7 Power Market Participation - a Profitability Driver

The German power market offers quarterly product trading, which can help mitigate the risk associated with trading anticipated excess energy from wind farms in the next hour. This is something that will be more relevant in the Nordic Market with time as the share of variable products in the energy mix increases. The model could possibly potentialize from 15 minute products as there is less risk of over-committing. In addition to previous discussions, it has been shown throughout several test instances in Section 8.1 that there are especially two factors that in this model that affects the value of power market participation. The two factors are the power transmission line and the true cost of under-delivery penalty. Capacity limits, and in this case of the power transmission line, are decided in the investment phase of the project. The operational value is measured against the investment costs. However, the operational value is also dependent on the true penalty cost. It is therefore difficult from an investment perspective to evaluate the true profitability of power transmission lines.

However, it has been seen that a large part of the operational value for power market participation is affected by the relative prices between hydrogen and power. It was shown in Section 8.1.6 that changes in hydrogen price did not have a large effect on system behaviour, that what was suspected to be a consequence of shedding costs. The electrolyzer capacity has been increased to 1 000 MW in an attempt to study the impact of power market access given different hydrogen prices. Contrary to the results in Section 8.1.6, Table 8.13 demonstrates that increases in hydrogen price reduces the activity in the power market. This is more in line with expected system behaviour in reaction to changes in relative prices. The power transmission capacity has been kept at 500 MW for the results in Table 8.13, as it stated in Section 8.2.6 that it would be difficult from a technical point of view to have a higher transmission cable than this.

Table 8.13: Key findings of hydrogen price test for 1 000 MW Electrolysis and 500 MW power transmission cable.

	Unit	2	4	5	6	8	10	15
Day-ahead Commitment	[MWh]	12 604.6	12 195.4	11 344.7	10 021.0	1 600.1	1.9	0.0
Intraday Purchase	[MWh]	125.0	117.2	120.6	131.9	23.5	0.0	0.0
Actual Day-ahead Deviation	[MWh]	7.5	7.5	7.5	6.3	0.0	0.0	0.0
Intraday Sale Commitment	[MWh]	45.5	44.6	38.6	28.6	6.1	0.0	0.0
Electrolysis	[MWh]	12 056.7	12 550.9	13 571.3	15 350.2	23 825.4	25 666.0	25 667.9
Battery Discharge	[MWh]	21.2	18.7	24.3	17.8	10.5	0.0	0.0
Fuel Cell	[MWh]	27.6	26.6	19.8	10.0	7.7	0.0	0.0
Energy Shed	[MWh]	1 106.3	1 068.0	897.8	490.4	309.0	56.6	56.6
Hydrogen Production	[kg]	194 014.8	201 970.4	218 388.5	247 012.2	383 422.9	413 041.8	413 072.8
Hydrogen Sales*	[EUR]	384 517.5	800 932.8	1 085 042.5	1 476 612.6	3 056 061.3	4 119 740.8	6 179 868.3
Day-Ahead Sales	[EUR]	1 217 600.8	1 194 305.8	1 136 831.9	1 038 478.6	226 243.7	316.5	0.0
Net Income*	[EUR]	1 594 180.8	1 987 789.9	2 214 136.0	2 505 326.5	3 280 055.5	4 120 062.0	6 179 868.3
Hydrogen Sales*	[%]	24.1	40.3	49.0	58.9	93.2	100.0	100.0
Electricity Sales*	[%]	75.9	59.7	51.0	41.1	6.8	0.0	0.0

The break-even price for hydrogen to become competitive falls within the range of 4 to 6 EUR/kg. These price levels correspond to hydrogen income percentages of 40.3% to 58.9%. At lower prices, the main source of income is the power markets. However, when prices exceed 6 EUR/kg, the profitability of hydrogen production significantly increases. In this case, day-ahead sales drop from 1 038 478.6 EUR to 226 243.7 EUR, resulting in an 84.0% reduction. The highest recorded spot prices for electricity are 177.4 EUR/MWh and 213.7 EUR/MWh. When the price of hydrogen reaches 8 EUR/kg, the price per unit of energy becomes 242.4 EUR/MWh. Once the price surpasses 10 EUR/kg, approximately equivalent to 300.3 EUR/MWh, all energy generated from the wind farm is directed towards the hydrogen market. This finding is significant since the investment in the transmission cable is heavily underutilized. High hydrogen price in combination with 1 000 MW of electrolysis can render the 500 MW transmission cable obsolete.

Further observations indicate that fuel cells and batteries become redundant when the system

primarily produces hydrogen. Without any commitments to the power market and the ability to utilize all the generated energy, the penalties associated with under-delivery and shedding are significantly reduced. While the wind energy availability consistently exceeds the minimum requirements for activating the fuel cells, it is challenging to accurately determine the relevance of investing in fuel cells and batteries. However, at hydrogen prices of 10 and 15 EUR/kg, the only remaining energy shedding occurs during the initial conditions when all electrolyzers are simultaneously shut down. These are interesting topics to be discussed for decision-makers in regard to investment decisions, when investment costs are also part of the economic assessment. The most important finding of this extended research is the break-even price of hydrogen.

CHAPTER

NINE

CONCLUDING REMARKS

A stochastic linear program has been formulated to account for uncertainty in wind power generation 36 hours ahead, by combining quantile regression with spline basis functions and a scenario generation method proposed by Pinson et al. (2009) to generate wind power scenarios from deterministic forecasts and historical observations. Deterministic forecasts are assumed for electricity market prices, and a rolling horizon approach is implemented that maximizes the net income with operational decisions taken every 15 minutes. A compromise between computational tractability and modeling precision was made when modeling electrolyzer characteristics, which includes ramping constraints between operational states. To accurately assess the model performance various test instances have been generated and tested.

The stochastic model has been compared to the case of having complete information about future power generation. High penalties from under-deliveries deteriorate the stochastic solution while all power market contracts are fulfilled under perfect information. An estimate of the value of perfect information is 170 140.1 EUR, or 8.4 % better. The expected value problem achieves, when including penalties, a higher objective function value than the stochastic solution. When accounting for financial implications from under-deliveries in the two cases, it is still difficult to accurately determine the value of the stochastic solution.

Substantial consideration of real-life operating conditions has been given in the development of the model presented in this thesis. A real-life application of the model imposes the expectations of short solution times while high accuracy is preserved, which is not always feasible. This work has seen the importance of coupling and aggregating individual electrolyzers into larger sets to control problem complexity. A high number of electrolyzers has inconclusive impacts on model performance despite being theoretically more accurate. The increase in computational cost does however suggest that the modelling of 20 electrolyzer units suffices for practical purposes.

A scenario description of stochastic wind power production has provided an approximation of real-life operating situations where the energy system must make first second-stage decisions. Modeling a higher number of scenarios provides a more accurate description of the uncertainty in wind power generation, which can make solutions more robust when penalties incur for under-deliveries. However, it is inconclusive evidence as to what is an appropriate number of scenarios. Statistically outlying scenario values can be generated due to random processes in the scenario generation procedure. A higher number of scenarios increases the likelihood of having an extreme scenario. Furthermore, the appropriate number of scenarios depends on the power market and energy shedding penalties. These two factors combined create situations where statistically deviant low-power scenario values are weighted heavily by the significant penalties, which results in model behavior that in hindsight is unreasonable. A reduction in penalty costs was seen to alleviate this issue significantly.

Power market participation has many implications for system design and modeling choices. The

profitability of power market participation depends on power prices, hydrogen prices and consequences of under-delivery. Access to intraday markets is pivotal to reducing day-ahead deviation and managing the risk of over-commitments in the day-ahead market. The unit value of the day-ahead deviation penalty has a large effect on profitability, and it is essential to have a high-quality approximation of this parameter to effectively evaluate overall profitability. In an energy system with 1 000 MW electrolysis capacity, the model will stop commitments to the day-ahead market for a hydrogen price of approximately 10 EUR/kg. The results suggest a break-even price of hydrogen at 4.9 EUR/kg for this configuration. At this price level, power sales are disfavored compared to more income-generating hydrogen even for the hybrid mode. The island configuration becomes competitive to the hybrid mode for hydrogen prices exceeding 5 EUR/kg when revenues are compared.

Uncertainty related to the exogenous factors influences the model performance in every aspect, as both wind speeds and power prices have strong variability. The effect of price differences between electricity and hydrogen markets is significant for revenue allocation in the short-term and is enhanced over longer time periods. A high-capacity power transmission line increases revenue significantly at the cost of higher deviation in the day-ahead market. However, this might not be technically feasible as it would demand substantial grid reinforcement.

Increasing the electrolyzer capacity in the hybrid system leads to a higher percentage of income from hydrogen as hydrogen sales sacrifice conversion losses for less risk compared to direct transmission to the power grid, however, it is not necessarily techno-economically feasible. The system can absorb more of the energy instead of making too high promises to the power markets that the model is comfortable when the power generation is maxed out. However, this is influenced by the forecasting accuracy and expected default cost of deviation from power market obligations, although in the absence of hydrogen purchasing agreements. Furthermore, the high cost associated with energy shedding would encourage higher electrolyzer capacity.

Fuel cells and batteries contribute to mitigating under-deliveries to the power market. Although their contributions are not sufficient alone, if their operation cost is less expensive than adjusting net position in the intraday market, they provide value to the system. However, it is uncertain how much they contribute to support the continuous operation of the electrolyzers in cases of low power generation. Fuel cells and batteries were not at any time activated for the island mode configuration. The intraday market proves essential to the wind power producer in adjusting the net position. Intraday purchases are prioritized because of the expected downside of under-delivery compared to the potential upside from additional sales, advocating risk-averse behavior. Future power market designs can decrease uncertainty related to commitments as short-time frame products become available and more variable production enters the energy mix leading to higher trading volumes.

The model presented in this thesis has allowed us to study the behaviour of an offshore energy system with hydrogen production with stochastic power generation. Approximations of revenues for different configurations of the energy system can provide decision-makers with information on the operational implications of early-stage investment decisions. The model proposed in this work can therefore be used as a decision-making tool. The contractual price of hydrogen will have a critical role for the profitability of electrolyzers in the offshore system, and to evaluate the competitiveness of the decoupled system. If the hydrogen price is too low, significant revenues are lost from the inability to trade in the power markets. On the other hand, a high hydrogen price would favor a decoupled configuration as the transmission cable becomes under-utilized. The break-even price of hydrogen lies just above 5 EUR/kg. This is the price at which the hybrid mode with 1 000 MW/500 MW hydrogen and 1 000 MW hydrogen island mode become competitive solutions. It has been seen that over-dimensioning of installed capacities provides operational value, and the question surrounding capacity expansion becomes a real option for decision-makers to consider. Thus, the model presented in this thesis could be used iteratively with project life-time profitability tools to optimize energy system designs. Future price estimations on electricity and hydrogen in combination with equipment costs can become decisive for the profitability and viability of projects with offshore hydrogen production.

CHAPTER

TEN

FUTURE RESEARCH

This thesis has presented a stochastic short-term optimization model and applied it to a hypothetical offshore energy system with hydrogen production. Several relevant focus areas for future research have been identified during the development, testing and analysis of the work presented in this thesis. The three main areas for future research can be highlighted as an extension of stochastic modelling, the development of energy system designs, and the integration of short-term optimization models into other decision-making tools.

The current methods to assess the stochastic behaviour of wind are generally designed for onshore applications. The development of both forecasting and scenario generation methods specifically for offshore applications is central in order to more accurately integrate the stochasticity of wind power generation in optimization models. In the context of modeling wind power generation scenarios, a scenario reduction method can effectively streamline power generation scenarios by clustering similar scenarios together. This approach significantly reduces the number of scenarios to be considered, and could provide value to the model. In terms of power market participation, an enhanced bidding process for intraday operations can be implemented to more accurately model demand and supply. Moreover, wind power producers have the opportunity to engage in reserve markets, which could be explored in future research. The energy system is heavily impacted by the penalty costs of energy shedding and over-commitment in the power markets. A study of the true costs associated with the operations of the offshore energy system could provide valuable insights to more accurately model economic viability and revenue streams.

Furthermore, existing literature underscores the potential for offshore energy systems with hydrogen production to significantly boost revenues through the inclusion of commercial oxygen sales. This work does not account for hydrogen demand in its modeling. The energy system could be under the obligation to deliver on an hourly, daily or weekly basis. Therefore, further investigation is required to assess the behavior of the model when it must consider both the power market and hydrogen market obligations. To address increasing modeling complexity, incorporating approximative solution methods becomes advantageous in order to overcome computational intractability. The application of specific solution algorithms can expedite the optimization process, enabling faster resolution of complex problems. This is particularly valuable when aiming to achieve higher modeling precision.

Detailed modeling of short-term operations has allowed us to assess revenue streams at high granularity. The model presented in this thesis could therefore be used as a tool to assess cash flows for a given design. It would therefore be interesting to integrate the presented model with economic tools that assess the overall profitability of investment decisions. The work in this thesis demonstrates that operating conditions and revenues are significantly affected by investment decisions, and some investment decisions could also be considered real options. The presented model could be used in a real options analysis to assess the value capacity expansion opportunities.

BIBLIOGRAPHY

Abdelghany, M. B., Shehzad, M. F., Liuzza, D., Mariani, V., & Glielmo, L. (2021). Optimal operations for hydrogen-based energy storage systems in wind farms via model predictive control [HYDROGEN ENERGY SYSTEMS]. *International Journal of Hydrogen Energy*, *46*(57), 29297–29313. https://doi.org/10.1016/j.ijhydene.2021.01.064

Abdelghany, M. B., Shehzad, M. F., Mariani, V., Liuzza, D., & Glielmo, L. (2022). Two-stage model predictive control for a hydrogen-based storage system paired to a wind farm towards green hydrogen production for fuel cell electric vehicles. *International Journal of Hydrogen Energy*, *47*(75), 32202–32222. https://doi.org/10.1016/j.ijhydene.2022.07.136

Aladwani, S., Al-Obaidi, M., & Mujtaba, I. (2021). Performance of reverse osmosis based desalination process using spiral wound membrane: Sensitivity study of operating parameters under variable seawater conditions. *Cleaner Engineering and Technology*, *5*, 100284. https://doi.org/10.1016/j.clet.2021.100284

Al-Mutaz, I., & Ghunaimi, M. (2001). Performance of reverse osmosis units at high temperatures. *Desalination and Water Reuse Proc., Bahrain*.

Andersson, J., & Grönkvist, S. (2019). Large-scale storage of hydrogen. *International Journal of Hydrogen Energy*, *44*(23), 11901–11919. https://doi.org/https://doi.org/10.1016/j.ijhydene.2019.03.063

Andrenacci, Choi, S., Raka, Y., Talic, Y., Belma, Colmenares-Rausseo & SINTEF, L. (n.d.). *Electrolysers towards mawp 2023 targets and beyond* (Rep.), European Union.

Ballard. (n.d.). *Fuel cell power module for marine applications* [Data sheet].

Beiter, P., Rand, J. T., Seel, J., Lantz, E., Gilman, P., & Wiser, R. (2022). Expert perspectives on the wind plant of the future. *Wind Energy*, *25*(8), 1363–1378. https://doi.org/10.1002/we.2735

Bødal, E. F., & Korpås, M. (2018). Production of hydrogen from wind and hydro power in constrained transmission grids, considering the stochasticity of wind power. *Journal of Physics: Conference Series*, *1104*(1), 012027. https://doi.org/10.1088/1742-6596/1104/1/012027

Bonacina, C. N., Gaskare, N. B., & Valenti, G. (2022). Assessment of offshore liquid hydrogen production from wind power for ship refueling. *International Journal of Hydrogen Energy*, *47*(2), 1279–1291. https://doi.org/10.1016/j.ijhydene.2021.10.043

Bordin, C., Anuta, H. O., Crossland, A., Gutierrez, I. L., Dent, C. J., & Vigo, D. (2017). A linear programming approach for battery degradation analysis and optimization in offgrid power systems with solar energy integration. *Renewable Energy*, *101*, 417–430. https://doi.org/https://doi.org/10.1016/j.renene.2016.08.066

Bossel, U., & Eliasson, B. (2003). *Energy and the hydrogen economy*. Retrieved 1st November 2022, from https://afdc.energy.gov/files/pdfs/hyd_economy_bossel_eliasson.pdf

Brändle, G., Schönfisch, M., & Schulte, S. (2021). Estimating long-term global supply costs for low-carbon hydrogen. *Applied Energy*, *302*, 117481. https://doi.org/10.1016/j.apenergy.2021.117481

Bremnes, J. B. (2004). Probabilistic wind power forecasts using local quantile regression. *Wind Energy*, *7*(1), 47–54. https://doi.org/https://doi.org/10.1002/we.107

Bremnes, J. B. (2006). A comparison of a few statistical models for making quantile wind power forecasts. *Wind Energy*, *9*(1-2), 3–11. https://doi.org/https://doi.org/10.1002/we.182

Carr, S., Zhang, F., Liu, F., Du, Z., & Maddy, J. (2016). Optimal operation of a hydrogen refuelling station combined with wind power in the electricity market. *International Journal of Hydrogen Energy*, *41*(46), 21057–21066. https://doi.org/10.1016/j.ijhydene.2016.09.073

Chi, J., & Yu, H. (2018). Water electrolysis based on renewable energy for hydrogen production. *Chinese Journal of Catalysis*, *39*(3), 390–394. https://doi.org/10.1016/S1872-2067(17)62949-8

Cockerill, R. (2020). *Electrolyser technologies pem vs alkaline electrolysis*. H2View. Retrieved 1st November 2022, from https://nelhydrogen.com/wp-content/uploads/2021/07/Electrolyser-technologies-PEM-vs-Alkaline-electrolysis-%E2%80%93-Single-Pages.pdf

Cryer, J. D., & Kellet, N. (1991). *Time series analysis*. Springer.

Cummins. (2021). *Hylyzer® water electrolyzers* [Data sheet]. https://mart.cummins.com/imagelibrary/data/assetfiles/0070327.pdf

DataArena. (2023). *Dataarena*. Retrieved 10th June 2023, from https://kart.dataarena.no/

Dinh, V. N., Leahy, P., McKeogh, E., Murphy, J., & Cummins, V. (2021). Development of a viability assessment model for hydrogen production from dedicated offshore wind farms [Recent Trends in Hydrogen Production and Utilization]. *International Journal of Hydrogen Energy*, *46*(48), 24620–24631. https://doi.org/10.1016/j.ijhydene.2020.04.232

Durakovic, G., del Granado, P. C., & Tomasgard, A. (2023). Powering europe with north sea offshore wind: The impact of hydrogen investments on grid infrastructure and power prices. *Energy*, *263*, 125654. https://doi.org/10.1016/j.energy.2022.125654

ECO Power. (n.d.). *Container Lithium ESS* [Data sheet]. http://energetechsolar.com/assets/images/30MWh%20Container%20ESS%20V1.pdf?redirect=1

Elberry, A. M., Thakur, J., Santasalo-Aarnio, A., & Larmi, M. (2021). Large-scale compressed hydrogen storage as part of renewable electricity storage systems. *International Journal of Hydrogen Energy*, *46*(29), 15671–15690. https://doi.org/10.1016/j.ijhydene.2021.02.080

Engmark, E., Sandven, H., Fleten, S.-E., & Klæboe, G. (2018). Stochastic multistage bidding optimisation in an intraday market with limited liquidity. *2018 15th International Conference on the European Energy Market (EEM)*, 1–5. https://doi.org/10.1109/EEM.2018.8469997

Espegren, K., Damman, S., Pisciella, P., Graabak, I., & Tomasgard, A. (2021). The role of hydrogen in the transition from a petroleum economy to a low-carbon society [Hydrogen Separation, Production and Storage]. *International Journal of Hydrogen Energy*, *46*(45), 23125–23138. https://doi.org/10.1016/j.ijhydene.2021.04.143

Europe, W. (2022). *North sea offshore wind to help repower the eu*. Wind Europe. Retrieved 26th October 2022, from https://windeurope.org/newsroom/press-releases/north-sea-offshore-wind-to-help-repower-the-eu/

European Commission. (2020a). *Communication from the commission to the european parliament, the council, the european economic and social committee and the committee of the regions a hydrogen strategy for a climate-neutral europe*. Retrieved 10th June 2022, from https://eur-lex.europa.eu/legal-content/EN/TXT/?uri=CELEX%5C%3A52020DC0299

European Commission. (2020b). *Communication from the commission to the european parliament, the council, the european economic and social committee and the committee of the regions an eu strategy to harness the potential of offshore renewable energy for a climate neutral*

future. Retrieved 10th June 2022, from https://eur-lex.europa.eu/legal-content/EN/TXT/?uri=COM%5C%3A2020%5C%3A741%5C%3AFIN

European Commission. (2020c). *Communication from the commission to the european parliament, the council, the european economic and social committee and the committee of the regions powering a climate-neutral economy: An eu strategy for energy system integration*. Retrieved 10th June 2022, from https://eur-lex.europa.eu/legal-content/EN/TXT/?uri=CELEX%5C%3A52020DC0299

Eyvindson, K., & Kangas, A. (2016). Evaluating the required scenario set size for stochastic programming in forest management planning: Incorporating inventory and growth model uncertainty. *Canadian Journal of Forest Research*, *46*(3), 340–347. https://doi.org/10.1139/cjfr-2014-0513

Falk, E. A., & Hansen, F. L. (2022). *Short-term optimization in energy systems with hydrogen production*. NTNU.

Felseghi, R.-A., Carcadea, E., Carcadea, R., Simona, M., TRUFIN, Nicolae, C., & Constantin, F. (2019). Hydrogen fuel cell technology for the sustainable future of stationary applications. *Energies*, *12*(23). https://doi.org/10.3390/en12234593

Ferchau, J. (2019). *Cummins perspective on fuel cells*. Cummins. Retrieved 15th November 2022, from https://www.energy.gov/sites/prod/files/2019/10/f68/fcto-h2-at-ports-workshop-2019-vi3-ferchau.pdf

Finnah, B., Gönsch, J., & Ziel, F. (2022). Integrated day-ahead and intraday self-schedule bidding for energy storage systems using approximate dynamic programming. *European Journal of Operational Research*, *301*(2), 726–746. https://doi.org/https://doi.org/10.1016/j.ejor.2021.11.010

Flamm, B., Peter, C., Büchi, F. N., & Lygeros, J. (2021). Electrolyzer modeling and real-time control for optimized production of hydrogen gas. *Applied Energy*, *281*, 116031. https://doi.org/10.1016/j.apenergy.2020.116031

Foley, A. M., Leahy, P. G., Marvuglia, A., & McKeogh, E. J. (2012). Current methods and advances in forecasting of wind power generation. *Renewable Energy*, *37*(1), 1–8. https://doi.org/https://doi.org/10.1016/j.renene.2011.05.033

Fragiacomo, P., & Genovese, M. (2020). Developing a mathematical tool for hydrogen production, compression and storage. *International Journal of Hydrogen Energy*, *45*(35), 17685–17701. https://doi.org/10.1016/j.ijhydene.2020.04.269

Franco, B. A., Baptista, P., Neto, R. C., & Ganilha, S. (2021). Assessment of offloading pathways for wind-powered offshore hydrogen production: Energy and economic analysis. *Applied Energy*, *286*, 116553. https://doi.org/10.1016/j.apenergy.2021.116553

Ghaffour, N., Missimer, T. M., & Amy, G. L. (2013). Technical review and evaluation of the economics of water desalination: Current and future challenges for better water supply sustainability. *Desalination*, *309*, 197–207. https://doi.org/10.1016/j.desal.2012.10.015

Grigonytė, E., & Butkevičiūtė, E. (2016). Short-term wind speed forecasting using arima model. *Energetika*, *62*. https://doi.org/10.6001/energetika.v62i1-2.3313

Grüger, F., Hoch, O., Hartmann, J., Robinius, M., & Stolten, D. (2019). Optimized electrolyzer operation: Employing forecasts of wind energy availability, hydrogen demand, and electricity prices [European Fuel Cell Conference & Exhibition 2017]. *International Journal of Hydrogen Energy*, *44*(9), 4387–4397. https://doi.org/10.1016/j.ijhydene.2018.07.165

Hanifi, S., Liu, X., Lin, Z., & Lotfian, S. (2020). A critical review of wind power forecasting methods-past, present and future. *Energies*, *13*. https://doi.org/10.3390/en13153764

He, Y., & Li, H. (2018). Probability density forecasting of wind power using quantile regression neural network and kernel density estimation. *Energy Conversion and Management*, *164*, 374–384. https://doi.org/https://doi.org/10.1016/j.enconman.2018.03.010

Heredia, F.-J., Cuadrado, M. D., & Corchero, C. (2018). On optimal participation in the electricity markets of wind power plants with battery energy storage systems. *Computers Operations Research*, *96*, 316–329. https://doi.org/https://doi.org/10.1016/j.cor.2018.03.004

Jang, D., Kim, K., Kim, K.-H., & Kang, S. (2022). Techno-economic analysis and monte carlo simulation for green hydrogen production using offshore wind power plant. *Energy Conversion and Management*, *263*, 115695. https://doi.org/10.1016/j.enconman.2022.115695

Jiang, Y., Huang, W., & Yang, G. (2021). Electrolysis plant size optimization and benefit analysis of a far offshore wind-hydrogen system based on information gap decision theory and chance constraints programming. *International Journal of Hydrogen Energy*, *47*(9), 5720–5732. https://doi.org/10.1016/j.ijhydene.2021.11.211

Jovan, D. J., & Dolanc, G. (2020). Can green hydrogen production be economically viable under current market conditions. *Energies*, *13*(24). https://doi.org/10.3390/en13246599

Kächele, F., Grothe, O., & Watermeyer, M. (2022). Dataset for the Paper: "Analyzing Europe's Biggest Offshore Wind Farms: a Data set With 40 Years of Hourly Wind Speeds and Electricity Production". https://doi.org/10.6084/m9.figshare.19139648.v1

Kaiser, S., Siems, F., Mostert, C., & Bringezu, S. (2022). Environmental and economic performance of co2-based methanol production using long-distance transport for h2 in combination with co2 point sources: A case study for germany. *Energies*, *15*(7). https://doi.org/10.3390/en15072507

Kall, P., & Wallace, S. W. (2003). *Stochastic programming second edition*. Institute for Operations Research; Mathematical Methods of Economics.

Karanfil, F., & Li, Y. (2017). The role of continuous intraday electricity markets: The integration of large-share wind power generation in denmark. *The Energy Journal*, *38*(2).

Khan, M. A., Young, C., & Layzell, D. B. (2021). The techno-economics of hydrogen pipelines. *Transition Accelerator Technical Briefs*, *1*(2), 1–40.

Koenker, R., & Bassett, G. (1978). Regression quantiles. *Econometrica*, *46*(1), 33–50. Retrieved 4th May 2023, from http://www.jstor.org/stable/1913643

Koenker, R., & Hallock, K. F. (2001). Quantile regression. *Journal of Economic Perspectives*, *15*(4), 143–156. https://doi.org/10.1257/jep.15.4.143

Kraft, E., Russo, M., Keles, D., & Bertsch, V. (2023). Stochastic optimization of trading strategies in sequential electricity markets. *European Journal of Operational Research*, *308*(1), 400–421. https://doi.org/https://doi.org/10.1016/j.ejor.2022.10.040

Kucuksari, S., Erdogan, N., & Cali, U. (2019). Impact of electrical topology, capacity factor and line length on economic performance of offshore wind investments. *Energies*, *12*(16). https://doi.org/10.3390/en12163191

Lebedeva, N. (2018). Li-ion batteries for mobility and stationary storage applications. *Publications Office of the European Union*.

Leo, E., & Engell, S. (2018). A two-stage stochastic programming approach to integrated day-ahead electricity commitment and production scheduling. In A. Friedl, J. J. Klemeš, S. Radl, P. S. Varbanov & T. Wallek (Eds.), *28th european symposium on computer aided process engineering* (pp. 1009–1014). Elsevier. https://doi.org/https://doi.org/10.1016/B978-0-444-64235-6.50177-7

Lucas, T. R., Ferreira, A. F., Santos Pereira, R., & Alves, M. (2022). Hydrogen production from the windfloat atlantic offshore wind farm: A techno-economic analysis. *Applied Energy*, *310*, 118481. https://doi.org/10.1016/j.apenergy.2021.118481

Luo, Z., Wang, X., Wen, H., & Pei, A. (2022). Hydrogen production from offshore wind power in south china [Hydrogen Sourced from Renewables and Clean Energy: Feasibility of Large-scale Demonstration Projects]. *International Journal of Hydrogen Energy*, *47*(58), 24558–24568. https://doi.org/10.1016/j.ijhydene.2022.03.162

Lyche, T., & Morken, K. (2008). Spline methods draft. *Department of Informatics, Center of Mathematics for Applications, University of Oslo, Oslo*, 3–8.

Maciejowska, K., Nowotarski, J., & Weron, R. (2016). Probabilistic forecasting of electricity spot prices using factor quantile regression averaging. *International Journal of Forecasting*, *32*(3), 957–965. https://doi.org/https://doi.org/10.1016/j.ijforecast.2014.12.004

Maggio, G., Nicita, A., & Squadrito, G. (2019). How the hydrogen production from res could change energy and fuel markets: A review of recent literature. *International Journal of Hydrogen Energy*, *44*(23), 11371–11384. https://doi.org/10.1016/j.ijhydene.2019.03.121

Marcjasz, G. (2020). Forecasting electricity prices using deep neural networks: A robust hyper-parameter selection scheme. *Energies*, *13*, 4605. https://doi.org/10.3390/en13184605

Martín, M., & Luceño, J. A. (2022). Chapter 9 - solar thermal energy. In M. Martín (Ed.), *Sustainable design for renewable processes* (pp. 355–396). Elsevier. https://doi.org/10.1016/B978-0-12-824324-4.00009-3

Matute, G., Yusta, J., Beyza, J., & Correas, L. (2021). Multi-state techno-economic model for optimal dispatch of grid connected hydrogen electrolysis systems operating under dynamic conditions. *International Journal of Hydrogen Energy*, *46*(2), 1449–1460. https://doi.org/10.1016/j.ijhydene.2020.10.019

May, T. W., Yeap, Y. M., & Ukil, A. (2016). Comparative evaluation of power loss in hvac and hvdc transmission systems. *2016 IEEE Region 10 Conference (TENCON)*, 637–641.

McKenna, R., D'Andrea, M., & González, M. G. (2021). Analysing long-term opportunities for offshore energy system integration in the danish north sea. *Advances in Applied Energy*, *4*, 100067. https://doi.org/10.1016/j.adapen.2021.100067

Mehrjerdi, H. (2020). Modeling and optimization of an island water-energy nexus powered by a hybrid solar-wind renewable system. *Energy*, *197*, 117217. https://doi.org/10.1016/j.energy.2020.117217

Meier, K. (2014). Hydrogen production with sea water electrolysis using norwegian offshore wind energy potentials - techno-economic assessment for an offshore-based hydrogen production approach with state-of-the-art technology. *International Journal of Energy and Environmental Engineering*, *5*. https://doi.org/10.1007/s40095-014-0104-6

MET Norway. (2023). *Met nordic dataset*. Retrieved 24th May 2023, from https://github.com/metno/NWPdocs/wiki/MET-Nordic-dataset

Møller, J. K., Nielsen, H. A., & Madsen, H. (2008). Time-adaptive quantile regression. *Computational Statistics Data Analysis*, *52*(3), 1292–1303. https://doi.org/https://doi.org/10.1016/j.csda.2007.06.027

Narajewski, M., & Ziel, F. (2020a). Econometric modelling and forecasting of intraday electricity prices. *Journal of Commodity Markets*, *19*, 100107. https://doi.org/https://doi.org/10.1016/j.jcomm.2019.100107

Narajewski, M., & Ziel, F. (2020b). Ensemble forecasting for intraday electricity prices: Simulating trajectories. *Applied Energy*, *279*, 115801. https://doi.org/https://doi.org/10.1016/j.apenergy.2020.115801

Narum, B. S. (2020). *Problem-based scenario generation in stochastic programming with binary distributions*. Retrieved 10th June 2022, from https://ntnuopen.ntnu.no/ntnu-xmlui/bitstream/handle/11250/2777017/no.ntnu%5C%3ainspera%5C%3a55508684%5C%3a57885811.pdf?sequence=1&isAllowed=y

NEL ASA. (2022). *Faq*. Retrieved 24th September 2022, from https://nelhydrogen.com/faq/

Nel Hydrogen. (2021). *Nel hydrogen electrolysers the world's most efficient and reliable electrolysers* [Data sheet]. https://nelhydrogen.com/wp-content/uploads/2020/03/Electrolysers-Brochure-Rev-D.pdf

Nielsen, H. A., Madsen, H., & Nielsen, T. S. (2006). Using quantile regression to extend an existing wind power forecasting system with probabilistic forecasts. *Wind Energy*, *9*(1-2), 95–108. https://doi.org/https://doi.org/10.1002/we.180

Nikolaidis, P., & Poullikkas, A. (2017). A comparative overview of hydrogen production processes. *Renewable and Sustainable Energy Reviews*, *67*, 597–611. https://doi.org/10.1016/j.rser.2016.09.04

Nord Pool AS. (2020). *Intraday market regulations*. Retrieved 13th April 2023, from https://www.nordpoolgroup.com/49e715/globalassets/download-center/rules-and-regulations/intraday-market-regulations_valid-from-1-july-2020.pdf

Pinson, P., Madsen, H., Nielsen, H., Papaefthymiou, G., & Klöckl, B. (2009). From probabilistic forecasts to statistical scenarios of short-term wind power production. *Wind Energy*, *12*, 51–62. https://doi.org/10.1002/we.284

Pisciella, P. (2012). *Methods for evaluation of business models for provision of advanced mobile services under uncertainty*. Norwegian University of Science and Technology.

POWER SONIC. (n.d.). *What is a battery c rating*. Retrieved 9th June 2023, from https://www.power-sonic.com/blog/what-is-a-battery-c-rating/

PowerCellution. (n.d.). *Powercellution marine system 200: Industrial ready marine megawatt solution* [Data sheet].

Rahman, S., Khan, I., Alkhammash, H. I., & Nadeem, M. F. (2021). A comparison review on transmission mode for onshore integration of offshore wind farms: Hvdc or hvac. *Electronics*, *10*(12), 1489.

Raluy, G., Serra, L., & Uche, J. (2006). Life cycle assessment of msf, med and ro desalination technologies [Double Special Issue: 2nd Dubrovnik Conference on Sustainable Development of Energy, Water and Environment Systems/PRES 03 and PRES 2004 Process Integration, Modelling and Optimisation for Energy Saving and Pollution Reduction]. *Energy*, *31*(13), 2361–2372. https://doi.org/10.1016/j.energy.2006.02.005

Schiebahn, S., Grube, T., Robinius, M., Tietze, V., Kumar, B., & Stolten, D. (2015). Power to gas: Technological overview, systems analysis and economic assessment for a case study in germany. *International Journal of Hydrogen Energy*, *40*(12), 4285–4294. https://doi.org/10.1016/j.ijhydene.2015.01.123

Schimpe, M., Naumann, M., Truong, C., Hesse, H., Santhanagopalan, S., Saxon, A., & Jossen, A. (2018). Energy efficiency evaluation of a stationary lithium-ion battery container storage system via electro-thermal modeling and detailed component analysis. *Applied Energy*, *210*, 211–229. https://doi.org/10.1016/j.apenergy.2017.10.129

Schrotenboer, A. H., Veenstra, A. A., uit het Broek, M. A., & Ursavas, E. (2022). A green hydrogen energy system: Optimal control strategies for integrated hydrogen storage and power generation with wind energy. *Renewable and Sustainable Energy Reviews*, *168*, 112744. https://doi.org/10.1016/j.rser.2022.112744

Sheffield, J., Martin, K., & Folkson, R. (2014). 5 - electricity and hydrogen as energy vectors for transportation vehicles. In R. Folkson (Ed.), *Alternative fuels and advanced vehicle technologies for improved environmental performance* (pp. 117–137). Woodhead Publishing. https://doi.org/10.1533/9780857097422.1.117

Solbrekke, I. M., & Sorteberg, A. (2022). Nora3-wp: A high-resolution offshore wind power dataset for the baltic, north, norwegian, and barents seas. *Scientific Data*, *9*(1), 362.

Stoughton, K. M. (2018). *Reverse Osmosis Optimization* (tech. rep. DOE-SLC-6903-1). U.S. Department of ENERGY. Salt Lake City, UT.

Taylor, J. W., & Bunn, D. W. (1999). A quantile regression approach to generating prediction intervals. *Management Science*, *45*(2), 225–237. Retrieved 4th May 2023, from http://www.jstor.org/stable/2634872

Tsiklios, C., Hermesmann, M., & Müller, T. (2022). Hydrogen transport in large-scale transmission pipeline networks: Thermodynamic and environmental assessment of repurposed and new

pipeline configurations. *Applied Energy*, *327*, 120097. https://doi.org/10.1016/j.apenergy.2022.120097

Varela, C., Mostafa, M., & Zondervan, E. (2021). Modeling alkaline water electrolysis for power-to-x applications: A scheduling approach. *International Journal of Hydrogen Energy*, *46*(14), 9303–9313. https://doi.org/10.1016/j.ijhydene.2020.12.111

Wallace, S., Maggioni, F., Thapalia, B. K., Kaut, M., & Crainic, T. G. (n.d.). *How useful is the deterministic solution?* Retrieved 22nd May 2023, from http://www.iot.ntnu.no/winterschool11/web/material/VSS-EVPI.pdf

Wang, J., Zhou, Q., & Zhang, X. (2018). Wind power forecasting based on time series arma model. *IOP Conference Series: Earth and Environmental Science*, *199*, 022015. https://doi.org/10.1088/1755-1315/199/2/022015

Weitzel, T., & Glock, C. H. (2018). Energy management for stationary electric energy storage systems: A systematic literature review. *European Journal of Operational Research*, *264*(2), 582–606. https://doi.org/https://doi.org/10.1016/j.ejor.2017.06.052

Wijayanta, A. T., Oda, T., Purnomo, C. W., Kashiwagi, T., & Aziz, M. (2019). Liquid hydrogen, methylcyclohexane, and ammonia as potential hydrogen storage: Comparison review. *International Journal of Hydrogen Energy*, *44*(29), 15026–15044. https://doi.org/10.1016/j.ijhydene.2019.04.112

Wind, T. O., & Gas, T. N. (2020). North sea energy technical assessment of hydrogen transport, compression, processing offshore. https://north-sea-energy.eu/static/f9c806827555f23ec1bcdc92c510b7af/5.-FINAL-NSE3-D3.1-Final-report-technical-assessment-of-Hydrogen-transport-compression-processing-offshore.pdf

Witkowski, A., Rusin, A., Majkut, M., & Stolecka, K. (2017). Comprehensive analysis of hydrogen compression and pipeline transportation from thermodynamics and safety aspects. *Energy*, *141*, 2508–2518. https://doi.org/10.1016/j.energy.2017.05.141

Wittholz, M. K., O'Neill, B. K., Colby, C. B., & Lewis, D. (2008). Estimating the cost of desalination plants using a cost database. *Desalination*, *229*(1), 10–20. https://doi.org/10.1016/j.desal.2007.07.023

Woznicki, M., Solliec, G. L., & Loisel, R. (2020). Far off-shore wind energy-based hydrogen production: Technological assessment and market valuation designs. *Journal of Physics: Conference Series*, *1669*(1), 012004. https://doi.org/10.1088/1742-6596/1669/1/012004

Yang, B., Zhong, L., Wang, J., Shu, H., Zhang, X., Yu, T., & Sun, L. (2021). State-of-the-art one-stop handbook on wind forecasting technologies: An overview of classifications, methodologies, and analysis. *Journal of Cleaner Production*, *283*, 124628. https://doi.org/https://doi.org/10.1016/j.jclepro.2020.124628

Zarnani, A., Karimi, S., & Musilek, P. (2019). Quantile regression and clustering models of prediction intervals for weather forecasts: A comparative study. *Forecasting*, *1*(1), 169–188. https://doi.org/10.3390/forecast1010012

Zhang, Y., Wang, L., Wang, N., Duan, L., Zong, Y., You, S., Maréchal, F., Van herle, J., & Yang, Y. (2019). Balancing wind-power fluctuation via onsite storage under uncertainty: Power-to-hydrogen-to-power versus lithium battery. *Renewable and Sustainable Energy Reviews*, *116*, 109465. https://doi.org/https://doi.org/10.1016/j.rser.2019.109465

Ziel, F. (2016). Forecasting electricity spot prices using lasso: On capturing the autoregressive intraday structure. *IEEE Transactions on Power Systems*, *31*(6), 4977–4987. https://doi.org/10.1109/TPWRS.2016.2521545

APPENDIX

A. 4.3 Technologies for Offshore Hydrogen Production Literature

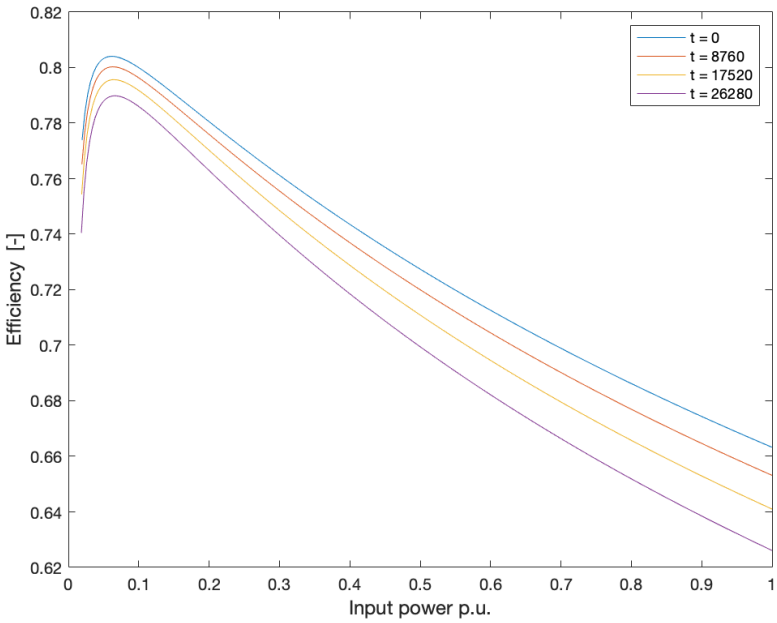

Figure A.1: Efficiency of a PEM electrolyzer as a function of the operating point.

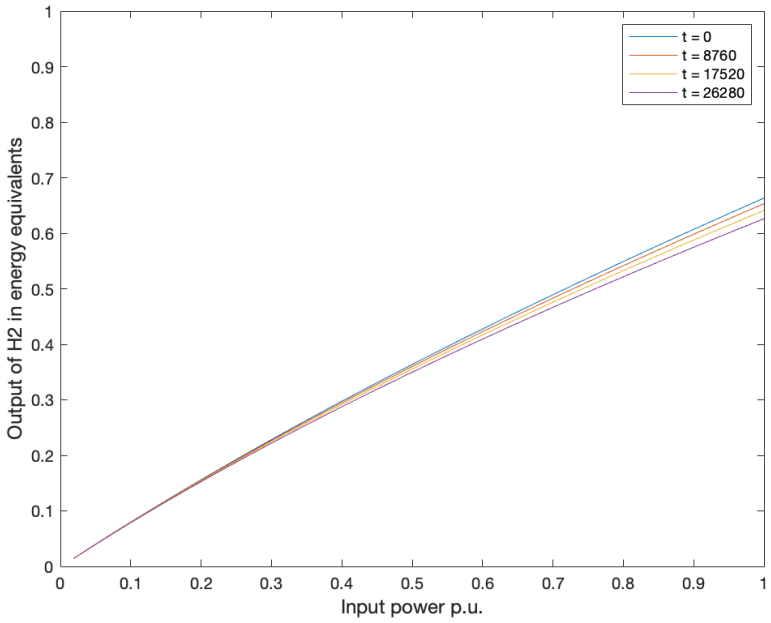

Figure A.2: Energy output in hydrogen per unit of energy input in a PEM electrolyzer

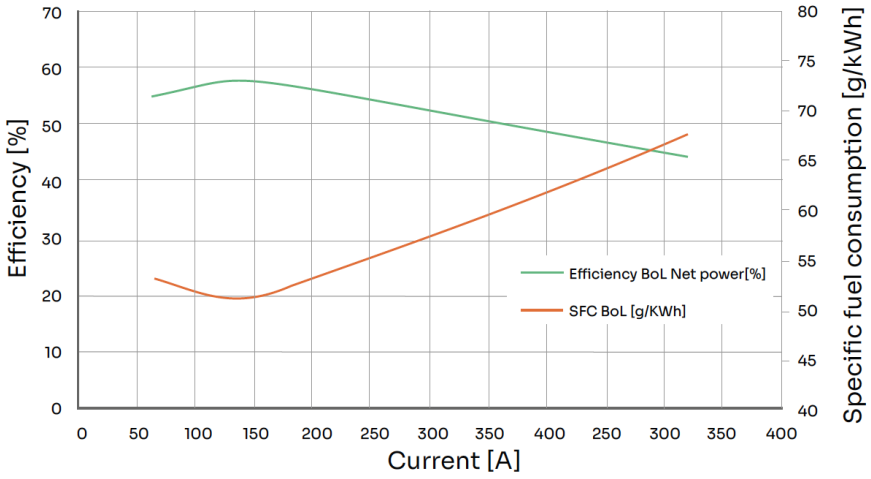

Figure A.3: Efficiency of PEMFC as a function of output current. Figure taken from PowerCellution (n.d.)

A. 7.2 Model Data

Table A.1: Technical parameter values in the model formulation.

Parameter	Value	Unit
η^{B}	0.85	[-]
η^{El}	0.95	[-]
η^{H2}	0.995	[-]
γAux	0.0009472	[MWh/kg H2]
γF	0.01538	[MWh/kg H2]
Γ^{B}	2	[MWh]
$\Gamma^{E,Min}$	0.625	[MWh]
$\Gamma^{E,Max}$	6.25	[MWh]
$\Gamma^{E,Agg,Min}$	1.25	[MWh]
$\Gamma^{E,Agg,Max}$	12.5	[MWh]
Γ^{F}	650.20	[kg]
$\Gamma^{P_{H2},Dis}$	4022.93	[kg]
$ET^{\mathcal{E}}$	0.3125	[MWh]
$ET^{\mathcal{E},Agg}$	0.625	[MWh]
$\Phi^{P_{H2}}$	123 800	[kg]
Φ^{B}	2	[MWh]
HHV^{H2}	0.039772	[MWh/kg]
P^{Max}	500	[kg]
L^{P}	10 000	[kg]
λ^{B}	100	[EUR]
λ^{Dah}	1 000 000	[EUR]
λ^{Int+}	1 000 000	[EUR]
λ^{Shed}	1 000	[EUR]
a	0.64	[-]
b	0	[-]

A. 7.4 Electricity Prices

Table A.2: Average day-ahead prices in 2022 by season for all hours.

Hour	Spring	Summer	Autumn	Winter
1	176.6	309.9	171.5	246.5
2	172.7	288.9	159.8	236.4
3	169.9	279.2	152.7	231.7
4	168.5	270.1	146.4	225.1
5	168.8	267.4	148.9	226.1
6	172	275.4	166	241.3
7	179.8	288.2	189	265.5
8	200.9	306.1	218.3	317.5
9	208.8	320.2	228.4	352.8
10	193.2	311.9	225.3	359
11	181.5	294.3	220.5	354.6
12	174.5	279.6	206.7	353.9
13	170	265.1	191.8	339.3
14	164	250.5	188.5	337.5
15	160.4	244.4	183.2	348.3
16	162.3	255.5	190.6	352.8
17	168.9	273.3	202.6	364.6
18	177.8	300.5	223.5	382.5
19	186.5	324.6	238.2	367.3
20	189.6	342.8	240.2	343.9
21	189.8	345	230.9	318.9
22	187.9	341.9	211.4	285.6
23	185.3	335.1	195.4	266.2
24	180.2	314.6	174.8	246.1
Average	**178.7**	**295.2**	**196**	**306.8**

Table A.3: Standard deviation of day-ahead prices in 2022 by season for all hours.

Hour	Spring	Summer	Autumn	Winter
1	30.1	134.1	131.2	57.1
2	32.3	124.4	122.3	56.2
3	34.2	124.6	119	55.7
4	35.8	120.7	117.3	59.4
5	36.7	122.6	118.2	61.3
6	39	134.1	132.2	59.6
7	40.1	143.3	146.4	64.7
8	75.5	150.1	157.3	100.7
9	77.4	156.8	159.6	119.8
10	55.6	156.7	152.2	117.5
11	43	153.2	146.6	108.8
12	39.4	152.9	138.3	107
13	40.2	146.3	132.1	98.3
14	44.8	145.6	128.5	96.1
15	49	145.7	127.1	102.2
16	45.7	146	130.8	108.5
17	41.3	148.7	138.9	115.4
18	37	150.3	150.3	130.4
19	32.9	158	159.3	116.7
20	27.9	165.1	170.2	106
21	25.7	162.3	167.8	100.1
22	24.4	154.4	154	72
23	23.3	146.8	139.3	63.2
24	24.7	136.5	127.5	57.7
Average	**39.8**	**145**	**140.3**	**88.9**

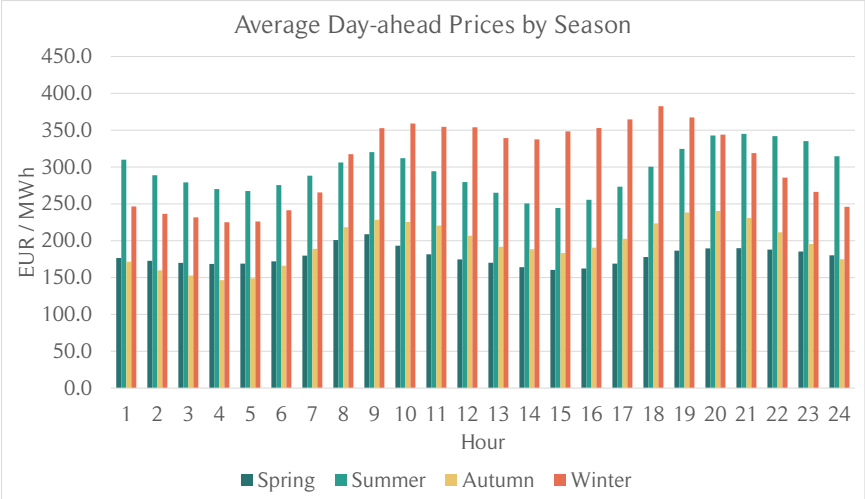

Figure A.4: Plot of Average day-ahead prices in 2022 by weekday for all hours.

Table A.4: Average day-ahead prices in 2022 by weekday for all hours.

Hour	Monday	Tuesday	Wednesday	Thursday	Friday	Saturday	Sunday
1	206.9	227.2	225.6	233.5	228.8	223.8	204.5
2	193.5	212.8	216.5	222.5	216.1	213.5	191.4
3	188.5	207	211	216.8	209.8	204.5	183.8
4	182.3	202.5	207.1	212.9	204.3	197.1	175.1
5	183.8	205.8	210	212.8	204.9	193.3	171.6
6	204.4	218.8	217.3	227.9	216.4	195.6	170.5
7	233.3	238	236.9	242.9	236.8	196.7	172.6
8	270.5	276.2	263.4	266.2	267.6	211.1	176.7
9	290.6	294.3	278.7	281.2	280.3	216	178.7
10	274	280.4	270	273.2	274.3	217.2	175.9
11	256	263.3	259.3	260.7	263.1	213	173.7
12	237.3	253.4	246.1	246.1	253.2	202.9	173.5
13	227.9	235.1	236.6	236.5	239.6	194.3	161.9
14	221.9	232.6	231.8	229.6	225.7	175.7	161.9
15	214.8	234.5	231.6	230.5	218.1	168.2	154.8
16	223.5	241.2	237.7	235.4	219.8	174.3	167.2
17	237.8	253	251.4	246.3	229.1	184	182.4
18	262.5	266.5	262.6	259.6	245.3	207.8	212.3
19	278	279.4	269.7	267.1	256.9	230.3	229.8
20	279.9	279.5	270.8	271.3	260.4	241.7	245.7
21	274.3	268.3	265.2	268	254.4	241.6	249.5
22	263	254.1	255.5	258	241.8	236	242.8
23	249.7	244.8	247.3	247	233.8	228	235.2
24	231.3	228.1	232.3	231.3	215.8	216.4	220.7
Average	**236.9**	**245.7**	**243.1**	**244.9**	**237.3**	**207.6**	**192.2**

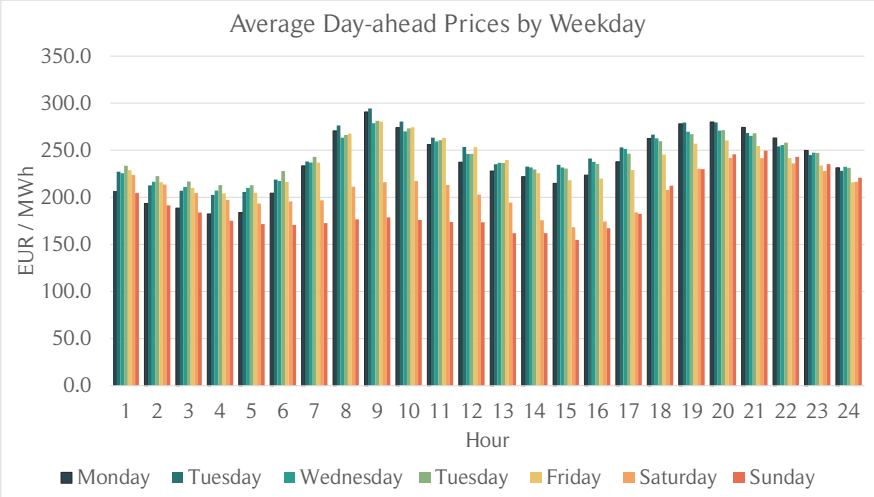

Figure A.5: Average day-ahead prices in 2022 by weekday.

Figure A.6: Original data set of intraday selling prices for 2022.

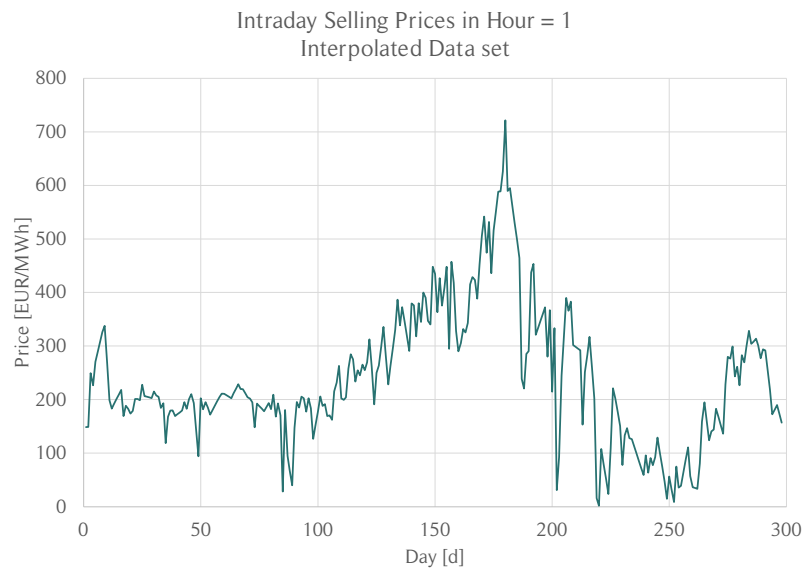

Figure A.7: Interpolated data set of intraday selling prices for 2022.

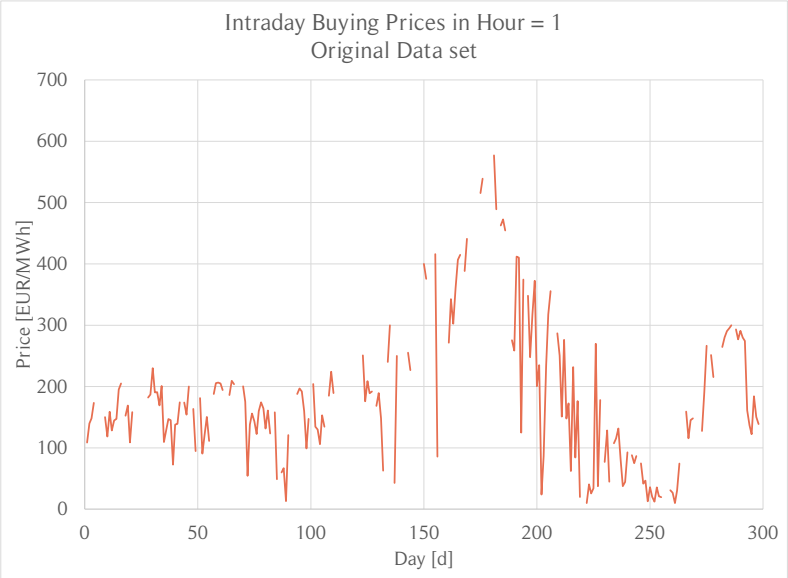

Figure A.8: Original data set of intraday buying prices for 2022.

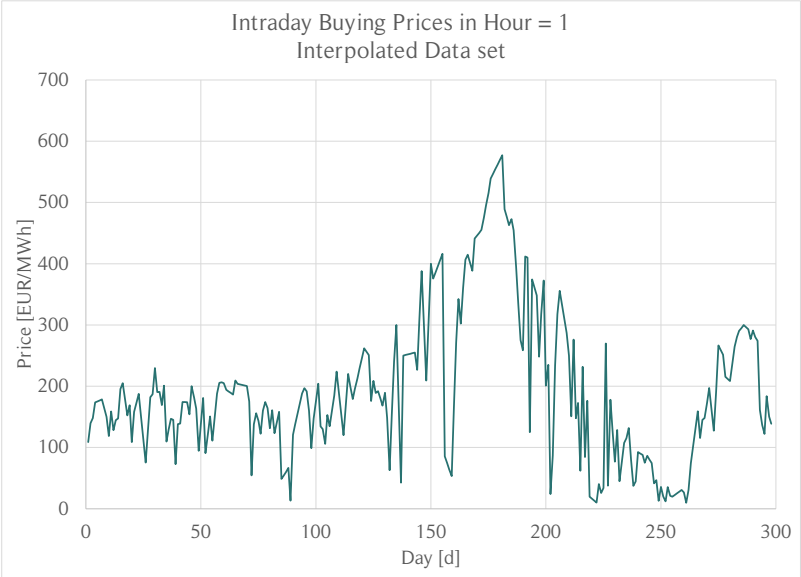

Figure A.9: Interpolated data set of intraday buying prices for 2022.

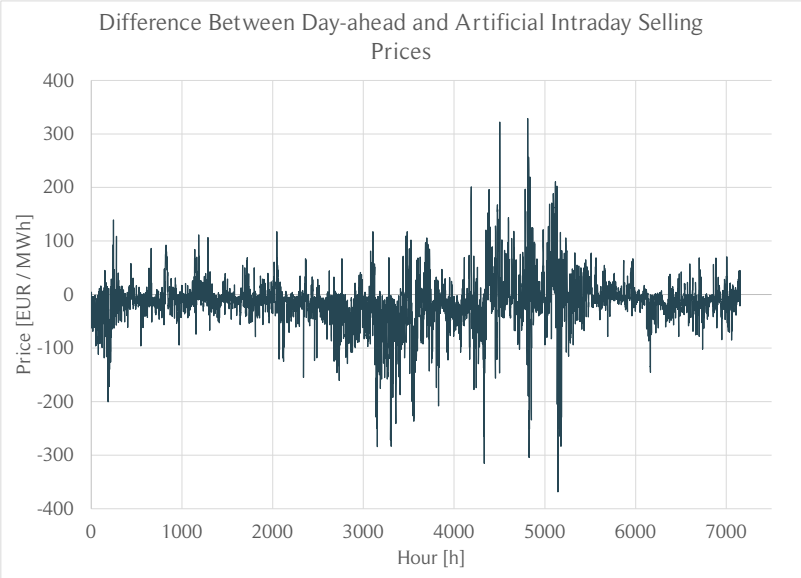

Figure A.10: Difference between day-ahead prices and artificial intraday selling prices in 2022.

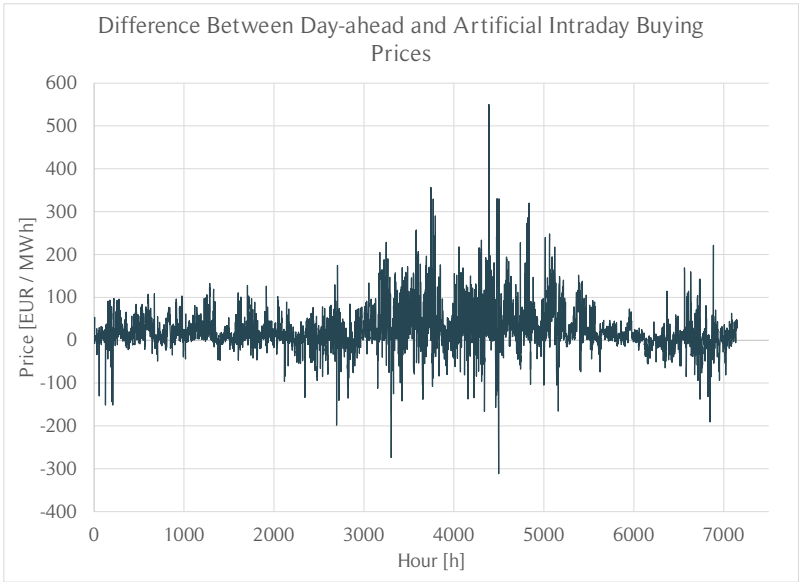

Figure A.11: Difference between day-ahead prices and artificial intraday buying prices in 2022.

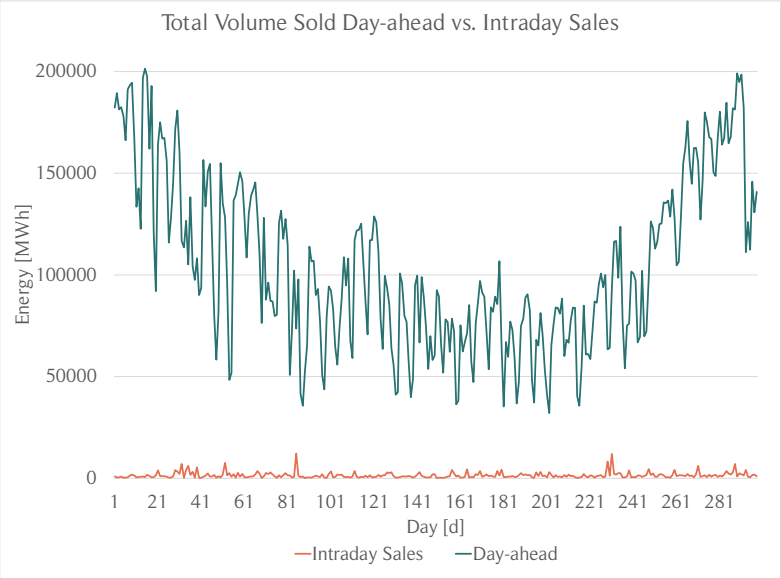

Figure A.12: Comparison of traded volume day-ahead versus intraday sales contracts in 2022.

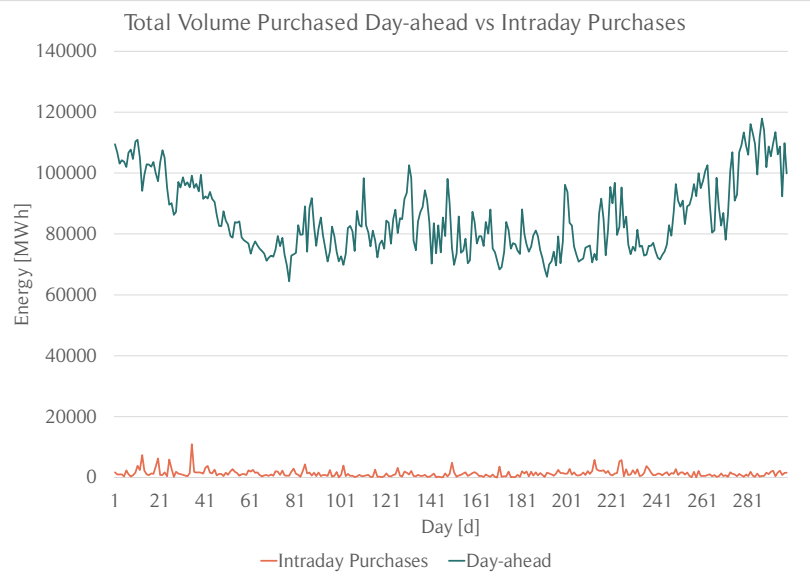

Figure A.13: Comparison of traded volume day-ahead versus intraday purchasing contracts in 2022.

A. 7.5 Wind Forecasting and Scenario Generation

Table A.5: Exponential alpha values for wind speed scaling

Month number	Unit	Value
1	[-]	1.177663
2	[-]	1.190666
3	[-]	1.219631
4	[-]	1.276513
5	[-]	1.284481
6	[-]	1.244307
7	[-]	1.203376
8	[-]	1.180236
9	[-]	1.181066
10	[-]	1.191049
11	[-]	1.179459
12	[-]	1.173860

A. 7.6 Test Instance Generation

Table A.6: Modeling parameters implemented in the base case of the model.

Parameter	Value
Number of Scenarios	20
Number of Electrolyzers units in $\mathcal{E}$	20
Number of Electrolyzers units in $\mathcal{E}^{Agg}$	10
Number of Batteries	5
Number of Desalination Units	1
Number of Fuel cell Units	1
Number of Compressors units	1
Number of Pipelines	1
Number of quarters of hour	146
Test horizon	24.10.2022:10:30 - 25.10.2022:23:00
Forecasting horizon length [h]	36
Time limit subproblem [minutes]	15

Table A.7: Initial values for all test instances of the rolling horizon model.

Parameter	Value	Unit
$\delta^{E}_{\varepsilon s0}$	0	[-]
e^{B}_{sb0}	0	[MWh]
$m^{P_{H2}}_{s0}$	1000	[kg]

A. 8.1.1 Seven Days Operation

Table A.8: Model results for one week of operation.

	Unit	Value
Day-ahead Commitments		
Day-ahead Commitment	[MWh]	45 580.8
Actual Day-ahead Delivery	[MWh]	42 796.8
Intraday Purchase	[MWh]	617.3
Actual Day-ahead Deviation	[MWh]	2 167.0
Actual Day-ahead Deviation	[%]	4.8
Intraday Sale Commitments		
Intraday Sale Commitment	[MWh]	114.3
Actual Intraday Sale Delivery	[MWh]	113.2
Actual Intraday Sale Deviation	[MWh]	1.1
Intraday Sale Delivery Ratio	[%]	99.0
Technical Performance		
Electrolysis	[MWh]	31 306.1
Auxiliary Processes	[MWh]	477.1
Electrolyzer Transitions	[MWh]	657.5
Battery Discharge	[MWh]	440.4
Fuel Cell	[MWh]	1 076.9
Energy Shed	[MWh]	6 447.1
Energy Shed	[%]	8.0
Hydrogen Production	[kg]	503 725.8
Financials		
Hydrogen Sales	[kg]	421 965.8
Hydrogen Sales	[EUR]	1 679 423.9
Hydrogen Sales*	[EUR]	1 730 248.5
Day-Ahead Sales	[EUR]	6 113 813.2
Intraday Sales	[EUR]	24 521.4
Cost Intraday Purchases	[EUR]	113 039.3
Net Income	[EUR]	7 704 719.3
Net Income*	[EUR]	7 755 543.9
Income Distribution		
Hydrogen Sales	[%]	21.8
Hydrogen Sales*	[%]	22.3
Electricity Sales	[%]	78.2
Electricity Sales*	[%]	77.7
Solver Performance		
Minimum Runtime	[s]	31.1
Maximum Runtime	[s]	901.2
Average Runtime	[s]	66.6
Minimum Optimality Gap	[%]	0.0002
Maximum Optimality Gap	[%]	0.0241
Average Optimality Gap	[%]	0.0040

A 8.1.2 Changing the Number of Wind Power Generation Scenarios

Table A.9: Model results for different number of scenarios.

	Unit	$\mathcal{S}$ = 10	$\mathcal{S}$ = 20	$\mathcal{S}$ = 30	$\mathcal{S}$ = 40	$\mathcal{S}$ = 50
Day-ahead Commitments						
Day-ahead Commitment	[MWh]	16 110.5	16 428.8	16 322.7	16 369.4	16 644.9
Actual Day-ahead Delivery	[MWh]	15 695.7	16 019.2	15 893.6	15 902.6	16 149.9
Intraday Purchase	[MWh]	184.2	231.7	256.7	276.0	303.4
Actual Day-ahead Deviation	[MWh]	231.5	178.1	172.8	190.9	191.2
Actual Day-ahead Deviation	[%]	1.4	1.1	1.1	1.2	1.1
Intraday Sale Commitments						
Intraday Sale Commitment	[MWh]	45.7	35.8	31.2	13.7	14.7
Actual Intraday Sale Delivery	[MWh]	44.4	35.8	31.2	13.7	14.7
Actual Intraday Sale Deviation	[MWh]	1.3	0.0	0.0	0.0	0.0
Intraday Sale Delivery Success	[%]	97.1	100.0	100.0	100.0	100.0
Technical Performance						
Electrolysis	[MWh]	8 380.8	8 173.3	7 507.1	7 687.0	7 841.2
Auxiliary Processes	[MWh]	127.7	124.6	114.4	117.2	119.5
Electrolyzer Transitions	[MWh]	202.2	195.0	248.8	215.0	199.4
Battery Discharge	[MWh]	111.0	82.7	98.2	93.1	100.3
Fuel Cell	[MWh]	85.7	95.7	123.9	139.5	188.8
Energy Shed	[MWh]	1 753.7	1 663.9	2 452.0	2 320.1	1 980.6
Energy Shed	[%]	6.7	6.4	9.4	8.9	7.6
Hydrogen Production	[kg]	134 857.1	131 513.9	120 794.8	123 688.6	126 165.3
Financials						
Hydrogen Sales	[kg]	16 092.0	80 020.4	45 034.0	32 808.6	86 692.5
Hydrogen Sales	[EUR]	64 046.2	318 481.2	179 235.3	130 578.2	345 036.2
Hydrogen Sales*	[EUR]	518 562.2	502 635.8	452 701.1	460 201.8	457 312.0
Day-Ahead Sales	[EUR]	1 514 038.1	1 556 594.7	1 542 645.0	1 539 629.8	1 576 850.0
Intraday Sales	[EUR]	6 730.3	4 667.5	3 761.6	1 655.2	1 758.7
Cost Intraday Purchases	[EUR]	19 884.0	26 041.9	28 404.4	30 177.2	33 458.5
Net Income	[EUR]	1 564 930.6	1 853 701.4	1 697 237.6	1 641 686.0	1 890 186.4
Net Income*	[EUR]	2 019 446.6	2 037 856.0	1 970 703.4	1 971 309.6	2 002 462.2
Income Distribution						
Hydrogen Sales	[%]	4.1	17.2	10.6	8.0	18.3
Hydrogen Sales*	[%]	25.7	24.7	23.0	23.3	22.8
Net Electricity Sales	[%]	95.9	82.8	89.4	92.0	81.7
Net Electricity Sales*	[%]	74.3	75.3	77.0	76.7	77.2
Runtime						
Minimum Runtime	[s]	15.3	39.9	59.5	81.0	102.9
Maximum Runtime	[s]	82.7	331.5	893.7	900.3	900.5
Average Runtime	[s]	21.5	55.1	87.7	118.9	171.2
Minimum Optitimality Gap	[%]	0.0006	0.0003	0.0007	0.0010	0.0003
Maximum Optimality Gap	[%]	0.0100	0.0098	0.0100	0.1061	0.6700
Average Optimality Gap	[%]	0.0038	0.0038	0.0040	0.0053	0.0095

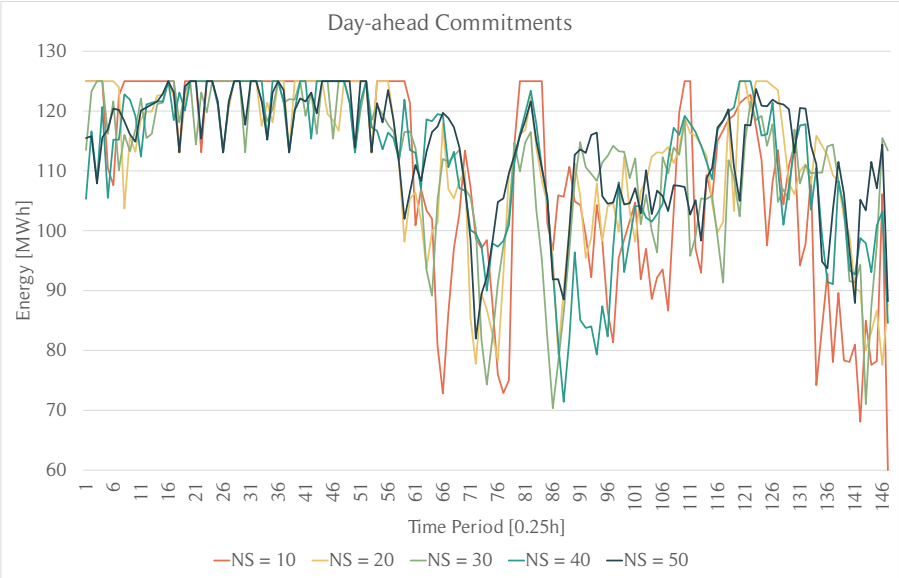

Figure A.14: The impact on day-ahead commitments when changing the number of scenarios.

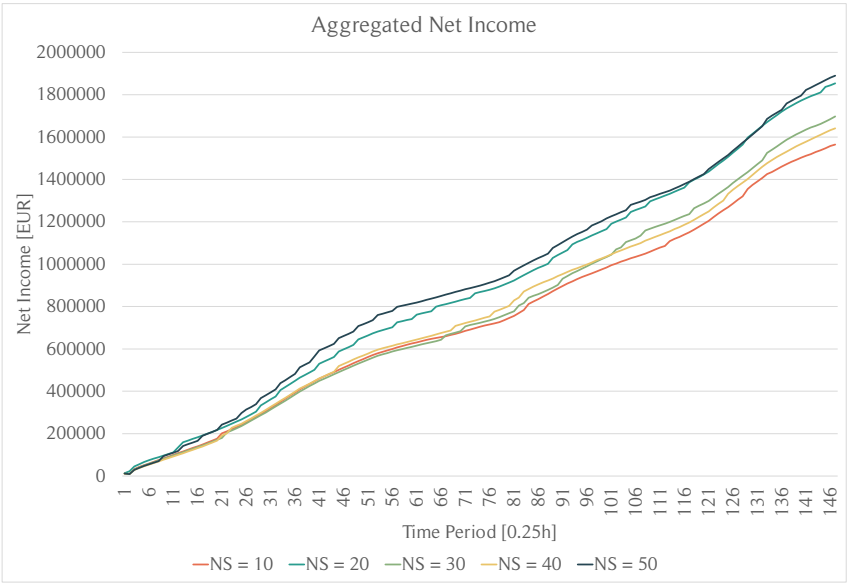

Figure A.15: The impact on net income when changing the number of scenarios.

A 8.1.3 The Role of the Intraday Market

Table A.10: Model results for intraday market policies.

	Unit	No Intraday Access	Limited Intraday Trading	Unlimited Intraday Trading
Day-ahead Commitments				
Day-ahead Commitment	[MWh]	16 423.4	16 428.8	16 426.9
Actual Day-ahead Delivery	[MWh]	16 229.5	16 019.2	12 176.9
Intraday Purchase	[MWh]	0.0	231.7	4 250.0
Actual Day-ahead Deviation	[MWh]	193.9	178.1	0.0
Actual Day-ahead Deviation	[%]	1.2	1.1	0.0
Intraday Sale Commitments				
Intraday Sale Commitment	[MWh]	0.0	35.8	271.5
Actual Intraday Sale Delivery	[MWh]	0.0	35.8	271.5
Actual Intraday Sale Deviation	[MWh]	0.0	0.0	0.0
Intraday Sale Delivery Success	[%]	0.0	100.0	100.0
Technical Performance				
Electrolysis	[MWh]	7 819.7	8 173.3	12 401.5
Auxiliary Processes	[MWh]	119.2	124.6	189.0
Electrolyzer Transitions	[MWh]	203.7	195.0	50.6
Battery Discharge	[MWh]	102.1	82.7	36.6
Fuel Cell	[MWh]	109.5	95.7	1.5
Energy Shed	[MWh]	1 852.5	1 663.9	1 019.5
Energy Shed	[%]	7.1	6.4	3.9
Hydrogen Production	[kg]	125 822.3	131 513.9	199 547.8
Financials				
Hydrogen Sales	[kg]	19 433.0	80 020.4	79 681.0
Hydrogen Sales	[EUR]	77 343.3	318 481.2	317 130.5
Hydrogen Sales*	[EUR]	476 537.3	502 635.8	797 914.5
Day-Ahead Sales	[EUR]	1 556 257.2	1 556 594.7	1 556 462.2
Intraday Sales	[EUR]	0.0	4 667.5	35 690.1
Cost Intraday Purchases	[EUR]	0.0	26 041.9	498 032.3
Net Income	[EUR]	1 633 600.6	1 853 701.4	1 411 250.4
Net Income*	[EUR]	2 032 794.6	2 037 856.0	1 892 034.4
Income Distribution				
Hydrogen Sales	[%]	4.7	17.2	22.5
Hydrogen Sales*	[%]	23.4	24.7	42.2
Electricity Sales	[%]	95.3	82.8	77.5
Electricity Sales*	[%]	76.6	75.3	57.8
Solver Performance				
Minimum Runtime	[s]	40.2	39.9	245.5
Maximum Runtime	[s]	317.7	331.5	903.9
Average Runtime	[s]	53.8	55.1	453.2
Minimum Optitimality Gap	[%]	0.0002	0.0003	0.0016
Maximum Optimality Gap	[%]	0.0099	0.0098	0.0160
Average Optimality Gap	[%]	0.0041	0.0038	0.0079

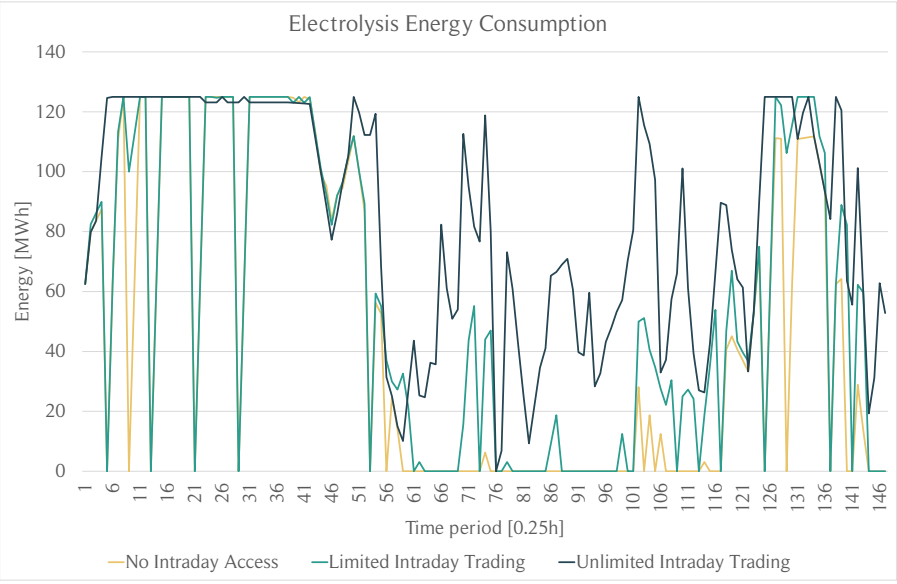

Figure A.16: The energy requirement for electrolysis over the planning period is modeled in the absence of the intraday market, with intraday trading volume restrictions and without any restrictions.

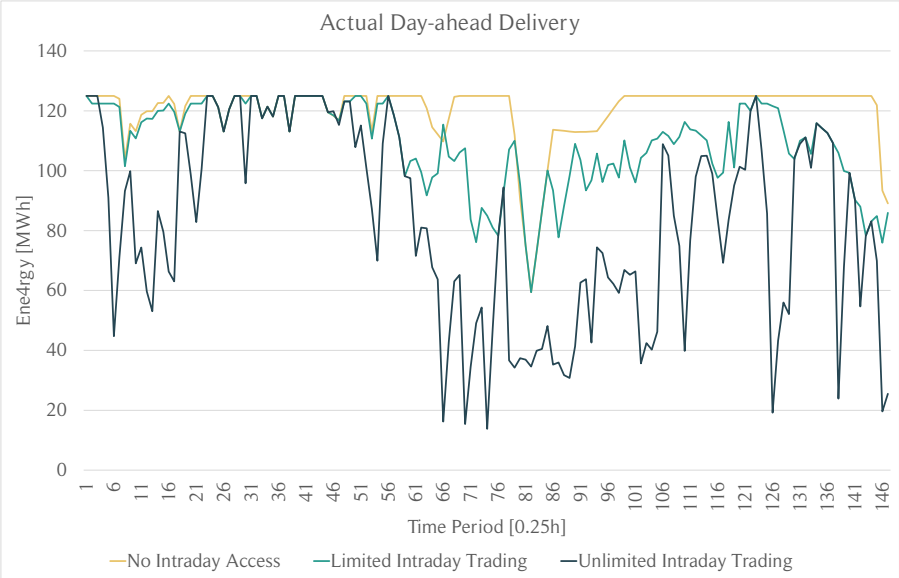

Figure A.17: The actual day-ahead delivery, equivalent to the amount of wind farm energy injected into the power grid, over the planning period is modeled in the absence of the intraday market, with intraday trading volume restrictions and without any restrictions.

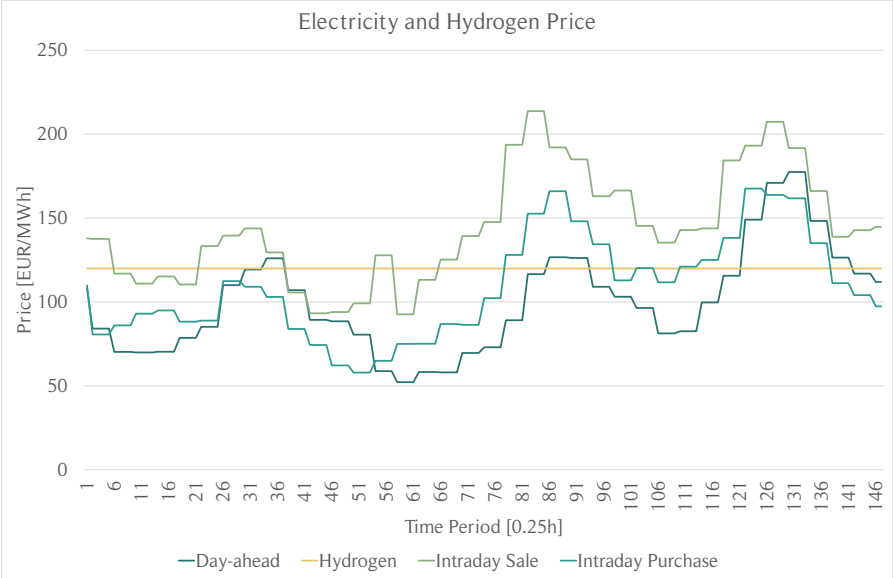

Figure A.18: The development of electricity prices and hydrogen price in the test instance when studying how the intraday market affects operations.

A 8.1.4 What if Analysis

Increased Electrolyzer Capacity

Table A.11: Model results for different electrolyzer capacities.

	Unit	500 MW	600 MW	700 MW	800 MW	1000 MW
Day ahead Commitment						
Day-ahead Commitment	[MWh]	16 428.8	14 408.1	13 130.5	12 462.2	12 195.4
Actual Day-ahead Delivery	[MWh]	16 019.2	14 182.2	12 990.1	12 335.2	12 071.3
Intraday Purchase	[MWh]	231.7	173.5	133.5	120.1	117.2
Actual Day-ahead Deviation	[MWh]	178.1	53.1	7.5	7.5	7.5
Actual Day-ahead Deviation	[%]	1.1	0.4	0.1	0.1	0.1
Intraday Sale Commitments						
Intraday Sale Commitment	[MWh]	35.8	46.4	49.1	48.0	44.6
Actual Intraday Sale Delivery	[MWh]	35.8	46.4	49.1	48.0	44.6
Actual Intraday Sale Deviation	[MWh]	0.0	0.0	0.0	0.0	0.0
Intraday Sale Delivery Success	[%]	100.0	100.0	100.0	100.0	100.0
Technical Performance						
Electrolysis	[MWh]	8 173.3	9 820.3	11 311.4	12 109.4	12 550.9
Auxiliary Processes	[MWh]	124.6	149.7	172.4	184.6	191.3
Electrolyzer Transitions	[MWh]	195.0	213.0	243.3	231.0	227.5
Battery Discharge	[MWh]	82.7	112.7	83.0	46.7	22.0
Fuel Cell	[MWh]	95.7	51.5	33.7	26.6	26.6
Energy Shed	[MWh]	1 663.9	1 747.1	1 383.6	1 237.1	1 068.0
Energy Shed	[%]	6.4	6.7	5.3	4.7	4.1
Hydrogen Production	[kg]	131 513.9	158 025.4	182 022.9	194 857.3	201 970.4
Financials						
Hydrogen Sales	[kg]	80 020.4	70 353.0	57 477.5	78 815.8	108 529.4
Hydrogen Sales	[EUR]	318 481.2	280 004.9	228 760.4	313 686.9	431 947.0
Hydrogen Sales*	[EUR]	502 635.8	619 618.3	719 892.4	772 580.9	800 932.8
Day-Ahead Sales	[EUR]	1 556 594.7	1 375 342.7	1 264 884.3	1 210 325.1	1 194 305.8
Intraday Sales	[EUR]	4 667.5	6 070.5	6 555.8	13 382.6	6 015.8
Intraday Purchases	[EUR]	26 041.9	19 350.0	15 152.7	13 630.3	13 464.4
Total Net Income	[EUR]	1 853 701.4	1 642 068.2	1 485 047.9	1 523 764.3	1 618 804.1
Total Net Income*	[EUR]	2 037 856.0	1 981 681.6	1 976 179.9	1 982 658.3	1 987 789.9
Income Distribution						
Hydrogen Sales	[%]	17.2	17.1	15.4	20.6	26.7
Hydrogen Sales*	[%]	24.7	31.3	36.4	39.0	40.3
Net Electricity Sales	[%]	82.8	82.9	84.6	79.4	73.3
Net Electricity Sales*	[%]	75.3	68.7	63.6	61.0	59.7
Solver Performance						
Minimum Runtime	[s]	42.5	41.1	37.3	38.8	46.1
Maximum Runtime	[s]	338.3	901.4	901.6	900.7	900.7
Average Runtime	[s]	57.2	66.2	61.0	72.6	95.0
Minimum Optimality Gap	[%]	0.0003	0.0001	0.0001	0.0005	0.0003
Maximum Optimality Gap	[%]	0.0098	0.0143	0.0961	0.1008	0.1577
Average Optimality Gap	[%]	0.0038	0.0060	0.0060	0.0063	0.0069

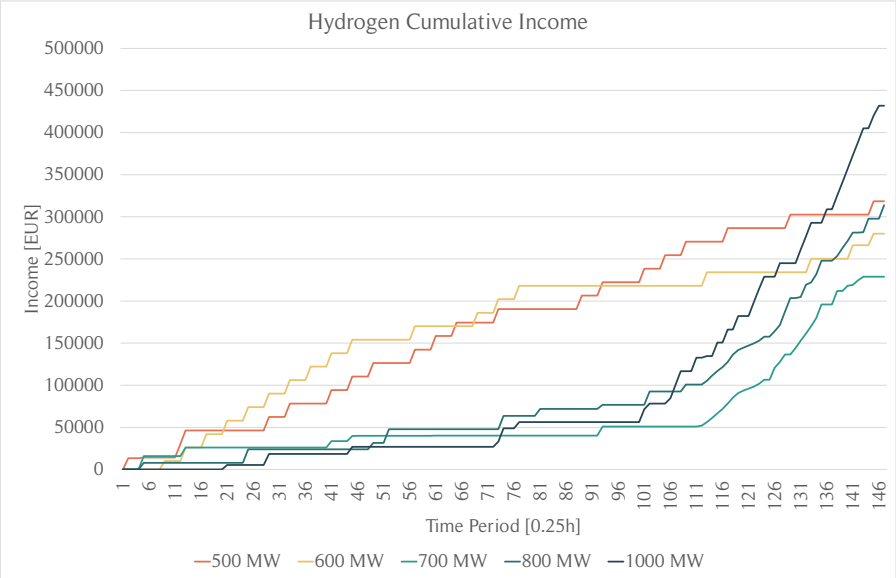

Figure A.19: Hydrogen sales does not follow the same sales pattern when comparing higher electrolyzer capacities to 500 MW.

Increased Fuel Cell Capacity

Table A.12: Model results for different fuel cell capacities.

	Unit	40 MW	50 MW	60 MW	70 MW	80 MW
Day-ahead Commitments						
Day-ahead Commitment	[MWh]	16 428.8	16 458.0	16 489.0	16 531.8	16 578.3
Actual Day-ahead Delivery	[MWh]	16 019.2	16 063.0	16 117.4	16 170.5	16 230.9
Intraday Purchase	[MWh]	231.7	235.8	227.4	230.1	228.1
Actual Day-ahead Deviation	[MWh]	178.1	160.0	144.8	132.1	120.1
Actual Day-ahead Deviation	[%]	1.1	1.0	0.9	0.8	0.7
Intraday Sale Commitments						
Intraday Sale Commitment	[MWh]	35.8	36.6	36.8	35.2	37.7
Actual Intraday Sale Delivery	[MWh]	35.8	36.6	36.8	35.2	37.7
Actual Intraday Sale Deviation	[MWh]	0.0	0.0	0.0	0.0	0.0
Intraday Sale Delivery Success	[%]	100.0	100.0	100.0	100.0	100.0
Technical Performance						
Electrolysis	[MWh]	8 173.3	8 236.7	8 245.8	8 302.5	8 299.0
Auxiliary Processes	[MWh]	124.6	125.5	125.7	126.5	126.5
Electrolyzer Transitions	[MWh]	195.0	182.5	185.0	175.6	165.0
Battery Discharge	[MWh]	82.7	87.7	94.6	89.0	80.1
Fuel Cell	[MWh]	95.7	115.4	134.2	159.5	180.7
Energy Shed	[MWh]	1 663.9	1 590.4	1 535.0	1 469.6	1 441.6
Energy Shed	[%]	6.4	6.1	5.9	5.6	5.5
Hydrogen Production	[kg]	131 513.9	132 534.5	132 680.7	133 589.6	133 535.8
Financials						
Hydrogen Sales	[kg]	80 020.4	94 322.4	94 041.0	85 870.0	62 346.1
Hydrogen Sales	[EUR]	318 481.2	375 403.2	374 283.2	341 762.6	248 137.5
Hydrogen Sales*	[EUR]	502 635.8	501 609.0	497 305.0	494 395.6	488 688.7
Day-Ahead Sales	[EUR]	1 556 594.7	1 560 282.3	1 564 015.6	1 568 425.6	1 573 472.4
Intraday Sales	[EUR]	4 667.5	4 779.9	4 737.4	4 526.6	4 872.8
Cost Intraday Purchases	[EUR]	26 041.9	26 236.4	25 539.9	25 579.9	25 390.1
Total Net Income	[EUR]	1 853 701.4	1 914 228.9	1 917 496.3	1 889 134.8	1 801 092.6
Total Net Income*	[EUR]	2 037 856.0	2 040 434.7	2 040 518.1	2 041 767.8	2 041 643.8
Income Distribution						
Hydrogen Sales	[%]	17.2	19.6	19.5	18.1	13.8
Hydrogen Sales*	[%]	24.7	24.6	24.4	24.2	23.9
Net Electricity Sales	[%]	82.8	80.4	80.5	81.9	86.2
Net Electricity Sales*	[%]	75.3	75.4	75.6	75.8	76.1
Solver Performance						
Minimum Runtime	[s]	41.6	38.8	37.4	38.5	42.8
Maximum Runtime	[s]	324.5	378.0	232.2	930.0	900.5
Average Runtime	[s]	56.3	53.9	53.0	67.5	64.1
Minimum Optimality Gap	[%]	0.0003	0.0001	0.0000	0.0008	0.0008
Maximum Optimality Gap	[%]	0.0098	0.0100	0.0098	0.0115	0.1938
Average Optimality Gap	[%]	0.0038	0.0038	0.0043	0.0041	0.0055

Increasing the Power Transmission Capacity

Table A.13: Model results for different transmission cable capacities.

	Unit	300 MW	400 MW	500 MW	600 MW	700 MW
Day-ahead Commitments						
Day-ahead Commitment	[MWh]	10 163.7	13 257.0	16 428.8	19 846.0	23 501.8
Actual Day-ahead Delivery	[MWh]	10 078.0	13 051.9	16 019.2	18 983.3	21 566.3
Intraday Purchase	[MWh]	81.7	150.3	231.7	354.9	459.1
Actual Day-ahead Deviation	[MWh]	4.0	54.8	178.1	506.8	1 476.4
Actual Day-ahead Deviation	[%]	0.0	0.4	1.1	2.6	6.3
Intraday Sale Commitments						
Intraday Sale Commitment	[MWh]	23.1	34.8	35.8	21.1	11.9
Actual Intraday Sale Delivery	[MWh]	23.1	34.8	35.8	21.1	11.9
Actual Intraday Sale Deviation	[MWh]	0.0	0.0	0.0	0.0	0.0
Intraday Sale Delivery Success	[%]	100.0	100.0	100.0	100.0	100.0
Technical Performance						
Electrolysis	[MWh]	14 450.1	11 250.1	8 173.3	6 238.7	4 017.8
Auxiliary Processes	[MWh]	220.2	171.5	124.6	95.1	61.2
Electrolyzer Transitions	[MWh]	225.8	179.3	195.0	105.5	70.1
Battery Discharge	[MWh]	59.6	75.5	82.7	84.4	73.0
Fuel Cell	[MWh]	27.3	50.9	95.7	305.6	489.7
Energy Shed	[MWh]	1 155.5	1 487.7	1 663.9	982.8	892.8
Energy Shed	[%]	4.4	5.7	6.4	3.8	3.4
Hydrogen Production	[kg]	232 520.3	181 053.3	131 513.9	100 384.9	64 657.0
Financials						
Hydrogen Sales	[kg]	107 948.5	72 015.0	80 020.4	81 455.4	33 145.0
Hydrogen Sales	[EUR]	429 634.9	286 619.7	318 481.2	324 192.5	131 917.1
Hydrogen Sales*	[EUR]	922 358.9	711 285.7	502 635.8	324 455.9	134 634.6
Day-Ahead Sales	[EUR]	968 001.5	1 262 226.5	1 556 594.7	1 880 514.5	2 228 076.6
Intraday Sales	[EUR]	2 929.0	4 318.6	4 667.5	2 845.2	1 524.7
Cost Intraday Purchases	[EUR]	9 481.0	16 994.6	26 041.9	38 694.8	50 051.0
Net Income	[EUR]	1 391 084.5	1 536 170.2	1 853 701.4	2 168 857.3	2 311 467.4
Net Income*	[EUR]	1 883 808.5	1 960 836.2	2 037 856.0	2 169 120.7	2 314 185.0
Income Distribution						
Hydrogen Sales	[%]	30.9	18.7	17.2	14.9	5.7
Hydrogen Sales*	[%]	49.0	36.3	24.7	15.0	5.8
Electricity Sales	[%]	69.1	81.3	82.8	85.1	94.3
Electricity Sales*	[%]	51.0	63.7	75.3	85.0	94.2
Solver Performance						
Minimum Runtime	[s]	48.5	41.4	39.9	41.4	41.6
Maximum Runtime	[s]	900.6	201.8	331.5	904.7	490.3
Average Runtime	[s]	76.3	58.4	55.1	102.4	112.4
Minimum Optimality Gap	[%]	0.0001	0.0008	0.0003	0.0003	0.0001
Maximum Optimality Gap	[%]	0.0308	0.0099	0.0098	0.0172	0.0100
Average Optimality Gap	[%]	0.0059	0.0050	0.0038	0.0039	0.0049

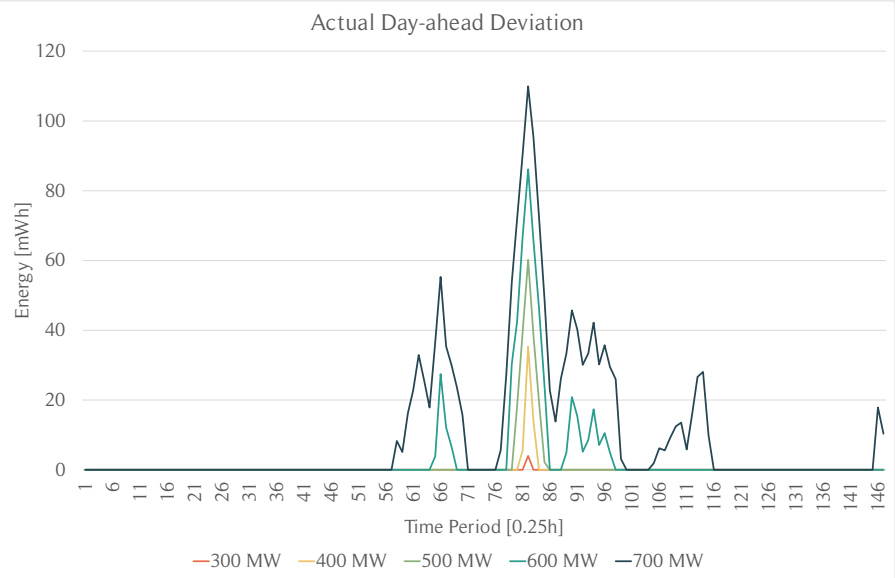

Figure A.20: Increasing the transmission cable capacity is associated with higher day-ahead deviations.

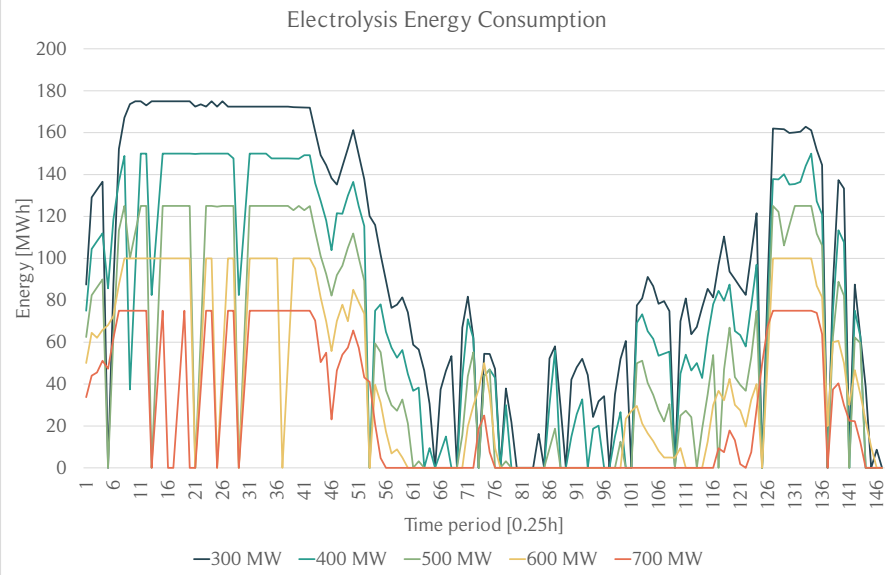

Figure A.21: The electrolysis energy requirements for different transmission cable capacities.

Number of Electrolyzers in $\mathcal{E}$

Table A.14: Model results with different electrolyzer modeling sets.

	Unit	$\mathcal{E} = 20$	$\mathcal{E} = 50$	$\mathcal{E} = 100$	$\mathcal{E} = 150$	$\mathcal{E} = 200$	$\mathcal{E} = 400$
Day-ahead Commitment							
Day-ahead Commitment	[MWh]	16 428.8	16 429.9	16 427.5	16 428.3	16 427.7	16 428.6
Actual Day-ahead Delivery	[MWh]	16 019.2	16 010.2	16 013.4	16 003.9	16 013.8	15 999.7
Intraday Purchase	[MWh]	231.7	243.0	236.0	247.0	237.6	252.1
Actual Day-ahead Deviation	[MWh]	178.1	177.5	178.6	178.5	177.0	177.5
Actual Day-ahead Deviation	[%]	1.1	1.1	1.1	1.1	1.1	1.1
Intraday Sale Commitments							
Intraday Sale Commitment	[MWh]	35.8	33.3	33.2	31.5	35.8	28.9
Actual Intraday Sale Delivery	[MWh]	35.8	33.3	33.2	31.5	35.8	28.9
Actual Intraday Sale Deviation	[MWh]	0.0	0.0	0.0	0.0	0.0	0.0
Intraday Sale Delivery Success	[%]	100.0	100.0	100.0	100.0	100.0	100.0
Technical Performance							
Electrolysis	[MWh]	8 173.3	8 636.6	8 693.5	8 621.8	8 500.6	8 847.6
Auxiliary Processes	[MWh]	124.6	131.6	132.5	131.4	129.6	134.9
Electrolyzer Transitions	[MWh]	195.0	165.0	156.3	161.3	177.8	137.9
Battery Discharge	[MWh]	82.7	84.3	89.9	82.4	76.5	84.9
Fuel Cell	[MWh]	95.7	94.5	92.9	97.0	97.1	92.5
Energy Shed	[MWh]	1 663.9	1 242.5	1 181.7	1 260.9	1 355.3	1 058.7
Energy Shed	[%]	6.4	4.8	4.5	4.8	5.2	4.1
Hydrogen Production	[kg]	131 513.9	138 967.8	139 880.2	138 725.5	136 779.6	142 365.7
Financials							
Hydrogen Sales	[kg]	131 513.9	138 967.8	139 880.2	138 725.5	136 779.6	142 365.7
Hydrogen Sales	[EUR]	318 481.2	530 077.5	534 131.9	522 466.1	515 086.8	544 111.8
Hydrogen Sales*	[EUR]	502 635.8	532 665.3	536 719.7	531 047.0	523 245.8	546 699.6
Day-Ahead Sales	[EUR]	1 556 594.7	1 556 695.9	1 556 537.9	1 556 623.7	1 556 546.9	1 556 651.4
Intraday Sales	[EUR]	4 667.5	4 251.0	4 437.5	3 888.2	4 666.3	3 803.4
Cost Intraday Purchases	[EUR]	26 041.9	27 295.3	26 362.1	27 991.9	26 404.9	27 932.2
Net Income	[EUR]	1 853 701.4	2 063 729.1	2 068 745.2	2 054 986.1	2 049 895.1	2 076 634.5
Net Income*	[EUR]	2 037 856.0	2 066 316.9	2 071 333.0	2 063 567.0	2 058 054.1	2 079 222.3
Income Distribution							
Hydrogen Sales	[%]	17.2	25.7	25.8	25.4	25.1	26.2
Hydrogen Sales*	[%]	24.7	25.8	25.9	25.7	25.4	26.3
Electricity Sales	[%]	82.8	74.3	74.2	74.6	74.9	73.8
Electricity Sales*	[%]	75.3	74.2	74.1	74.3	74.6	73.7
Solver Performance							
Minimum Runtime	[s]	38.8	46.0	68.4	82.4	98.4	172.2
Maximum Runtime	[s]	332.2	334.3	545.5	739.8	414.8	901.3
Average Runtime	[s]	54.3	71.1	90.4	119.3	145.8	300.8
Minimum Optimality Gap	[%]	0.0003	0.0001	0.0001	0.0001	0.0000	0.0000
Maximum Optimality Gap	[%]	0.0098	0.0100	0.0100	0.0100	0.0099	0.1882
Average Optimality Gap	[%]	0.0038	0.0045	0.0040	0.0041	0.0036	0.0052

System Performance With Different Hydrogen Prices [500 MW Electrolysis]

Table A.15: Model results with different hydrogen prices and 500 MW electrolyzer capacity.

	Unit	2	3	4	6	8	10	15	20
Day-ahead Commitments									
Day-ahead Commitment	[MWh]	16 441.7	16 441.7	16 428.8	16 292.9	16 129.6	16 117.6	16 075.7	16 069.1
Actual Day-ahead Delivery	[MWh]	16 035.7	16 035.8	16 019.2	15 875.8	15 709.7	15 695.6	15 642.0	15 638.6
Intraday Purchase	[MWh]	228.1	228.1	231.7	238.2	237.7	240.2	251.5	248.5
Actual Day-ahead Deviation	[MWh]	178.5	178.0	178.1	179.2	182.4	181.9	182.4	182.3
Actual Day-ahead Deviation	[%]	1.1	1.1	1.1	1.1	1.1	1.1	1.1	1.1
Intraday Sale Commitments									
Intraday Sale Commitment	[MWh]	35.8	35.8	35.8	34.7	34.7	31.1	29.7	29.6
Actual Intraday Sale Delivery	[MWh]	35.8	35.8	35.8	34.7	34.7	31.1	29.7	29.6
Actual Intraday Sale Deviation	[MWh]	0.0	0.0	0.0	0.0	0.0	0.0	0.0	0.0
Intraday Sale Delivery Success	[%]	100.0	100.0	100.0	100.0	100.0	100.0	100.0	100.0
Technical Performance									
Electrolysis	[MWh]	7 929.6	8 062.1	8 173.3	8 159.2	8 273.6	8 494.9	8 341.0	8 716.8
Auxiliary Processes	[MWh]	120.9	122.9	124.6	124.4	126.1	129.5	127.1	132.9
Electrolyzer Transitions	[MWh]	210.0	189.4	195.0	199.4	197.8	185.6	197.2	170.3
Battery Discharge	[MWh]	79.8	82.5	82.7	88.5	98.6	101.9	93.8	98.1
Fuel Cell	[MWh]	98.8	97.9	95.7	89.6	86.6	86.5	87.7	85.3
Energy Shed	[MWh]	1 888.9	1 765.5	1 663.9	1 810.6	1 859.5	1 670.1	1 861.1	1 509.4
Energy Shed	[%]	7.2	6.8	6.4	6.9	7.1	6.4	7.1	5.8
Hydrogen Production	[kg]	127 587.2	129 721.3	131 513.9	131 284.2	133 123.0	136 682.9	134 206.6	140 253.0
Financials									
Hydrogen Sales	[kg]	82 582.2	106 847.0	80 020.4	107 263.9	97 403.2	109 390.6	52 159.6	133 194.1
Hydrogen Sales	[EUR]	164 338.6	318 938.3	318 481.2	640 365.5	775 329.5	1 088 436.5	778 482.0	2 650 562.6
Hydrogen Sales*	[EUR]	243 102.8	371 205.6	502 635.8	754 989.5	1 022 885.5	1 314 003.0	1 932 930.8	2 700 710.6
Day-Ahead Sales	[EUR]	1 557 467.7	1 557 470.9	1 556 594.7	1 545 171.5	1 528 890.2	1 528 164.4	1 523 954.7	1 523 529.6
Intraday Sales	[EUR]	4 666.8	4 667.6	4 667.5	4 512.3	4 538.1	4 230.6	3 850.6	3 863.9
Cost Intraday Purchases	[EUR]	25 808.1	25 810.5	26 041.9	26 381.2	26 440.2	26 626.2	27 891.5	27 716.5
Net Income	[EUR]	1 700 664.9	1 855 266.2	1 853 701.4	2 163 668.1	2 282 317.6	2 594 205.3	2 278 395.8	4 150 239.7
Net Income*	[EUR]	1 779 429.1	1 907 533.6	2 037 856.0	2 278 292.1	2 529 873.6	2 819 771.8	3 432 844.6	4 200 387.7
Income Ditribution									
Hydrogen Sales	[%]	9.7	17.2	17.2	29.6	34.0	42.0	34.2	63.9
Hydrogen Sales*	[%]	13.7	19.5	24.7	33.1	40.4	46.6	56.3	64.3
Electricity Sales	[%]	90.3	82.8	82.8	70.4	66.0	58.0	65.8	36.1
Electricity Sales*	[%]	86.3	80.5	75.3	66.9	59.6	53.4	43.7	35.7
Solver Performance									
Minimum Runtime	[s]	41.6	40.4	40.1	41.4	40.9	31.0	36.8	35.7
Maximum Runtime	[s]	447.0	294.2	345.6	264.0	431.5	554.4	377.5	422.7
Average Runtime	[s]	58.1	58.6	55.5	57.5	57.0	58.3	54.9	56.8
Min Optimality Gap	[%]	0.0006	0.0002	0.0003	0.0008	0.0004	0.0005	0.0010	0.0009
Max Optimality Gap	[%]	0.0099	0.0100	0.0098	0.0097	0.0099	0.0097	0.0100	0.0100
Average Optimality Gap	[%]	0.0041	0.0039	0.0038	0.0042	0.0047	0.0044	0.0047	0.0050

A. 8.1.7 Value of Perfect Information

Table A.16: Model results under perfect information.

Solution	Value
Scenario 1	1 982 720.0
Scenario 2	1 955 730.7
Scenario 3	1 916 534.1
Scenario 4	1 959 490.6
Scenario 5	1 873 809.7
Scenario 6	1 955 854.0
Scenario 7	1 815 337.4
Scenario 8	1 879 046.9
Scenario 9	1 635 405.5
Scenario 10	1 871 512.9
Scenario 11	1 624 777.7
Scenario 12	1 831 764.3
Scenario 13	1 985 992.6
Scenario 14	1 911 671.4
Scenario 15	1 897 383.4
Scenario 16	1 894 268.2
Scenario 17	1 915 866.3
Scenario 18	1 863 913.1
Scenario 19	1 912 421.8
Scenario 20	1 951 432.2
SS	1 853 733.2

A. 8.2.4 Decoupling From Power Markets - *Island Mode*

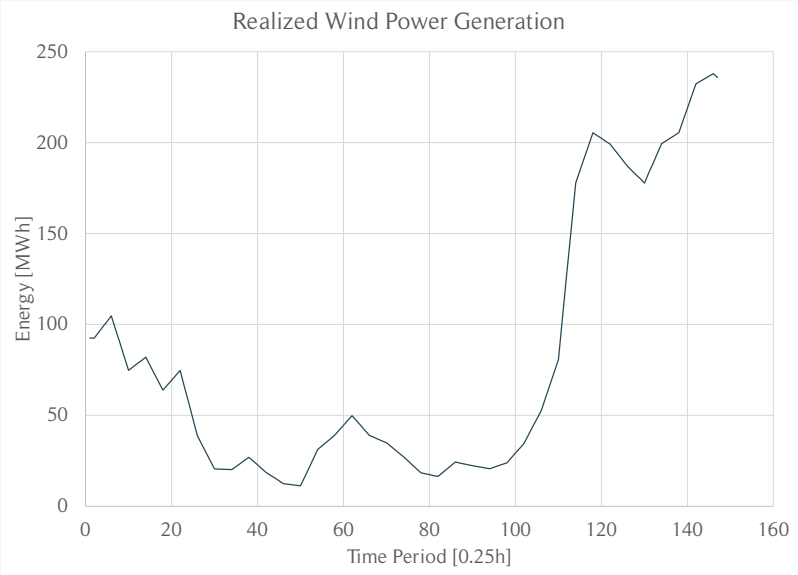

Figure A.22: Wind power generation profile when testing for fuel cell and battery activation in island mode configuration.

A. 8.2.7 Power Market Participation - A Profitability Driver

Table A.17: Model results with different hydrogen prices and 1000 MW electrolyzer capacity.

	Unit	2 EUR	4 EUR	5 EUR	6 EUR	8 EUR	10 EUR	15 EUR
Day-ahead Commitments								
Day-ahead Commitment	[MWh]	12 604.6	12 195.4	11 344.7	10 021.0	1 600.1	1.9	0.0
Actual Day-ahead Delivery	[MWh]	12 472.5	12 071.3	11 217.1	9 883.8	1 576.5	1.9	0.0
Intraday Purchase	[MWh]	125.0	117.2	120.6	131.9	23.5	0.0	0.0
Actual Day-ahead Deviation	[MWh]	7.5	7.5	7.5	6.3	0.0	0.0	0.0
Actual Day-ahead Deviation	[%]	0.1	0.1	0.1	0.1	0.0	0.0	NA
Intraday Sale Commitments								
Intraday Sale Commitment	[MWh]	45.5	44.6	38.6	28.6	6.1	0.0	0.0
Actual Intraday Sale Delivery	[MWh]	45.5	44.6	38.6	28.6	6.1	0.0	0.0
Actual Intraday Sale Deviation	[MWh]	0.0	0.0	0.0	0.0	0.0	0.0	0.0
Intraday Sale Delivery Success	[%]	100.0	100.0	100.0	100.0	100.0	NA	NA
Technical Performance								
Electrolysis	[MWh]	12 056.7	12 550.9	13 571.3	15 350.2	23 825.4	25 666.0	25 667.9
Auxiliary Processes	[MWh]	183.8	191.3	206.9	234.0	363.2	391.2	391.2
Electrolyzer Transitions	[MWh]	286.3	227.5	206.3	142.5	56.9	12.5	12.5
Battery Discharge	[MWh]	21.2	18.7	24.3	17.8	10.5	0.0	0.0
Fuel Cell	[MWh]	27.6	26.6	19.8	10.0	7.7	0.0	0.0
Energy Shed	[MWh]	1 106.3	1 068.0	897.8	490.4	309.0	56.6	56.6
Energy Shed	[%]	4.2	4.1	3.4	1.9	1.2	0.2	0.2
Hydrogen Production	[kg]	194 014.8	201 970.4	218 388.5	247 012.2	383 422.9	413 041.8	413 072.8
Financials								
Hydrogen Sales	[kg]	122 404.8	108 529.4	122 709.0	144 238.8	307 007.3	377 164.3	367 891.5
Hydrogen Sales	[EUR]	243 585.7	431 947.0	610 477.3	861 105.6	2 443 778.1	3 752 784.8	5 490 781.1
Hydrogen Sales*	[EUR]	384 517.5	800 932.8	1 085 042.5	1 476 612.6	3 056 061.3	4 119 740.8	6 179 868.3
Day-Ahead Sales	[EUR]	1 217 600.8	1 194 305.8	1 136 831.9	1 038 478.6	226 243.7	316.5	0.0
Intraday Sales	[EUR]	6 146.7	6 015.8	5 610.5	4 195.6	1 111.7	4.8	0.0
Cost Intraday Purchases	[EUR]	14 084.2	13 464.4	13 348.9	13 960.4	3 361.2	0.0	0.0
Net Income	[EUR]	1 453 249.0	1 618 804.1	1 739 570.8	1 889 819.5	2 667 772.3	3 753 106.0	5 490 781.1
Net Income*	[EUR]	1 594 180.8	1 987 789.9	2 214 136.0	2 505 326.5	3 280 055.5	4 120 062.0	6 179 868.3
Income Ditribution								
Hydrogen Sales	[%]	16.8	26.7	35.1	45.6	91.6	100.0	100.0
Hydrogen Sales*	[%]	24.1	40.3	49.0	58.9	93.2	100.0	100.0
Electricity Sales	[%]	83.2	73.3	64.9	54.4	8.4	0.0	0.0
Electricity Sales*	[%]	75.9	59.7	51.0	41.1	6.8	0.0	0.0
Solver Performance								
Minimum Runtime	[s]	47.0	50.8	49.0	51.6	49.3	51.1	53.8
Maximum Runtime	[s]	900.8	900.6	900.5	545.1	901.4	901.7	509.6
Average Runtime	[s]	115.8	95.9	113.5	108.4	170.5	181.4	145.8
Min Optimality Gap	[%]	0.0001	0.0003	0.0002	0.0005	0.0003	0.0015	0.0021
Max Optimality Gap	[%]	0.0219	0.1577	0.0240	0.0100	0.2643	0.0879	0.0100
Average Optimality Gap	[%]	0.0059	0.0069	0.0063	0.0063	0.0077	0.0085	0.0072

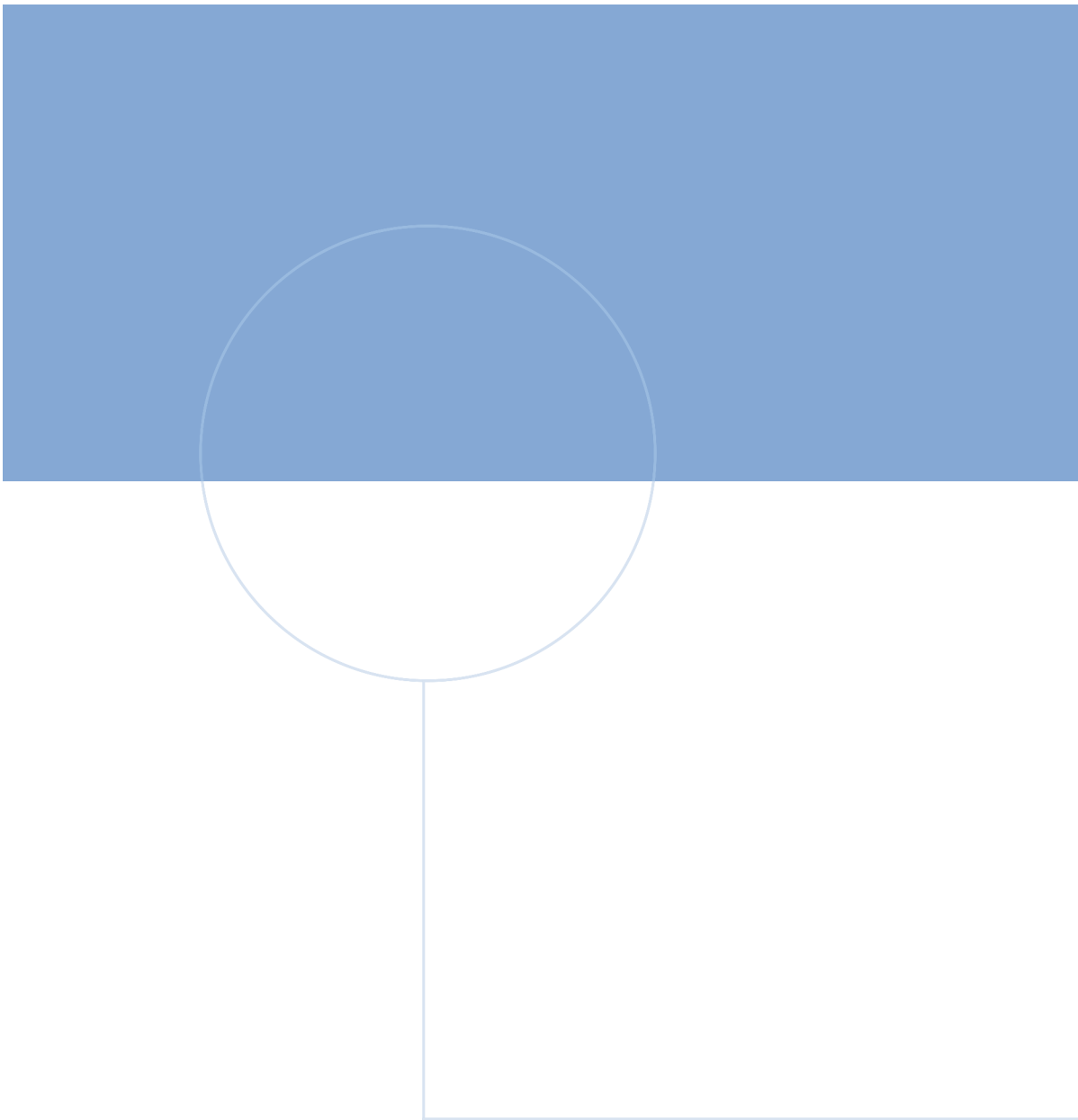

NTNU

Norwegian University of
Science and Technology